INFORMATION TO USERS

This manuscript has been reproduced from the microfilm master. UMI films the text directly from the original or copy submitted. Thus, some thesis and dissertation copies are in typewriter face, while others may be from any type of computer printer.

The quality of this reproduction is dependent upon the quality of the copy submitted. Broken or indistinct print, colored or poor quality illustrations and photographs, print bleedthrough, substandard margins, and improper alignment can adversely affect reproduction.

In the unlikely event that the author did not send UMI a complete manuscript and there are missing pages, these will be noted. Also, if unauthorized copyright material had to be removed, a note will indicate the deletion.

Oversize materials (e.g., maps, drawings, charts) are reproduced by sectioning the original, beginning at the upper left-hand corner and continuing from left to right in equal sections with small overlaps.

Photographs included in the original manuscript have been reproduced xerographically in this copy. Higher quality 6" x 9" black and white photographic prints are available for any photographs or illustrations appearing in this copy for an additional charge. Contact UMI directly to order.

Bell & Howell Information and Learning
300 North Zeeb Road, Ann Arbor, MI 48106-1346 USA
800-521-0600

UMI®

UNIVERSITÉ DE MONTRÉAL

Counter–Current and Flooding in Vertical and Horizontal Tubes with and without Obstructions

PETER TYE

DÉPARTEMENT DE GÉNIE MÉCANIQUE

ÉCOLE POLYTECHNIQUE DE MONTRÉAL

THÈSE PRÉSENTÉE EN VUE DE L'OBTENTION

DU DIPLÔME DE PHILOSOPHIÆ DOCTOR (Ph.D.)

(GÉNIE NUCLÉAIRE)

Avril 1998

©Peter Tye, 1998.

National Library of Canada
Bibliothèque nationale du Canada

Acquisitions and Bibliographic Services
Acquisitions et services bibliographiques

395 Wellington Street
Ottawa ON K1A 0N4
Canada

395, rue Wellington
Ottawa ON K1A 0N4
Canada

Your file Votre référence

Our file Notre référence

The author has granted a non-exclusive licence allowing the National Library of Canada to reproduce, loan, distribute or sell copies of this thesis in microform, paper or electronic formats.

L'auteur a accordé une licence non exclusive permettant à la Bibliothèque nationale du Canada de reproduire, prêter, distribuer ou vendre des copies de cette thèse sous la forme de microfiche/film, de reproduction sur papier ou sur format électronique.

The author retains ownership of the copyright in this thesis. Neither the thesis nor substantial extracts from it may be printed or otherwise reproduced without the author's permission.

L'auteur conserve la propriété du droit d'auteur qui protège cette thèse. Ni la thèse ni des extraits substantiels de celle-ci ne doivent être imprimés ou autrement reproduits sans son autorisation.

0-612-46641-8

Canada

UNIVERSITÉ DE MONTRÉAL

ÉCOLE POLYTECHNIQUE

Cette thèse intitulée:

Counter–Current Flow and Flooding in Vertical and Horizontal Tubes with and without Obstructions

présentée par: TYE Peter

en vue de l'obtention du diplôme de: Philosophiæ Doctor (Ph.D.)

a été dûment acceptée par le jury d'examen constitué de:

M.ROZON Daniel, Ph.D., président

M.TEYSSEDOU Alberto, Ph.D., membre et directeur de recherche

M.TAPUCU Altan, D.Sc.A., membre et codirecteur

M.SHOUKRI Mamdouh, Ph.D., membre externe

M.CAMARERO, Ricardo, Ph.D., membre

To my mother.

To the memory of my father, who beleived that the greatest gift a parent could give a child was an education. Thanks dad I wish you'd been here to see this...

and

To Bill.

Acknowledgements

I would like to thank my thesis directors Drs. A. Teyssedou and A. Tapucu for their guidance, support and encouragement during the course of this research project. The work presented in this thesis was funded by the CANDU Owners Group (COG) whose support is greatfully acknowledged. I would also like to express my very special thanks to Dr. W.I. Midvidy whose unwavering support as the COG contract officer made this research project possible and whose technical suggestions helped guide the course of this work.

I also wish to thank Mr. J.C. Juneau for his help in constructing the test facility, Mr. P. Champagne for his help with the electronics and Mr. P. Hernu for his help with the French corrections. I also wish to express my thanks to all the students and the staff of the IGN for making my stay here so enjoyable.

I would also like to thank all the members of my jury for taking the time to read my thesis and particularly for doing so on very short notice.

Résumé

Au cours de cette thèse, nous présenterons les résultats des travaux effectués dans le but d'étudier les écoulements à contre-courant ainsi que le point d'engorgement pour des écoulements vertical et vertical à horizontal. Pour réaliser ces travaux, deux sections d'essais de 63.5 *mm* de diamètre intérieur ont été utilisées; la première ayant uniquement une branche verticale et la seconde une branche verticale et une branche horizontale. Dans les deux cas, les expériences ont été effectuées avec et sans orifices de différentes grandeurs placés dans la section d'essais. Pour la section d'essais ayant une branche verticale et une branche horizontale l'orifice était placé dans la partie horizontale. Nous présentons aussi les résultats concernant les pertes de pression expérimentales en écoulements à contre-courant obtenus uniquement avec la section d'essais verticale.

Pour les deux sections d'essais, nous avons trouvé que pour un débit de liquide donné, la présence d'un orifice réduit de façon significative le débit de gaz correspondant au point d'engorgement. De plus, nous avons constaté que cette réduction était inversement proportionnelle au rapport β de l'orifice. Un autre point intéressant à signaler est que pour les deux sections d'essais, le débit de liquide délivré (le débit de liquide qui se rend à la sortie de la section d'essais) est fonction uniquement du débit de gaz et du rapport β de l'orifice; il est indépendant du débit de liquide injecté. Nous avons aussi constaté que pour tous les cas étudiés, la vitesse superficielle du gaz nécessaire au refoulement total du liquide (point de pénétration nulle) est fonction uniquement du rapport β de l'orifice; il est aussi indépendant du débit de liquide injecté.

En ce qui concerne le point d'engorgement seulement, nous avons comparé les résultats expérimentaux obtenus avec la section d'essais ayant une branche verticale et une branche horizontale avec ceux d'autres chercheurs. Malgré le fait qu'aucune des sec-

tions d'essais utilisées par les autres chercheurs ne soit identique à celle utilisée dans cette étude, leurs résultats sont en accord avec les nôtres. Nous avons également constaté que la corrélation d'Ardron et Banerjee [1986] prédit relativement bien nos résultats expérimentaux pour les cas sans orifice.

Des expériences ont également été réalisées dans le but d'étudier l'effet d'hystérésis en utilisant la section d'essais ayant une branche verticale et une branche horizontale. Ces expériences ont été menées avec et sans orifices de différentes grandeurs installés dans la branche horizontale. Pour tous les cas étudiés, nous avons observé des effets d'hystérésis importants. Nous avons constaté qu'il était nécessaire de réduire de façon importante le débit de gaz sous celui qui correspond au point d'engorgement afin de rétablir l'acheminement total du liquide. De plus, nous nous sommes aperçus que, suite à l'engorgement, les débits de liquide déchargé obtenus avec des débits de gaz décroissants et inférieurs à celui correspondant au point d'engorgement, suivent les mêmes courbes de décharge partielle que celles obtenues avec des débits de gaz croissants.

Nous avons développé deux modèles phénoménologiques pour la prédiction du point d'engorgement pour des écoulements à contre–courant verticaux. Nous présenterons une comparaison entre les prédictions de ces modèles et les résultats expérimentaux obtenus aux cours de ces travaux.

Nous avons développé un modèle pour prédire le point d'engorgement pour des écoulements à contre–courant vertical et horizontal utilisant une extension d'un modèle pour le début de l'entraînement appliqué à la crête du saut hydraulique. La hauteur du saut hydraulique est calculée en utilisant des méthodes tirées du domaine de l'étude des écoulements à surfaces libres. Nous avons comparé les prédictions de ce modèle avec nos résultats expérimentaux ainsi qu'avec ceux d'autres chercheurs. Nous verrons que les prédictions concordent très bien avec les résultats expérimentaux. Une extension a été apportée à ce modèle afin de tenir compte de l'effet de l'orifice sur la hauteur du niveau de liquide dans la section horizontale à la crête du saut hydraulique. De plus nous présenterons une comparaison des prédictions de ce modèle avec nos résultats expérimentaux obtenus avec un orifice placé dans la branche horizontale ainsi qu'avec ceux d'autres chercheurs. De manière générale, ce modèle prédit très bien les résultats expérimentaux.

Nous avons réalisé une revue bibliographique sur les écoulements diphasiques à contre–

courants. Une attention spéciale à été accordée aux phénomènes qui pourraient être pertinents au refroidissement d'urgence d'un réacteur CANDU suite à une perte de caloporteur. Ceux-ci incluent les pertes de charges, l'effet d'hystérésis, l'épaisseur de film et le point d'engorgement. Nous émettrons aussi certaines recommandations sur les meilleures corrélations empiriques et théoriques permettant la détermination du point d'engorgement. Pour conclure, nous suggérerons également des sujets de recherches futures qui pourraient approfondir nos connaissances dans ce domaine.

Abstract

This thesis presents the results of the work carried out to study counter-current flow and flooding phenonema under conditions of both vertical and vertical to horizontal flow. Two different 63.5 *mm.* I.D. test sections were used for this work. The first containing only a vertical leg and the second having both a vertical and a horizontal leg. In both cases the experiments were carried out both with and without various size orifices placed in the test section. For the test section containing both the vertical and the horizontal legs the orifice was placed in the horizontal leg. Results on the pressure drop under counter-current flow conditions obtained in the vertical test section only are also presented.

For both the vertical and the horizontal test sections, it was found that for a given liquid flow rate the presence of an orifice greatly reduced the gas flow rate at which flooding occured. Furthermore, this decrease was found to be inversely proportional to the orifice β ratio. A further point of interest is that for both test sections the delivered liquid flow rate (the liquid flow rate that actually reaches the outlet of the test section) is a function of the gas flow rate and the orifice β ratio only and is independent of the inlet liquid flow rate. It was further observed that for all the cases studied the zero penetration point was only a function of the orifice β ratio and of the gas flow rate, and was also seen to be independent of the inlet liquid flow rate.

The experimental results, for the flooding point only, obtained in the test section containing both the vertical and the horizontal legs have been compared to the results of other researchers. In spite of the fact, that none of the test facilities used by the other researchers are identical to the one used in the present study, the results of the other researchers are in good agreement with the present results. The Ardron & Banerjee [1986] correlation was found to do a reasonably good job of predicting our experimental flooding results in the no orifice case.

Experiments were also carried out to study the hysteresis effect in a test section containing both a vertical and a horizontal leg. These experiments were performed both with and without various sized orifices placed in the horizontal leg. For all the cases studied, a significant hysteresis effect was observed. It was found that in order to re–establish full liquid delivery after flooding had occured it was necessary to significantly decrease the gas flow rate below that required to initiate flooding. It was also observed that in the post flooding state, the delivered liquid flow rate with decreasing gas flow rate followed the partial liquid delivery curves obtained with increasing gas flow rates.

Two phenomenological models for the prediction of the flooding point for vertical counter–current two–phase flows are developed. The first represented flooding as being linked to the mechanism of droplet entrainment while the second related the flooding point to the mechanism of film reversal. A comparison between the predictions of these model and the experimental results obtained during the course of this investigation will be presented. It will be shown that the models were very sensitive to the choice of correlation used for the interfacial friction factor. Using an appropriate choice of the correlation to represent the interfacial friction, the model based on the mechanism of droplet entrainment predicts our experimental results reasonably well. The model based on the mechanism of flow reversal on the other hand under–predicts the flooding points at high liquid flow rates.

A model to predict the flooding point in a test section containing vertical and horizontal legs using an extension of a model for entrainment inception applied at the crest of the hydraulic jump has been developed. The height of the hydraulic jump is calculated using methods taken from the study of open channel flows. The results of a comparison between this model and our experimental results as well as those of other researchers is presented. The predictions are seen to be in very good agreement with the experimental results. An extension to this model to take into account the influence of the various size orifices on the height of the liquid level in the horizontal leg at the crest of the hydraulic jump has been developed. A comparison of the predictions of this model against both our experimental results and those of other researchers is presented. The agreement between the predictions and the experimental results is in general very good.

A review of literature in the area of counter–current gas–liquid flow has been carried

out. Special emphasis is put on the phenomena that might be of relevance to the emergency core cooling during a postulated loss of coolant accident in a CANDU reactor. This includes pressure drop, hysteresis effect, film thickness and counter-current flooding limits. Recommendations are made for the best available empirical and theoretical correlations for the counter-current flooding limit. The problems of practical importance that need to be examined in greater detail have been pointed out.

Condensé en français

1 Introduction (Chapitre 1)

Les écoulements à contre-courants en général et la limite d'engorgement en particulier sont d'une importance capitale dans le domaine de l'analyse de sûreté des réacteurs nucléaires. Dans les réacteurs CANDU, suite à certaines pertes de caloporteur hypothétiques, l'eau de refroidissement qui vient des collecteurs d'entrées et de sorties est acheminée aux canaux de combustible par les tuyaux d'alimentation. Ceux-ci comportent des sections verticales et horizontales; dans certains des tuyaux d'alimentation des orifices et/ou des venturis sont installés pour fin de contrôle ou mesure de débit. La vapeur produite dans les tuyaux d'alimentation et/ou dans les canaux de combustible peut s'écouler dans la direction opposée à celle de l'eau de refroidissement créant ainsi un écoulement diphasique à contre–courant dans les tuyaux d'alimentation. Dans de telles conditions, le débit de l'eau de refroidissement qui se rend aux canaux de combustible peut être limité par le phénomène d'engorgement. Suite à l'amorce de l'engorgement, l'eau de refroidissement est partiellement entraînée dans le même sens que la vapeur. Le débit de liquide délivré aux canaux de combustible est donc grandement influencé par la géométrie des tuyaux d'alimentation, le type et le nombre de raccords, les restrictions hydrauliques et la façon que les tuyaux d'alimentation sont connectés aux collecteurs et aux canaux de combustible. Ainsi, une compréhension plus profonde du phénomène d'engorgement dans une géométrie similaire à celle qu'on retrouve dans le système d'alimentation d'un réacteur CANDU est d'une importance capitale dans le domaine de l'analyse de sûreté des réacteurs nucléaires, particulièrement pour l'amélioration de la prédiction du temps requis pour que le système d'alimentation d'urgence remplisse les canaux de combustible. Les objectifs de cette recherche sont donc d'étudier tous les aspects des écoulements à contre-courant et du phénomène d'engorgement applicable dans

des systèmes géométriquement similaire à celui de l'alimentation d'eau d'un réacteur CANDU.

2 Revue bibliographique (Chapitre 2)

Au cours des 40 dernières années, un grand nombre de travaux expérimentaux et analytiques ont été effectués dans le but d'étudier les écoulements à contre-courant (ÉCC) et le phénomène d'engorgement. Dans le passé, trois critères différents ont été utilisés pour la caractérisation de la limite d'engorgement. Ceux-ci incluent:

1. le point où débute l'entraînement des gouttelettes,
2. le point où le film de liquide commence à s'écouler vers le haut, et
3. le point de pénétration nulle.

Cependant, il est important de noter que pour un débit de liquide donné, ces trois phénomènes se produisent à des débits de gaz différents. Il est donc évident qu'un manque de clarté et d'uniformité dans la définition du point d'engorgement aura une influence majeure sur l'interprétation des résultats expérimentaux. Certaines des corrélations les plus connues pour la prédiction du point d'engorgement en écoulement à contre-courant vertical seront présentées.

Écoulements verticaux

Un écoulement vertical à contre-courant s'établit dû à la différence entre les forces gravitationnelles par unité de volume qui s'exercent sur les deux phases. Les forces de traînée à l'interface gaz–liquide agissent en opposition aux forces gravitationnelles. De plus, cette traînée s'accroît avec une augmentation de la vitesse relative entre les deux phases. Il est donc clair qu'il existe une vitesse relative au delà de laquelle un écoulement à contre-courant pur ne peut exister. Cette limite est connue sous le nom de *point d'engorgement.* Comme nous l'avons mentionné auparavant, plusieurs critères contradictoires ont été utilisés pour caractériser cette limite. Une définition plus claire qui n'est pas sujet a multiples interprétations s'impose donc. La définition du point d'engorgement que nous allons utiliser aux cours de ces travaux est: *le point où la décharge du liquide dans sa totalité ne peut plus être soutenue correspond au point d'engorgement.* De manière générale, les expériences faites au cours des années ont démontré que le débit de gaz correspondant au point d'engorgement diminue

avec des débits de liquide qui augmentent. De plus, nous avons trouvé que, pour un débit de liquide donné, la perte de pression augmente graduellement avec une augmentation du débit de gaz jusqu'au point d'engorgement où un saut brusque de sa valeur se produit. Une mesure de la perte de pression en écoulement à contre-courant peut donc être utilisée comme critère expérimental pour la détermination du point d'engorgement.

La corrélation la plus connue pour la prédiction du point d'engorgement en écoulement à contre-courant vertical est celle de Wallis [1969] qui est donnée par:

$$j_g^{*1/2} + m j_l^{*1/2} = C$$

où la vitesse superficielle adimensionnelle est définie comme:

$$j_k^* = \frac{j_k \rho_k^{1/2}}{\left[gD\left(\rho_l - \rho_g\right)\right]^{1/2}}$$

où k représente soit la phase liquide l soit la phase gazeuse g. Les constantes m, C tiennent compte des effets d'entrée et de sortie.

Écoulements horizontaux

Krowlewski [1980] a effectué des expériences sur le point d'engorgement dans une conduite verticale ou inclinée reliée à une conduite horizontale par un coude à 90° ou à 45°, selon le cas. La section d'essais était composée d'une conduite horizontale d'une longueur de 584 *mm* et d'un diamètre intérieur de 51 *mm*. L'eau et l'air aux conditions atmosphériques ont été utilisés comme fluides de travail. La limite d'engorgement était déterminée lorsqu'une augmentation soudaine de la perte de pression dans la section d'essais était observée. Les données ont été collectées pour différentes configurations géométriques. L'auteure a observé que le débit de gaz nécessaire pour provoquer un engorgement dans une conduite horizontale est beaucoup plus faible que celui requis pour une conduite verticale de même diamètre intérieur.

Siddiqui *et al.* [1986] ont effectué des expériences dans une conduite verticale reliée à une conduite horizontale par un coude à 90° et ce, pour différents diamètres et longueurs de conduites ainsi que pour différents rayons de courbure du coude. Les auteurs ont observé que pour un débit de liquide injecté élevé, un saut hydraulique se

forme dans la partie horizontale près du coude. Dans ces conditions, l'engorgement est causé par un bouchon qui se form à la crête du saut hydraulique. Sur toute la plage de diamètres intérieurs étudiés, lorsque le débit de liquide injecté est faible, le saut hydraulique est petit et difficile à observer. Les auteurs ont constaté que la limite d'engorgement dépendait du diamètre intérieur de la conduite, de la longueur de la conduite horizontale et du rayon de courbure du coude. Les résultats ont montré que le débit de gaz nécessaire pour provoquer un engorgement est beaucoup plus faible dans les configurations étudiées que dans une conduite verticale équivalente. Les auteurs ont également observé que, sur la plage de diamètres intérieurs étudiés, la racine carrée de la vitesse superficielle non-dimensionnelle du gaz au point de pénétration nulle est constante.

Wan [1986] a effectué des expériences sur les écoulements diphasiques à contre-courant dans une section d'essais ayant un coude à 90°. Les fluides de travail utilisés étaient l'eau et la vapeur d'eau. L'auteur a identifié trois configurations différentes d'écoulement caractérisant ses expériences: i) écoulement diphasique à contre-courant en régime stationnaire sans bouchon, ii) bouchon avec refoulement de liquide et iii) bouchon accompagné d'une colonne pulsative dans la conduite verticale mais sans refoulement de liquide.

Kawaji *et al.* [1989] ont étudié la limite d'engorgement dans une conduite verticale et dans une conduite verticale reliée par des coudes de différents angles à des conduites inclinées ou horizontales. Dans tous les cas, les conduites utilisées avaient un diamètre intérieur de 51 mm. Pour les expériences effectuées dans une conduite verticale reliée à une conduite horizontale par un coude, deux longueurs ont été utilisées pour la conduite horizontale: 0.1 m et 2.54 m. Pour la conduite horizontale la plus longue et pour de faibles débits de liquide injecté, les auteurs ont observé la formation d'un saut hydraulique dans la conduite horizontale près du coude. Dans ces conditions, la cause de l'engorgement était la formation d'un bouchon à la crête du saut hydraulique. De plus, les auteurs ont observé que, pour un débit de liquide injecté donné, le débit de gaz nécessaire à l'obtention d'un engorgement était beaucoup plus faible dans un écoulement vertical-horizontal (avec une longue conduite horizontale) que dans un écoulement vertical. Pour de grands débits de liquide injecté, les auteurs ont observé un changement dans le mécanisme causant l'engorgement. Dans ces conditions, l'engorgement était provoqué par un bouchon près de la sortie de la conduite

horizontale.

Pour la conduite horizontale la plus courte, l'engorgement dû à un saut hydraulique a été observé pour de faibles débits de liquide injecté seulement. Dans ces conditions, les résultats étaient comparables à ceux obtenus dans une longue conduite horizontale. Pour des débits de liquide injecté plus important, la cause de l'engorgement provenait de la formation d'un bouchon (sans saut hydraulique) dans la conduite horizontale. Dans ces conditions, le débit de gaz au point d'engorgement était nettement supérieur à celui dans la longue conduite horizontale et même supérieur à celui dans une conduite verticale seule.

Pour les expériences dans une conduite verticale reliée à une conduite inclinée, trois coudes ont été utilisés: 112.5°, 135.0° et 157.5°. Les débits de gaz au point d'engorgement pour les coudes de 112.5° et 135.0° étaient presque identiques et correspondent au débit maximal des géométries étudiées. Le débit de gaz au point d'engorgement dans le coude de 157.5° était légèrement inférieur à celui dans les coudes de 112.5° et 135.0° mais tout de même supérieur à celui dans un écoulement vertical et à celui dans un coude de 90° avec une courte conduite horizontale. Dans toutes les conduites inclinées, l'engorgement s'est formé dans la conduite inclinée environ 15 à 50 *cm* plus bas que le coude, tout dépendant du débit de liquide injecté et de l'angle du coude. Les auteurs ont également fait des comparaisons avec une corrélation d'écoulement par bouchon et un modèle de refoulement du liquide.

Kawaji *et al.* [1993] ont effectué des expériences dans le but de déterminer la limite d'engorgement dans une section d'essais de 51 mm de diamètre intérieur contenant plusieurs coudes et une obstruction. Les rapports $\beta = D_{orifice}/D_{tube}$ des orifices utilisés dans ces expériences étaient 0.550, 0.670 et 0.865. Trois configurations différentes ont été étudiées: section d'essais contenant trois coudes dont le premier et le troisième sont dans le plan vertical, section d'essais contenant trois coudes dont le premier et le troisième sont dans le plan horizontal et section d'essais contenant trois coudes dont le deuxième et le troisième sont à 45 par rapport au plan vertical. Bien qu'il y ait certaines différences dans les résultats obtenus pour ces trois géométries, plusieurs observations qualitatives ont pu être faites sur l'effet de la dimension de l'obstruction sur la limite d'engorgement. Les auteurs ont observé que l'obstruction la plus petite (rapport β le plus grand) avait une faible influence sur la limite d'engorgement comparée aux expériences effectuées sans obstruction. Pour

les deux obstructions les plus importantes (rapport β les plus faibles), les auteurs ont observé que, pour un débit de liquide injecté donné, le débit de gaz nécessaire pour déclencher l'engorgement était beaucoup plus faible que celui observé dans les cas avec faible obstruction ou sans obstruction. De plus, le débit de gaz au point d'engorgement diminuait en diminuant le rapport β (augmentant la dimension de l'obstruction).

Ardron et Banerjee [1986] ont développé une corrélation pour prédire le début de l'engorgement pour un écoulement à contre-courant horizontal. Cette corrélation donne la vitesse adimensionnelle du gaz à l'engorgement en fonction de la fraction de vide à l'endroit où se situe le saut hydraulique. Des comparaisons ont montré que cette corrélation prédit très bien les résultats de plusieurs chercheurs. Il est important de souligner que cette corrélation est incapable de tenir compte de l'effet de l'orifice.

3 Montages et procédures expérimentaux (Chapitre 3)

Le montage expérimental permet l'utilisation de sections d'essais ayant uniquement une branche verticale ou ayant une branche verticale et une branche horizontale. L'eau et l'air à pression atmosphérique sont utilisés comme fluides de travail. Les deux sections d'essais sont fabriqués de plexiglass pour permettre la visualisation de l'écoulement. Leur diamètre intérieur est 63.5 mm. La section d'essais verticale a une longueur de 2578 mm. Une bride dans laquelle une obstruction peut être installée est située à 1744 mm de l'entrée d'eau. La seconde section d'essai est composée d'une branche verticale de 2022 mm de longueur reliée à une branche horizontale de 3327 mm de longueur par un coude en PVC de 90°. Une bride dans laquelle une obstruction peut être installée est située dans la branche horizontale à 1638 mm du coude. Pour les expériences faites dans la section d'essais verticale, des orifices ayant des rapports β de 0.90, 0.83, 0.72, et 0.66 on été utilisés. Pour les expériences faites dans la section d'essais ayant une branche verticale et une horizontale, deux orifices additionnels ayant des rapports β de 0.77 et 0.55 ont également été utilisés. Les deux sections d'essais partagent certaines pièces communes, telles que:

- le système d'injection d'eau qui consiste en un tube de 63.5 mm de diamètre intérieur ayant 800 trous de 1 mm percés dans sa paroi et des brides qui permettent sa fixation aux sections d'essais,
- le réservoir inférieur qui comprend le système d'entrée d'air ainsi que le système

de décharge d'eau, et

- le réservoir supérieur qui sert de système de séparation et de collecte de l'eau entraînée par l'air.

Instrumentation

Le montage expérimental est instrumenté pour mesurer les débits de liquide et de gaz, leurs températures, ainsi que la pression absolue du système. La section d'essais verticale est également équipée pour permettre la mesure des pertes de pressions axiales. Le débit de liquide est mesuré en utilisant des débitmètres à turbine de type "Flow Technology". Ces débitmètres peuvent couvrir la plage allant de 0.05 à 4.54 m^3/h avec une précision supérieure à 1% de la pleine échelle. Le débit de gaz est mesuré en utilisant un groupe de cinq rotamètres "Brook" qui couvrent la plage allant de 0.085 à 132.5 m^3/h à une pression de 2 *bar*. La précision des rotamètres est de 2% de la pleine échelle. La température du gaz est mesurée à l'aide d'un thermocouple installé au centre de la conduite d'entrée d'air. La température du liquide est également mesurée et contrôlé à une température de 20 $\pm$ 0.5 $°C$. La pression absolue dans le réservoir inférieur est mesurée à l'aide d'un capteur de pression "Sensotec". La plage de pression absolue couverte est de 1 à 1.14 *bar* avec une précision de 0.25% de la pleine échelle. Les pertes de pressions dans la section d'essais verticale sont mesurées à l'aide de deux capteurs de pressions différentielles "Validyne" couvrant une plage de pression différentielle allant de 0 à 103.4 Pa et de 0 à 689.5 Pa. La précision de ces capteurs est de 0.25% de la pleine échelle.

Procédures expérimentales

Deux types d'expériences ont été effectuées dans le cadre de cette recherche; des expériences pour la détermination du point d'engorgement, du débit de liquide délivré, et de l'effet d'hystérésis et des expériences pour la détermination des pertes de pressions en écoulement à contre-courant dans la section d'essais verticale.

La procédure expérimentale utilisée pour déterminer le point d'engorgement et le débit de liquide délivré est la suivante:

1. Fixer le débit de liquide injecté à l'entrée de la section d'essais;
2. augmenter le débit du gaz jusqu'à l'obtention du point d'engorgement;

3. continuer d'augmenter le débit du gaz (augmentation par palier) en collectant et pesant le liquide entraîné jusqu'à l'obtention du point de pénétration nulle.

Cette procédure expérimentale doit être répétée pour tous les débits de liquide et tous les orifices étudiés. Pour l'étude de l'effet d'hysérésis, la procédure est la même. Mais suite à l'engorgement, le débit de gaz est graduellement réduit par palier jusqu'au point où la décharge totale du débit de liquide est rétablie. La variation de la perte de pression dans la section d'essais verticale est déterminée en mesurant la pression à une position axiale donnée par rapport à une pression de référence (atmosphérique). Afin d'obtenir une mesure plus précise de la pression dans la section d'essais, trois prises de pressions sont situées à 120° les unes des autres autour de la section d'essais à chaque position axiale. Les prises de pressions sont connectées au système de mesure à l'aide de colliers spéciaux.

4 Résultats expérimentaux (Chapitre 4)

Résultats des expériences d'ÉCC verticale

Les résultats expérimentaux obtenus dans la section d'essais verticale ont démontré que le débit de gaz correspondant au point d'engorgement diminue avec des débits de liquide qui augmentent. Pour le cas sans orifice, nous avons constaté que pour les débits de liquide élevé au point d'engorgement il y à une transition subite jusqu'au débit de liquide délivré tandis que pour des débits de liquide faibles la transitions se fait d'une façon beaucoup plus graduelle. Dans tous les cas où un orifice est présent, la transition entre la livraison totale du débit liquide et la livraison partielle se fait d'une façon très graduelle. Nous avons également trouvé que, pour un débit de liquide donné, la présence d'un orifice réduit de façon significative le débit de gaz correspondant au point d'engorgement. De plus, nous avons constaté que cette réduction est inversement proportionnelle au rapport β de l'orifice.

Résultats des expériences d'ÉCC verticale et horizontale

Pour les résultats expérimentaux obtenus avec la section d'essais ayant une branche verticale et une branche horizontale, nous avons observé que le débit de gaz correspondant au point d'engorgement suit les mêmes tendances que le cas vertical vu précédemment; il diminue avec des débits de liquide qui augmentent. Contrairement à ce que nous avons trouvé dans la section d'essais ayant uniquement une branche verticale, nous avons observé que dans tous les cas (avec et sans orifice) la transi-

tion entre la livraison totale du débit liquide et la livraison partielle se fait de façon subite. Nous avons également constaté que l'effet de l'orifice provoquant la réduction du débit de gaz pour lequel l'engorgement a lieu pour un débit de liquide donné est aussi présent dans le cas d'un écoulement à contre–courant horizontal. De plus, nous nous sommes aperçus que cette réduction était inversement proportionnelle au rapport β de l'orifice tel qu'observé pour les cas verticaux. Suite à l'engorgement, nous avons observé que le débit de liquide délivré est fonction uniquement du débit de gaz et du rapport β de l'orifice; il ne dépend pas du débit de liquide injecté. Ceci est également vrai pour le point de pénétration nulle.

En ce qui concerne le point d'engorgement seulement, nous avons comparé les résultats expérimentaux obtenus avec la section d'essais ayant une branche verticale et une branche horizontale avec ceux d'autres chercheurs. Malgré le fait qu'aucune des sections d'essais utilisées par les autres chercheurs ne soit identique à celle utilisée dans cette étude, leurs résultats sont en accord avec les nôtres. Nous avons également constaté que la corrélation d'Ardron et Banerjee [1986] prédit relativement bien nos résultats expérimentaux pour les cas sans orifice.

Des expériences ont également été réalisées dans le but d'étudier l'effet d'hystérésis en utilisant la section d'essais ayant une branche verticale et une branche horizontale. Ces expériences ont été menées avec et sans orifices de différentes grandeurs installés dans la branche horizontale. Pour tous les cas étudiés, nous avons observé des effets d'hystérésis importants. Nous avons constaté qu'il était nécessaire de réduire de façon importante le débit de gaz sous celui qui correspond au point d'engorgement afin de rétablir l'acheminement total du liquide. De plus, nous nous sommes aperçus que, suite à l'engorgement, les débits de liquide déchargé obtenus avec des débits de gaz décroissants et inférieurs à celui correspondant au point d'engorgement, suivent les mêmes courbes de décharge partielle que celles obtenues avec des débits de gaz croissants.

Expérience de pertes de pression

Nous avons effectué des expériences pour mesurer les pertes de pression en écoulement à contre-courant dans la section d'essais ayant uniquement une branche verticale. Nous avons trouvé que pour un débit de liquide donné, les pertes de pression s'accroissent en augmentant le débit de gaz. De plus, pour un débit de gaz donné, les pertes de pression augmentent quand on accroit le débit de liquide.

5 Modélisation du point d'engorgement (Chapitre 5)

Nous avons développé deux modèles phénoménologiques pour la prédiction du point d'engorgement pour des écoulements à contre–courant verticaux. Le premier représente la point d'engorgement en fonction du débit de gaz nécessaire pour entraîner une gouttelette dans le courant de gaz contre les forces gravitationnelles. Le deuxième modèle que nous avons développé représente le point d'engorgement en fonction du débit de gaz nécessaire pour rendre nulle la vitesse du film de liquide situé à l'interface gaz–liquide. Nous avons constaté que les prédictions des deux modèles sont fortement dépendantes du choix de la corrélation utilisée pour représenter le facteur de friction à l'interface. En utilisant une corrélation appropriée, nous trouvons que le modèle basé sur le mécanisme d'entraînement de gouttelettes réussit bien à prédire les résultats expérimentaux tandis que le modèle basé sur le mécanisme de l'écoulement du film sous–estime les résultats expérimentaux pour les débits de liquide élevés.

Nous avons également développé un modèle pour prédire le point d'engorgement pour des écoulements à contre–courant vertical et horizontal utilisant une extension d'un modèle pour le début de l'entraînement appliqué à la crête du saut hydraulique. La hauteur du saut hydraulique est calculée en utilisant des méthodes tirées du domaine de l'étude des écoulements à surfaces libres. Nous avons comparé les prédictions de ce modèle avec nos résultats expérimentaux ainsi qu'avec ceux d'autres chercheurs. Nous voyons que les prédictions concordent très bien avec les résultats expérimentaux. Une extension a été apportée à ce modèle afin de tenir compte de l'effet de l'orifice sur la hauteur du niveau de liquide dans la section horizontale à la crête du saut hydraulique. De plus nous présentons une comparaison des prédictions de ce modèle avec nos résultats expérimentaux obtenus avec un orifice placé dans la branche horizontale ainsi qu'avec ceux d'autres chercheurs. De manière générale, ce modèle prédit très bien les résultats expérimentaux.

6 Conclusion et recommandation (Chapitre 6)

Au cours de cette thèse, nous avons présenté les résultats des travaux effectués dans le but d'étudier les écoulements à contre–courant ainsi que le point d'engorgement pour des écoulements vertical et vertical à horizontal. Pour les deux sections d'essais, nous avons trouvé que pour un débit de liquide donné, la présence d'un orifice réduit de façon significative le débit de gaz correspondant au point d'engorgement. De plus, nous avons constaté que cette réduction était inversement proportionnelle au rapport

β de l'orifice. Un autre point intéressant à signaler est que pour les deux sections d'essais, le débit de liquide délivré est fonction uniquement du débit de gaz et du rapport β de l'orifice; il est indépendant du débit de liquide injecté. Nous avons aussi constaté que pour tous les cas étudiés, la vitesse superficielle du gaz nécessaire au refoulement total du liquide (point de pénétration nulle) est fonction uniquement du rapport β de l'orifice; il est aussi indépendant du débit de liquide injecté.

Des expériences ont également été réalisées dans le but d'étudier l'effet d'hystérésis en utilisant la section d'essais ayant une branche verticale et une branche horizontale. Ces expériences ont été menées avec et sans orifices de différentes grandeurs installés dans la branche horizontale. Pour tous les cas étudiés, nous avons observé des effets d'hystérésis importants. Nous avons constaté qu'il était nécessaire de réduire de façon importante le débit de gaz sous celui qui correspond au point d'engorgement afin de rétablir l'acheminement total du liquide. De plus, nous nous sommes aperçus que, suite à l'engorgement, les débits de liquide déchargé obtenus avec des débits de gaz décroissants et inférieurs à celui correspondant au point d'engorgement, suivent les mêmes courbes de décharge partielle que celles obtenues avec des débits de gaz croissants.

Nous avons développé deux modèles phénoménologiques pour la prédiction du point d'engorgement pour des écoulements à contre–courant verticaux. Nous avons trouvés que le modèle basé sur le mécanisme d'entraînement de gouttelettes réussit bien à prédire les résultats expérimentaux tandis que le modèle basé sur le mécanisme de l'écoulement du film sous–estime les résultats expérimentaux pour les débits de liquide élevés.

Nous avons développé un modèle pour prédire le point d'engorgement pour des écoulements à contre–courant vertical et horizontal avec et sans orifice placé dans la branche horizontale. Nous avons comparé les prédictions de ce modèle avec nos résultats expérimentaux ainsi qu'avec ceux d'autres chercheurs. Nous avons démontré que les prédictions concordent très bien avec les résultats expérimentaux.

Table of Contents

Dedication iv

Acknowledgements v

Résumé vi

Abstract ix

Condensé en français xii

Table of Contents xxiii

List of Figures xxvii

List of Tables xxxiv

List of Appendices xxxv

List of Symbols xxxvi

1 INTRODUCTION 1

1.1 Organization of this Thesis 2

2 LITERATURE REVIEW 3

2.1 Vertical CCF and CCFL Experiments 4

2.1.1 Counter–Current Flow Generalities 4

2.1.2 Pressure Drop 5

2.1.3 Mean Film Thickness 8

2.1.4 Flooding and Liquid Delivery 9

2.1.5 Counter–Current Flows Through Obstructions 11

2.1.6 Hysteresis Effect 11

2.2 Inclined and Vertical–to–Horizontal CCF and CCFL Experiments . . 12

2.3 Models and Correlations for CCFL Prediction 16

2.3.1 Empirical Correlations for Vertical CCFL 16

2.3.2 Theoretical Correlations for Vertical CCFL 18

2.3.3 Inclined and Vertical–to–Horizontal CCFL Prediction 19

3 COUNTER–CURRENT TWO–PHASE FLOW TEST FACILITY AND PROCEDURE 30

3.1 VERTICAL CCF TEST SECTION 30

3.2 CCF TEST SECTION CONTAINING VERTICAL AND HORIZONTAL RUNS 31

3.3 Instrumentation 32

3.3.1 Liquid Flow Rate 32

3.3.2 Gas Flow Rate 33

3.3.3 Absolute Pressure 34

3.3.4 Differential Pressure 34

3.4 Experimental Procedure 34

3.4.1 Flooding and Liquid Delivery Experiments 35

3.4.2 Procedure for Experiments to Study the Hysteresis Effect . . . 36

3.4.3 Axial Pressure Drop – Vertical Test Section 36

3.4.4 Validation of Pressure Measurement System and Identification of Possible Systematic Errors 37

4 EXPERIMENTAL RESULTS 47

4.1 Liquid Delivery Experiments 47

4.1.1 Results of Vertical CCF Experiments 47

4.1.2 Results of CCF Experiments for Vertical to Horizontal Legs . 49

4.2 Flooding Results 52

4.2.1 Results of Vertical CCFL Experiments 53

4.2.2 Results of CCFL Experiments for Vertical to Horizontal Legs . 54

4.3 Results of Hysteresis Experiments 55

4.4 Pressure Drop Experiments 55

4.5 Comparison of Flooding Results 56

4.5.1 Vertical Flooding Results 56

4.5.2 Flooding Results for Test Section with Vertical and Horizontal Legs 57

5 CCFL MODEL DEVELOPMENT 110

5.1 Model for Vertical CCFL 110

5.2 Droplet Force Balance 112

5.2.1 Drop Size Modelling 113

5.2.2 Algorithm for Model Based on Droplet Force Balance 119

5.3 Film Flow Modelling 120

5.4 Comparison of Predicted and Experimental Flooding Points - Vertical Flow 121

5.5 Model for Horizontal CCFL 122

5.5.1 Modification of the Model for Horizontal CCFL to Take into Account the Influence of the Orifice 127

5.5.2 Comparison of Predicted and Experimental Flooding Points–Horizontal Flow 128

6 CONCLUSIONS AND RECOMMENDATIONS 157

6.1 Recommendations 159

BIBLIOGRAPHY 161

List of Figures

2.1 CCFL data bank [McQuillan & Whalley 1985]. 22

2.2 Flow regime transition in vertical counter-current annular flow. . . . 23

2.3 Pressure drop vs. liquid inlet flow rate [Clift *et. al.* 1966]. 24

2.4 Pressure gradient in counter-current flow [Bharathan *et. al.* 1979]. . . 25

2.5 Pressure drop variation and flow regime [Hawley & Wallis 1982]. . . . 26

2.6 Pressure drop results of Zabaras [1985]. 27

2.7 Mean film thickness including flooding state [Zabaras 1985]. 28

2.8 Various entrance and exit geometries used in flooding experiments [Bankoff & Lee 1986]. 29

3.1 CCF test facility. 41

3.2 Vertical test section. 42

3.3 Test section with vertical and horizontal legs. 43

3.4 Schematic of pressure measurement system. 44

3.5 Pressure measurement validation system. 45

3.6 Validation of pressure measurement system. 46

4.1 J_ℓ delivered vs. J_g vertical test section no orifice. 59

4.2 J_ℓ delivered vs. J_g vertical test section with orifices. 60

4.3 Beginning of buildup of liquid column above the orifice, test section with vertical leg only. 61

4.4 Continuation of buildup of liquid column above the orifice, test section with vertical leg only. 62

4.5 Further buildup of liquid column above the orifice, test section with vertical leg only. 63

4.6 Liquid column fills the entire region above the orifice, test section with vertical leg only. 64

4.7 Liquid column formed above the smallest orifices at zero gas flow, test section with vertical leg only. 65

4.8 J_ℓ delivered vs. J_g test section containing vertical and horizontal legs. 66

4.9 J_ℓ delivered vs. J_g test section containing vertical and horizontal legs (cont.). 67

4.10 J_ℓ delivered vs. J_g test section containing vertical and horizontal legs (cont.). 68

4.11 Onset of entrainment above the elbow, test section containing vertical and horizontal legs. 69

4.12 Pulsating column formed in the vertical leg, test section containing vertical and horizontal legs. 70

4.13 Wave in horizontal leg formed by pulsating column, test section containing vertical and horizontal legs. 71

4.14 Wave traveling towards the orifice, test section containing vertical and horizontal legs. 72

4.15 Wave reflected from the orifice, test section containing vertical and horizontal legs. 73

4.16 Wave traveling towards the orifice and wave reflected from the orifice, test section containing vertical and horizontal legs. 74

4.17 Liquid slug formed in the horizontal leg, test section containing vertical and horizontal legs. 75

4.18 Liquid slug and gas bubble in the vertical leg, test section containing vertical and horizontal legs. 76

4.19 J_ℓ delivered vs. J_g and flooding points, test section with vertical leg only (no orifice). 77

4.20 J_ℓ delivered vs. J_g and flooding points, test section with vertical leg only (orifices). 78

4.21 Experimental flooding points, test section with vertical leg only (all cases studied). 79

4.22 J_ℓ delivered vs. J_g and flooding points, test section with vertical and horizontal legs (orifice $\beta = 0.77$). 80

4.23 J_ℓ delivered vs. J_g and flooding points, test section with vertical and horizontal legs (no orifice). 81

4.24 J_ℓ delivered vs. J_g and flooding points, test section with vertical and horizontal legs (orifice $\beta = 0.90$). 82

4.25 J_ℓ delivered vs. J_g and flooding points, test section with vertical and horizontal legs (orifice $\beta = 0.83$). 83

4.26 J_ℓ delivered vs. J_g and flooding points, test section with vertical and horizontal legs (orifice $\beta = 0.77$). 84

4.27 J_ℓ delivered vs. J_g and flooding points, test section with vertical and horizontal legs (orifice $\beta = 0.72$). 85

4.28 J_ℓ delivered vs. J_g and flooding points, test section with vertical and horizontal legs (orifice $\beta = 0.66$). 86

4.29 J_ℓ delivered vs. J_g and flooding points, test section with vertical and horizontal legs (orifice $\beta = 0.55$). 87

4.30 Flooding points, test section with vertical and horizontal legs 88

4.31 Flooding points, test section with vertical and horizontal legs (cont.) 89

4.32 Partial delivery results with decreasing gas flow, test section with vertical and horizontal legs (no orifice) 90

4.33 Partial delivery results with decreasing gas flow, test section with vertical and horizontal legs (orifice $\beta = 0.90$) 91

4.34 Partial delivery results with decreasing gas flow, test section with vertical and horizontal legs (orifice $\beta = 0.83$) 92

4.35 Partial delivery results with decreasing gas flow, test section with vertical and horizontal legs (orifice $\beta = 0.77$) 93

4.36 Partial delivery results with decreasing gas flow, test section with vertical and horizontal legs (orifice $\beta = 0.72$) 94

4.37 Partial delivery results with decreasing gas flow, test section with vertical and horizontal legs (orifice $\beta = 0.66$) 95

4.38 Partial delivery results with decreasing gas flow, test section with vertical and horizontal legs (orifice $\beta = 0.55$) 96

4.39 Pressure drop $Q_l = 0.1$ (m^3/h), test section with vertical leg only. . . 97

4.40 Pressure drop $Q_l = 0.25$ (m^3/h), test section with vertical leg only. . 98

4.41 Pressure drop $Q_l = 0.5$ (m^3/h), test section with vertical leg only. . . 99

4.42 Pressure drop $Q_l = 1.0$ (m^3/h), test section with vertical leg only. . . 100

4.43 Pressure drop $Q_l = 1.5$ (m^3/h), test section with vertical leg only. . . 101

4.44 Pressure drop $Q_l = 1.75$ (m^3/h), test section with vertical leg only. . 102

4.45 Pressure drop $Q_g = 50.88$ (m^3/h) for various liquid flow rates, test section with vertical leg only. 103

4.46 Three dimensional view of pressure drop $Q_g = 50.88$ (m^3/h) for various liquid flow rates, test section with vertical leg only. 104

4.47 Comparison of flooding points obtained in the test section with a vertical leg only and Wallis' correlation (no orifice). 105

4.48 Comparison of flooding points obtained in the test section with a vertical leg only and Wallis' correlation (orifices). 106

4.49 Comparison of flooding results with those of other researchers test section with vertical and horizontal leg (no orifice). 107

4.50 Comparison of flooding results with those of other researchers test section with vertical and horizontal leg (orifices). 108

4.51 Comparison of flooding points obtained in the test section with vertical and horizontal leg and the Ardron and Banerjee flooding correlation (no orifice). 109

5.1 Force balance on a drop. 131

5.2 Comparison of interfacial friction factor vs. data of Dukler *et al.* [1984] 132

5.3 Comparison of experimental flooding points and correlations obtained from the literature. 133

5.4 Comparison of experimental flooding points and Wallis' correlation. . 134

5.5 Comparison of experimental and predicted flooding points test section with vertical leg only using droplet force balance model with Nusselt film thickness and various interfacial friction correlations. 135

5.6 Comparison of experimental and predicted flooding points test section with vertical leg only using droplet force balance model with film thickness from $V_{il} = 0$ and various interfacial friction correlations. . . 136

5.7 Comparison of experimental and predicted flooding points test section with vertical leg only using droplet force balance model with interfacial friction from best fit of Dukler *et al.* [1984] data. 137

5.8 Comparison of experimental and predicted flooding points test section with vertical leg only using film reversal model and interfacial friction from the correlation Bharathan [1979]. 138

5.9 Comparison of experimental and predicted flooding points test section with vertical leg only using film reversal model and interfacial friction from best fit of Dukler *et al.* [1984] data. 139

5.10 Offset region caused by the orifice. 140

5.11 Flowchart showing the calculation procedure for the application of the horizontal CCFL model. 141

5.12 Comparison of experimental and predicted flooding points, test section with vertical and horizontal legs no orifice using the horizontal CCFL model. 143

5.13 Comparison of experimental and predicted flooding points using the horizontal CCFL model and the data of Krowlewski [1980]. 144

5.14 Comparison of experimental and predicted flooding points using the horizontal CCFL model and the data of Wan & Krishnan [1986]. . . . 145

5.15 Comparison of experimental and predicted flooding points using the horizontal CCFL model and the data of Siddiqui [1986]. 146

5.16 Comparison of experimental and predicted flooding points using the horizontal CCFL model and the data of Kawaji [1991]. 147

5.17 Comparison of experimental and predicted flooding points, test section with vertical and horizontal legs orifice $\beta = 0.90$ using the horizontal CCFL model. 148

5.18 Comparison of experimental and predicted flooding points, test section with vertical and horizontal legs orifice $\beta = 0.83$ using the horizontal CCFL model. 149

5.19 Comparison of experimental and predicted flooding points, test section with vertical and horizontal legs orifice $\beta = 0.77$ using the horizontal CCFL model. 150

5.20 Comparison of experimental and predicted flooding points, test section with vertical and horizontal legs orifice $\beta = 0.72$ using the horizontal CCFL model. 151

5.21 Comparison of experimental and predicted flooding points, test section with vertical and horizontal legs orifice $\beta = 0.66$ using the horizontal CCFL model. 152

5.22 Comparison of experimental and predicted flooding points, test section with vertical and horizontal legs orifice $\beta = 0.55$ using the horizontal CCFL model. 153

5.23 Comparison of experimental and predicted flooding points using the horizontal CCFL model and the data of Kawaji *et al.* [1993] orifice $\beta = 0.865$. 154

5.24 Comparison of experimental and predicted flooding points using the horizontal CCFL model and the data of Kawaji *et al.* [1993] orifice $\beta = 0.67$. 155

5.25 Comparison of experimental and predicted flooding points using the horizontal CCFL model and the data of Kawaji *et al.* [1993] orifice $\beta = 0.55$. 156

A.1 Test of offset height correction calculated with equation A-1, test section with vertical and horizontal legs orifice $\beta = 0.90$ using the horizontal CCFL model. 169

A.2 Test of offset height correction calculated with equation A-1, test section with vertical and horizontal legs orifice $\beta = 0.83$ using the horizontal CCFL model. 170

A.3 Test of offset height correction calculated with equation A-1, test section with vertical and horizontal legs orifice $\beta = 0.77$ using the horizontal CCFL model. 171

A.4 Test of offset height correction calculated with equation A-1, test section with vertical and horizontal legs orifice $\beta = 0.72$ using the horizontal CCFL model. 172

A.5 Test of offset height correction calculated with equation A-1, test section with vertical and horizontal legs orifice $\beta = 0.66$ using the horizontal CCFL model. 173

A.6 Test of offset height correction calculated with equation A-1, test section with vertical and horizontal legs orifice $\beta = 0.55$ using the horizontal CCFL model. 174

List of Tables

3.1 Ranges of Turbine Flow Meters 33

3.2 Ranges of Rotameters 34

5.1 Standard Deviation of Model Predictions vs. Experiments. 130

List of Appendices

A ORIFICE OFFSET 168

List of Symbols

a	Wave amplitude (m).
A	Cross sectional area (m^2).
C_d	Drag coefficient.
C_s	Interfacial shape factor.
C_w	Surface tension factor.
d	Droplet diameter (m).
D	Tube diameter (m).
f_i	Interfacial friction factor.
F_d	Drag force.
F_g	Force of gravity.
F_σ	Surface tension force.
g	Acceleration due to gravity (m/s^2).
h_o	Height of offset region (m)
J	Superficial velocity (m/s).
L	Length (m).
$\dot{m}_l$	Mass flow rate (kg/s).
Q	Volumetric flow rate (m^3/s).
v	Velocity (m/s).
α	Void fraction.
β	Orifice ratio ($= D_{orifice}/D_{tube}$).
δ	Film thickness (m).
λ	Wave length (m).
ν	Kinematic viscosity (m^2/s).
μ	Viscosity (Ns/m^2).
ρ	Density (kg/m^3).
σ	Surface tension (N/m).

τ	Interfacial shear stress (N/m^2).

Dimensionless Groups

Bo	Bond number	$\left[\frac{D^2 g(\rho_l-\rho_g)}{\sigma}\right]$
Fr	Froude number Equation (2.15)	$\frac{Q_l}{P_w}\left[\frac{g(\rho_l-\rho_g)^3}{\sigma^3}\right]^{1/4}$
Fr	Froude number Equation (5.38)	$\frac{\lvert v_l\rvert}{\sqrt{g\delta_h}}$
K	Kutateladze number	$\frac{J_k\rho_k^{1/2}}{\lvert g\sigma(\rho_l-\rho_g)\rvert^{1/4}}$
N_μ	Viscosity number	$\frac{\mu_l}{\left(\rho_l\sigma\sqrt{\frac{\sigma}{g(\rho_l-\rho_g)}}\right)^{1/2}}$
Re	Reynolds number	$\frac{\rho_l\lvert v_l\rvert\delta_j}{\mu_l}$
Re_f	Film Reynolds number	$\frac{\dot{m}_l}{P_w\mu_l}$
We	Weber number	$\frac{\tau d_{max}}{2\sigma}$

Subscripts and Superscripts

c	critical.
d	drop.
ℓ	liquid.
g	gas.
h	horizontal.
i	interfacial.
j	jump.
r	relative.
max	maximum.
w	wall.
$*$	non dimensional quantity.

Chapter 1

INTRODUCTION

Counter–Current Flow (CCF) in general and the Counter–Current Flooding Limit (CCFL) in particular are of great importance in the area of nuclear reactor safety analysis. In CANDU reactors, during some postulated loss of coolant accident (LOCA), the water coming from the inlet and outlet headers enters the fuel channels through the feeder pipes. These pipes consist of vertical and horizontal legs; in some feeders, orifices and/or venturi type flow obstructions are installed for flow adjustments and measurements. Steam produced in the feeders and/or in the fuel channels may flow in the direction opposite to that of the water, thereby creating vertical and horizontal counter–current two–phase flows in the feeder pipes. Under these conditions, the rate at which cooling water can enter the fuel channels may be limited by the flooding phenomena. At flooding, the liquid is partly entrained in the same direction as the steam flow. The liquid delivery is greatly affected by the geometry of the feeder pipes, shape and number of fittings, flow area restrictions and the way the feeder pipe is connected to the header and to the end–fitting. Thus, knowledge of the flooding phenomena in a geometry similar to the header–feeder system in a CANDU reactor is of prime importance in the safety analysis of nuclear reactors in order to improve the prediction of the time required for the emergency cooling injection system to refill the fuel channels. The objectives of this research are thus, to study all aspects of CCF and the flooding phenomena as they apply to systems having a geometry similar to that seen in the header–feeder system of a CANDU nuclear reactor. These aspects include the study of all counter–current flow phenomena from the flooding point through the entire range of partial liquid delivery, up to the point of zero liquid penetration as well as the hysteresis effect. Work has also been done on the devel-

opment of phenomenological models for the prediction of the flooding point in such systems.

The research project presented in this thesis was carried out as part of an industrial contract with the CANDU Owners Group (contract # WPIR–1513). Therefore, most of the work carried out was presented to COG in several technical reports (Tye *et al.*[1993], Tye *et al.*[1995], Tye *et al.*[1996] , Tye *et al.*[1997]).

1.1 Organization of this Thesis

Chapter One introduces and outlines the work that has been done.

Chapter Two reviews the domain of counter-current two phase flow and flooding. The review includes the work done on the experimental determination of the flooding point under conditions of both vertical and vertical to horizontal flow. A review of the various models and correlations available for the prediction of the flooding point for vertical and for vertical to horizontal counter-current flows is also presented.

Chapter Three presents the experimental facility and the experimental procedures used in the current research.

Chapter Four presents both the experimental results obtained in the current research and a comparison of these results with the work of other researchers.

Chapter Five presents the development of a phenomenological model for the prediction of the flooding point for vertical counter-current two-phase flows. The development of a phenomenological model for the prediction of the flooding point for horizontal counter-current two-phase flows without an orifice as well as its extension to include the influence of an orifice in the horizontal leg on the CCFL is also presented.

Chapter Six gives the conclusions and recommendations for future work.

Chapter 2

LITERATURE REVIEW

Over the last 40 years a great deal of experimental and analytical work has been done in the area of counter–current two–phase flows and the flooding phenomena. The number of different experiments that have been carried out to determine the flooding point under vertical counter–current two–phase flow conditions is so vast as to make a complete review impossible. Furthermore a lack of clarity and consistency in the definition of the flooding point used by the various researchers would render such a review almost useless. This point may best be illustrated by examining Figure 2.1 taken from McQuillan & Whalley [1985] who compiled a data bank containing 2762 flooding points obtained by different researchers around the world. It is clear from the scatter in the data presented in this figure that a great deal of confusion exists as to the exact phenomena which corresponds to flooding. As described by Tien *et. al.* [1979], three criteria have, in the past, been used for the characterization of the counter–current flooding limit:

a) point of inception of liquid entrainment,

b) inception of liquid film upflow, and

c) zero liquid penetration.

However, for a given liquid flow rate these events occur at significantly different gas flow rates. Thus, it is obvious that a lack of clarity and consistency in the definition of flooding will significantly influence the interpretation of the experimental results.

For the prediction of the CCFL in vertical flows the number of available correlations is huge and this review cannot claim to be exhaustive. However, a number of the more common correlations will be presented. For a more detailed review the interested reader is referred to McQuillan & Whalley [1985] and Bankoff & Lee [1986].

For the case of counter-current two-phase flows occuring in an elbow between a vertical and a horizontal tube the amount of experimental information available in the open literature is quite limited and the models available for the prediction of the CCFL even more so. For the specific case of the CCFL occuring in an elbow between a vertical and a horizontal tube in which an orifice is located, the literature is limited to the work of only one other researcher [Kawaji *et al.* 1993]. To the best of the author's knowledge no correlations or models exist which were developed to predict flooding behaviour due to the interactions of an elbow between a vertical and a horizontal run, and an orifice.

2.1 Vertical CCF and CCFL Experiments

As has already been stated the amount of available information regarding the experimental study of counter-current flow and flooding is quite vast. This review will therefore focus on some of the more commonly observed experimental results. What little information available on the influence of flow obstructions on the CCFL under vertical flow conditions will also be examined. Experiments carried out to study the zero liquid penetration point and pressure drop in counter-current two-phase flow will also be reviewed as will the hysteresis effect.

2.1.1 Counter–Current Flow Generalities

Vertical counter-current flow of two phases can be sustained only as a result of the differences in the gravitational force per unit volume on each phase. For the case of an annular gas-liquid counter-current flow where the liquid flows downward and the gas flows upward, as shown in Figure 2.2a, a qualitative map of the various flow regimes has been given by Bankoff & Lee [1986]. The counter-current flow is opposed by interfacial friction between the phases. The interfacial friction increases as the relative velocity of the phases increases. Thus, there is a maximum relative

velocity for a pure counter–current flow beyond which there is a partial liquid flow reversal. At this point the flow becomes counter–current below and co–current above the liquid injection point (Fig. 2.2b). This limit is known as the flooding point. In the past, several different physical phenomena have been used to characterize the flooding point. Some authors identified it as liquid bridging, surface wave instabilities, inception of droplet entrainment, etc. However, none of these phenomena necessarily leads to a net upward liquid flow. The liquid that is entrained above the liquid inlet may subsequently flow downward. Therefore, a more reasonable definition of the flooding limit is *the point where full liquid delivery out the bottom of the tube may no longer be sustained.* Such a definition is rigorous but not very convenient for practical experimental use. An objective and practical criterion for the detection of the flooding point should be found by studying the coincidence between the flooding point as defined above and other accompanying phenomena which may be more easily measured experimentally. Beyond the CCFL, a further increase in the gas flow rate results in a partial liquid entrainment (Fig. 2.2c) in which droplets are carried upward by the gas core. An even further increase in the gas flow rate results in a complete liquid flow reversal, i.e., there is no net flow below the liquid inlet. This is known as the zero downward liquid penetration limit (Fig. 2.2d). In turn, when the gas flow rate is decreased a point is reached where a part of the liquid starts flowing downward (Fig. 2.2e). As for the flooding point, the partial downward flow reversal should not be confused with the appearance of the liquid below the liquid inlet. The liquid may appear below the liquid inlet in the form of a hanging film as reported by Wallis & Makkenchery [1974]. Thus, only the onset of the net downward liquid flow may be identified as the point of partial downward flow reversal. To reestablish a fully counter–current flow the gas flow rate must be decreased well below that of the flooding point. This is known as complete downward flow reversal or deflooding point (Fig. 2.2g).

2.1.2 Pressure Drop

The overall pressure drop for vertical counter–current flow was studied by Clift *et. al.* [1966]. It was defined as the pressure difference between the air pressure in the lower plenum at the gas inlet and the atmospheric pressure. They detected abrupt pressure drop changes at the flooding and deflooding points. Their results are shown

in Figure 2.3. The overall pressure drop is plotted versus the inlet liquid flow rate for a fixed gas flow rate. As the liquid flow rate increases (line $O'A'$) the pressure drop is almost constant. At point A' the pressure drop abruptly jumps up to point B'. This occurs at the flooding point. A further increase in the liquid flow rate causes only a slight increase in the pressure drop ($B'C'$). Once the column is flooded the liquid flow rate may be reduced well below the flooding value without significantly altering of the pressure drop ($C'D'$). At point D' the pressure drop abruptly jumps down to point D'' and this is accompanied by the appearance of pure counter–current flow in the pipe (deflooding point). These sharp changes of the pressure drop have been used as objective criteria for the experimental detection of the flooding (A' to B' transition) and deflooding (D' to D'' transition) points.

Bharathan *et. al.* [1979] measured the pressure gradient by the use of three pressure taps; two of them installed in the test section and the third one in the lower plenum. Their experimental results are presented qualitatively in Figure 2.4 using the dimensionless superficial velocities and the dimensionless pressure gradient, where the dimensionless superficial velocity of the kth phase is defined as:

$$J_k^* = \frac{\rho_k^{1/2} J_k}{[gD(\rho_l - \rho_g)]^{1/2}} \quad , \tag{2.1}$$

the dimensionless pressure gradient is given by:

$$\left(\frac{dp}{dz}\right)^* = \frac{dp/dz}{[g(\rho_l - \rho_g)]} \quad , \tag{2.2}$$

and $k = g$ or l represent the gas and liquid phases respectively. The pressure gradient shows the same sharp variation as the gas flow rate is increased to the flooding point. Similar results have also been reported by Dukler *et. al.* [1979].

Hawley & Wallis [1982] measured the pressure drop under counter–current flow conditions across a 1.83 m long 51 mm I.D. test section. It should be pointed out that for these experiments the gas was drawn into the bottom of the test section, which was open to the atmosphere, by a vacuum blower. They presented the dimensionless pressure drop which is defined as:

$$\Delta P^* = \frac{\Delta P}{[gD(\rho_l - \rho_g)]} \quad , \tag{2.3}$$

as a function of the dimensionless superficial gas velocity and compared the various characteristic stages in the pressure gradient variation with the observed stages of the film flow. At low gas flow rates (stage 1 Fig. 2.5) a smooth falling film is observed in the tube with a correspondingly small pressure gradient. As the gas flow rate was increased a region of increased pressure drop was observed where the gas pulled the water exiting the tube into a neck, or contraction, as shown in Figure 2.5 (stage 2). At yet higher gas flow rates (stage 3 Fig. 2.5) the air entering the test section rips droplets from the water exiting the tube. The entrained droplets are only seen to occur in the lower 10–30 *cm* of the test section. The impact of the droplets on the liquid film causes waves to form, variations are also observed in the film thickness. In the upper portion of the tube the film remains smooth. At this stage a slight pressure rise from that of stage 2 is observed. Stage 3, however, is unstable and the rough film region grows successively larger (stage 4 Fig. 2.5) until it covers the entire length of the tube as shown in Figure 2.5 (stage 5). In the transition from stage 3 to stage 5 a sharp increase in the pressure drop across the tube was observed. Hawley & Wallis [1982] considered stage 5 to correspond to the onset of flooding. Due to the nature of the liquid inlet used by these researchers, which was by overflow at the top of the tube, the onset of flooding limited the inlet liquid flow and a decrease in the pressure drop was thus observed (stage 6 and 6a Fig. 2.5). It can again be seen from these results that the flooding point corresponds to the point where a sharp increase in the pressure drop occurs.

Dukler *et. al.* [1984] measured a pressure gradient in the liquid phase above and below a liquid inlet for a fixed liquid flow rate and a range of the gas flow rates covering the flooding point. They found that the pressure gradient exhibits a sharp increase, both above and below the liquid inlet, as the gas flow rate approaches the flooding point.

Zabaras [1985] measured the pressure drop under counter-current two phase flow conditions in a 4.56 *m* long vertical 51 *mm* I.D. test section. The pressure drop was measured using a movable measurement station with the pressure taps spaced 89 *mm* apart which was located either 0.15 or 1.7 *m* from the liquid injection point. Four different liquid flow rates were studied for a number of different gas flow rates covering the entire range from zero gas flow up to almost that required to cause zero downward liquid flow. The results of Zabaras [1985] are shown in Figures 2.6a and 2.6b for the two different positions of the measurement station. In general it

was found that below the flooding point the pressure gradient increases very slightly with increasing liquid flow rate. For a given gas flow an order of magnitude increase in the liquid flow rate caused a 50% increase in the pressure gradient. It was also found that for all the liquid flow rates studied, below the flooding point the pressure gradient increased smoothly with increasing gas flow rate. A significant increase in the pressure gradient was observed at the flooding point. The increase in the pressure gradient became sharper with increasing liquid flow rates.

2.1.3 Mean Film Thickness

The classical theory of falling liquid film was first developed by Nusselt [1916], the film thickness corresponding to the idealized case where the equation of motion for steady, laminar, one dimensional flow is solved with zero interfacial shear is known as the Nusselt film thickness and is given by the following equation:

$$\delta_N = \left[\frac{3\mu_l \dot{m}_l}{g\rho_l^2 \pi D}\right]^{1/3} \quad . \tag{2.4}$$

Hewitt & Wallis [1963] measured the film thickness under counter-current flow conditions with zero gas flow and with a gas flow just below the flooding point. They found that the measured film thicknesses were in very close agreement with those given by equation 2.4 not only for the case of zero gas flow but also for the gas flow rate just below the flooding point. The results of Hawley & Wallis [1982] covering a wide range of liquid flow rates with no gas flow and with a gas flow below the flooding point also confirm these observations.

Zabaras [1985] also measured the film thickness under counter-current two phase flow for the same conditions as those described in the previous section. The results are shown in Figures 2.7a and 2.7b for the two different positions of the measurement station. The figures also show the Nusselt film thickness corresponding to the four liquid flow rates studied. These results confirm those of Hewitt & Wallis [1963]. Zabaras [1985] also found that just before flooding the mean film thickness increases rapidly. While after flooding it decreases and is almost independent of the total inlet liquid flow rate.

If the equation of motion for steady, laminar, one dimensional flow is solved with the

boundary condition of zero liquid velocity at the gas liquid interface the film thickness is given by the following expression:

$$\delta_Z = \left[\frac{12\mu_l \dot{m}_l}{g\rho_l^2 \pi D}\right]^{1/3} \quad . \tag{2.5}$$

The film thickness calculated using equation 2.5 corresponding to the four liquid flow rates studied by Zabaras [1985] are also shown in Figures 2.7a and 2.7b for the two different positions of the measurement station. It is interesting to note that the film thicknesses corresponding to the condition of zero liquid velocity at the gas liquid interface correspond quite well with the measured film thicknesses at the flooding point particularly for the case were the measurement station is located further from the liquid inlet.

2.1.4 Flooding and Liquid Delivery

A great deal of work has been done to experimentally study the flooding phenomena; the liquid flow rates, both upward and downward in the post flooding region; as well as the point of zero liquid penetration or complete liquid holdup. Although a great deal of scatter exists in the experimental results some qualitative knowledge about flooding and the influence of certain parameters on its onset has been acquired.

Flooding depends on the combination of liquid and gas flow rates. For a fixed inlet liquid flow rate, the higher the inlet liquid flow rate the lower the gas flow rate will be at which flooding occurs, similarly, for a fixed gas flow rate the higher the gas flow rate the lower the inlet liquid flow rate will be at which flooding occurs.

It has been found, that while, for a given set of experimental conditions the point of onset of flooding may be clearly defined [Hewitt 1989] a minor change in the configuration of secondary parameters such as the inlet and exit geometries may have a large influence of the measured flooding point. Figures 2.8 a–l [Bankoff & Lee 1986] show some of the experimental geometries used by different researchers. All other parameters being identical the flooding point is highest for the case where a porous liquid inlet and exit are used as illustrated in Figure 2.8j, next highest for the smooth inlet geometries of which Figure 2.8b is an example and finally lowest for sharp end geometries as illustrated by Figure 2.8a. Data clearly illustrating the

influence of inlet and outlet geometries on the flooding point are given by Hawley & Wallis [1982], Hewitt [1989] and Govan [1990].

Hewitt [1989] presented results showing the influence of the tube length on flooding. For a test section having a porous liquid inlet and exit, his results show a clear influence of the tube length with, for a given inlet liquid flow rate, the gas flow rate at the flooding point decreasing substantially with increasing length. Results were also presented for a test section having a porous liquid inlet and a sharp edged exit. For this case no difference in the flooding point was observed even with a doubling of the tube length. It is clear that for this case the flooding occurs as a result of certain phenomena taking place at the exit and not as a results of the interaction between the gas core and the liquid film inside the tube.

There is a clear influence of the tube diameter on the flooding point. Obviously, for a given liquid flow rate the gas flow rate at flooding increases with increasing tube diameter. Further, when the gas and liquid flows are expressed in terms of the superficial velocities it is found that as the tube diameter increases the gas superficial velocity at the flooding point increases for a fixed inlet liquid superficial velocity. Experimental evidence to support these statements is presented by Suzuki & Ueda [1977], Chung [1978], and Celata [1989].

Suzuki & Ueda [1977] examined other factors affecting the flooding gas flow rate. They presented experimental results on the flooding gas flow rate in vertical tubes over a wide range of tube diameter; tube length; liquid flow rate; liquid viscosity and surface tension. They found that for a given liquid flow rate the flooding gas flow rate increases with increasing tube diameter and decreases with increasing tube length. For their particular case, the effect of tube length was small for low liquid flow rates but was significant for high liquid flow rates. The effect of tube length is less important in the case of high viscosity liquids. This is due to the fact that the viscosity attenuates the waves. The flooding gas flow rate has a tendency to increase with increasing liquid viscosity, but this trend is not very clear for thick liquid films. It seems that the viscosity is less important for thick films where inertial effects are significant. The effect of surface tension is complicated; this may be due to the fact that dynamic tension of a newly formed surface differs from that of a static one.

Dukler and Smith [1979] carried out experiments to study the delivered liquid flow rate in the post flooding region. They found that beyond the flooding point the

delivered liquid flow rate was a function of the gas flow rate only and was completely independent of the inlet liquid flow rate. The results of both Zabaras [1985] and Govan [1990] confirm this observation. The results of both Dukler & Smith [1979] and Zabaras [1985] also show that the gas flow at the zero liquid penetration point depends only on the geometry of the test section and not on the inlet liquid flow rates.

2.1.5 Counter–Current Flows Through Obstructions

Celata *et. al.* [1989] performed experiments with air–water counter–current flows in a vertical 20 *mm* I.D. 500 *mm* long circular test section. Orifices of different diameters ranging from 12 to 19 *mm* were placed concentrically in the test section 300 *mm* downstream from the liquid inlet. Tests were also carried out with four non–concentric orifices, drilled in the same disk, with the total area equal to the area of one of the concentric orifices (D=14 *mm*). The disk thickness was equal to 1/10 of the hole diameter. The flooding point was defined as a point at which the falling film began to be entrained by the upward–flowing gas. The experimental data were presented in terms of the superficial velocity calculated with *the free flow area offered by the obstruction (and not to the area of the test section).* At the flooding point the delivered liquid mass flow rate (i.e., the mass flow rate of the liquid flowing downward) or delivered superficial velocity was expressed in terms of the gas superficial velocity. Pressure drop data were also reported. It was found that the gas flow rate at zero downward liquid penetration decreases with decreasing perforation ratio ($A_{Orif.}/A_{Tube}$). The same is true for the gas flow rate at the onset of flooding.

2.1.6 Hysteresis Effect

From the time some of the earliest experiments on the flooding phenomena were carried out, it has been known that a significant hysteresis effect exists under counter–current flow conditions when the flooding point was reached [Wallis *et al.* 1963]. Clift *et al.* [1966] termed the point were full liquid delivery was re–established, in the post flooding state, the de–flooding point. Both of these early results indicated that for a given inlet liquid flow rate, the gas flow rate at the flooding point was significantly larger than at the de–flooding point. Thus a significant hysteresis effect was found to

exist for counter–current two–phase flows in the post flooded state. For vertical flows Celata *et al.* [1989] carried out experiments in a 20 *mm* I.D. test section in order to study the hysteresis effect in counter–current two–phase flows. They found that in order to re–establish full liquid delivery a significant decrease in the gas flow rate was required below the gas flow rate at the flooding point. Similar experiments were also carried out by Shoukri *et al.* [1991] who also observed a significant hysteresis effect in their results.

2.2 Inclined and Vertical–to–Horizontal CCF and CCFL Experiments

The number of studies which have been carried out on counter–current flows in inclined and vertical–to–horizontal flows is quite limited. Krowlewski [1980] carried out experiments to study both flooding and de–flooding for vertical to horizontal and inclined to horizontal flows. The test facility consisted of a 51 *mm* I.D. 584 *mm* long horizontal leg connected to a vertical or inclined leg by either a 90° or a 45° elbow. Air and water at atmospheric conditions were used as the working fluids. The point of onset of flooding was determined to be the point at which a sudden increase in the pressure drop across the test section occured. Data were reported for a number of different geometrical configurations. For the one most closely resembling the test facility used in the present study, the author's results indicate that there is a significant decrease in the gas flow rate required to provoke flooding as compared to that which would be required for the same tube diameter under vertical flow conditions. It was also found that the hysteresis was much more pronounced than what had previously been observed by other researchers in a vertical test section.

Siddiqui *et al.* [1986] carried out experiments on air–water flows in a pipe consisting of a vertical leg connected to a horizontal leg by an elbow. They found that the gas velocities at flooding were well below those expected for vertical pipes, and were found to depend on tube diameter, the length of the horizontal leg and on the radius of curvature of the bend. The wave instability causing flooding occurs in the horizontal part of the test section. The range of parameters studied were:

$$36.5 < \text{pipe diameter} < 47\ mm$$

$$24 < \text{horizontal leg length to diameter ratio} < 95$$

$$\text{square edge} < \text{elbow radius of curvature} < 300\ mm$$

Their findings may be summarized as follows:

1. for a given liquid flow rate the onset of flooding in bends took place at lower air flow rates than in vertical tubes,
2. the inception of flooding was identified with the occurrence of slugging at the hydraulic jump in the horizontal leg near the bend,
3. larger bend radii led to onset of flooding at lower gas flow rates,
4. in general, the higher tube diameter led to the onset of flooding at lower non-dimensional superficial gas velocities,
5. the use of smooth exit geometry led to a significant increase in the air flow rates needed to cause flooding, and
6. for a slight upward inclination of 0.6° the air flow rate needed to cause flooding was greatly reduced, whereas for an equal downward inclination the opposite was seen.

Siddiqui *et al.* [1986] found that for a vertical-to-horizontal pipe the flooding points corresponded to the equation:

$$J_g^* = J_{gc}^* \alpha^{3/2} \quad , \tag{2.6}$$

where:

$$J_{gc}^* = 0.2 \quad , \tag{2.7}$$

and α is the local void fraction at the crest of the hydraulic jump. The complete flow reversal limit, i.e., no liquid flow at the gas inlet, is predicted reasonably well by the following relation:

$$J_g^{*\frac{1}{2}} = 0.45 \quad , \tag{2.8}$$

which was seen to hold for all tube diameters, bend radii and the liquid supply rates.

Flooding velocities are very sensitive to the inclination of the horizontal leg. For upward inclinations there is a point at which the slope of the interface is such that the liquid bridges the pipe at the elbow. The bridging occurs at the inclination angle, ϕ, that fulfills the following condition:

$$\sin \phi_{cr} = \frac{D}{L} \quad , \tag{2.9}$$

where ($\phi > 0$ for an upward inclination).

Wan & Krishnan [1986] performed experiments on air–water counter–current flows in vertical–to–horizontal and in vertical–to–slightly inclined pipes. Experimental data obtained for the vertical-to-horizontal pipes are in good agreement with the experimental data of Siddiqui *et al.* [1986] and with the predictions by Ardron & Banerjee [1986] for low liquid flow rates ($J_l^{*\frac{1}{2}} < 0.5$). In this case the hydraulic jump was actually observed near the elbow and flooding was due to slugging at its crest. However, for higher liquid flow rates the hydraulic jump moved towards the horizontal pipe exit and the flooding mechanism was due to slugging at the exit. Ardron & Banerjee [1986] predictions fail in this case due to a change in the flooding mechanism. They observed that a slight upward inclination of the lower leg significantly reduces the gas flow rate needed to cause flooding, whereas for a slight downward inclination the opposite was seen.

Wan [1986] carried out experiments on steam–water counter–current flows in vertical–to–horizontal or slightly inclined pipes. For low liquid flow rates there is general agreement between the steam–water data for various subcoolings ($\Delta T < 6°C$), and the air–water data. For $J_l^{*\frac{1}{2}} > 0.4$, there is considerably more scatter in the data points and the overall trend is for $J_g^{*\frac{1}{2}}$ to increase with $J_l^{*\frac{1}{2}}$, which is opposite to that seen in the air–water tests. This trend is also seen in vertical systems and is probably due to the condensation effects of the steam in the subcooled water. Three flow regimes were observed:

1. a regime characterized by a counter–current flow of steam and water,

2. a regime characterized by a partial or complete carryover of injected water from the vertical leg of the elbow, and

3. a regime characterized by an unsteady water column in the vertical leg on top of a counter–current steam–water region with no water carryover.

Kawaji *et al.* [1989] studied air–water counter–current flows in vertical–to–horizontal and in vertical–to–downwardly inclined pipes containing elbows of varying angle. For low liquid flow rates ($J_l^{*\frac{1}{2}} < 0.4$) in vertical–to–horizontal pipes they confirmed the qualitative observations and experimental results of Siddiqui *et al.* [1986] as well as the predictions obtained by Ardron & Banerjee [1986]. For higher liquid flow rates they confirmed the observations of Wan & Krishnan [1986] that the Ardron & Banerjee model [1986] fails to reproduce experimental data, because liquid flow is supercritical in the lower leg. For still higher liquid flow rates ($J_l^{*\frac{1}{2}} > 0.8$), they observed that flooding occurred in the vertical section near the porous liquid inlet. In all vertical–to–downwardly inclined pipes, the flooding was initiated in the inclined section, however, no hydraulic jump was observed. Kawaji *et al.* [1989] suggested that flooding in vertical–to–downwardly inclined pipes is caused by slugging at low liquid flow rates and by liquid entrainment at high liquid flow rates.

Kawaji *et al.* [1993] carried out experiments to determine the flooding limit in a 51 *mm* I.D. test section with multiple elbows and orifices having $\beta = D_{Orif}/D_{Tube}$ ratios of 0.550, 0.670 and 0.865. Three different geometrical configurations were studied: double–vertical elbow in which the second and third elbow are in the vertical plane, double–horizontal elbow in which the second and third elbow are in the horizontal plane, and double–inclined elbow in which the second and third elbow are at 45° to the vertical plane. Although there are some differences in the results for the three different geometries studied, qualitative observations can be made as to the effects of the orifice size on the flooding point. The authors found that the orifice having the largest β ratio had very little effect on the flooding point as compared to the results without the orifice. For the two smaller orifices it was found that, for a given liquid flow rate, the flooding gas velocities were much smaller than those observed with the largest orifice and in the no orifice case. Further, the flooding gas velocity was found to decrease with decreasing orifice β ratio.

Noel *et al.* [1994] carried out experiments to study the hysteresis effect in an even more

complex geometry. They studied both the flooding and de–flooding point in a complex test section containing multiple vertical and horizontal or near horizontal legs. Similar to that observed for vertical flows, their results show a significant difference in the gas flow rates at the flooding and de–flooding points for all of the liquid flow rates studied.

2.3 Models and Correlations for CCFL Prediction

The models and correlations for vertical CCFL and those for CCFL occuring under conditions of inclined or vertical to horizontal flow will be examined separately.

The correlations for the prediction of the flooding point in a vertical tube may be regarded as being of two main types: empirical and theoretical. The first group are based in large part on experimental flooding data supplemented by dimensional analysis. The second group are based on physical and mathematical models for the flooding mechanism. These models however frequently make use of empirical correlations to specify certain parameters required in the model.

2.3.1 Empirical Correlations for Vertical CCFL

A number of empirical correlations have been proposed to predict the onset of flooding. Generally, they are valid for the experimental conditions under which they were obtained and frequently fail to give reliable predictions for other experimental conditions. One of the oldest and the best known is the correlation proposed by Wallis [1961]:

$$J_g^{*\frac{1}{2}} + mJ_l^{*\frac{1}{2}} = C \quad , \tag{2.10}$$

where the dimensionless superficial velocity of the kth phase is defined by equation 2.1. The coefficients m and C are chosen to fit the experimental data. They are known to depend mainly on the tube–end conditions. The following values are commonly used for m and C : $m = 0.8 \rightarrow 1.0$ and $C = 0.7 \rightarrow 1.0$. It is worth mentioning here that the Wallis correlation may be derived from the separated cylinders model [Wallis 1961]. The coefficients m and C obtained in this manner are equal to 1.

Several investigators [Bankoff & Lee 1986] have suggested a correlation using the surface tension, σ, instead of the tube diameter for defining the appropriate dimensionless quantity. Such correlations have the following form:

$$K_g^{\frac{1}{2}} + mK_l^{\frac{1}{2}} = C \quad , \tag{2.11}$$

where K_g and K_l are the gas and liquid Kutateladze numbers respectively. The Kutateladze number for the kth phase is given by:

$$K_k = \frac{J_k \rho_k^{1/2}}{\left[g\sigma\left(\rho_l - \rho_g\right)\right]^{1/4}} \quad . \tag{2.12}$$

McQuillan & Whalley [1985] compiled 2762 experimental flooding points for vertical tubes and used them to test 17 empirical and 5 theoretical flooding correlations. They ignored tube–end effects and tube length. However, they included the effects of tube diameter and the physical properties of the gas and the liquid. They found that the empirical correlations were generally more successful than the theoretical correlations. The correlations which use dimensionless superficial velocities are noticeably less accurate than the other empirical correlations, particularly for high liquid velocities and for non air–water systems. For their data McQuillan & Whalley [1985] found that the most accurate prediction of the available data was obtained by the modified Alekseev *et al.* [1972] correlation which has the following form:

$$K_g = 0.286 Bo^{0.26} Fr^{-0.22} \left\{1 + \frac{\mu_l}{\mu_w}\right\}^{-0.18} \quad , \tag{2.13}$$

where μ_l is the viscosity of the liquid under consideration, and μ_w is the viscosity of water. Bo is the Bond number given by:

$$Bo = \left[\frac{D^2 g\left(\rho_l - \rho_g\right)}{\sigma}\right] \quad , \tag{2.14}$$

and Fr is the Froude number given by:

$$Fr = \frac{Q_l}{P_w}\left[\frac{g\left(\rho_l - \rho_g\right)^3}{\sigma^3}\right]^{1/4} \quad . \tag{2.15}$$

The modification of the Alekseev *et al.* [1972] correlation was introduced by McQuillan & Whalley [1985] to account for the effect of liquid viscosity.

2.3.2 Theoretical Correlations for Vertical CCFL

McQuillan & Whalley [1985] found that among the five theoretical correlation the modified Bharathan correlation [Bharathan *et al.* 1978] yielded the best predictions for the experimental data. This correlation has the following form:

$$\frac{2f_w\, J_l^{*2}}{(1-\alpha)^2} + \frac{2f_i\, J_g^{*2}}{\alpha^{2.5}} = (1-\alpha) \quad , \tag{2.16}$$

where the wall and interfacial friction factors are $f_w = 0.005$, and

$$f_i = f_w + 14.6\,(1-\alpha)^{1.87} \quad , \tag{2.17}$$

respectively. Instead of allowing α to vary and obtaining the limiting CCF curve, as was done by Bharathan *et al.* [1978], McQuillan & Whalley [1985] eliminated α from Eq. 2.17 by using an equation relating the dimensionless film thickness which is given by:

$$\delta^* = \delta \left[\frac{\rho_l(\rho_l - \rho_g)g}{\mu_l{}^2}\right]^{1/3} \tag{2.18}$$

to the film Reynolds number, Re_f, defined by:

$$Re_f = \frac{\dot{m}_l}{P_w \mu_l} \quad , \tag{2.19}$$

where P_w is the wetted perimeter. McQuillan & Whalley [1985] used

$$\delta^* = 0.908 Re_f{}^{1/3} \quad , \tag{2.20}$$

for film Reynolds numbers less than 2064 and

$$\delta^* = 0.304 Re_f{}^{7/12} \quad , \tag{2.21}$$

for Reynolds number greater than or equal to 2064.

2.3.3 Inclined and Vertical–to–Horizontal CCFL Prediction

Ardron & Banerjee [1986] developed a model to predict the experimental results of Siddiqui *et al.* [1986] for flooding in vertical–to–horizontal pipes. They assumed a one–dimensional, steady, stratified and incompressible flow. They also neglected interphase mass transfer and surface tension effects. The pressure variations over the cross section of each phase were assumed to be due to hydrostatic forces only. Mass and momentum balance equations were written for the horizontal part of a tube. Boundary conditions were imposed at the crest of the hydraulic jump and at the water outlet. It was further assumed that at the time of flooding the dimensionless superficial gas velocity at the crest of the hydraulic jump was given by: $J_g^* = 0.2\alpha^{3/2}$ while the critical flow condition ($d\alpha/dx \rightarrow \infty$) was satisfied at the water outlet. The balance equations were solved analytically and a system of algebraic equations was then obtained. The data resulting from a numerical solution of this system of algebraic equations was then fit to yield the following flooding correlation:

$$J_g^{*1/2} = 1.444 - 0.004\lambda - \cosh(\lambda^p \kappa^q (J_l^{*1/2})^r) \quad , \tag{2.22}$$

where: $p = 0.057$; $q = -0.02$; $r = 0.7$; $\lambda = \frac{L(Re^*)^{-n}}{D}$; and $n = 0.2$,

$$Re^* = \frac{D}{\nu_g}\left[\frac{gD(\rho_l - \rho_g)}{\rho_g}\right]^{1/2} \quad , \tag{2.23}$$

and

$$\kappa = \frac{\nu_g}{\nu_l}\left[\frac{\rho_g}{\rho_l}\right]^{1/2} \quad , \tag{2.24}$$

and L is the distance between the crest of hydraulic jump and the liquid outlet. For the range of parameters:

$$1 \leq \lambda \leq 16 \quad ,$$

$$0.5 \leq \kappa \leq 1.8 \quad ,$$

$$0 \leq J_l^{*\frac{1}{2}} \leq 0.6 \quad .$$

The correlation given by Equation 2.22 differs from the numerical solution of the system of equations by less than 2%. It should be noted that this model does not apply for an inclination higher than the critical one as described in the previous section. Furthermore, Ardron & Banerjee's model fails to account for the observed effect of the radius of curvature of the bend on the flooding limit. For a downward inclination, flow is supercritical in the lower limb, i.e., the average liquid velocity is higher than the propagation velocity of small surface waves, and this model is not valid in this case.

Kawaji *et. al.* [1989] suggested that flooding in vertical–to–downwardly inclined pipes is caused by slugging at low liquid flow rates and by liquid entrainment at high liquid flow rates. At low liquid flow rates they proposed the following correlation for flooding:

$$\frac{J_g}{\alpha} + \frac{J_l}{1-\alpha} = 0.5\alpha^{1/2}\sqrt{(\rho_l - \rho_g)gD\frac{\cos\phi}{\rho_g}} \quad , \tag{2.25}$$

where:

$$\alpha = \left(1 - \frac{2\delta}{D}\right)^2 \quad , \tag{2.26}$$

and the film thickness, δ, is expressed using the following correlation [Wallis 1969]:

$$\frac{\delta}{D} = 0.063 J_l^{*\frac{2}{3}} \quad . \tag{2.27}$$

At high liquid flow rates a liquid jet forms at the elbow and droplets are generated as a results of breakup of its surface. The droplets are then entrained by the gas stream and the flooding begins. In this case the correlation for flooding is expressed in the following form:

$$\frac{J_g}{\alpha} + \frac{J_l}{1-\alpha} = \frac{2}{\sqrt{3}}\left[\frac{g(\rho_l - \rho_g)d_d}{\rho_g C_D \sin(-\phi)}\right]^{1/2} \quad , \tag{2.28}$$

where d_d is a droplet diameter which is calculated using:

$$We = \frac{\rho_l v_l^2 d_d}{\sigma} \quad . \tag{2.29}$$

Kawaji *et. al.* [1989] suggested the use a critical Weber number of 100. There are two points about this correlation that may be regarded as being arguable. The first is that, as this correlation represents a force balance required to suspend a droplet

of diameter d_d against the force of gravity, the relative velocity acting on the droplet should be $(v_g - v_d)$ and the liquid film velocity should not intervene, further if the droplet is "just" suspended in the gas stream $v_d = 0$. The other point is that the use of the liquid density and velocity in the definition of the Weber number implies that the drop size is controlled at formation. Kocamustafaogullari *et. al.* [1993, 1994] state that the droplet size is controlled by breakup mechanisms caused by the interaction of the droplet and the gas stream. Further, this correlation yields physically unrealistic droplet sizes at low liquid velocities.

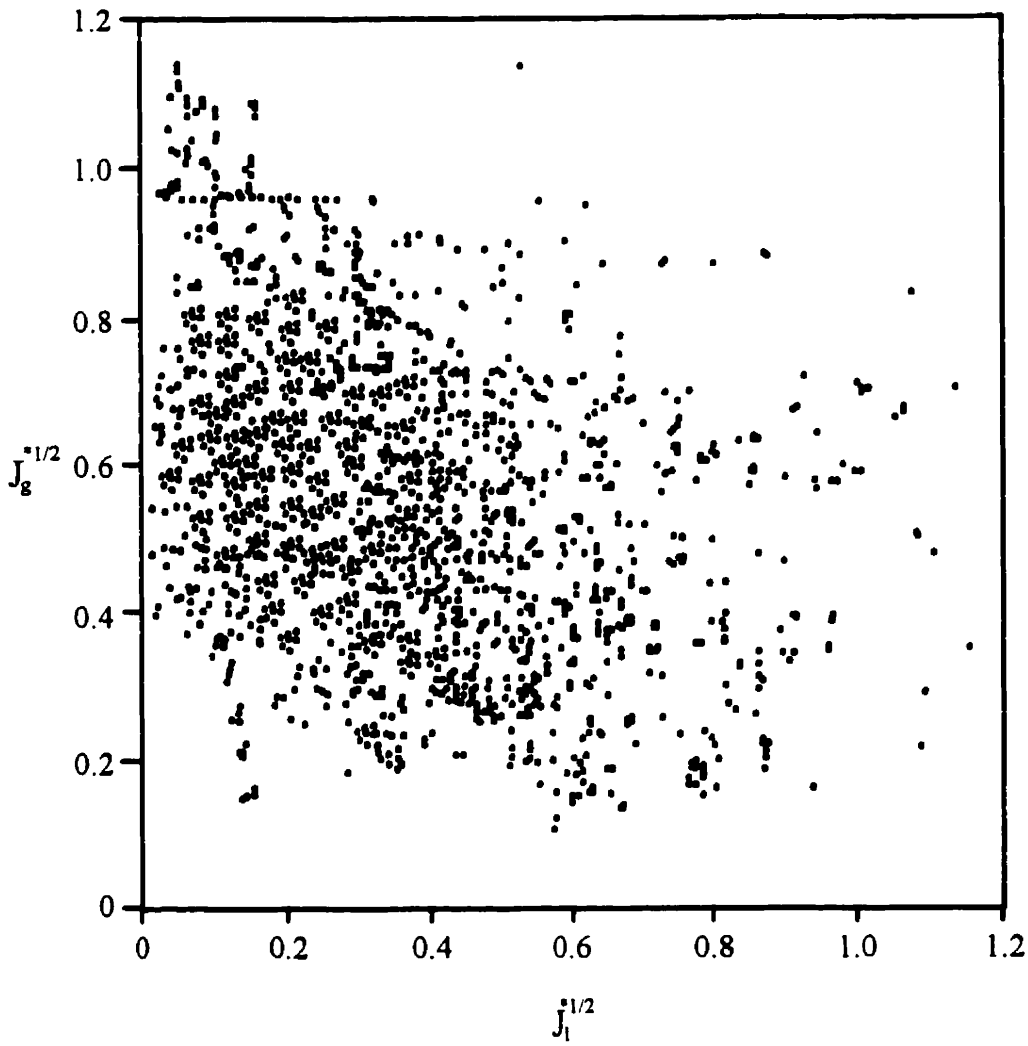

Figure 2.1: CCFL data bank [McQuillan & Whalley 1985].

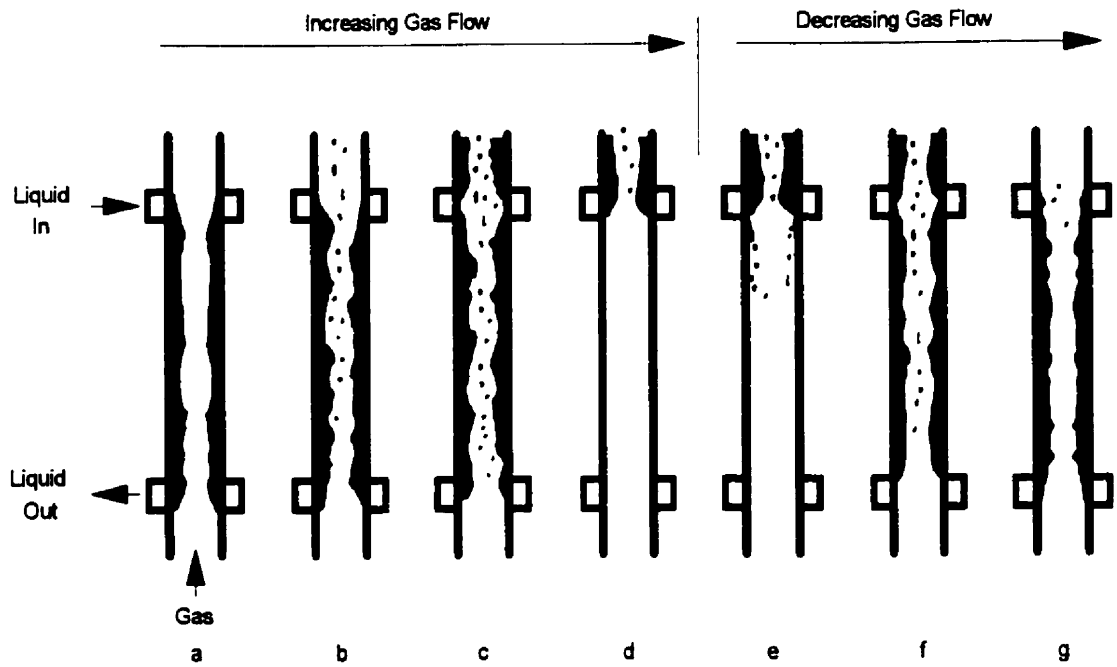

Figure 2.2: Flow regime transition in vertical counter-current annular flow.

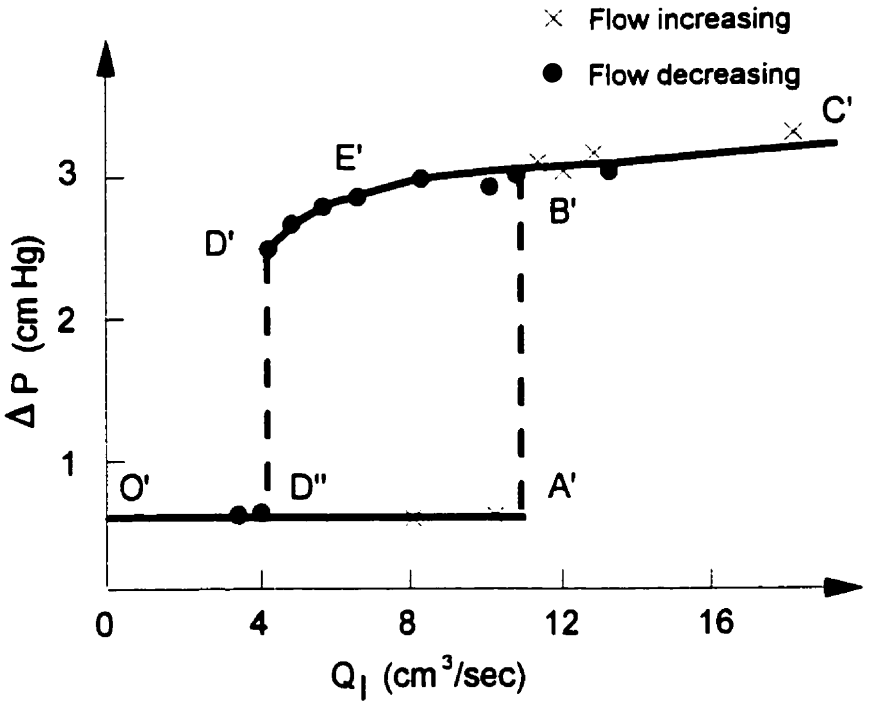

Figure 2.3: Pressure drop vs. liquid inlet flow rate [Clift *et. al.* 1966].

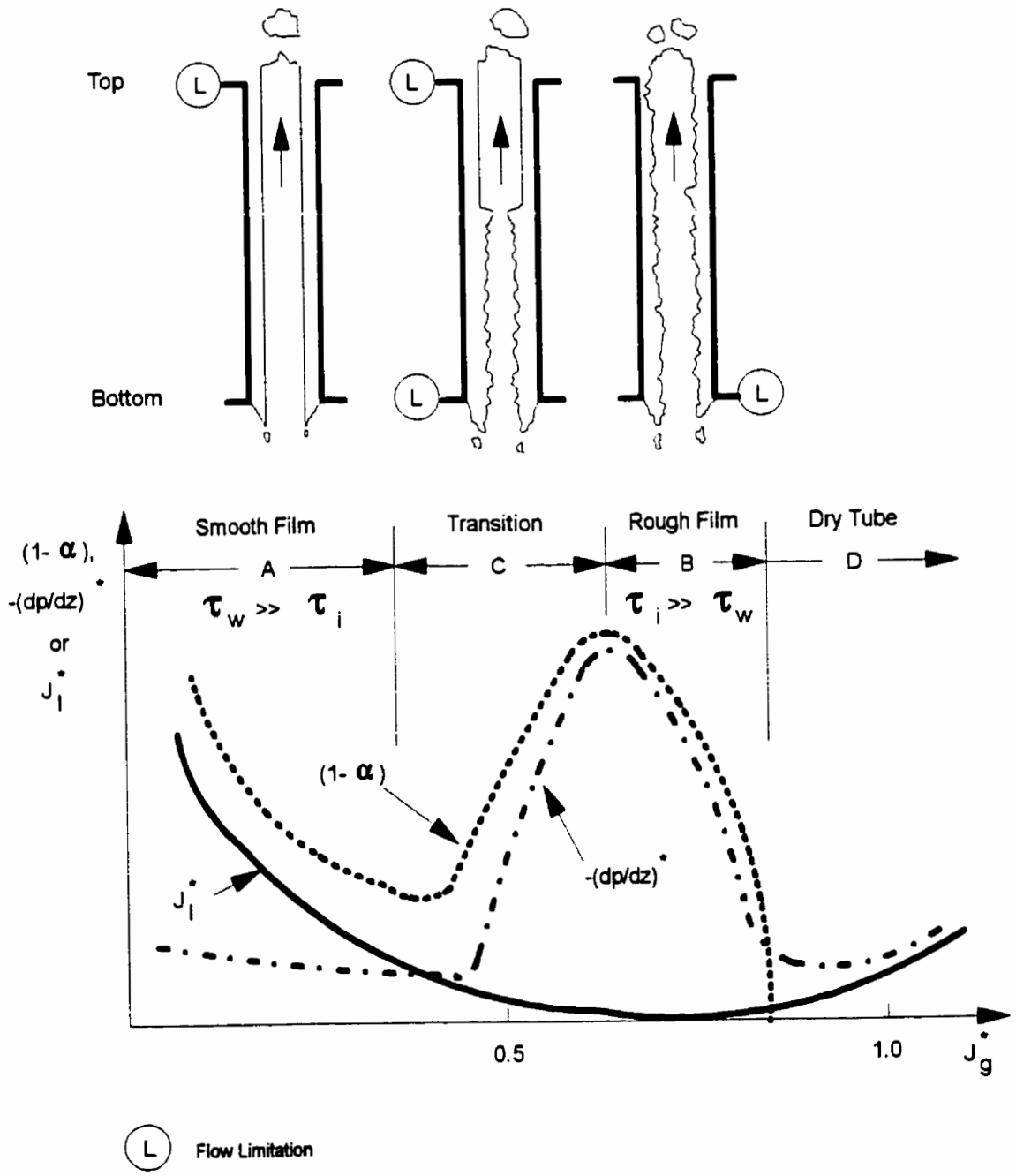

Figure 2.4: Pressure gradient in counter-current flow [Bharathan *et. al.* 1979].

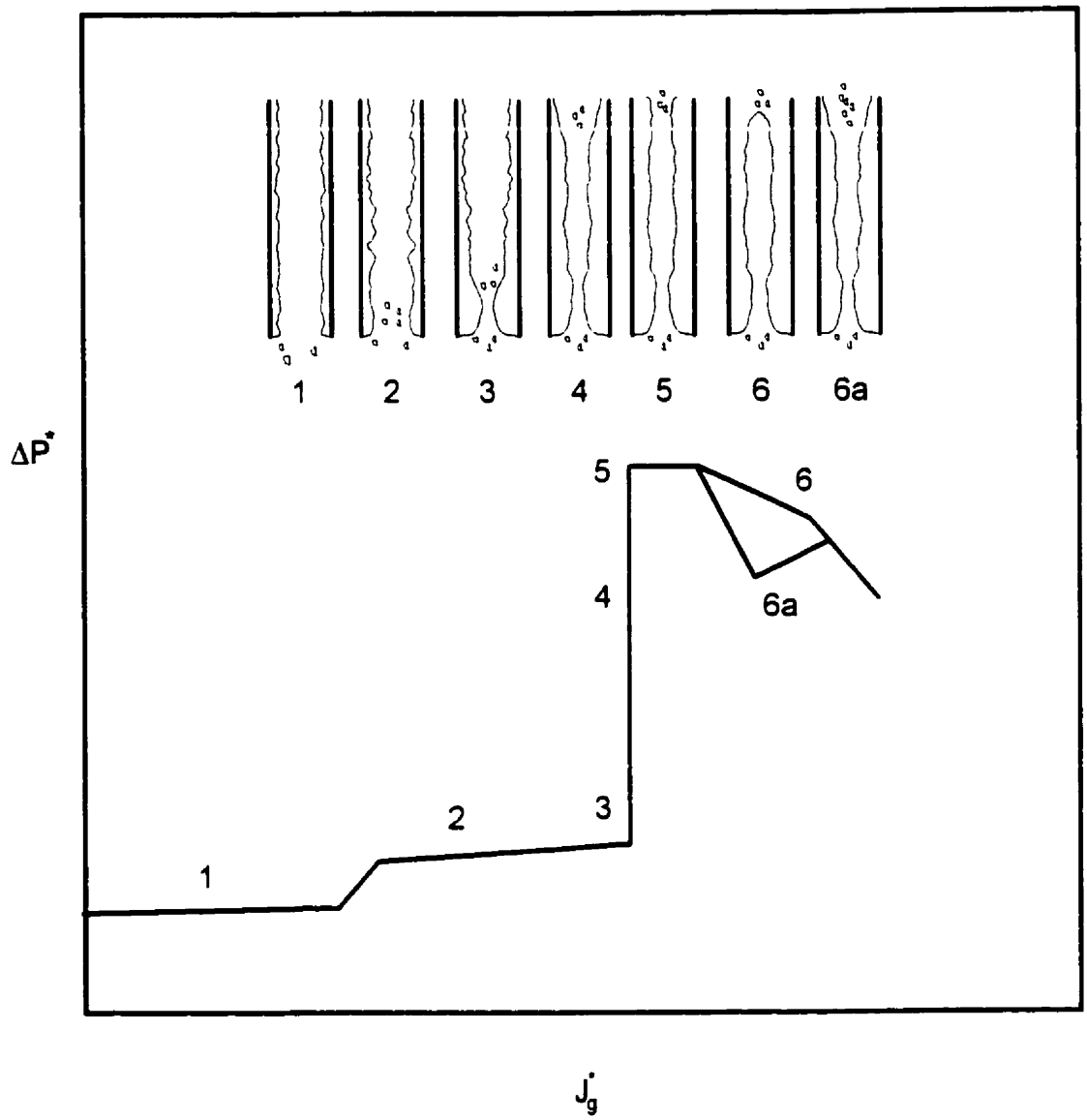

Figure 2.5: Pressure drop variation and flow regime [Hawley & Wallis 1982].

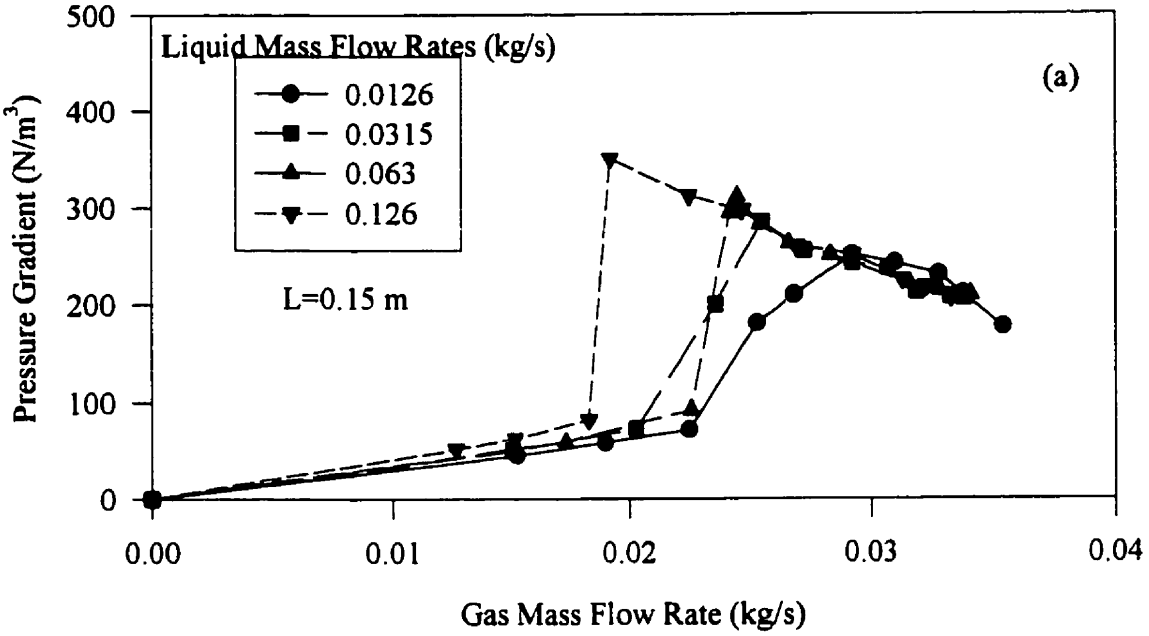

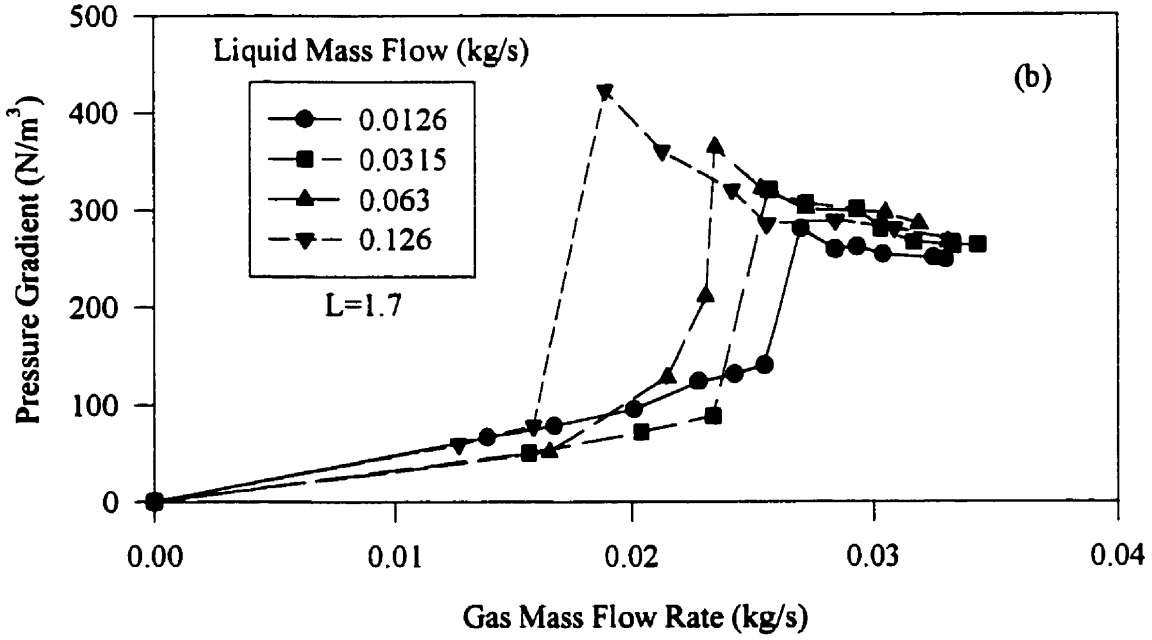

Figure 2.6: Pressure drop results of Zabaras [1985].

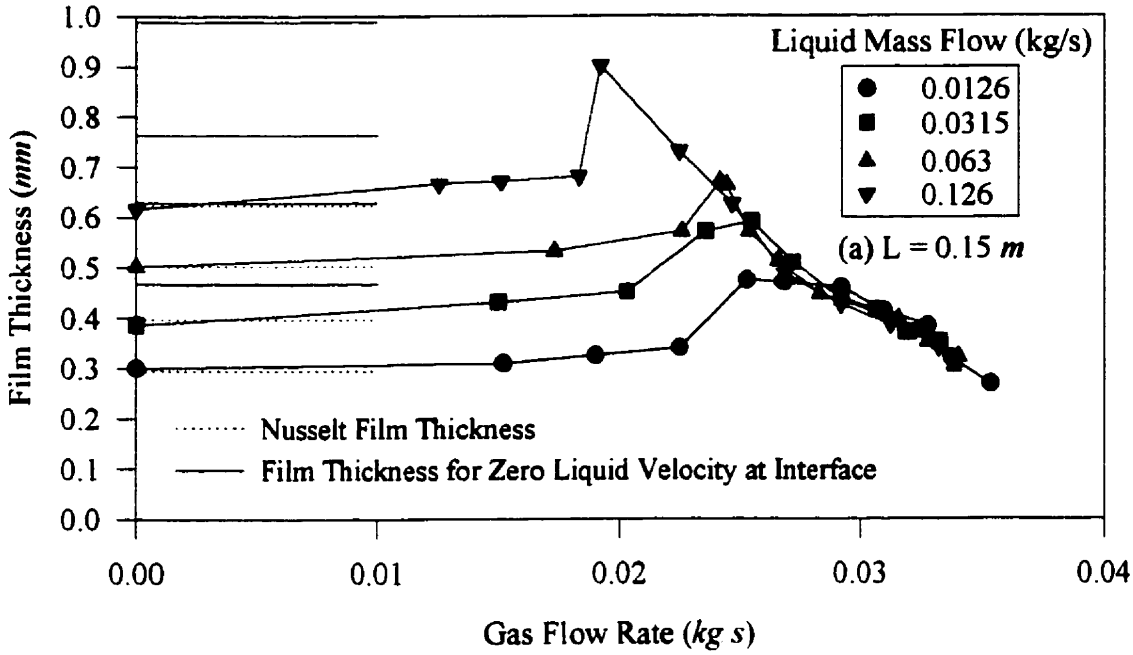

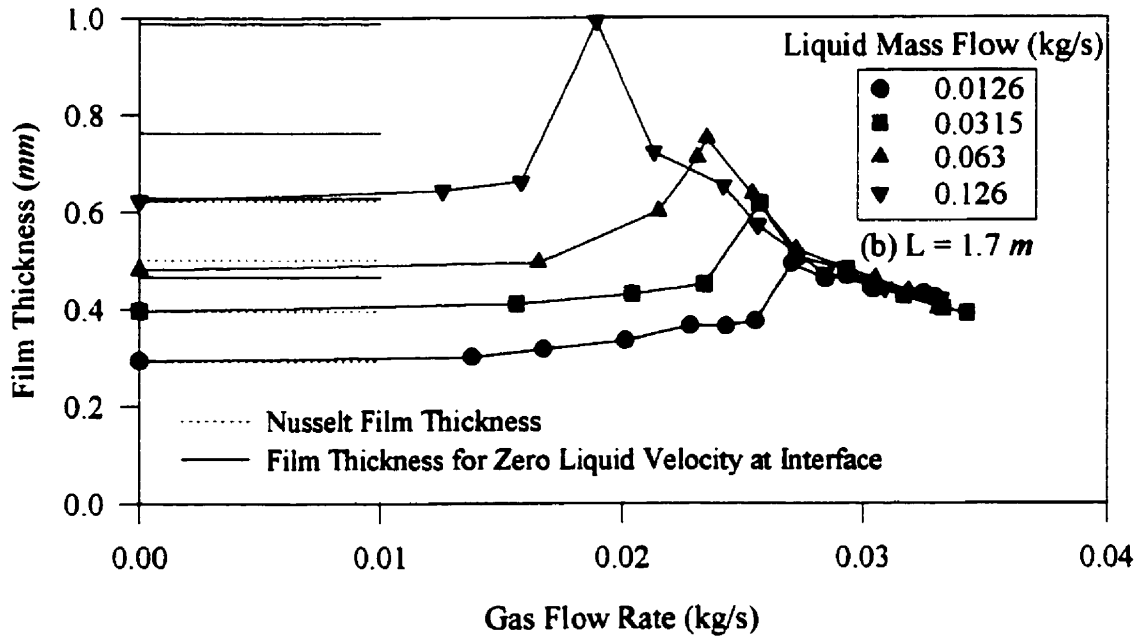

Figure 2.7: Mean film thickness including flooding state [Zabaras 1985].

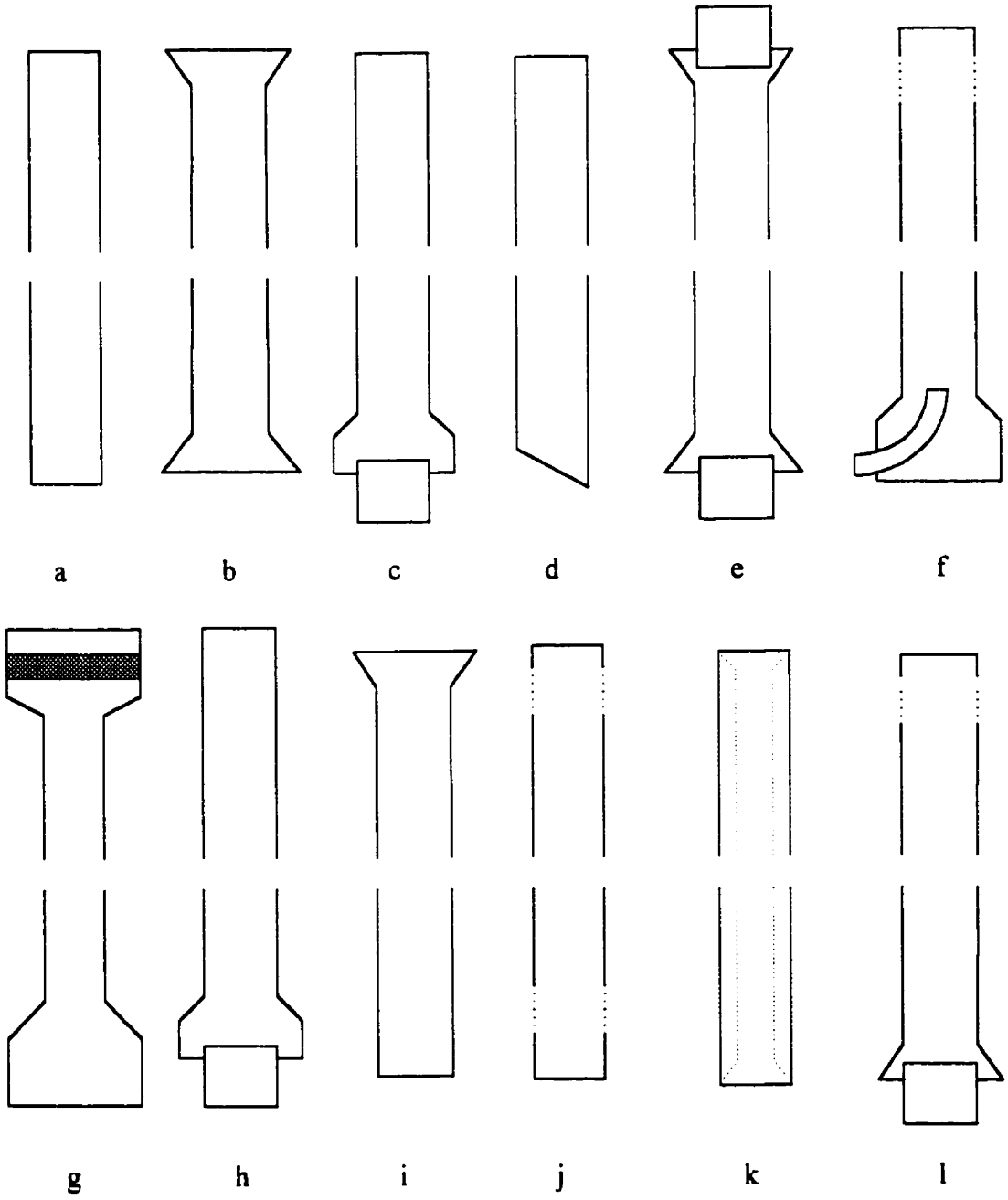

Figure 2.8: Various entrance and exit geometries used in flooding experiments [Bankoff & Lee 1986].

Chapter 3

COUNTER–CURRENT TWO–PHASE FLOW TEST FACILITY AND PROCEDURE

The CCF test facility shown in Figure 3.1 can support vertical test sections as well as test sections containing both vertical and horizontal legs. The water is supplied to the test section by a pump connected to a constant head water tank. The liquid flow rate is controlled in two steps: the coarse control is done using a set of valves and a by–pass circuit at the pump outlet, and the fine control is done using a set of two different size parallel needle valves located close to the test section. The temperature of the inlet water is held constant at $20 \pm 0.5°C$. The description of the CCF test sections will be presented in two parts:

1. the vertical test section, and
2. the test section containing both vertical and horizontal runs.

3.1 VERTICAL CCF TEST SECTION

Figure 3.2 shows a schematic diagram of the vertical CCF test section. It is constructed of 63.5 *mm* I.D. clear plexiglass tubes to allow flow visualization. The vertical structure is supported by an aluminum I–beam and the test section is positioned vertically using 4 adjustable supports. The major components are:

- the upper plenum which is used as a collector/separator for any liquid hold up during CCF and CCFL experiments,
- the porous wall water injector which consists of a 63.5 *mm* I.D. tube with 800 1 *mm* holes in the wall,
- the tubular test section with the flanges for orifice insertion and 12 sets of three pressure taps distributed angularly around the test section at each axial location, and spaced essentially every 200 *mm* along its entire length,
- the lower plenum contains the liquid outlet including a water level control system and the air inlet system. The level control system consists of a 3.45 kPa (0.5 PSID) pressure transducer used as a liquid level transducer. The signal produced by this transducer is used as the process variable input of an electronic level controller developed at IGN. The level control system is capable of maintaining the water level in the lower plenum constant through a wide range of liquid flow rates, i.e., from full delivery up to the zero liquid penetration point.
- the orifices are made of 1.5 *mm* thick stainless steel plates without a chamfered edge. The β ratios ($= D_{orif}/D_{tube}$) of the orifices used in this research are 0.90, 0.83, 0.72, and 0.66.

A more detailed description of the major mechanical components of this test section is given in Tye *et.al.* [1993] and Davidson [1994].

3.2 CCF TEST SECTION CONTAINING VERTICAL AND HORIZONTAL RUNS

Figure 3.3 shows a schematic diagram of the test section containing both vertical and horizontal runs. It is constructed of 63.5 *mm* I.D. clear plexiglass tubes. The vertical run is supported by the same aluminum I–beam as is used to position the vertical test section. The horizontal run is also supported by an aluminum I–beam structure; it is positioned horizontally using 6 adjustable supports of the same type as those used to position the vertical run. The I–beam is supported by 3 adjustable tubular

steel legs bolted to the floor. The angle of the test section from the horizontal can be varied as required. The major components are:

- the upper plenum same as that used in the vertical test section (Section 3.1),
- the water injector same as that used in the vertical test section (Section 3.1),
- the tubular test section consists of a 2022 mm long vertical section and a 3327 mm long horizontal run. The L/D ratio of the horizontal leg is 52. Both the vertical and horizontal runs contain flanges in which an orifice may be placed. The vertical and horizontal runs are connected by an opaque 90° PVC elbow. The horizontal and vertical runs are centered in the elbow by two plexiglass collars and are sealed using O-rings.
- the lower plenum same as that used in the vertical test section (Section 3.1),
- the orifices are same as those used with the vertical test section (Section 3.1), however for this test section two additional orifice having β ratios of 0.77 and 0.55 were used.

A more detailed description of this test section is given in Tye *et.al.* [1994].

3.3 Instrumentation

The test facility is instrumented to measure liquid and gas flow rates, inlet flow temperatures, and absolute pressures. For the experiments carried out in the vertical test section, the test section is also instrumented to measure the axial pressure drop in the liquid film.

3.3.1 Liquid Flow Rate

The water flow rate at the inlet of the test section is measured with a bank of three "Flow Technology" flow meters covering a range of 0.05 to 4.54 m^3/h. The detailed range of liquid flow rates covered by the set of flow meters is given in Table 3.1. According to the manufacturer the accuracy of these meters is better than 1% of the

readings. This has been confirmed during a number of verification experiments where the readings of the turbine flow meters were compared to the weight of water collected over a given time period. The temperature of the inlet water is kept almost constant at $20 \pm 0.5°C$. A calming tank is located upstream of the flow meters to damp out any oscillations that may be produced by the pump (see Figure 3.1). Due to the fact that turbine flow meters are sensitive to swirl, flow straighteners are located both upstream and downstream of the flow meters. These flow straighteners provide a smooth transition between the diameter of the lines and the bore of the flow meters and extend 20 hydraulic diameters upstream and 10 hydraulic diameters downstream of the meters.

Table 3.1: Ranges of Turbine Flow Meters

Flowmeter	Q_{lmin} m^3/h	Q_{lmax} m^3/h
#1	0.05	0.58
#2	0.22	2.30
#3	0.45	4.54

3.3.2 Gas Flow Rate

The air flow rate is measured with a bank of five "Brooks" rotameters, covering a range of 0.085 to 132.5 m^3/h at an outlet pressure of 2 bars. The rotameters have been calibrated to an accuracy of 1% of full scale. The pressure at the outlet of the rotameters is kept constant and is continuously measured with a bourdon type pressure gauge. The temperature of the air is continuously monitored with a thermocouple installed in the air flow line. Figure 3.1 also shows the arrangement used in the gas flow rate measurement system. The complete range of gas flow rates covered by this system is given in Table 3.2.

Table 3.2: Ranges of Rotameters

Rotameters	Q_{gmin} m^3/hr	Q_{gmax} m^3/hr
#1	0.08495	0.76455
#2	0.25485	2.5485
#3	0.8495	9.3445
#4	5.2669	52.669
#5	13.2522	132.522

3.3.3 Absolute Pressure

The absolute pressure in the lower plenum is measured using a "Sensotec" pressure transducer; the range of the absolute pressure covered is from 1 to 1.14 *bars* with an accuracy of ±0.25% of full scale.

3.3.4 Differential Pressure

For the experiments carried out in the vertical test section, the pressure in the liquid film is measured with respect to the atmospheric pressure at 12 points along the test section using "Validyne" variable reluctance differential pressure transducers, the ranges of the differential pressures covered are from 0 to 103.4 Pa $(0 - 0.015PSID)$ and from 0 to 689.5 Pa $(0 - 0.1PSID)$ with an accuracy of ±0.25% of full scale. The three pressure taps which are separated by 120° are drilled into the wall of the test section at each axial plane. They are connected to the measurement system by special pressure collars designed for this purpose. Further details of the pressure taps and collars are given in Tye *et.al.* [1993] and Davidson [1994].

3.4 Experimental Procedure

The experimental procedures used for both types of experiments carried out will now be presented. The procedure used to carry out the experiments to study the delivered liquid flow rate as a function of the inlet gas flow rate will be given first, then the procedure used to carry out the experiments to study the pressure drop profile in the

vertical test section will be presented.

3.4.1 Flooding and Liquid Delivery Experiments

The first objective of this research is to study the entire range of counter-current flow phenomena from the onset of flooding up to the zero penetration limit in tubes both with and without flow area restrictions. The influence of an elbow between a vertical and a horizontal run on the counter-current flow is also studied as is the influence of the interaction between the elbow and an orifice which is placed in the horizontal leg.

The flow area restrictions (orifices) are installed in the test sections by means of the flanges designed for this purpose. The positions of these flanges for the test section with only a vertical leg and for the test section containing both a vertical and a horizontal leg are shown in Figures 3.2 and 3.3 respectively.

Before detailing the procedure used to carry out the flooding experiments we will clearly state the definition of flooding and the experimental criterion that we will be using in this research. The standard definition of the counter-current flooding limit is (Bankoff and Lee [1986]): *"for a given downward liquid flow the maximum upward gas flow rate for which full liquid delivery out the bottom of the tube is maintained, corresponds to the counter-current flooding limit."* It is important to note that the counter-current flooding limit is just a **limit** for the gas flow rate beyond which only partial liquid delivery out of the lower end of the test section will occur. This point corresponds to the maximum gas flow rate for which full liquid delivery still exists, and it is the most widely accepted experimental criterion for the point of flooding (Bankoff & Lee [1986] and Dukler *et al.* [1984]).

Having defined our criterion for the experimental detection of the flooding point we will now describe the experimental procedure. For these experiments the liquid flow rate was first fixed and then a gas flow rate was fixed and the entrained liquid was then collected and weighed using the collection system located in the upper plenum. In this manner the entire range of CCF phenomena from the point of inception of entrainment to the zero penetration point was studied for each liquid flow rate.

3.4.2 Procedure for Experiments to Study the Hysteresis Effect

Before describing the procedure used for the experiments to study the hysteresis effect, it will be useful to present a definition of the de–flooding point that will be used in this research. Further, this definition should be consistent with the definition of the flooding point given in the previous section. The de–flooding point is therefore defined as the point where *for a given inlet liquid flow rate and a given gas flow rate full liquid delivery out the bottom of the tube is restored* (Clift *et al.* [1966]). The hysteresis that is associated with the flooding and de–flooding points corresponds to the difference in the gas flow rates at these two points.

For the experiments carried out to study the hysteresis effect, the liquid flow rate was first fixed, flooding was then initiated using as relatively large gas flow rate. The gas flow rate was then slowly decreased by steps all the way down to the point were full liquid delivery was re–established. At each step of the gas flow the entrained liquid is collected using the collection system located in the upper plenum and weighed. In this manner the entire range of CCF phenomena in the region of hysteresis from the flooding point all the way to the de–flooding point is studied for each liquid flow rate.

3.4.3 Axial Pressure Drop – Vertical Test Section

The second objective of this research program is to obtain data on the axial pressure variation in counter–current two–phase flow. Thus, the variation of the pressure drop in the test section is determined by measuring the pressure at a given axial location in the test section with respect to a reference pressure (atmospheric). In order to get a good idea of the average pressure prevailing in the test section, three pressure taps are located every 120° around the test section at every axial location as detailed in section 3.3.4. They are connected to the measurement system by special pressure collars designed for this purpose. The distance between each station ($\simeq 200\ mm$) has been measured with a digital caliper to the nearest 0.01 mm Davidson [1994].

The pressure measurement system is shown schematically in Figure 3.4. The pressure is measured using a ±689.5 Pa ($0-0.1\ PSID$) Validyne variable reluctance pressure transducer one side of which is open to the atmosphere. The pressure transducer is connected to the test section by means of gas filled manometric tubes and an air

water separator pot. Each pressure measurement station can be isolated from the manometric line by a valve. The signal from the pressure transducer was averaged over 60 readings with a sampling rate of 50 ms using a Wavetek data logger. The pressure signals were also recorded, on line, with a Yokagawa chart recorder.

3.4.4 Validation of Pressure Measurement System and Identification of Possible Systematic Errors

The performance of the pressure measurement system described above was evaluated using a second system shown schematically in Figure 3.5. It consists of the same set of pressure collars, separation pots, manometric tubes, and the Validyne pressure transducer as described above. However, a second pressure measurement pot open to the atmosphere and equipped with an impedance probe mounted on a micrometer having a resolution of ± 0.01 mm was connected in parallel with the first separation pot connecting the collar to the pressure transducer. This second pot was used as a manometer where the liquid level in the pot balanced the pressure in the test section. The performance of the pressure measurement system was evaluated by comparing the two sets of readings for a number of different liquid and gas flow rate combinations. A detailed error analysis of the pressure measurement system was also carried out. It is important to note that the system consisting of the manometer/micrometer setup was not judged to be suitable for carrying out all the experiments as it yielded only instantaneous readings and could not take into account any variations due to local entrainment which caused the pressure to fluctuate slightly. Further, it could only be used for a limited range of gas flow rates.

At the start of an experiment the zero of the pressure transducer is fixed with both sides open to the atmosphere. The collars and the connection lines between the collars and the separator pots are purged of any air bubbles that could interfere with the measurement. A liquid flow rate is then fixed in the test section with zero gas flow while all the separator pots are open to the atmosphere. An equilibrium liquid level, h_o, corresponding to these conditions is thus established in the separator pots. Once these initial equilibrium liquid levels stabilize, the separator pots are connected to the manometric tubes. A gas flow rate is then fixed and the valve connecting a given pot to the pressure transducer is opened. As the pressure in the test section is higher than that for the case with zero gas flow rate, the liquid level in the pot rises

slightly and a new equilibrium liquid level, h, is reached. The increase in the liquid level causes the gas in the manometric tubing to be compressed to a value P_g. The corresponding transducer readings are denoted as P_m. The difference between the transducer reading and the pressure of the gas in the manometric tube is mainly due to the difference in gas densities for atmospheric pressure and the actual pressure in the manometric tube:

$$P_m = P_g + (\rho_g - \rho_g^\circ)gH \quad , \tag{3.1}$$

where ρ_g° is the density of the air at atmospheric pressure, ρ_g is the density of air at the actual pressure in the manometric tube, g is the acceleration due to gravity, and H is the position of the separator pot with respect to the pressure transducer. The density is proportional to the pressure, thus:

$$\frac{\rho_g}{\rho_g^\circ} = \frac{P_{at} + P_g}{P_{at}} \quad , \tag{3.2}$$

where P_{at} is the atmospheric pressure. Combining this equation with equation 3.1 yields:

$$P_g = \frac{P_m}{1 + \frac{\rho_g^\circ gH}{P_{at}}} \quad . \tag{3.3}$$

Since $\rho_g^\circ gH << P_{at}$, the transducer reading can be considered to be almost equal to the actual pressure in the manometric tube:

$$P_g \approx P_m \quad . \tag{3.4}$$

The actual pressure in the test section can be expressed in the following form:

$$P = P_g + \rho_\ell gh \quad , \tag{3.5}$$

or using equation 3.4:

$$P = P_m + \rho_\ell gh \quad , \tag{3.6}$$

where ρ_ℓ is the liquid density, and h is the water level in the separator pot when the equilibrium is reached. An approximate estimation of this liquid level can be obtained in the following manner. Assuming that the gas in the manometric tube undergoes an isothermal transition. Thus, the pressure in the manometric tube is

inversely proportional to the total volume of the tube, the fittings, the valve and the space in the pot occupied by the gas:

$$\frac{P_m + P_{at}}{P_m^o + P_{at}} = \frac{\mathcal{V}_0}{\mathcal{V}} \quad , \tag{3.7}$$

where $\mathcal{V}_0$ and $\mathcal{V}$ are the volumes of the air in the manometric tubing at the zero gas flow rate and at a fixed non–zero gas flow rate respectively. P_m^o is the transducer reading at the zero gas flow rate, and is assumed to be equal to zero. Furthermore, if one assumes that the manometric volume (i.e., tubes, fittings, valve and free space of the pot) has an equivalent constant cross sectional area, the pressure of the manometric air is inversely proportional to the total length of the manometric volume. This length varies from l_o at the zero gas flow rate to l at the fixed non–zero gas flow rate. These lengths are related to the equilibrium liquid levels by:

$$l = l_o - (h - h_o) \quad . \tag{3.8}$$

Combining equations 3.7 and 3.8 the following relationship is obtained:

$$h = h_o + l_o \frac{P_m}{P_m + P_{at}} \quad . \tag{3.9}$$

Substituting equation 3.9 into equation 3.6 and assuming that:

$$\frac{P_m}{P_{at}} \ll 1 \quad , \tag{3.10}$$

the following relationship between the actual pressure in the test section and the transducer reading results:

$$P = P_m \left(1 + \frac{\rho_\ell g h_o}{P_m} + \frac{\rho_\ell g l_o}{P_{at}} \right) \quad . \tag{3.11}$$

This equation yields a qualitative estimate of the systematic errors which exist in these pressure measurements. As the second and third terms on the RHS of equation 3.11 are always positive:

$$P_m \leq P \quad . \tag{3.12}$$

Thus, the transducer readings underestimate the actual pressure in the test section. The second term on the RHS of equation 3.11 is due to the non–zero equilibrium liquid

level in the pot at the zero gas flow rate and is related to friction between the liquid film and the wall of the test section. The third term is due to the compressibility of the air in the manometric tubes. Equation 3.11 may be presented in the following form:

$$P = aP_m + b \quad , \tag{3.13}$$

with: $a = 1 + \frac{\rho_\ell g l_o}{P_{at}}$ and $b = \rho_\ell g h_0$

Equation 3.13 has been fitted to experimental data, where P was determined from measurements of the liquid level in the manometer using the micrometer/conductance system and P_m was the transducer reading. The constant a in equation 3.13 varied between $0.96 - 1.06$ and b was found to vary between $14 - 21$ Pa The values of a and b averaged over all liquid and gas flow rates and all pressure tap positions were 0.975 and 20 Pa respectively. The results of this fitting are shown in Figure 3.6 and are then used to determine the actual pressure drop in the test section from the pressure readings It is important to note that in the determination of the differential pressures presented in chapter 4, the b terms will all cancel each other.

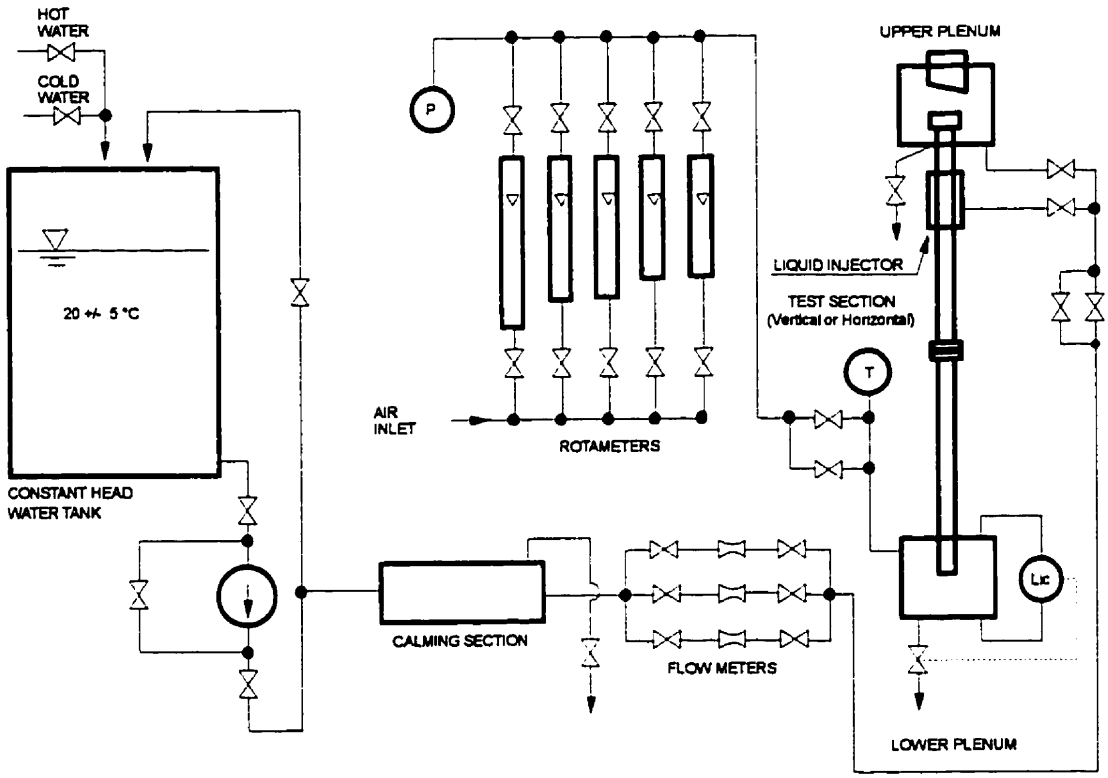

Figure 3.1: CCF test facility.

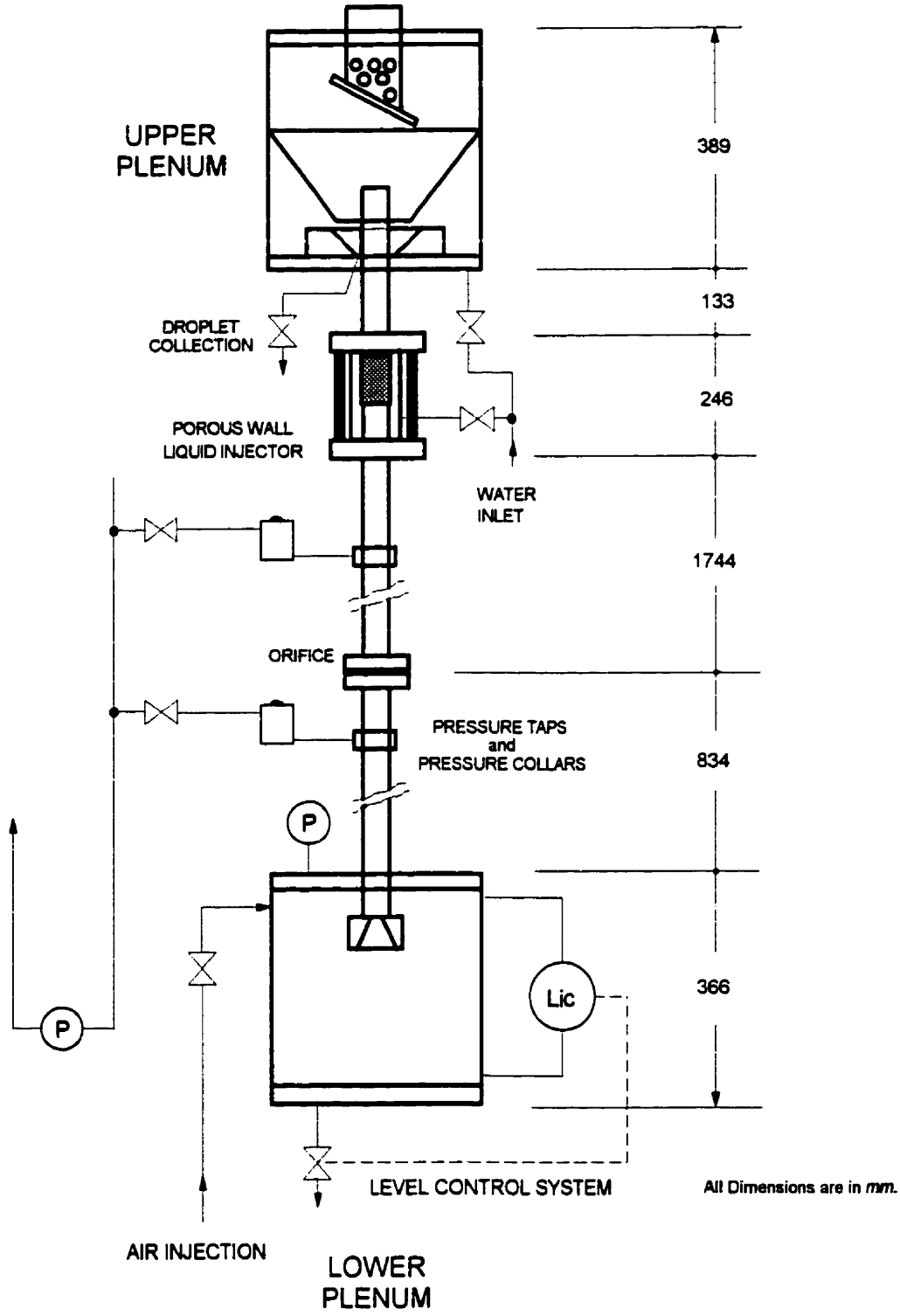

Figure 3.2: Vertical test section.

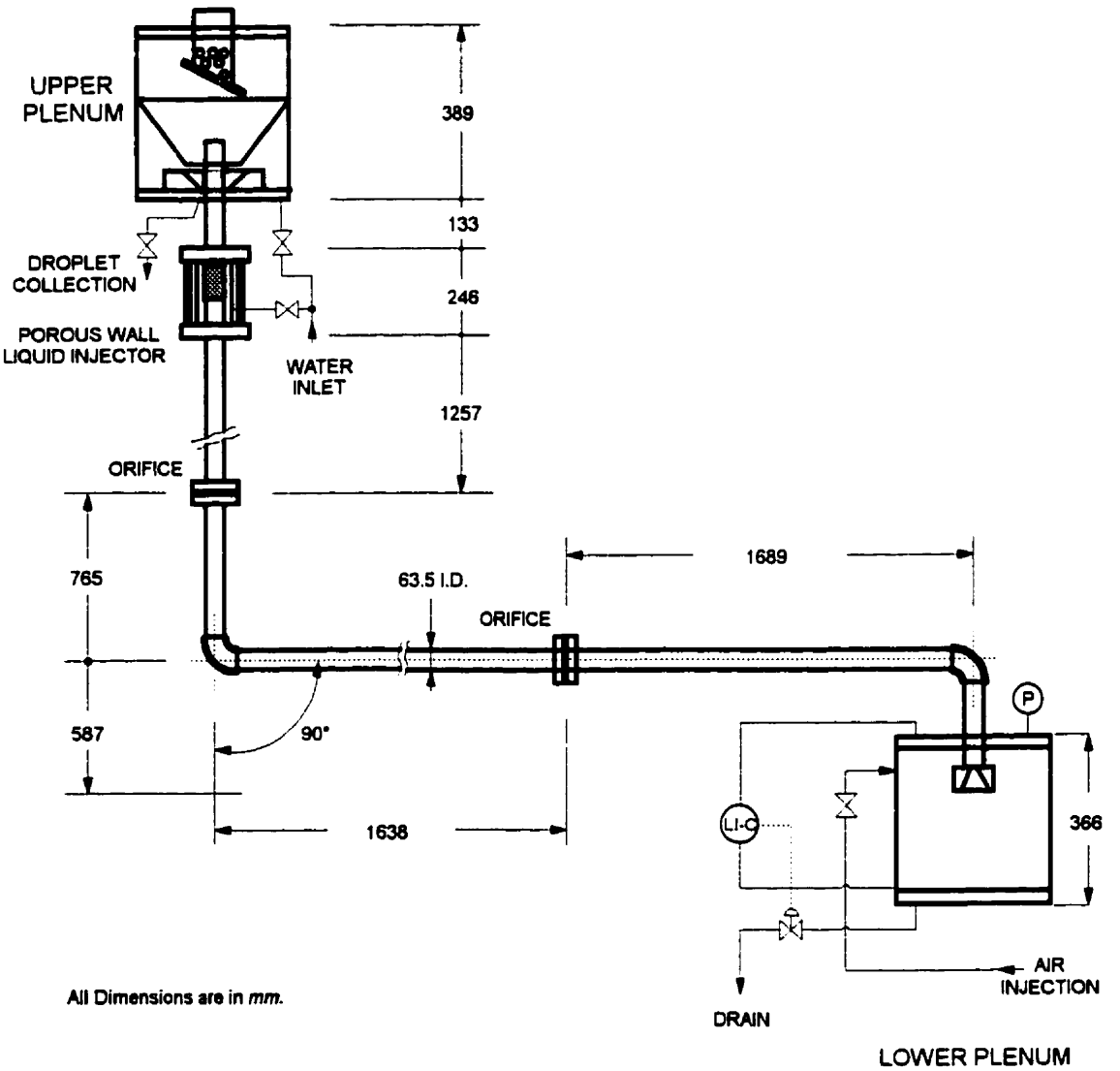

Figure 3.3: Test section with vertical and horizontal legs.

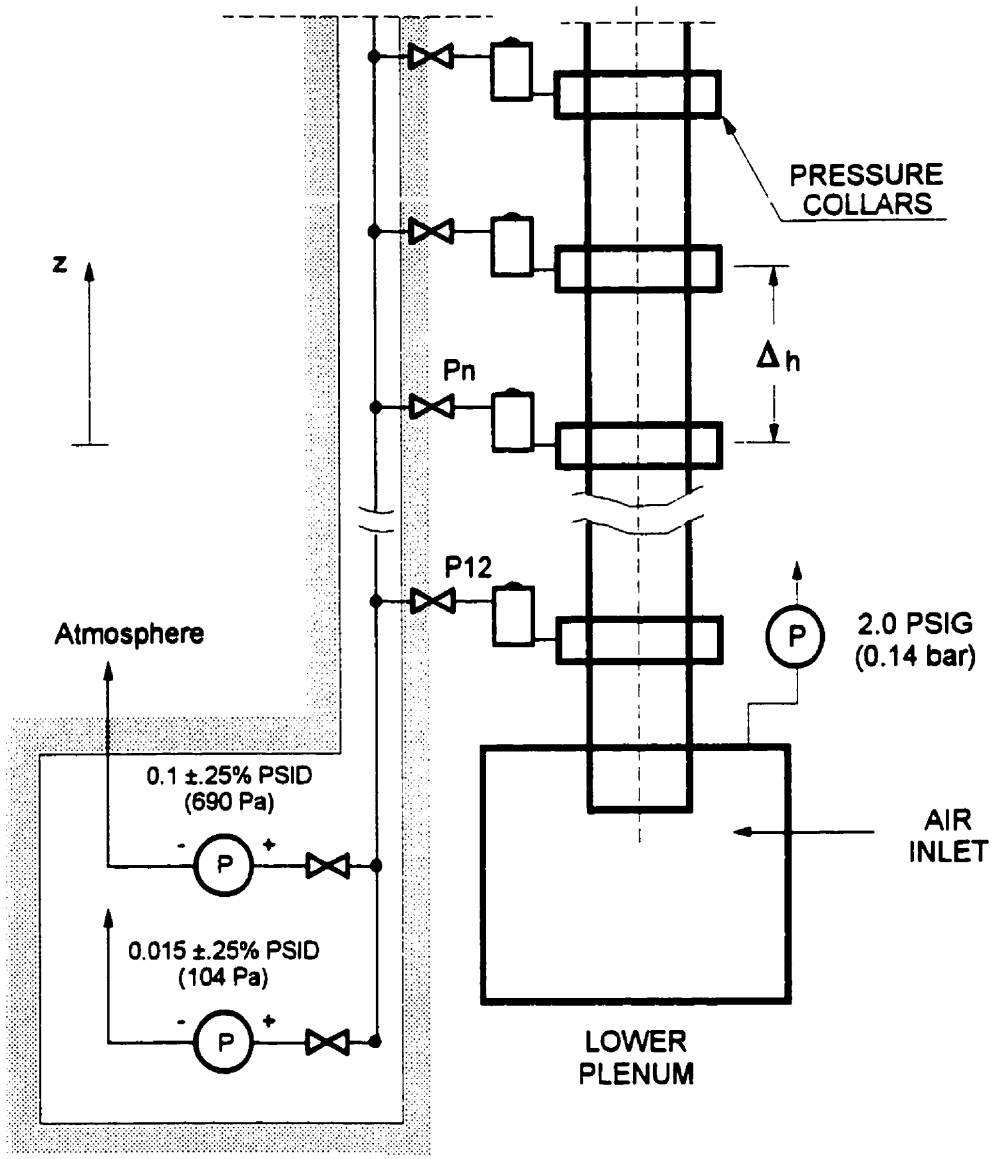

Figure 3.4: Schematic of pressure measurement system.

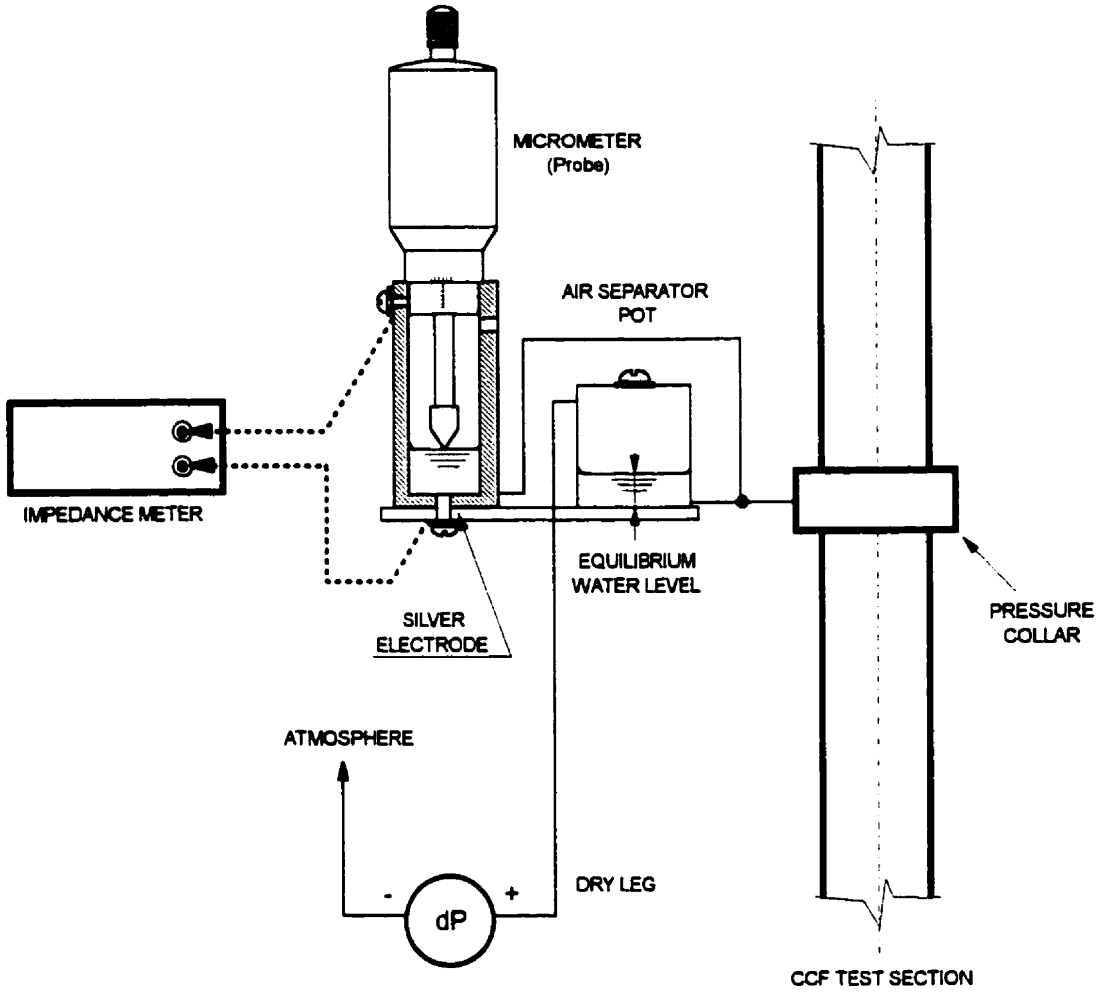

Figure 3.5: Pressure measurement validation system.

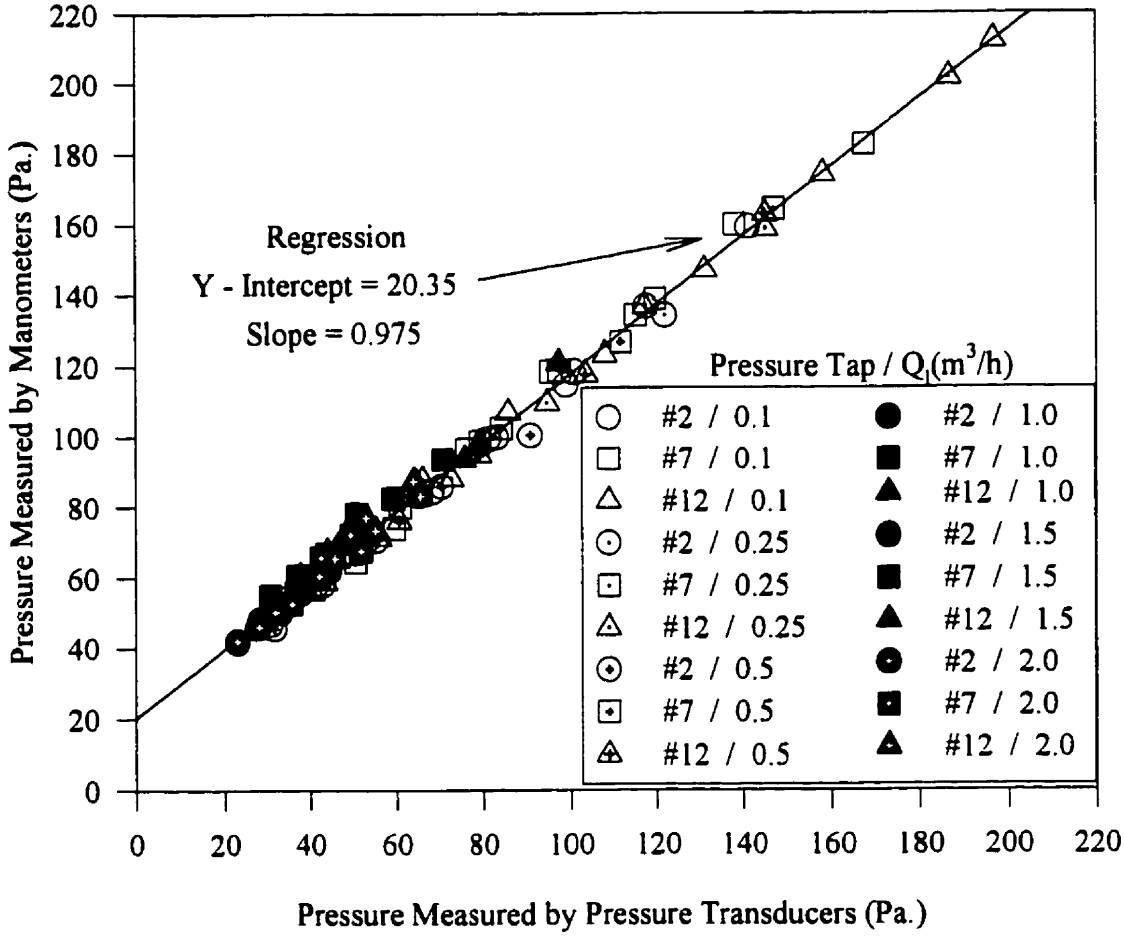

Figure 3.6: Validation of pressure measurement system.

Chapter 4

EXPERIMENTAL RESULTS

The results for all the experiments carried out during the course of this research project will now be presented. A number of different types of experimental results have been obtained. These are the results for the liquid delivery, which include the zero liquid penetration point, the flooding results, the results of the hysteresis experiments and the pressure drop results. These results will be presented separately.

4.1 Liquid Delivery Experiments

The liquid delivery experiments will be presented in two parts, the first part will be the experiments carried out in the vertical test section and the second will be the experiments carried out in the test section containing both vertical and horizontal legs.

4.1.1 Results of Vertical CCF Experiments

The results for the vertical tube without an orifice are shown in Figure 4.1 where they are presented in terms of the delivered liquid superficial velocity, $J_{\ell\ delivered}$, vs. the gas superficial velocity, J_g. It can be seen that the gas superficial velocity required to provoke the transition from full to partial delivery decreases with increasing liquid superficial velocities. In the partial delivery region our results show the same trends as those observed by Zabaras [1985] for inlet liquid superficial velocities up to 0.01754 m/s. At higher liquid superficial velocities our results are similar to those of

Celata [1989]. For the two lowest inlet liquid superficial velocities 0.00877 m/s and 0.01754 m/s the variation of the delivered liquid superficial velocity with increasing gas superficial velocity is very smooth throughout the entire partial delivery region. At higher liquid superficial velocities it can be seen that there is a large drop in the delivered liquid superficial velocity at a given gas superficial velocity. In the region of gas superficial velocities between 5 and 10 m/s a plateau is observed in the delivered liquid superficial velocity. At still higher inlet liquid superficial velocities, the delivered liquid superficial velocity region exhibits a smooth decrease with increasing gas superficial velocities. It has been observed visually that in the partial delivery region the liquid upflow occurs due to two mechanisms. At lower gas superficial velocities the liquid upflow is due to entrained drops carried upwards by the gas flow while at higher gas superficial velocities the liquid upflow is due to a combination of both entrained drops and film upflow. The delivered liquid (i.e., that which reaches the lower plenum) is in the form of a liquid film that becomes thinner with increasing gas flow rate. The sharp transition from full to partial delivery at the highest inlet liquid superficial velocities imposes a maximum limit on the inlet liquid flows that can be studied with the actual experimental facility. This is due to the fact that as soon as partial delivery is reached for these high inlet liquid superficial velocities the entrained liquid flow rate is beyond the capacity of the entrainment collection system.

Figure 4.2 shows the results of the experiments carried out for vertical counter–current flow with orifices of various sizes installed in the test section. They are presented in terms of the delivered liquid superficial velocity, $J_{\ell\ delivered}$, vs. the gas superficial velocity, J_g, calculated using the unobstructed tube diameter. It can be seen that for a given orifice, the delivered liquid superficial velocity depends only on the counter–current gas superficial velocity and not on the inlet liquid superficial velocity. It can also be seen that for a given gas superficial velocity the delivered liquid superficial velocity decreases with decreasing β ratios (i.e., decreasing orifice diameter). For the experiments with an orifice installed, the phenomena governing the liquid delivery is different than that described for the experiments without the orifice. The gas flow causes a pulsating column of gas and entrained liquid to form just above the orifice. The steps of the formation of this pulsating column are shown in Figures 4.3 to 4.6. As the gas superficial velocity is slowly increased a certain amount of liquid gets trapped above the orifice as shown in Figure 4.3. At this point the delivered liquid superficial velocity is less than the inlet liquid superficial velocity. The quantity of

liquid injected into the test section that makes up the difference between $J_{\ell\ delivered}$ and $J_{\ell\ injected}$ adds to the size of the pulsating column, this is shown in Figure 4.4 and 4.5. Eventually the pulsating column builds up sufficiently that it completely fills the part of the test section above the orifice, Figure 4.6. At this point, the column has reached its maximum possible size and any difference between $J_{\ell\ delivered}$ and $J_{\ell\ injected}$ is recovered by the entrainment collection system. The magnitude of the gas superficial velocity determines how much liquid penetrates the orifice and how much gets trapped above it and thus carried upwards by the gas. This phenomena was much more apparent for the smaller orifices.

For the two smallest orifices studied $\beta = 0.66$ and $\beta = 0.72$ an inlet liquid superficial velocity was reached where a bubble filled liquid column formed in the test section without any gas being injected into the lower plenum. Such a column is shown in Figure 4.7. The presence of this column resulted in an upper limit to the inlet liquid superficial velocities that could be studied.

4.1.2 Results of CCF Experiments for Vertical to Horizontal Legs

Figures 4.8 to 4.10 show the delivered liquid superficial velocity, $J_{\ell\ delivered}$, vs. the gas superficial velocity, J_g, for the present tests; seven different cases were studied. They are the no orifice case and the cases for orifices having β ratios of 0.90, 0.83, 0.77 0.72, 0.66, and 0.55 installed in the horizontal leg.

The results for the case without an orifice, $\beta = 1$ in Figure 4.8, show that the delivered liquid superficial velocities decrease smoothly with increasing gas superficial velocity. For the case without an orifice a hydraulic jump was observed to occur in the horizontal leg. As the gas flow rate was increased the hydraulic jump was seen to travel back towards the elbow and eventually enter it. As the gas flow rate was increased beyond that required to drive the hydraulic jump into the elbow, entrained droplets were observed in the gas stream in the vertical leg just above the elbow, these droplets did not, however, necessarily lead to the onset of flooding as they were frequently seen to be redeposited into the liquid film only a few centimeters above the elbow. In this region, it was observed that the flow was in the form of an annular film with entrained droplets in the gas core. As the gas flow rate was increased

an increasing number of droplets were visible in the gas core just above the elbow which could not reach the upper plenum. At the flooding point, the flow pattern was seen to change from a stable counter–current annular flow with entrained droplets, to counter–current churn flow. This churn flow was in the form of a pulsating column in the vertical leg. This pulsating column caused large amplitude waves to form in the horizontal leg that were subsequently driven back into the elbow by the counter–current gas flow and upward to the collection system. The results shown in Figures 4.8 to 4.10 are similar to those of Kawaji *et al.* [1991] in that largest orifice used in these experiments had almost no influence on the delivered liquid flow rate as compared to the unobstructed case ($\beta = 1$ in Figure 4.8 and $\beta = 0.90$ in Figure 4.9). Further, our results show that this observation can be extended from the flooding limit studied by Kawaji *et al.* [1991], through the entire partial liquid delivery region right up to the zero penetration point.

The results for the largest orifice studied ($\beta = 0.90$) shown in Figure 4.9 are very similar to those observed for the case without an orifice described above. However, for the cases with an orifice placed in the horizontal leg no hydraulic jump was observed in the horizontal leg. Since the flow in the vertical leg is supercritical and the flow in the horizontal leg is subcritical the transition must therefore take place inside the elbow. It can be seen that for this case the delivered liquid superficial velocities decrease smoothly with increasing gas superficial velocity as observed in the case without an orifice. For the case having an orifice of $\beta = 0.83$ (Figure 4.8) at superficial gas velocities greater than 1 m/s the results are quite similar to the results for $\beta = 0.90$ in that the delivered liquid superficial velocities decrease smoothly with increasing gas superficial velocity. For largest inlet liquid superficial velocities and for gas superficial velocities between 0.5 and 1.0 m/s it can be seen that a plateau region is reached in the delivered liquid superficial velocity. For gas superficial velocities less than 0.5 m/s it can be seen that the delivered liquid superficial velocity decreases very rapidly with increasing gas superficial velocity. For the smaller orifices ($\beta = 0.77$ to $\beta = 0.55$ see Figures 4.9 and 4.10) the results are clearly different than those observed for the cases of $\beta = 1.0$ and $\beta = 0.90$. At very low gas superficial velocities and high inlet liquid superficial velocities the delivered liquid superficial velocity decreases very rapidly with increasing gas superficial velocity. It was visually observed that in this region a very densely packed bubble column, with the occasional Taylor bubble rising through it, was formed in the vertical leg. The liquid upflow was mostly due to entrainment

in this bubble column. The passage of the Taylor bubbles caused periodic increases in the liquid upflow. In the horizontal leg large slow moving plugs carried the gas into the elbow. At gas superficial velocities between approximately 0.5 and 2.5 (m/s) (see Figures 4.9 and 4.10) it can be seen that a plateau is reached in the delivered liquid superficial velocity and that the liquid delivery is almost independent of the gas superficial velocity. The size of this plateau seems to increase with decreasing β ratios (i.e., increasing the severity of the obstruction). In this region it was visually observed that the liquid upflow was mostly in the form of very fast moving slugs. This region is qualitatively similar to region 2 identified by Wan [1986]. The slugging frequency decreased with increasing gas superficial velocity. At even higher gas superficial velocities, the delivered liquid superficial velocity was seen to decrease quite smoothly with increasing gas superficial velocity. In this region a wavy stratified flow existed in the horizontal leg, the waves were seen to travel in the direction of the gas flow, while the liquid substrate traveled in the opposite direction. The liquid level of this stratified flow decreased with increasing distance from the elbow. It appears that the case having an orifice of $\beta = 0.83$ is a transition between two distinct regions of flow behaviour. At high gas superficial velocities the results for $\beta = 0.83$ are similar to those of $\beta = 1.0$ and $\beta = 0.90$, while at lower gas superficial velocities there are a number of similarities with the results for $\beta = 0.77$ to $\beta = 0.55$ described above. It is also interesting to note that in the region were the transition takes place, gas superficial velocities between $(0.4\ to\ 1.0\ m/s)$, the results for this orifice exhibit more experimental scatter than any of the other cases studied.

For all the cases studied it was visually observed that the disturbance that lead to partial liquid delivery always formed in the elbow. The mechanism governing the partial delivery was very similar to the case of a vertical tube containing an orifice. A pulsating column was formed in the vertical leg which caused large amplitude waves to form in the horizontal leg that were subsequently driven back into the elbow by the counter-current gas flow. For the experiments with an orifice installed in the horizontal leg the mechanism was similar to that observed in the case without the orifice. The major difference was that the wave produced by the pulsating column was seen to be reflected by the orifice and traveled back towards the elbow; it was then possible for this wave to interfere constructively with those waves generated by the pulsating column above the elbow. If the height of the wave resulting from the meeting of the two incident waves was sufficient to bridge the tube, a liquid slug

resulted which was then blown violently back into the elbow and into the vertical leg. This sequence of events is shown in Figures (4.11–4.18). Figure 4.11 shows the onset of entrainment above the elbow. Figure 4.12 shows the pulsating column formed in the vertical leg. This results in the production of waves in the horizontal leg shown in Figure 4.13. Figure 4.14 shows the wave traveling towards the orifice plate and the reflection is shown in Figure 4.15 (note also the very low liquid height on the downstream side of the orifice). Figure 4.16 shows the incident and reflected waves traveling towards each other. The slug formed by the interference of these waves is shown in Figure 4.17. The large liquid plug formed in the vertical leg is shown in Figure 4.18 where a bullet shaped gas pocket driving the water slug upward may also be seen. For smaller orifices the height of the liquid film in the horizontal leg and the size of the wave reflected from the orifice both increased. This resulted in more frequent and more violent slugging behaviour being observed for the smaller orifice. For the experiments with the $\beta = 0.90$ orifice no reflection of the wave by the orifice was seen to occur. At higher gas superficial velocities a region was reached where the liquid level in the horizontal leg was insufficient to allow bridging to occur and a region of steady counter-current flow without slugging but with liquid carryover (similar to region 1 of Wan [1986]) was established. Another observation is that the gas superficial velocity corresponding to the point of zero liquid penetration for a given orifice as well as for the no orifice case is the same for all the inlet liquid superficial velocities. A similar observation for results without an orifice was made by Siddiqui *et al.* [1986]. A further point of interest is that, while by strict definition as soon as J_ℓ delivered is less than J_ℓ injected the flooding limit has been reached, a large increase in the gas superficial velocity is still required to reach the point of zero liquid penetration as shown in Figures 4.8 to 4.10. This is an important point for the refilling of a nuclear reactor following a LOCA.

4.2 Flooding Results

The results for the flooding point will be presented in two parts, the first part will be the experiments carried out in the test section with only a vertical leg and the second will be the experiments carried out in the test section containing both vertical and horizontal legs.

4.2.1 Results of Vertical CCFL Experiments

For the partial delivery results obtained in the vertical test section shown in Figure 4.1 two distinct sets of data points can be seen. This is the result of the sharp decrease in the delivered liquid superficial velocity that occur at the transition from full to partial delivery. The first curve is the locus of partial delivery whose behaviour has been described in the previous section. The second curve is the locus of flooding. For a given inlet liquid superficial velocity, these points correspond to the maximum gas superficial velocity for which full liquid delivery out the bottom of the test section is maintained. The relationship between the partial delivery, which is simply represented as a best fit to all the experimental data, and the flooding limit is illustrated in Figure 4.19. The insert in this figure shows the flooding limit as well as the partial delivery results for one particular inlet liquid superficial velocity (0.08771 m/s in Figure 4.1). It can be seen that for this case the locus of flooding points lie considerably above the locus of partial delivery points. The two curves approach each other at the extreme of very low inlet liquid superficial velocities. Similar loci of partial liquid delivery also exist for the cases with the various orifices installed in the test section. These are shown in Figure 4.20, it can be seen that due to the very smooth transition from full to partial delivery when an orifice is present in the test section, the locus of flooding for any given orifice is nearly identical to the locus of partial delivery.

The results of the flooding limits only, for both the experiments without an orifice and for the various orifices studied are presented in Figure 4.21. They are given in terms of the square root of the non-dimensional superficial velocities, $J_g^{*\frac{1}{2}}$ and $J_\ell^{*\frac{1}{2}}$, where $J_k^{*\frac{1}{2}}$ is defined as:

$$J_k^{*\frac{1}{2}} = \left\{ \frac{\rho_k^{\frac{1}{2}} J_k}{[gD(\rho_f - \rho_g)]^{\frac{1}{2}}} \right\}^{\frac{1}{2}} \quad . \tag{4.1}$$

It is important to point out that the non-dimensional superficial velocities used in Figure 4.21 are all calculated using the unobstructed tube diameter in equation 4.1. It can be seen that in all cases studied the non-dimensional superficial velocity of the gas at the flooding point decreases smoothly with increasing non-dimensional superficial velocity of the of the liquid. It can also be seen that for a given non-dimensional superficial liquid velocity the values of the non-dimensional superficial

velocity of the gas at the flooding point decrease with decreasing orifice β ratios.

4.2.2 Results of CCFL Experiments for Vertical to Horizontal Legs

It is important to point out that Figures 4.8 to 4.10 represent the locus of partial delivery for all the cases studied and **not** the flooding limits. As was done for the results obtained in the vertical test section, the relationship between the partial liquid delivery and the flooding limit is illustrated for a given orifice, ($\beta = 0.77$), in Figure 4.22. The insert in this figure shows the flooding limit as well as the partial liquid delivery results for one particular inlet liquid superficial velocity (0.12 m/s in Figure 4.9). It can be seen that for this orifice the locus of flooding points lie considerably above the locus of partial delivery points for most of the range of gas superficial velocities covered. The two curves approach each other at the extremes of very low and very high inlet liquid superficial velocities. Figures 4.23 to 4.29 show the relationship between the partial liquid delivery and the flooding limit for all the cases studied. The partial liquid delivery results have been replaced by a best fit of the data to clarify the presentation. In general, it can be seen that the relative drop between the locus of flooding points and the locus of partial delivery increases with decreasing β ratio.

In examining Figures 4.23 to 4.29 it is important to recall that the flooding limit corresponds to the maximum gas superficial velocity for which full liquid delivery still exists. From the insert in Figure 4.22 we can see that as the superficial velocity of the gas is increased the delivered liquid superficial velocity remains constant at its inlet value until a particular gas superficial velocity is reached; at this point the delivered liquid superficial velocity drops suddenly. The maximum gas superficial velocity for which the delivered liquid superficial velocity retains its inlet value corresponds to the flooding limit. The abrupt transition from full to partial delivery may be related to the hysteresis effect observed by many other researchers [Shoukri *et al.* 1991]. The mechanisms governing the transition from full to partial liquid delivery have been described in detail in the previous section.

The flooding limits were obtained in the manner described above for all of the inlet liquid superficial velocities and for all of the cases studied. The results of the flooding

limits only are presented in Figures 4.30 and 4.31 in terms of the square root of the non dimensional superficial velocities, $J_g^{*\frac{1}{2}}$ and $J_\ell^{*\frac{1}{2}}$ calculated using the unobstructed tube diameter. A fit of the ($\beta = 1.0$) data has been added to Figure 4.31 for reference purposes. It can be seen that the flooding limits decrease with decreasing β ratios. For the case with no orifice in the horizontal leg (Figure 4.30) the results are quite similar to those of Siddiqui *et al.* [1986]. Further, it can be seen that the largest orifice used ($\beta = 0.90$) had almost no effect on the flooding limit as compared to the case without an orifice. The same observation can be made about the next largest orifice ($\beta = 0.83$) for values of $J_\ell^{*\frac{1}{2}}$ less than 0.4. For the other orifices ($\beta < 0.83$) that were studied it is quite clear from both Figures 4.30 and 4.31 that for a given value of $J_\ell^{*\frac{1}{2}}$ a decrease in the β ratio leads to a decrease in the value of $J_g^{*\frac{1}{2}}$ at the flooding limit. This result is qualitatively similar to the observations for vertical pipes presented in the previous section. However, the flooding limits are well below those presented for vertical flow.

4.3 Results of Hysteresis Experiments

Figures 4.32 to 4.38 show the locus of deflooding points for the no orifice case as well as for the cases where orifices having β ratios of 0.90, 0.83, 0.77, 0.72, 0.66, and 0.55 were located in the horizontal leg. The best fit curves to the partial delivery experiments and to the flooding points are also presented on the same graphs. It can be seen that for all the orifice sizes studied, the deflooding points follow almost exactly the curve of partial liquid delivery results. This indicates that in the post flooded state these curves define a unique relationship between the delivered liquid superficial velocity and the gas superficial velocity which do not depend on whether the gas flow is increasing or decreasing. For all the cases studied the differences found between gas superficial velocity corresponding to the flooding point and the gas superficial velocity corresponding to deflooding point indicate that there is a significant hysteresis effect.

4.4 Pressure Drop Experiments

Pressure drop experiments were carried out in the 63.5 mm I.D. vertical test section for liquid flow rates ranging from 0.1 to 1.75 m^3/h at a number of different gas

flow rates. The results are shown in Figures 4.39 to 4.44 for the pressure drop profiles measured in the liquid film for liquid flow rates of 0.1, 0.25, 0.5, 1.0, 1.5, and 1.75 m^3/h respectively. These pressure differences are measured with respect to the pressure tap located at the top of the test section. They indicate that the pressure decreases in the upward direction, i.e., in the direction of the gas flow. It can be seen that the total pressure difference increases with increasing gas flow rate. Figure 4.45 shows the comparison of the pressure difference results for a fixed gas flow rate of 50.88 m^3/h, for five different inlet liquid flow rates of 0.1, 0.25, 0.5, 1.0, and 1.5 m^3/h. It can be observed that the pressure difference increases with increasing liquid flow rate. This is seen even more clearly in Figure 4.46 which shows the same results in term of a three dimensional figure where the pressure difference is clearly seen to increase with increasing gas flow rate for a fixed inlet liquid flow rate.

4.5 Comparison of Flooding Results

In this section the comparison of the flooding results will be presented. First the flooding results obtained in the vertical test section are compared against the Wallis [1969] flooding correlation. Then the flooding results obtained in the test section containing both vertical and horizontal legs will be compared against other experimental data and for the case with no orifice a comparison will also be presented against the model of Ardron & Banerjee [1986].

4.5.1 Vertical Flooding Results

The results for the case without an orifice are compared to the well known flooding correlation of Wallis [1969] given by equation 2.10 in Figure 4.47 where the best fit of this equation to the experimental results is obtained using $m = 0.694$ and $C = 0.74$.

The results for the cases with an orifice are shown in Figure 4.48 where they are also compared to the Wallis flooding correlation. It can be seen that all the curves can be represented quite well by equation 2.10 where the slope of the curve is almost constant ($m = 0.85 - 0.91$) and C is seen to decrease with decreasing β ratios. The cases for which an orifice is placed in the test section can not be compared to any other results due to the fact that no such data is available in the open literature. The

results of Celata [1989] and Davidson [1994] can not be used for this comparison due to the fact that they were carried out in test sections of much smaller diameter than that used in the present experiments and that there are well known effects of scale [Bankoff & Lee 1986] which are not accounted for by the use of a representation using the dimensionless superficial velocities.

4.5.2 Flooding Results for Test Section with Vertical and Horizontal Legs

The flooding results for the test section with vertical and horizontal legs without an orifice installed in the horizontal leg will be compared to other experimental results obtained on geometrically similar test facilities. They will also be compared to the one model available in the literature which is able to predict the flooding point for this type of geometry. For the cases where an orifice is installed in the horizontal leg, the results will only be compared to other experimental results due to the fact that, as yet, no model exists which is able to predict the flooding behaviour due to the interactions of an elbow between a vertical and a horizontal run containing an orifice.

a) Comparison with Other Experimental Results: No Orifice

Figure 4.49 shows a comparison of our experimental results for the case without an orifice with the results of Krowlewski [1980], Siddiqui *et al.* [1986], Kawaji *et al.* [1991], and Wongwises [1994]. The geometric arrangement of their various test sections is also shown in the same figure. In all these cases the various authors studied the influence of different parameters, i.e., the radius of curvature of the elbow, the L/D ratio of the horizontal leg, the influence of the tube diameter, and the influence of the angle of inclination of the lower leg from the horizontal plane. It should be noted that none of the test facilities of the other researchers who's data have been used for this comparison is identical in all respects to the one used in the present study. However, for the comparisons the results of each author obtained on the geometry most similar to the one in the present study were used. At the lower values of $J_\ell^{*1/2}$ the results of Krowlewski [1980], Siddiqui *et al.* [1986] and Kawaji *et al.* [1991] are in reasonably good agreement with our results. At values of $J_\ell^{*1/2} > 0.4$ the results of Krowlewski [1980] and those of Kawaji *et al.* [1991] start to diverge from ours. This divergence could be due to the influence of parameters that differ between the

various test facilities. The results of Wongwises [1994] are in total disagreement with all the other available data for the flooding in a test section containing a vertical and a horizontal leg connected by an elbow.

b) Comparison with Other Experimental Results: Orifice

Figure 4.50 shows a comparison of the present flooding results with those of Kawaji *et al.* [1993]. A schematic of the test facility used by Kawaji *et al.* [1993] is also shown in the same figure. It consists of a 1 m long vertical leg connected to a 1.5 m long horizontal leg containing an orifice 1.1 m downstream, with respect to the liquid flow, of the first elbow. The horizontal leg was connected to a second 1 m long vertical leg which was in turn connected to a third 1 m long horizontal leg. At high values of $J_\ell^{*1/2}$ Kawaji *et al.* [1993] reported that flooding occured in the second vertical leg of the test facility. Since the geometrical arrangement used by Kawaji *et al.* [1993] is different than the one used in the present study the data reflecting the occurrence of the flooding in the second vertical leg were not used for comparison. In the region where Kawaji *et al.* [1993] reported that the flooding occured as a result of the orifice their data are in very good agreement with that obtained in the present study. In general both sets of results indicate that the gas superficial velocity required to provoke flooding for a given gas flow rate, decrease with decreasing orifice β ratio.

c) Comparison with Model: No Orifice

The only model available for the prediction of the flooding in an elbow between a vertical and a horizontal leg is that of Ardron & Banerjee [1986] given by equation 2.22.

Figure 4.51 shows the results of a comparison of the above flooding correlation with the experimental flooding limits obtained in this study for the no orifice case. We can see that the correlation is in reasonably good agreement with the experimental results over most of the range of $J_\ell^{*\frac{1}{2}}$ studied, but begins to diverge from the experimental results for $J_\ell^{*\frac{1}{2}} > 0.45$.

This correlation is not applicable to the cases having an orifice in the horizontal leg and to the best of the authors knowledge no correlations exist which were developed to predict flooding behaviour due to the interactions of an elbow between a vertical and a horizontal run, and an orifice.

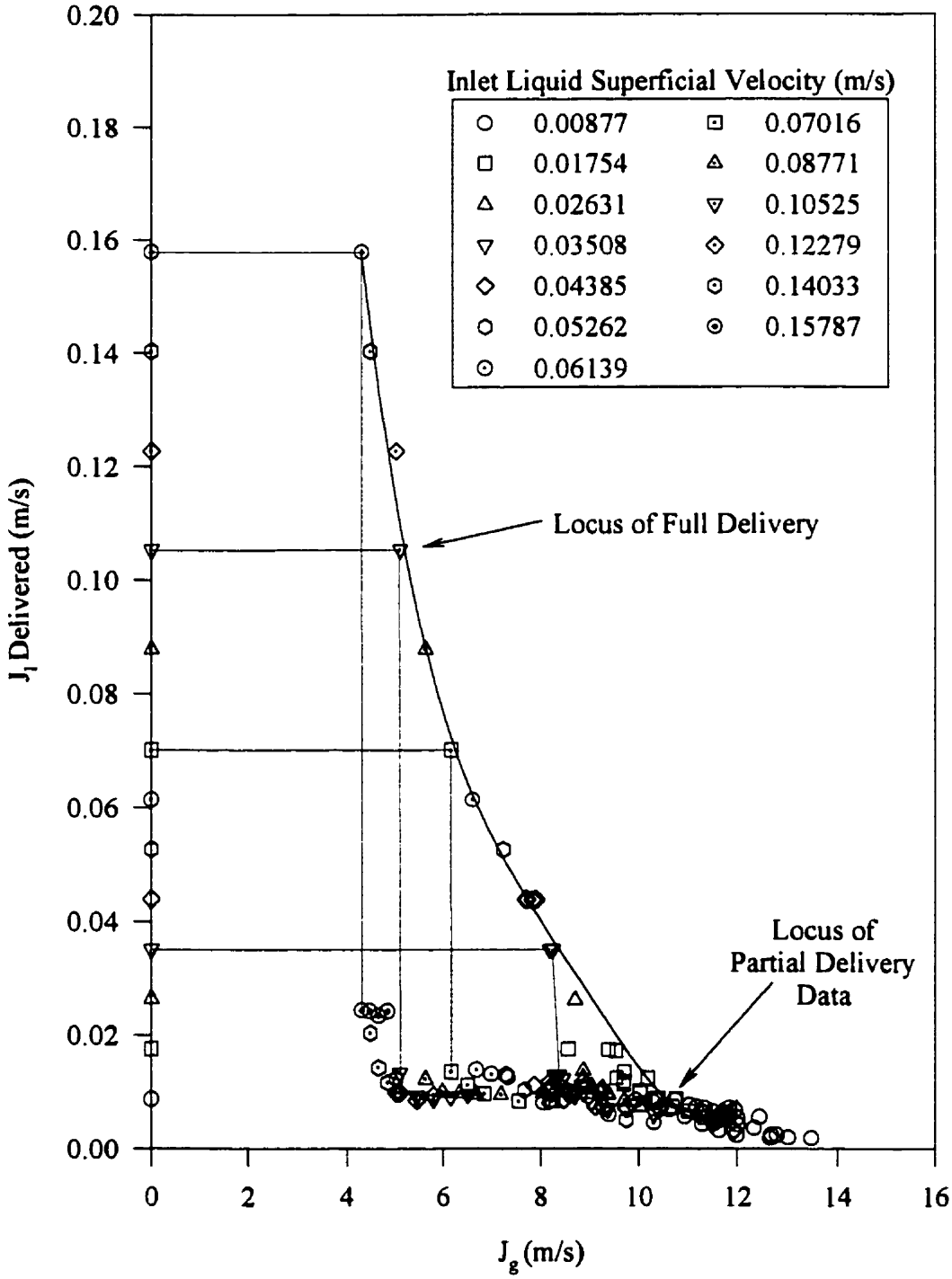

Figure 4.1: J_ℓ delivered vs. J_g vertical test section no orifice.

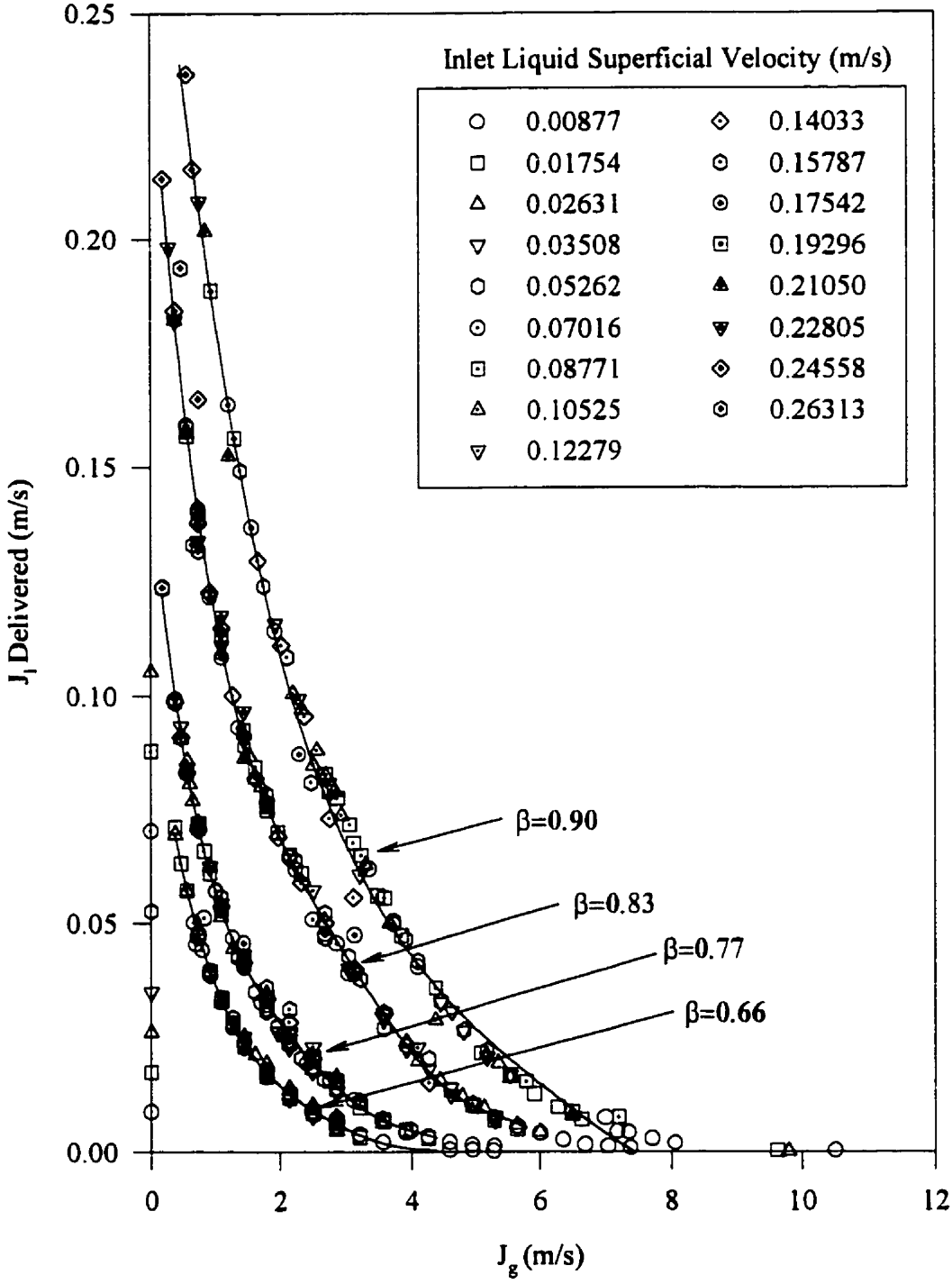

Figure 4.2: J_ℓ delivered vs. J_g vertical test section with orifices.

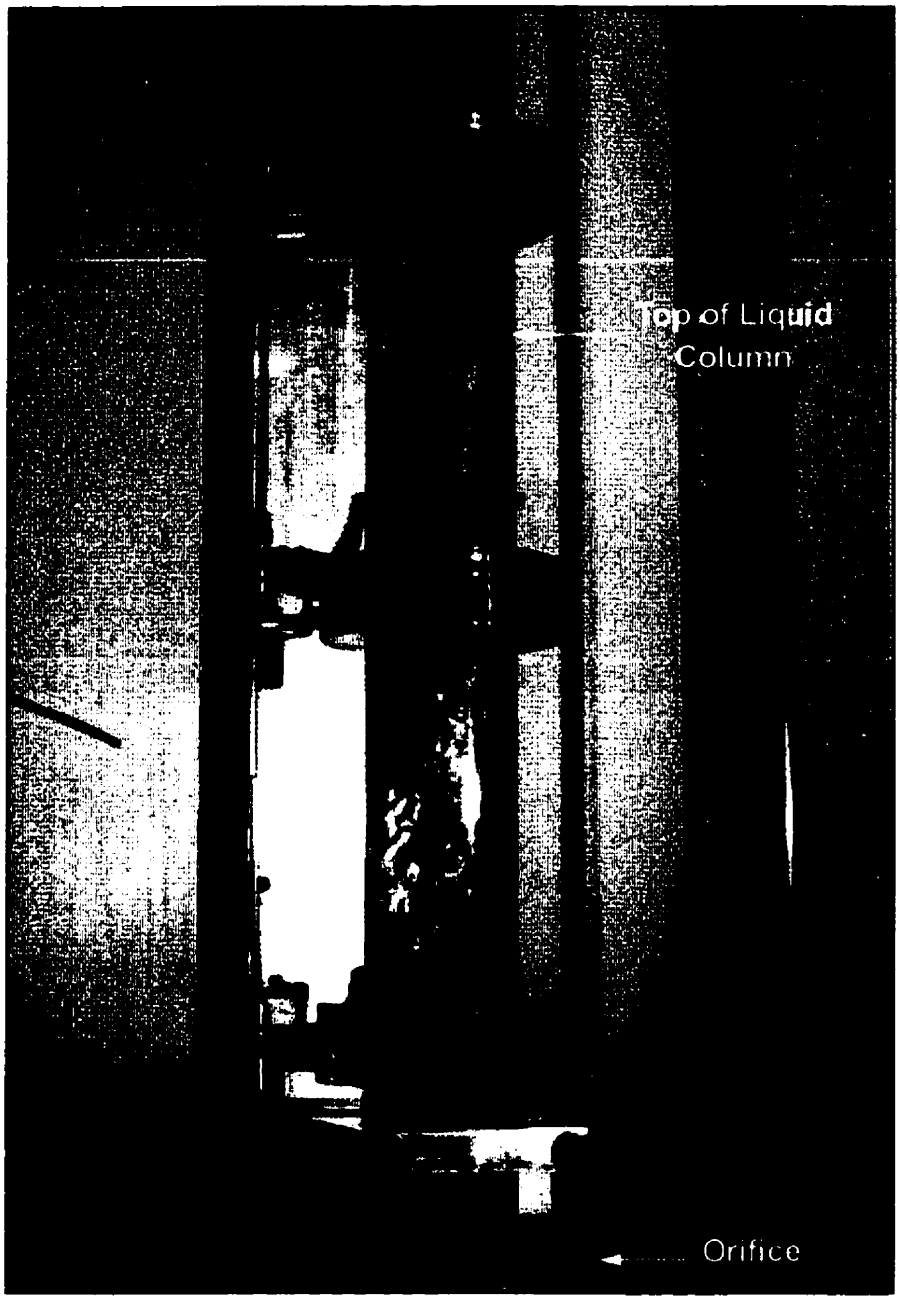

Figure 4.3: Beginning of buildup of liquid column above the orifice, test section with vertical leg only.

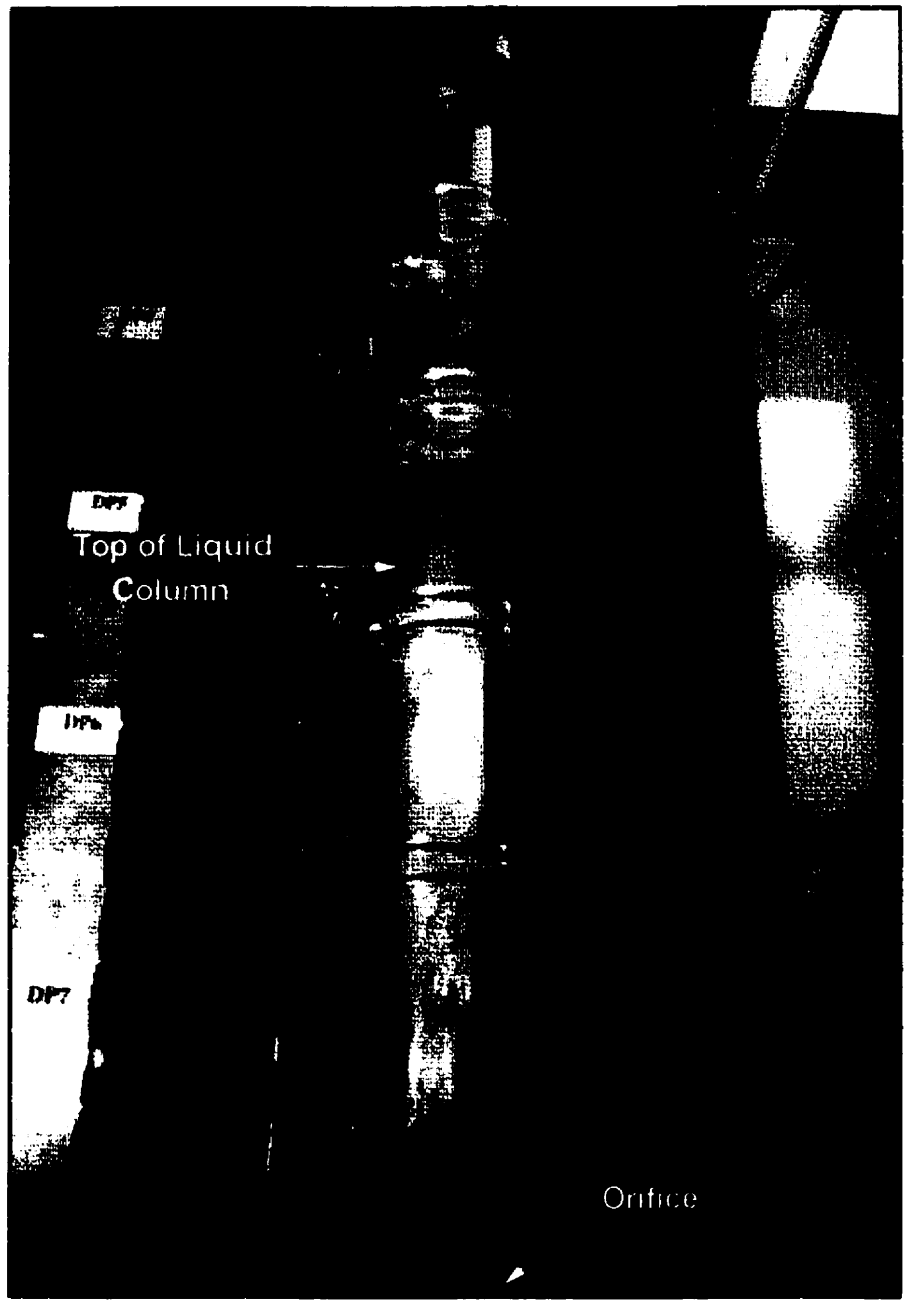

Figure 4.4: Continuation of buildup of liquid column above the orifice, test section with vertical leg only.

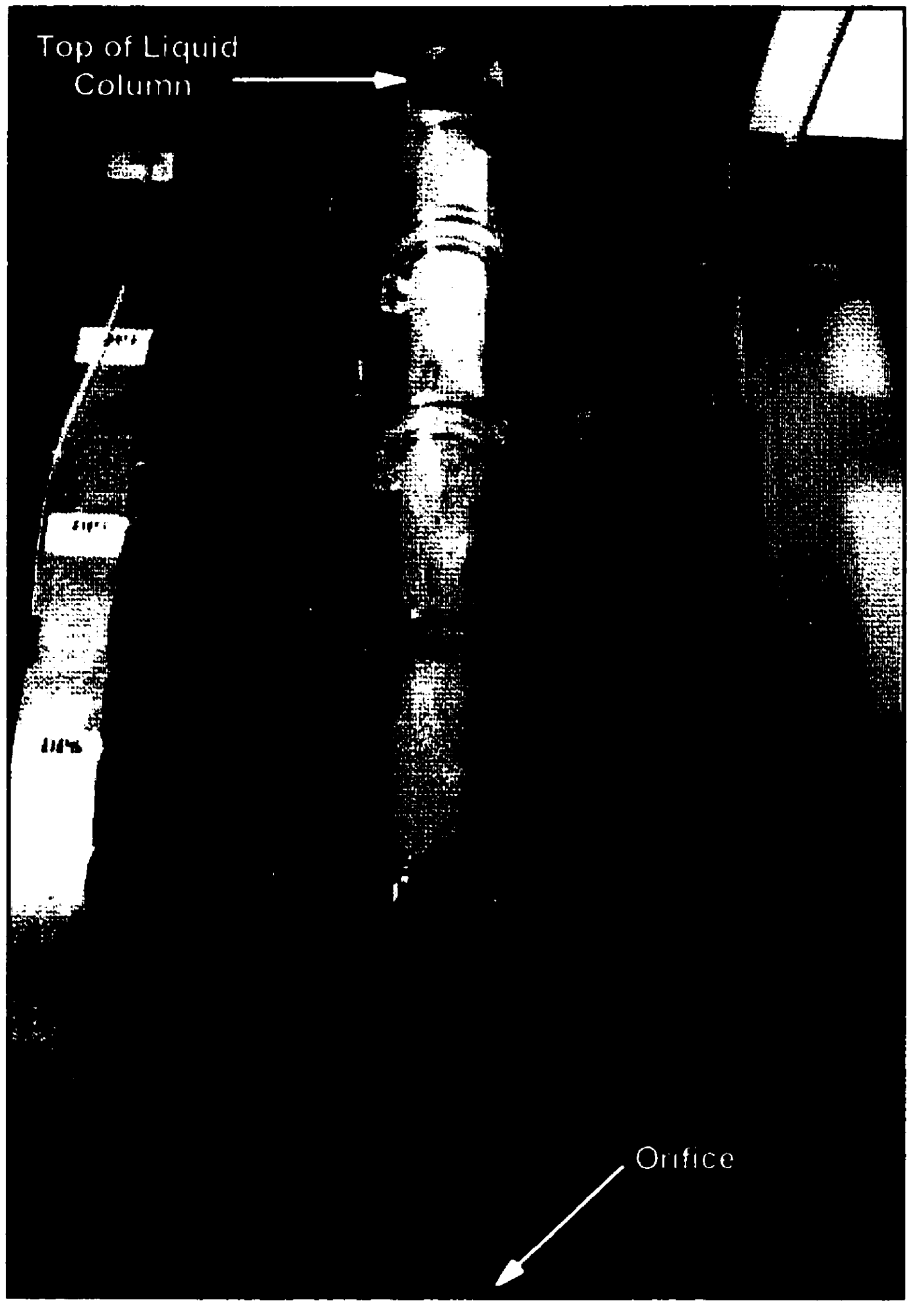

Figure 4.5: Further buildup of liquid column above the orifice, test section with vertical leg only.

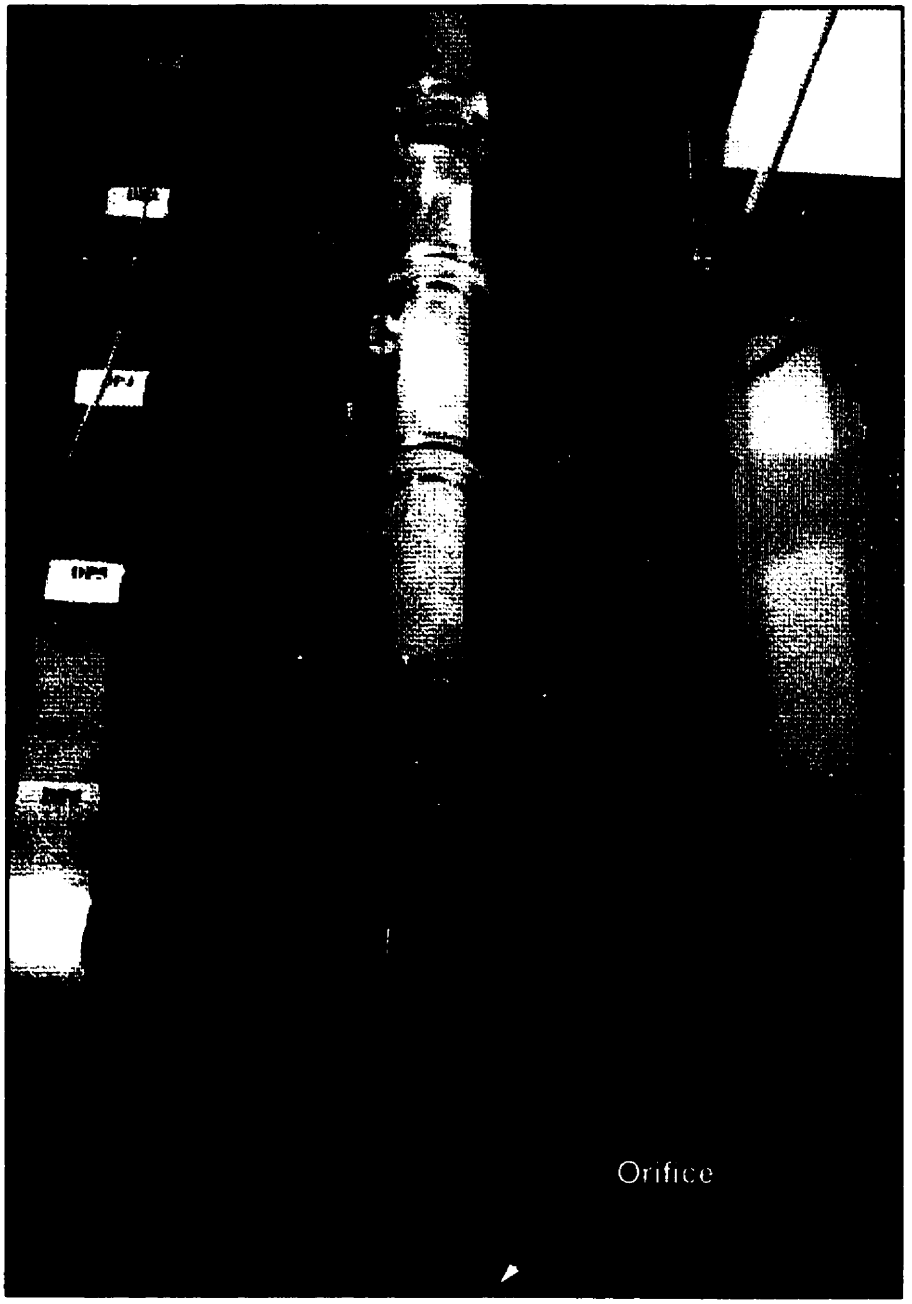

Figure 4.6: Liquid column fills the entire region above the orifice, test section with vertical leg only.

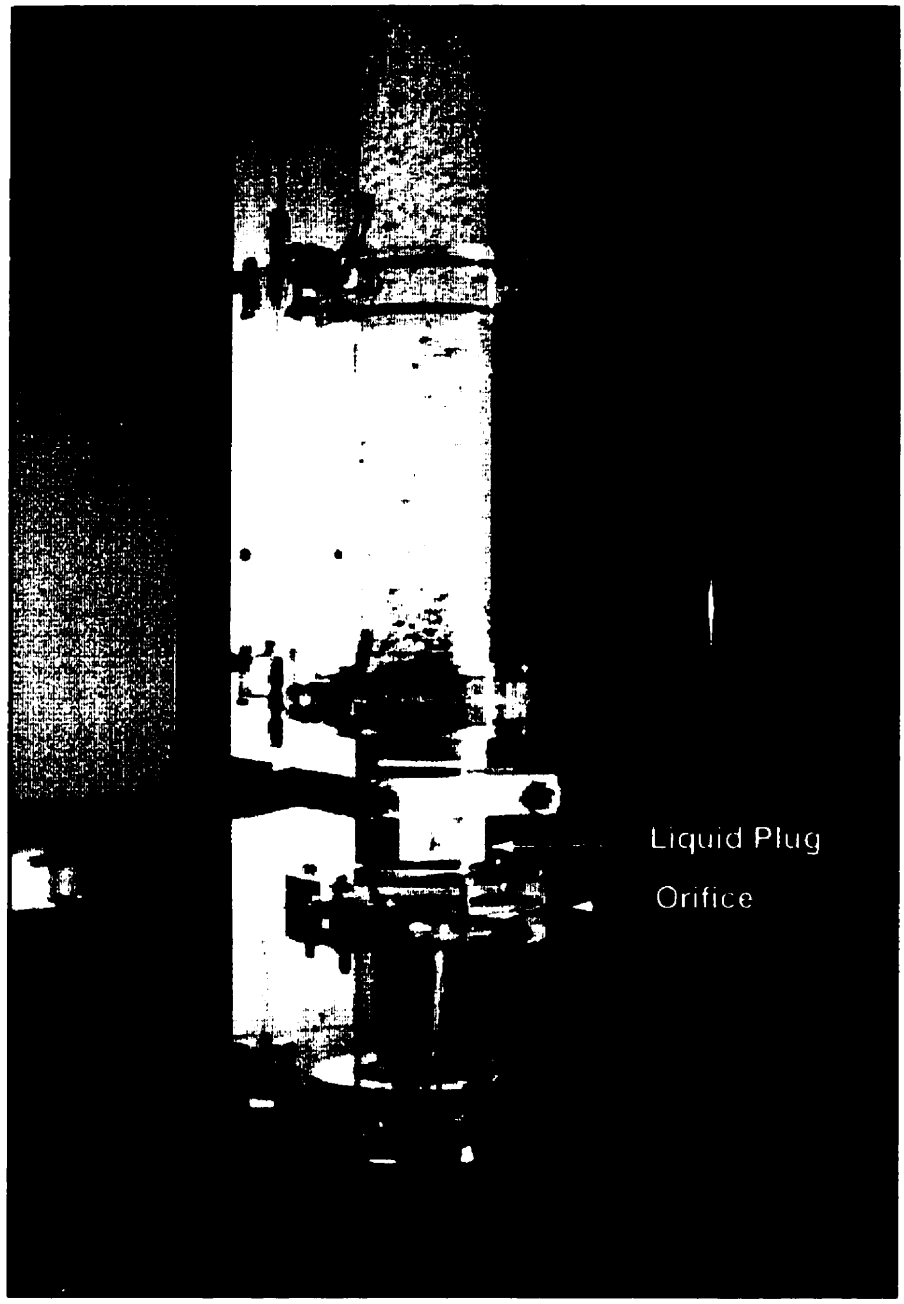

Figure 4.7: Liquid column formed above the smallest orifices at zero gas flow, test section with vertical leg only.

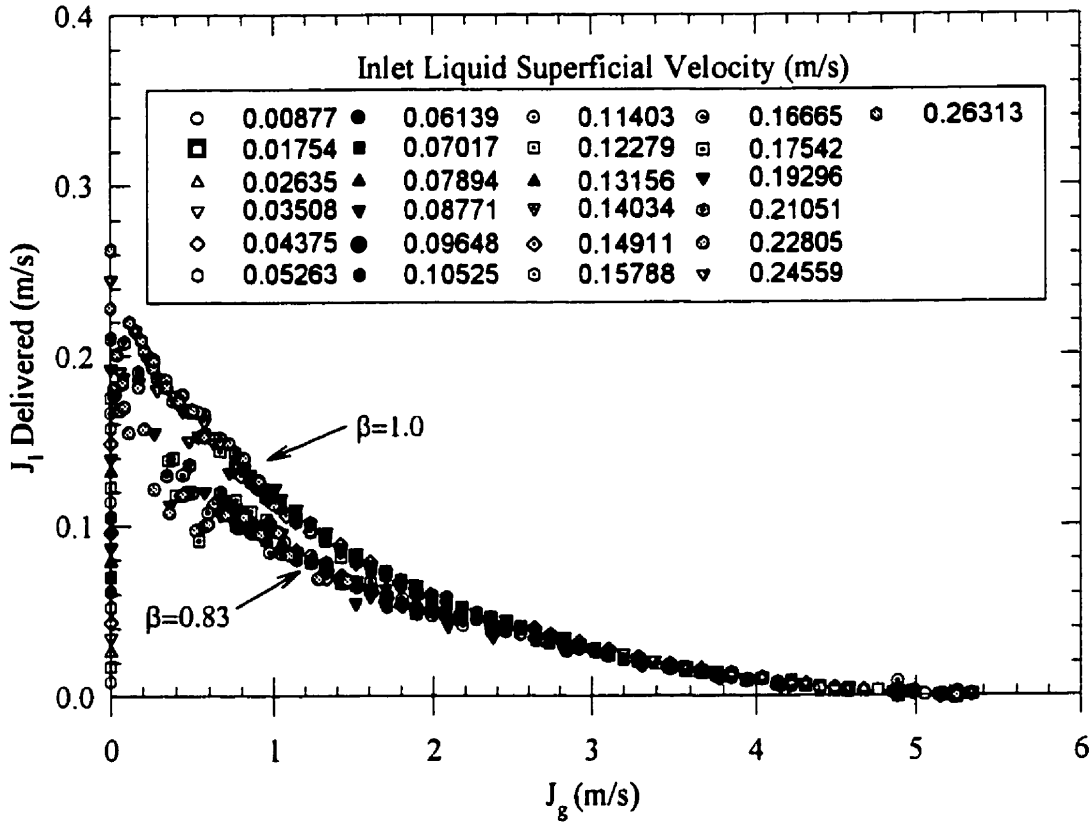

Figure 4.8: J_ℓ delivered vs. J_g test section containing vertical and horizontal legs.

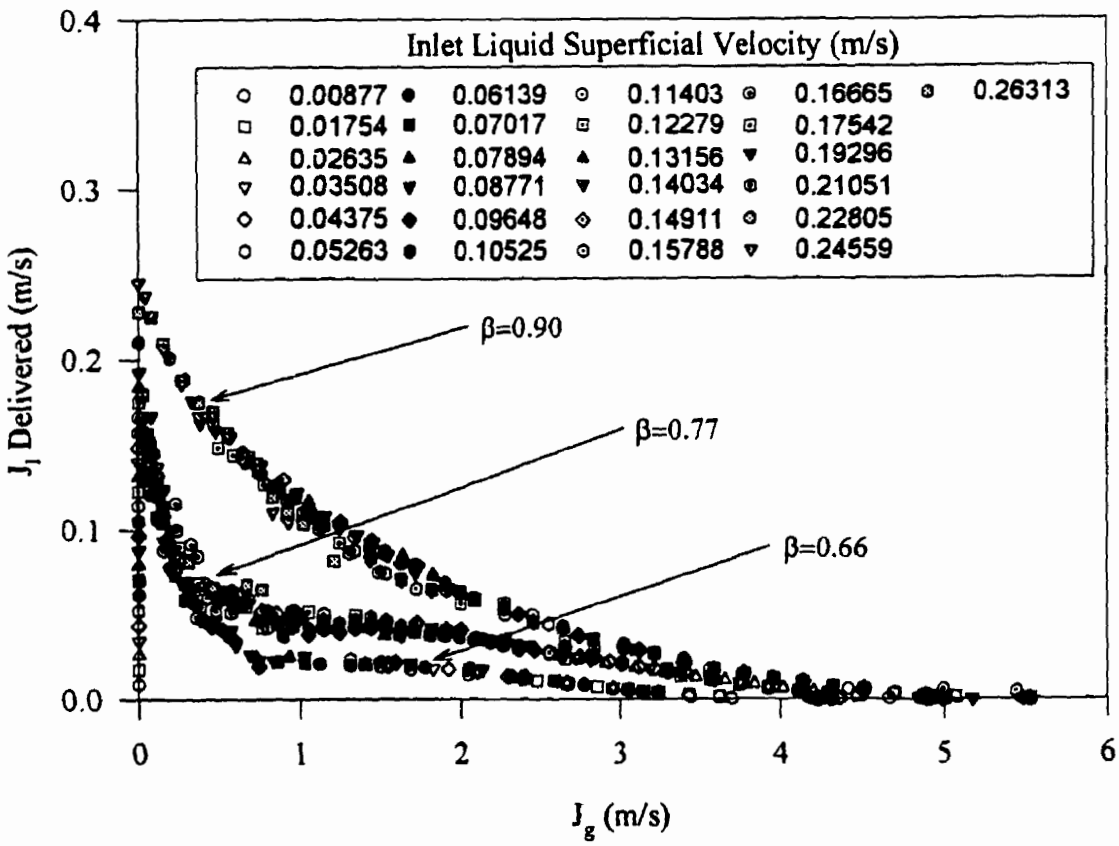

Figure 4.9: J_ℓ delivered vs. J_g test section containing vertical and horizontal legs (cont.).

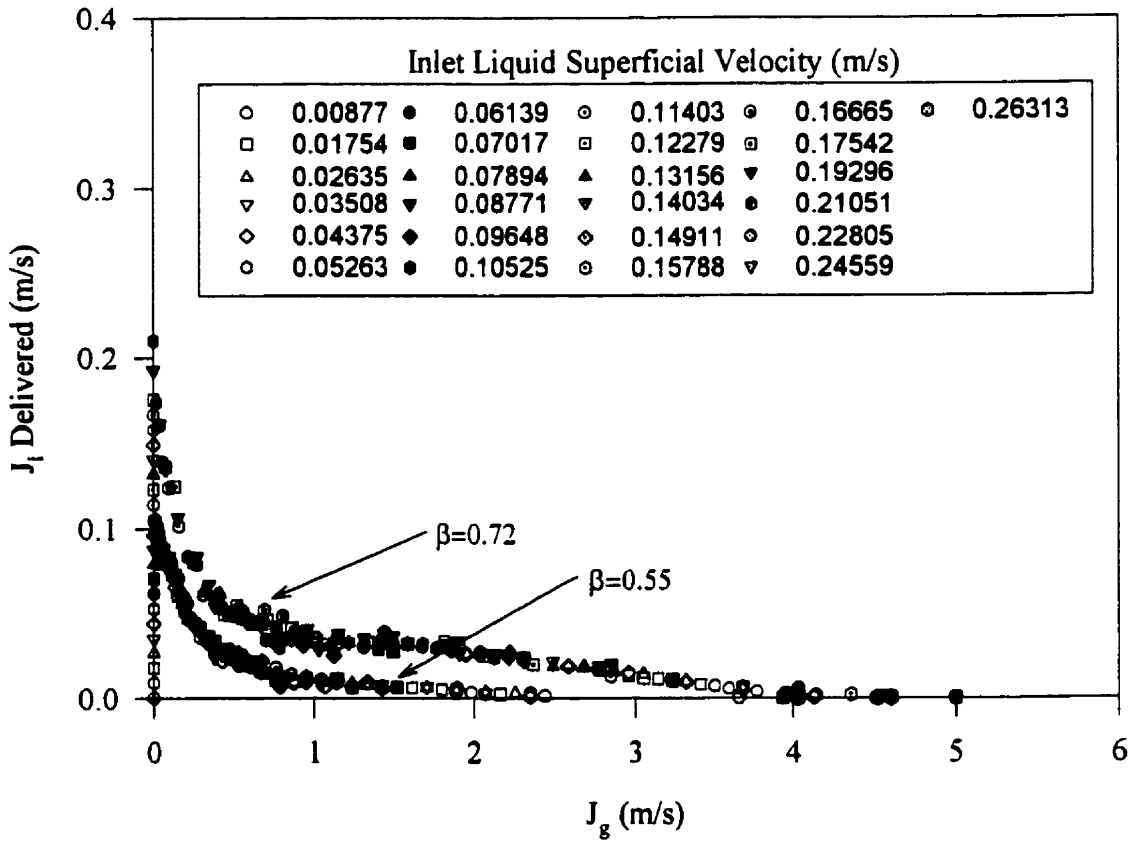

Figure 4.10: J_ℓ delivered vs. J_g test section containing vertical and horizontal legs (cont.).

Figure 4.11: Onset of entrainment above the elbow, test section containing vertical and horizontal legs.

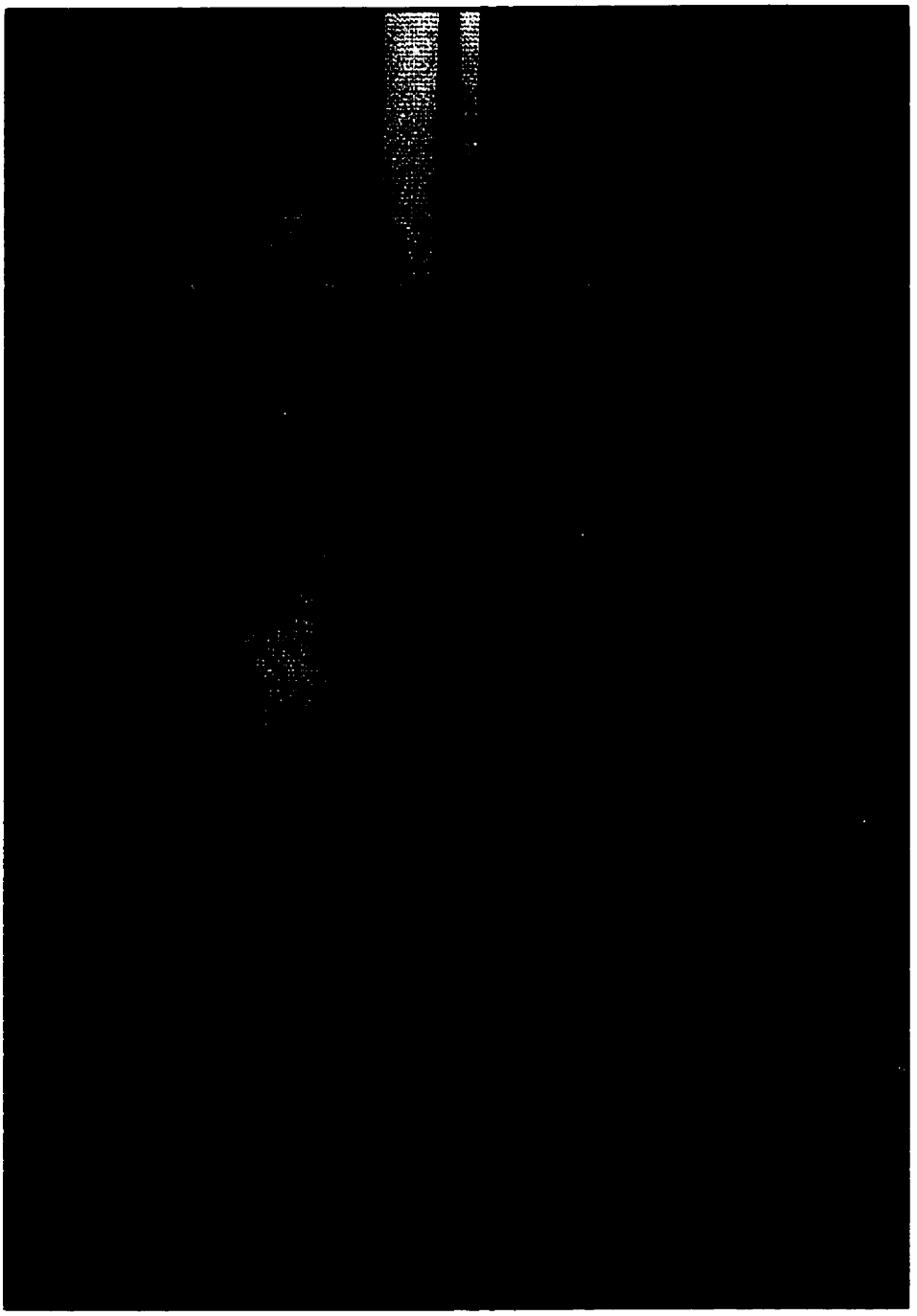

Figure 4.12: Pulsating column formed in the vertical leg, test section containing vertical and horizontal legs.

Figure 4.13: Wave in horizontal leg formed by pulsating column, test section containing vertical and horizontal legs.

Figure 4.14: Wave traveling towards the orifice, test section containing vertical and horizontal legs.

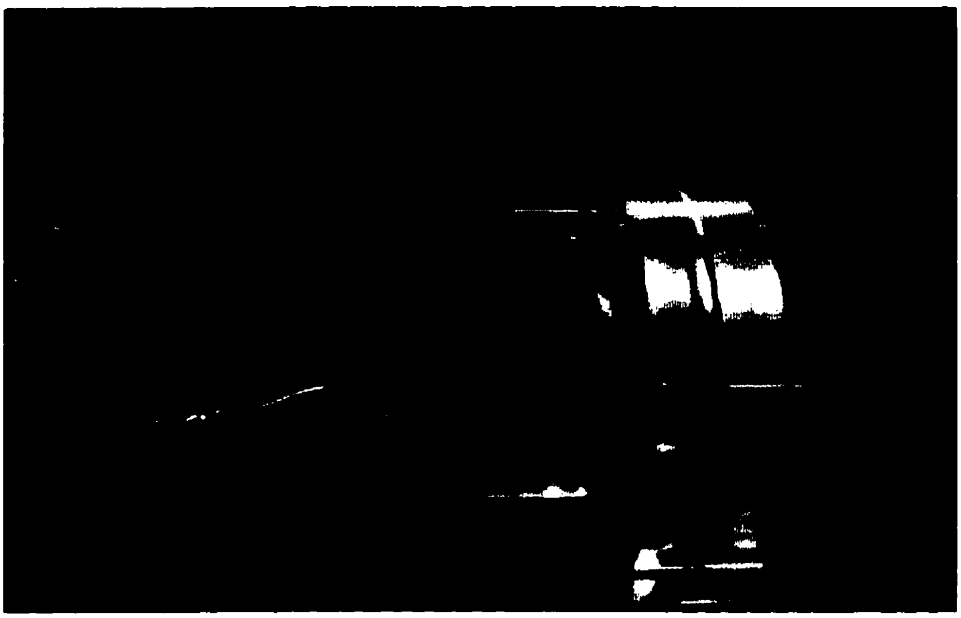

Figure 4.15: Wave reflected from the orifice, test section containing vertical and horizontal legs.

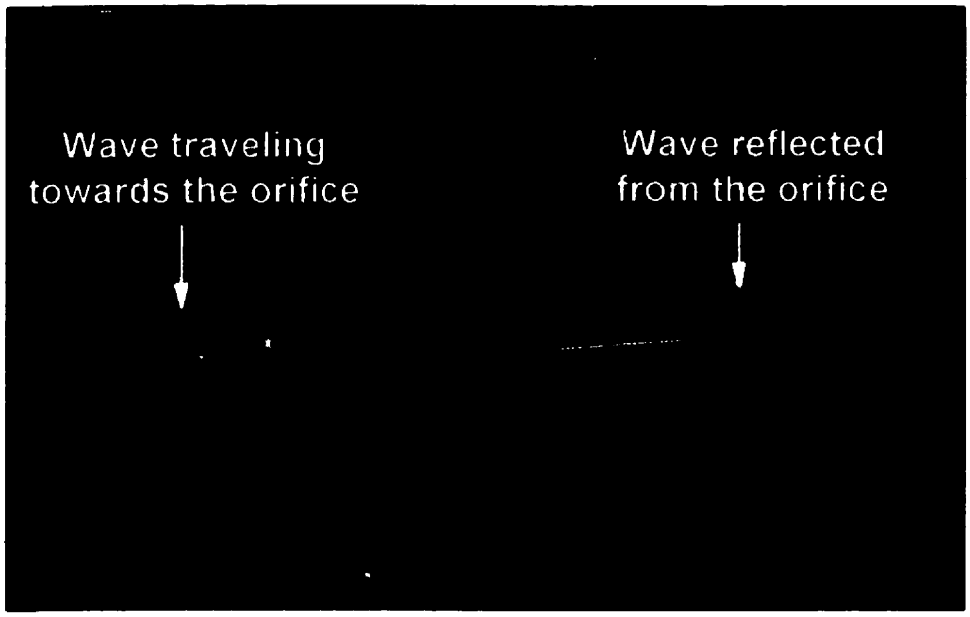

Figure 4.16: Wave traveling towards the orifice and wave reflected from the orifice, test section containing vertical and horizontal legs.

Figure 4.17: Liquid slug formed in the horizontal leg, test section containing vertical and horizontal legs.

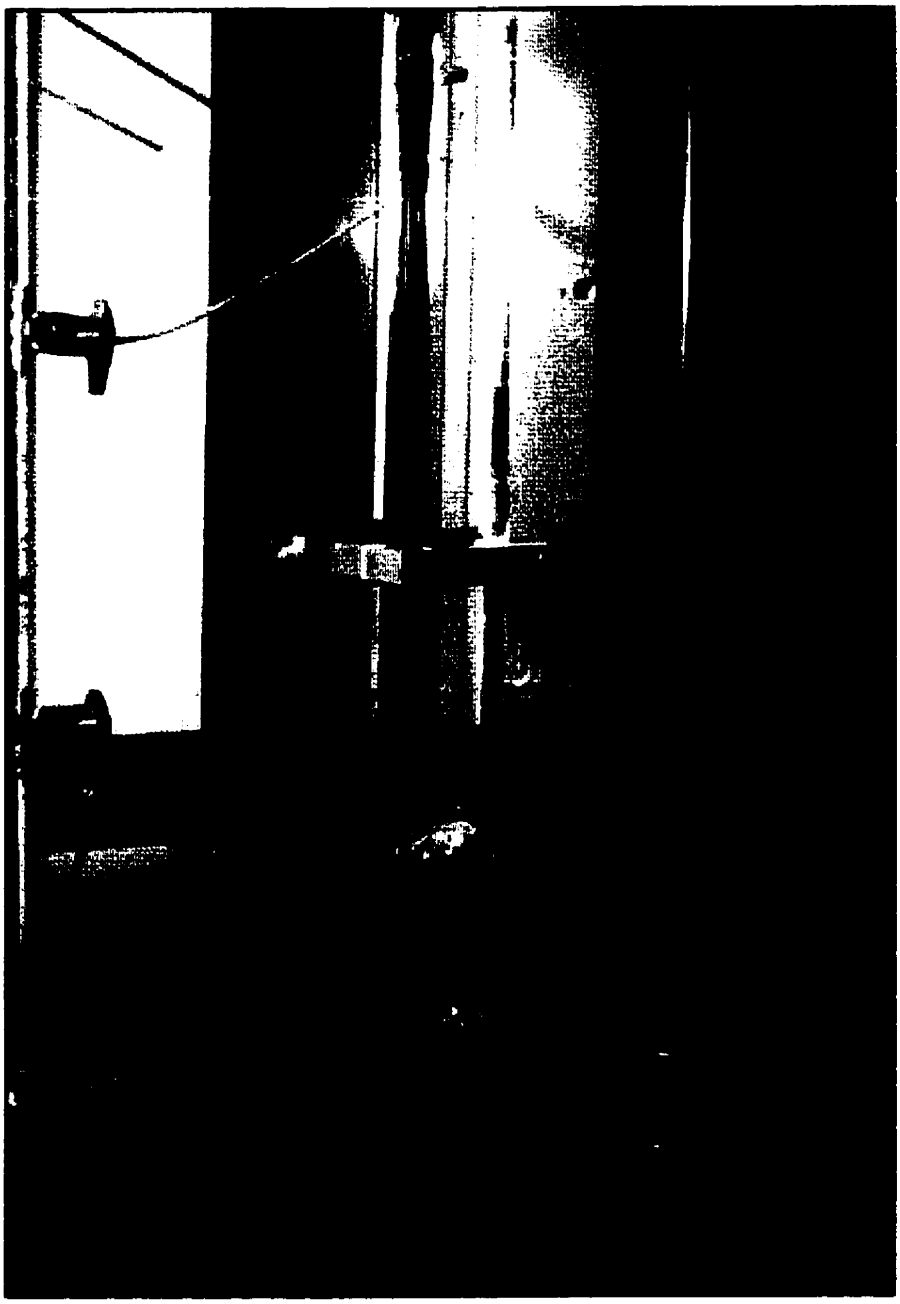

Figure 4.18: Liquid slug and gas bubble in the vertical leg, test section containing vertical and horizontal legs.

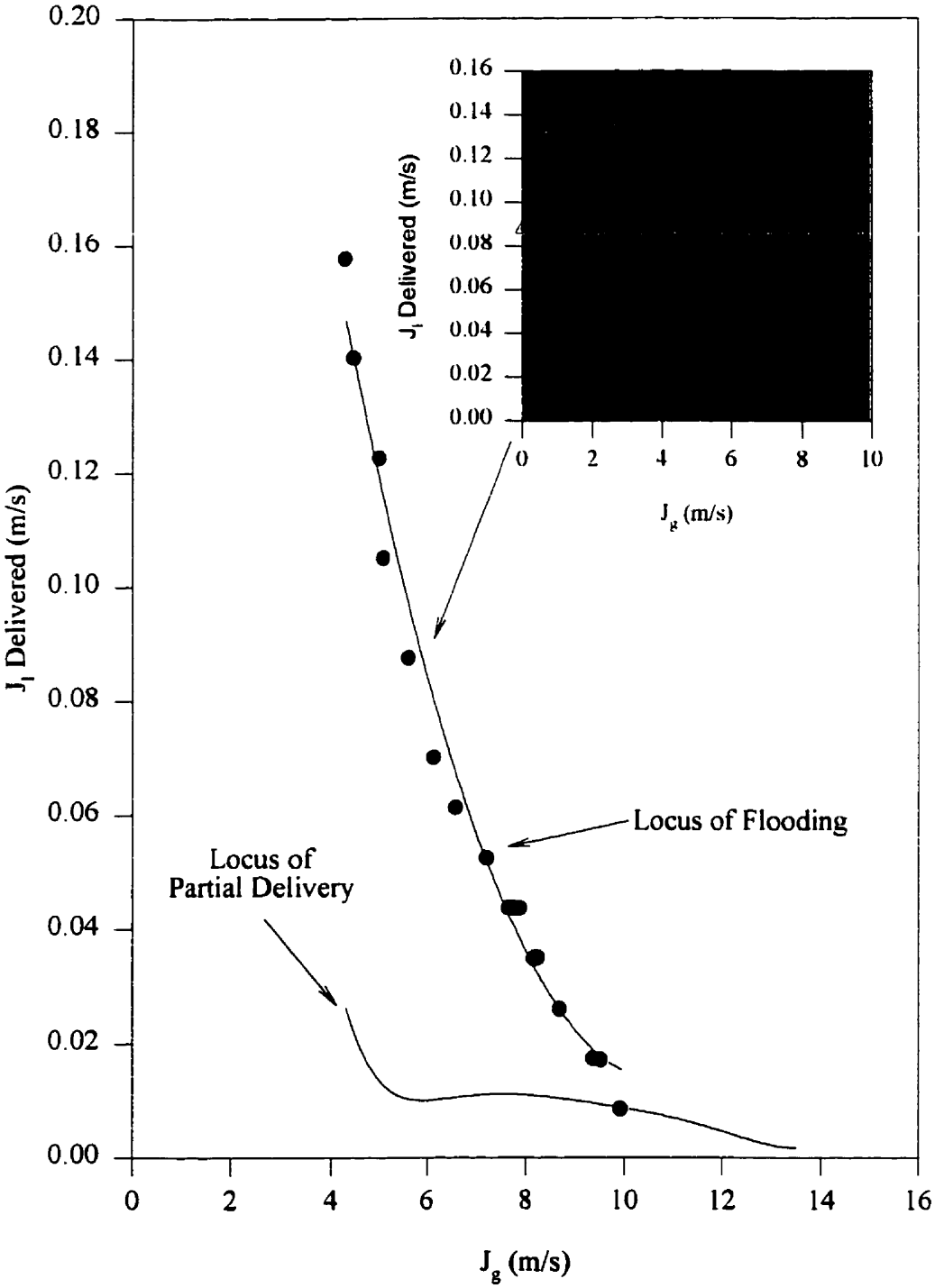

Figure 4.19: J_ℓ delivered vs. J_g and flooding points, test section with vertical leg only (no orifice).

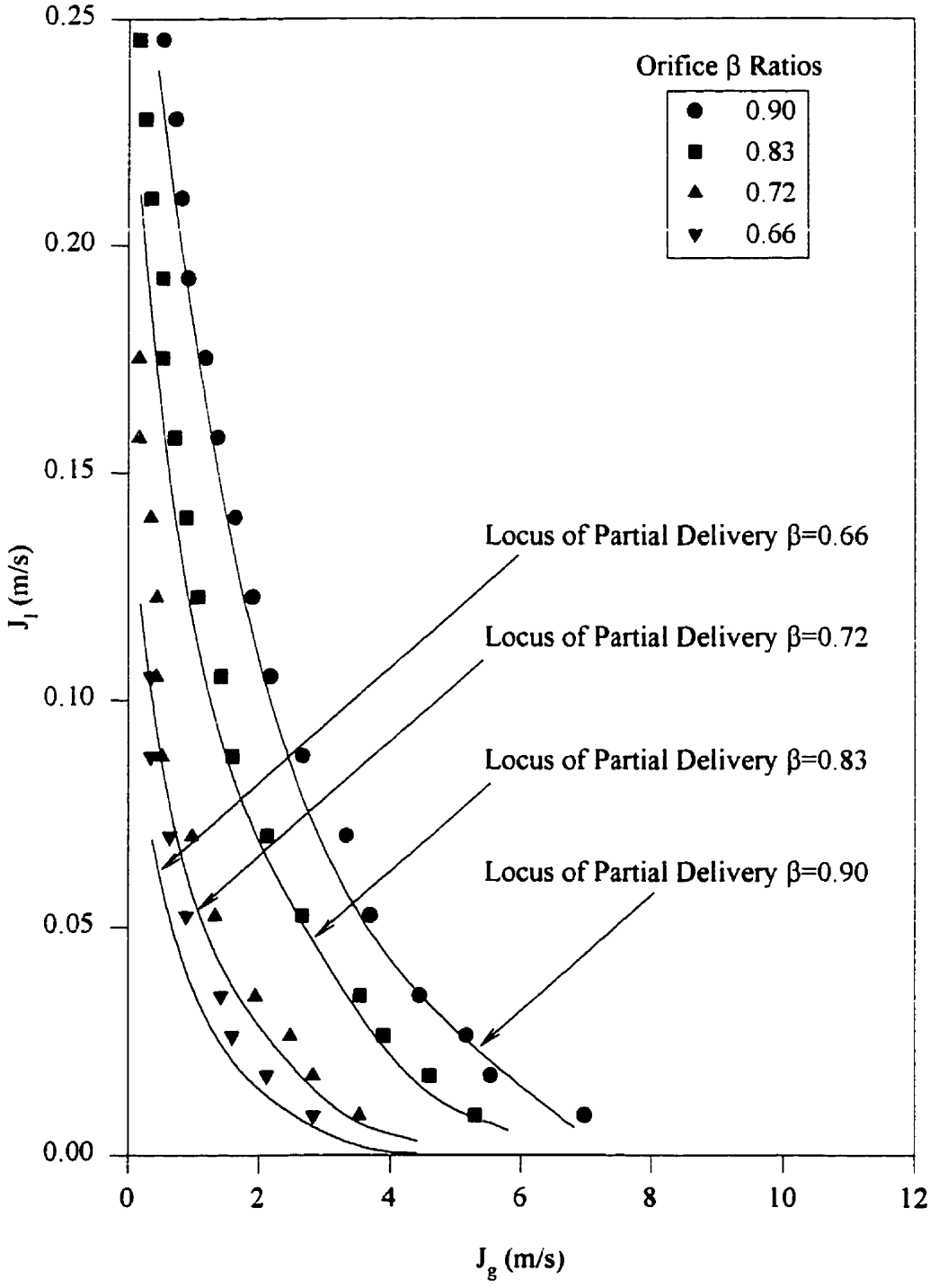

Figure 4.20: J_ℓ delivered vs. J_g and flooding points, test section with vertical leg only (orifices).

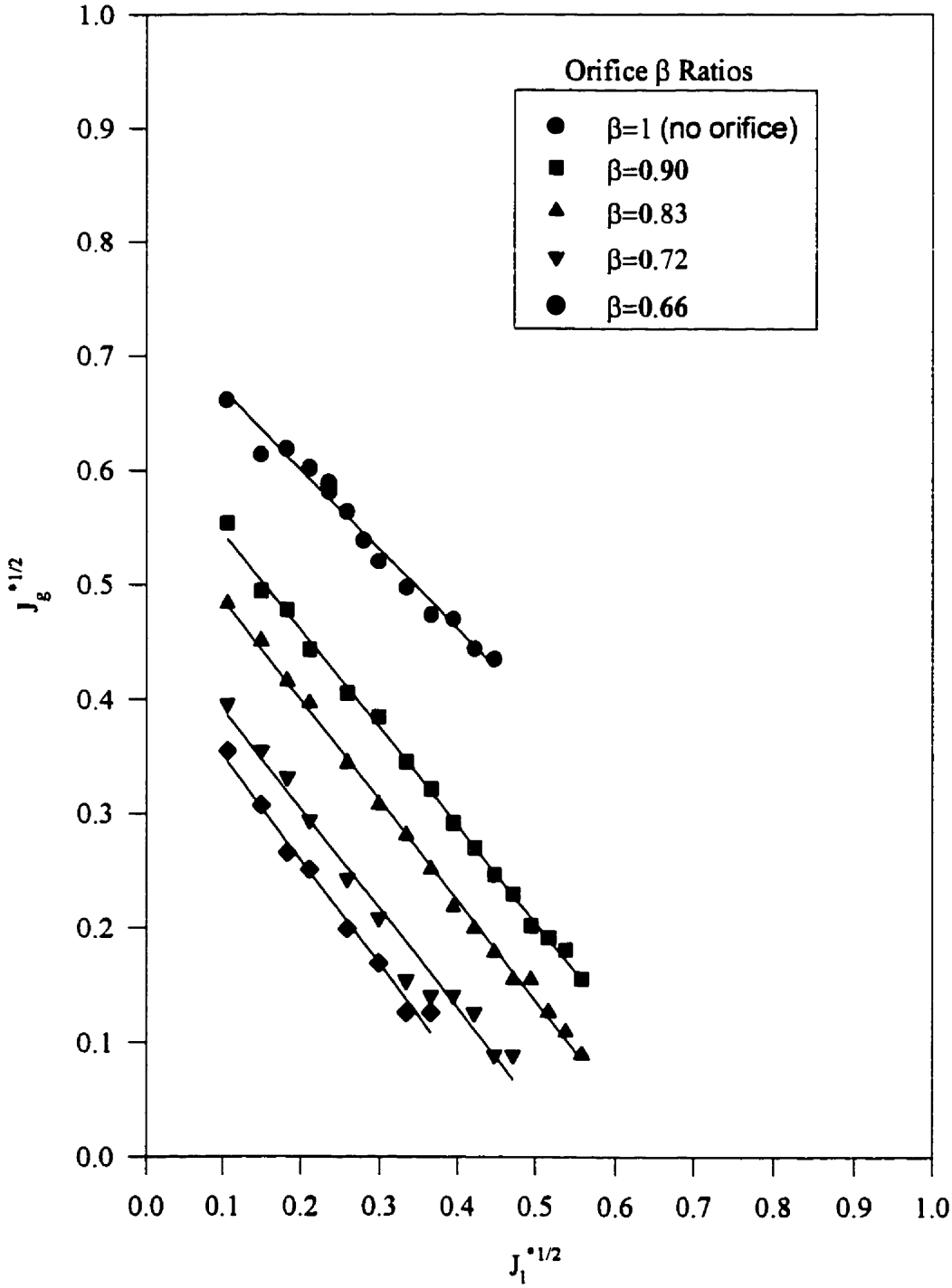

Figure 4.21: Experimental flooding points, test section with vertical leg only (all cases studied).

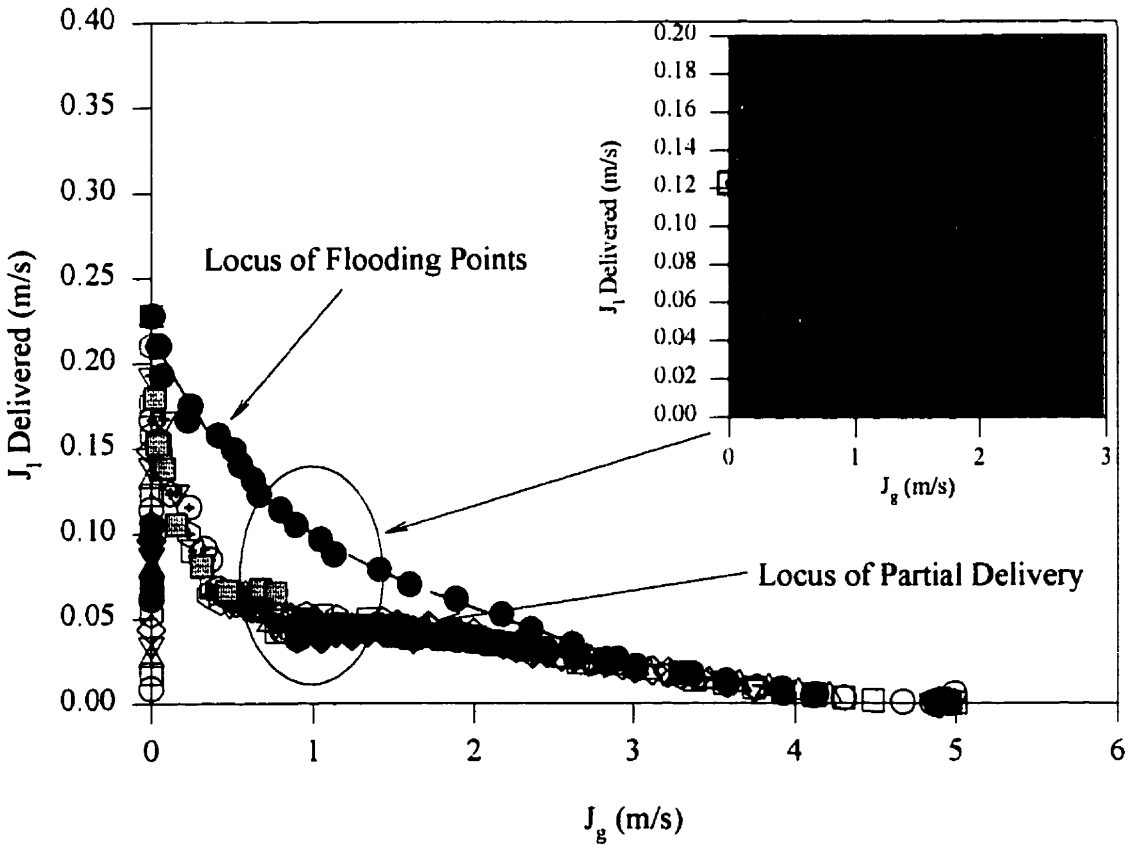

Figure 4.22: J_ℓ delivered vs. J_g and flooding points, test section with vertical and horizontal legs (orifice $\beta = 0.77$).

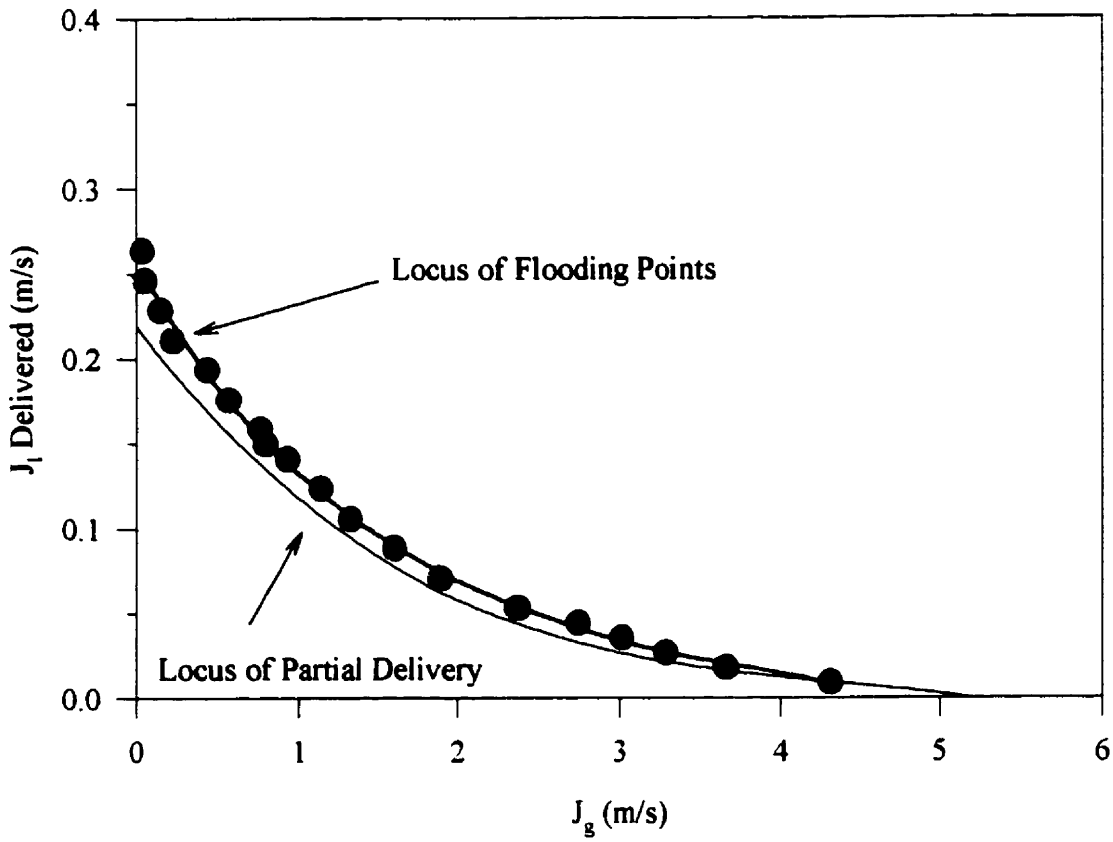

Figure 4.23: J_ℓ delivered vs. J_g and flooding points, test section with vertical and horizontal legs (no orifice).

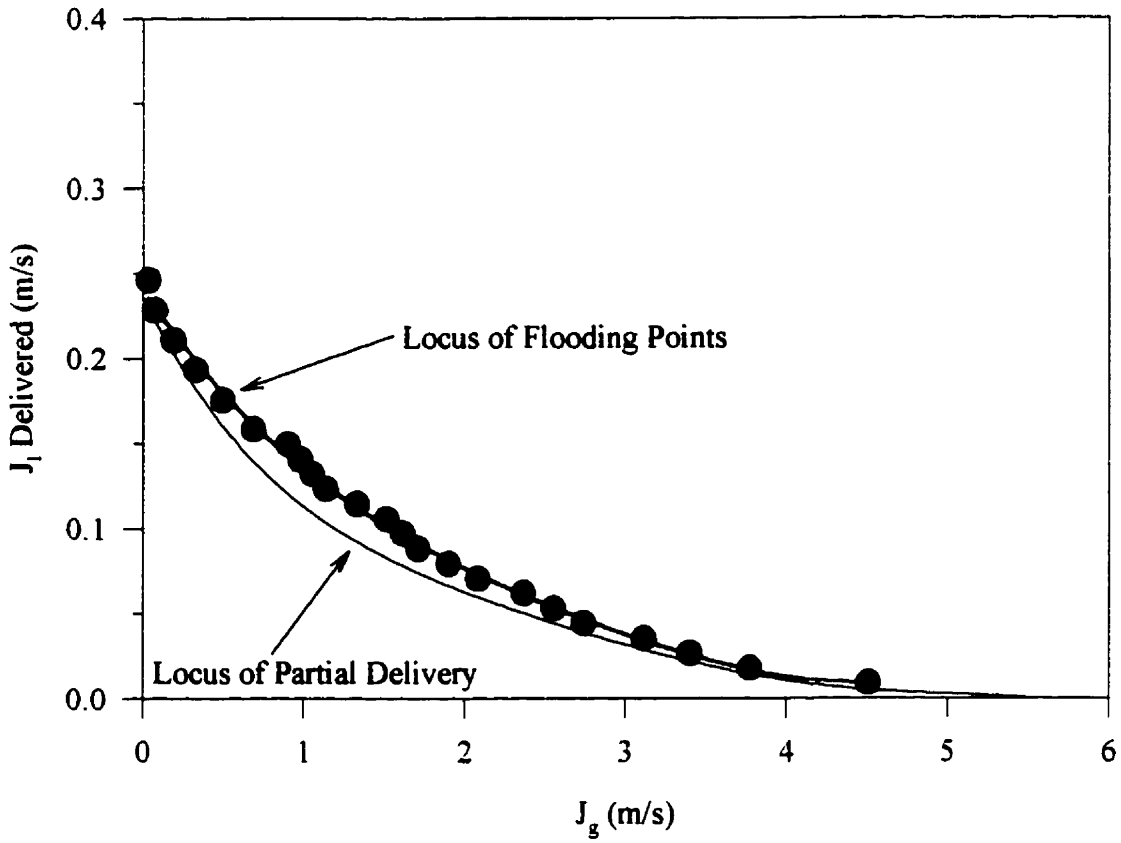

Figure 4.24: J_ℓ delivered vs. J_g and flooding points, test section with vertical and horizontal legs (orifice $\beta = 0.90$).

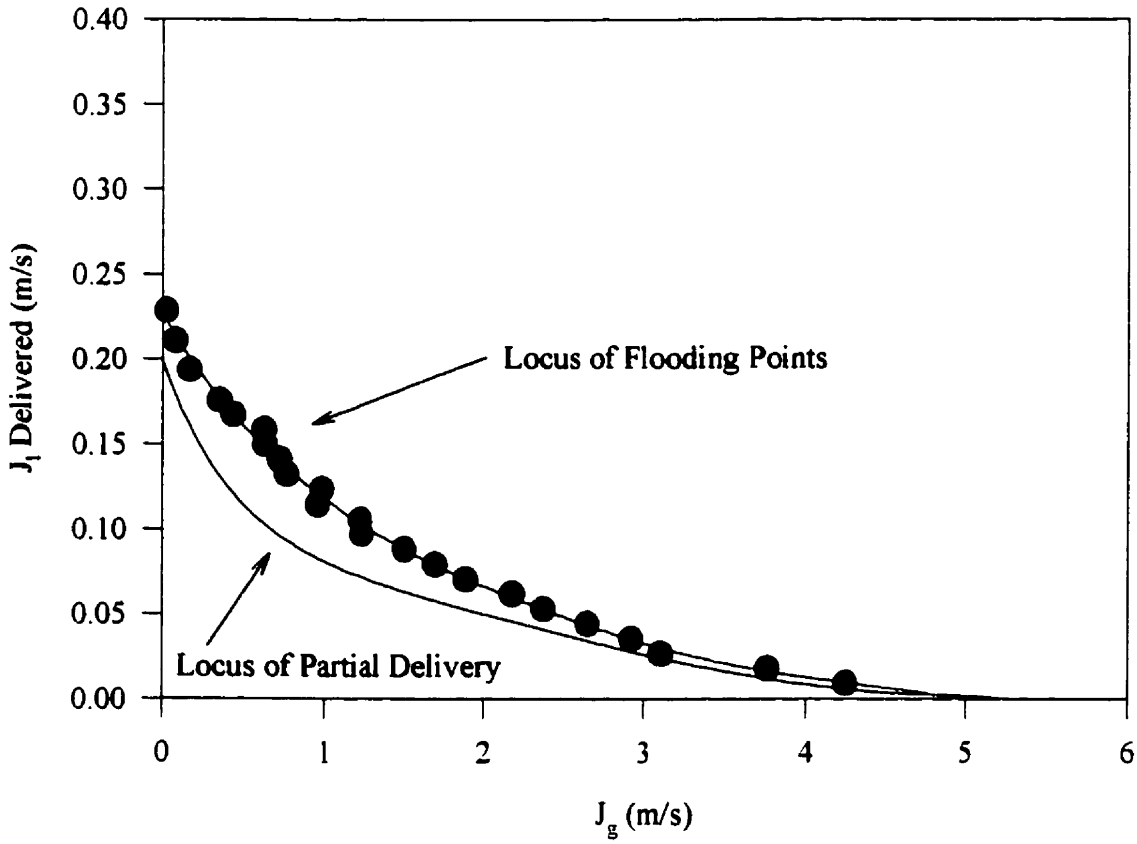

Figure 4.25: J_ℓ delivered vs. J_g and flooding points, test section with vertical and horizontal legs (orifice $\beta = 0.83$).

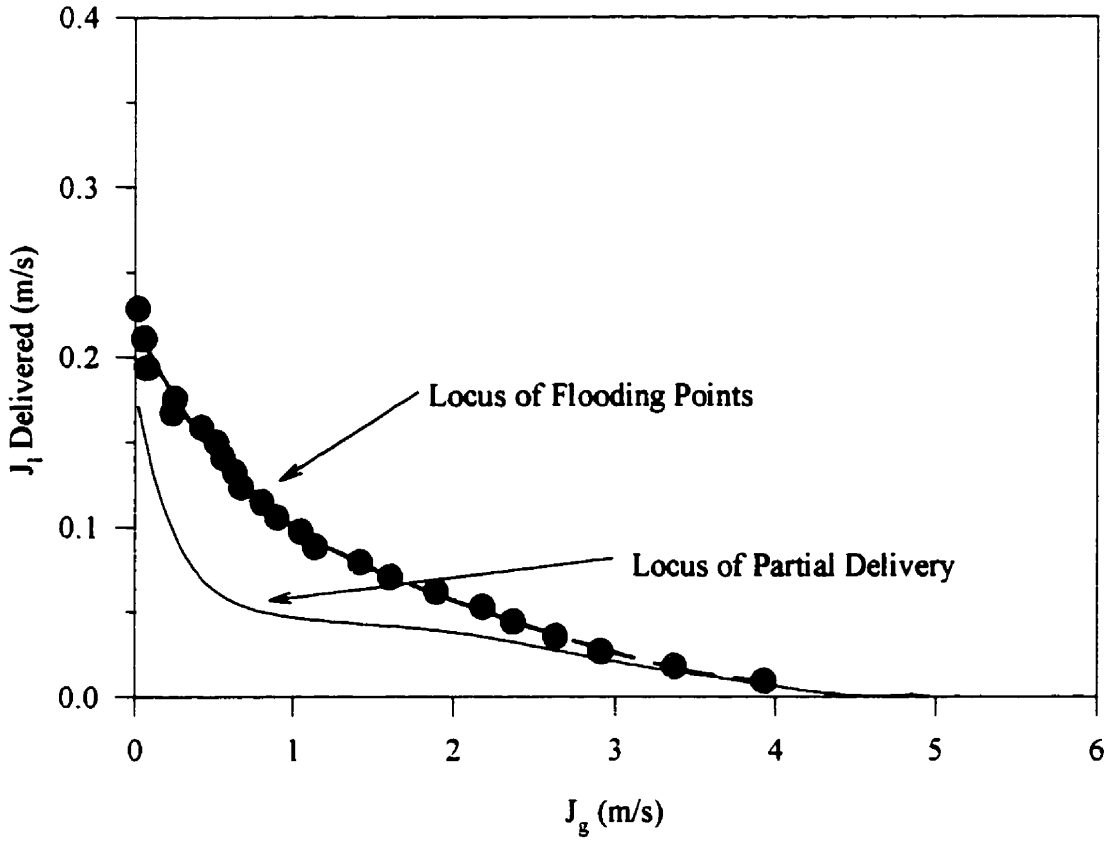

Figure 4.26: J_ℓ delivered vs. J_g and flooding points, test section with vertical and horizontal legs (orifice $\beta = 0.77$).

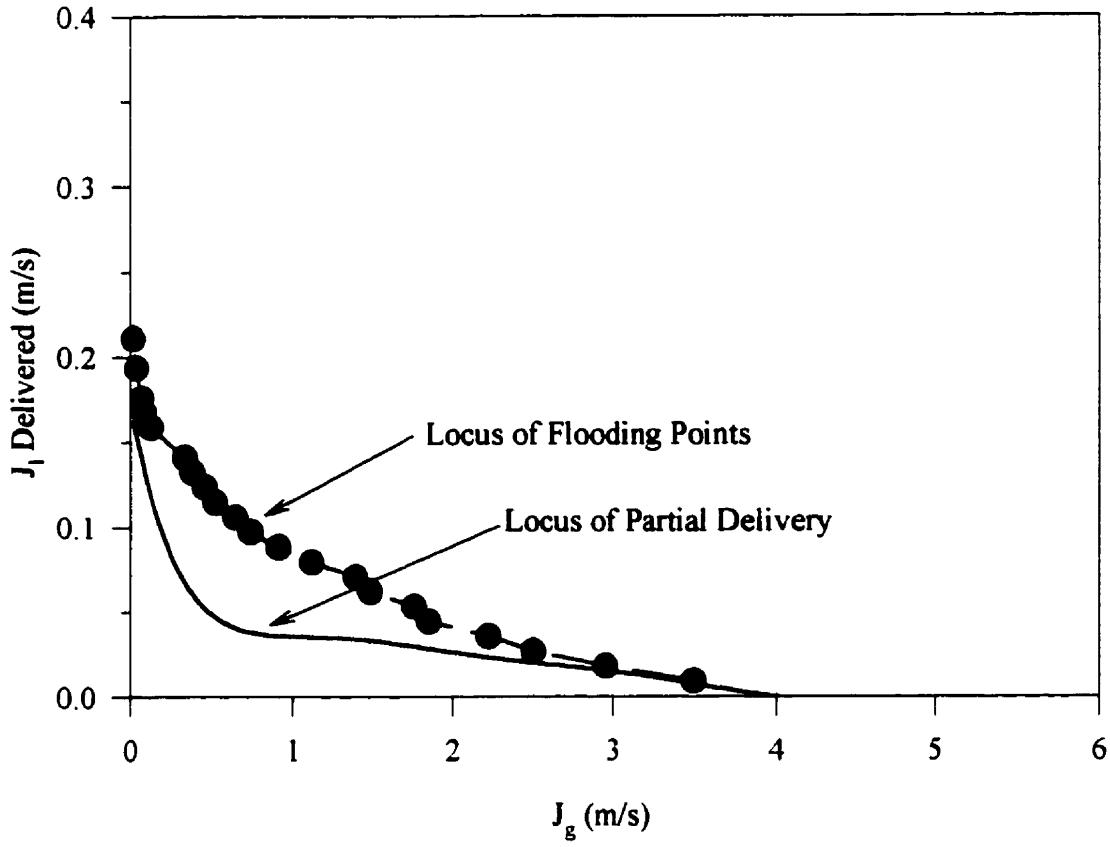

Figure 4.27: J_ℓ delivered vs. J_g and flooding points, test section with vertical and horizontal legs (orifice $\beta = 0.72$).

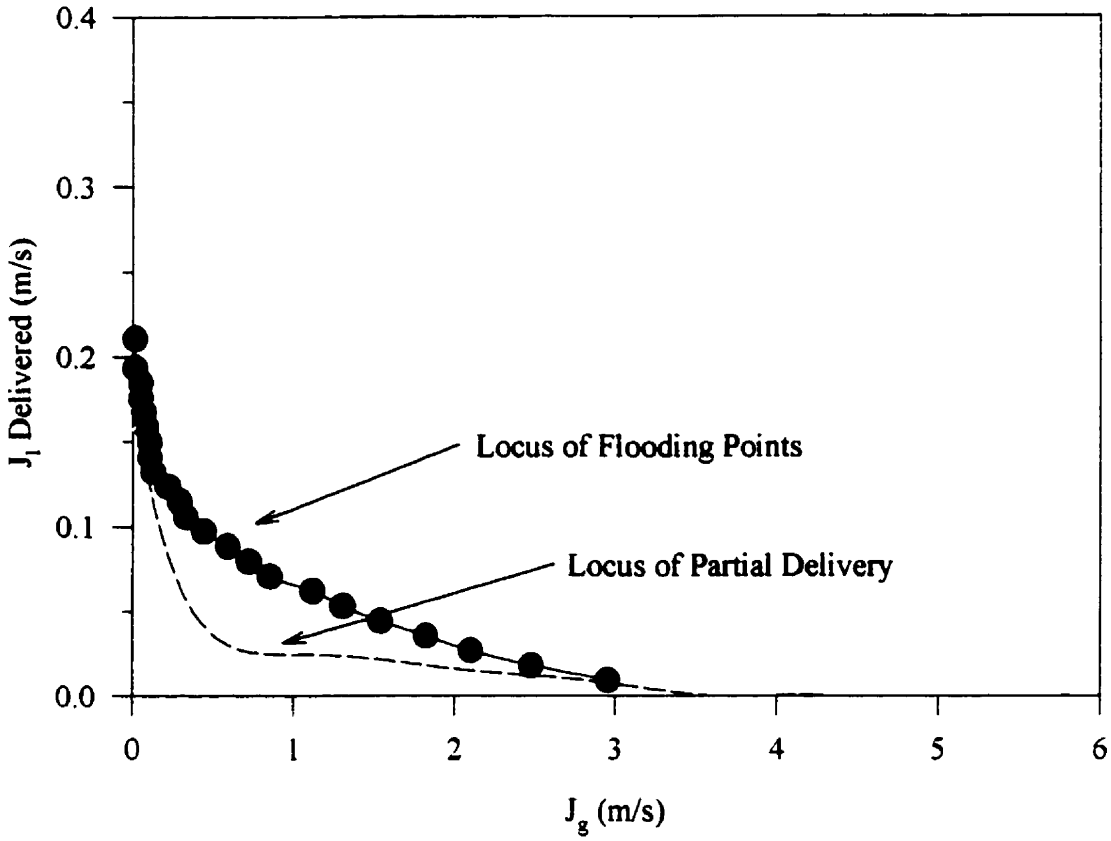

Figure 4.28: J_ℓ delivered vs. J_g and flooding points, test section with vertical and horizontal legs (orifice $\beta = 0.66$).

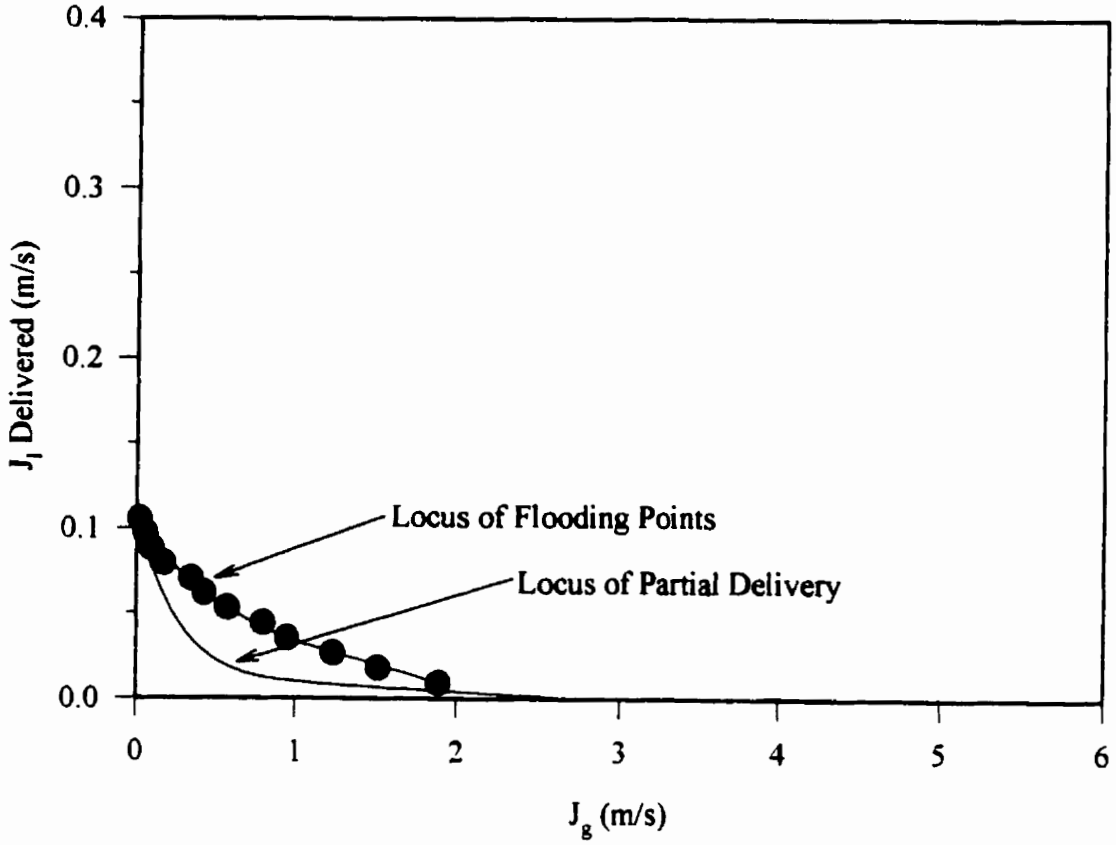

Figure 4.29: J_ℓ delivered vs. J_g and flooding points, test section with vertical and horizontal legs (orifice $\beta = 0.55$).

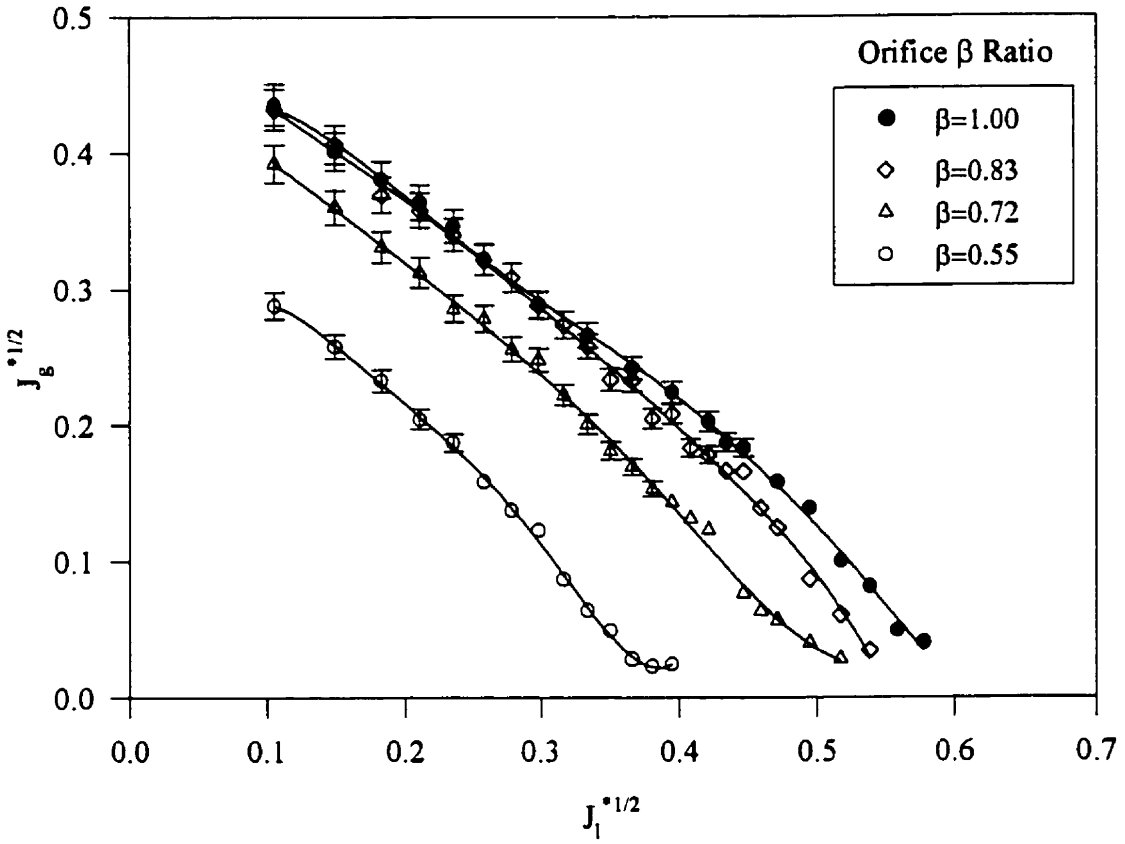

Figure 4.30: Flooding points, test section with vertical and horizontal legs

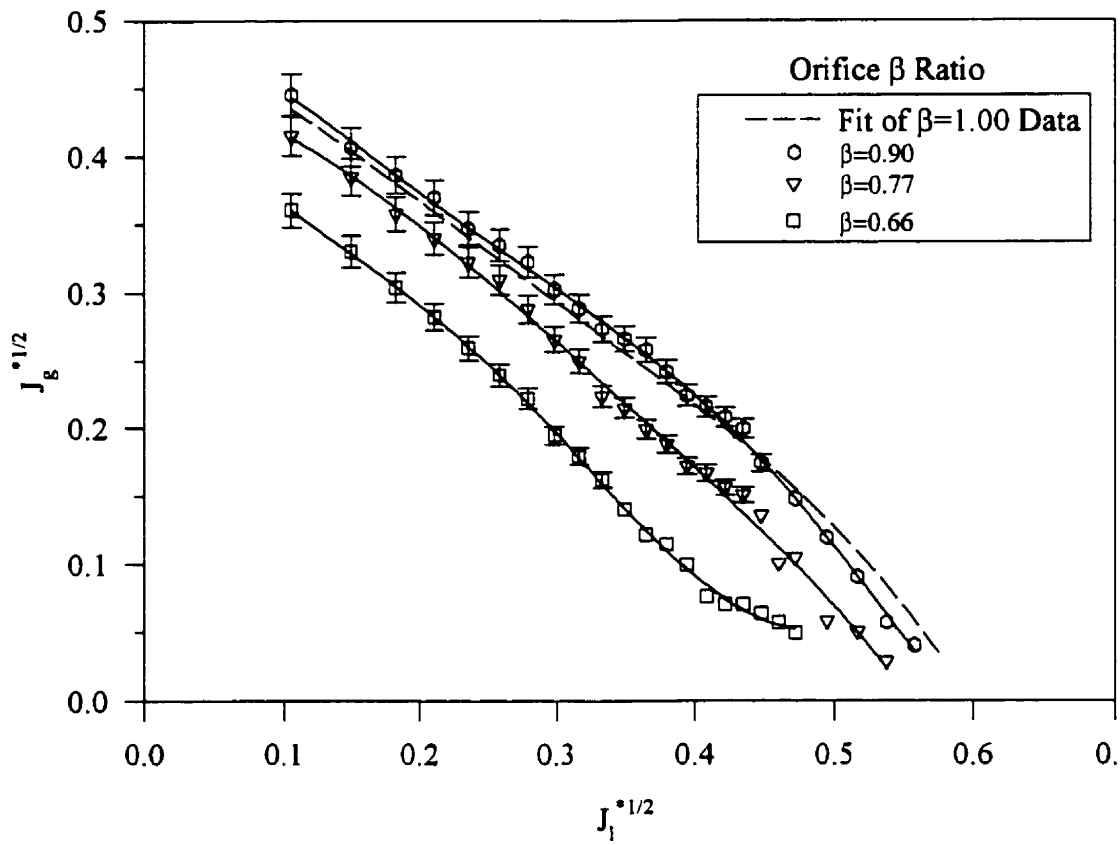

Figure 4.31: Flooding points, test section with vertical and horizontal legs (cont.)

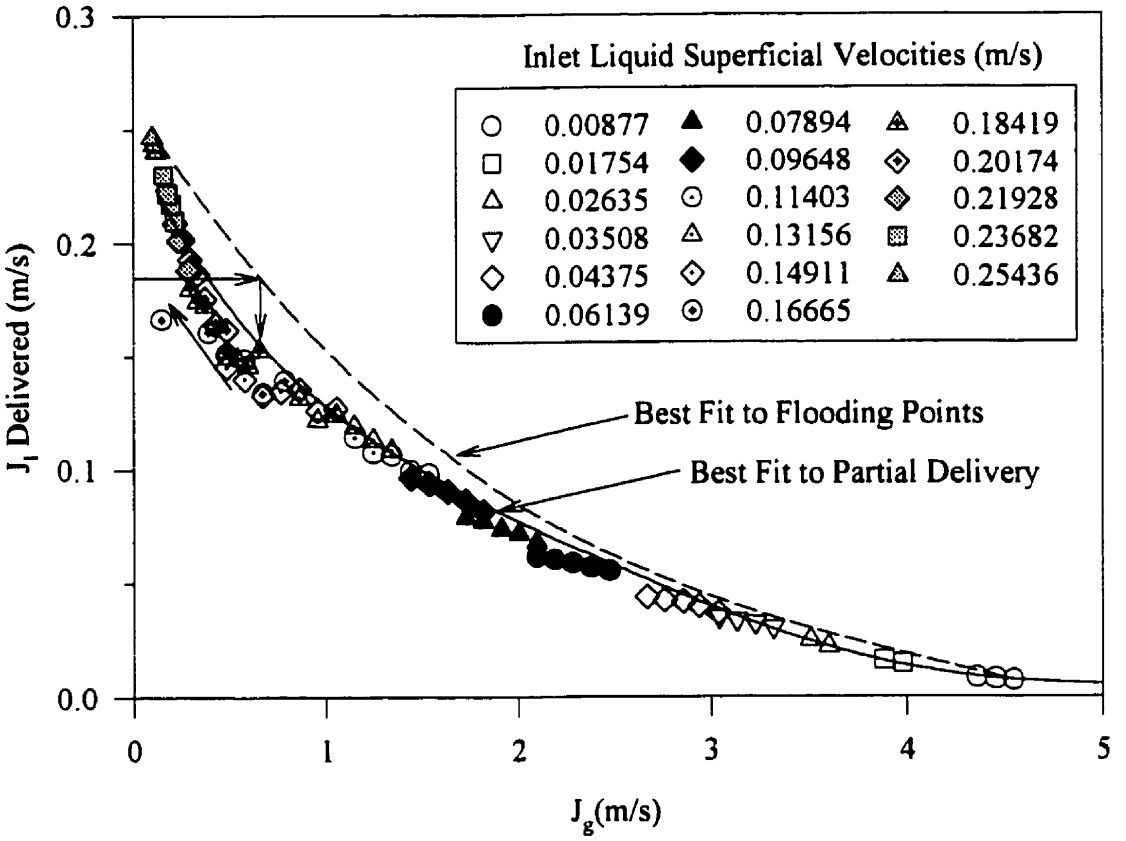

Figure 4.32: Partial delivery results with decreasing gas flow, test section with vertical and horizontal legs (no orifice)

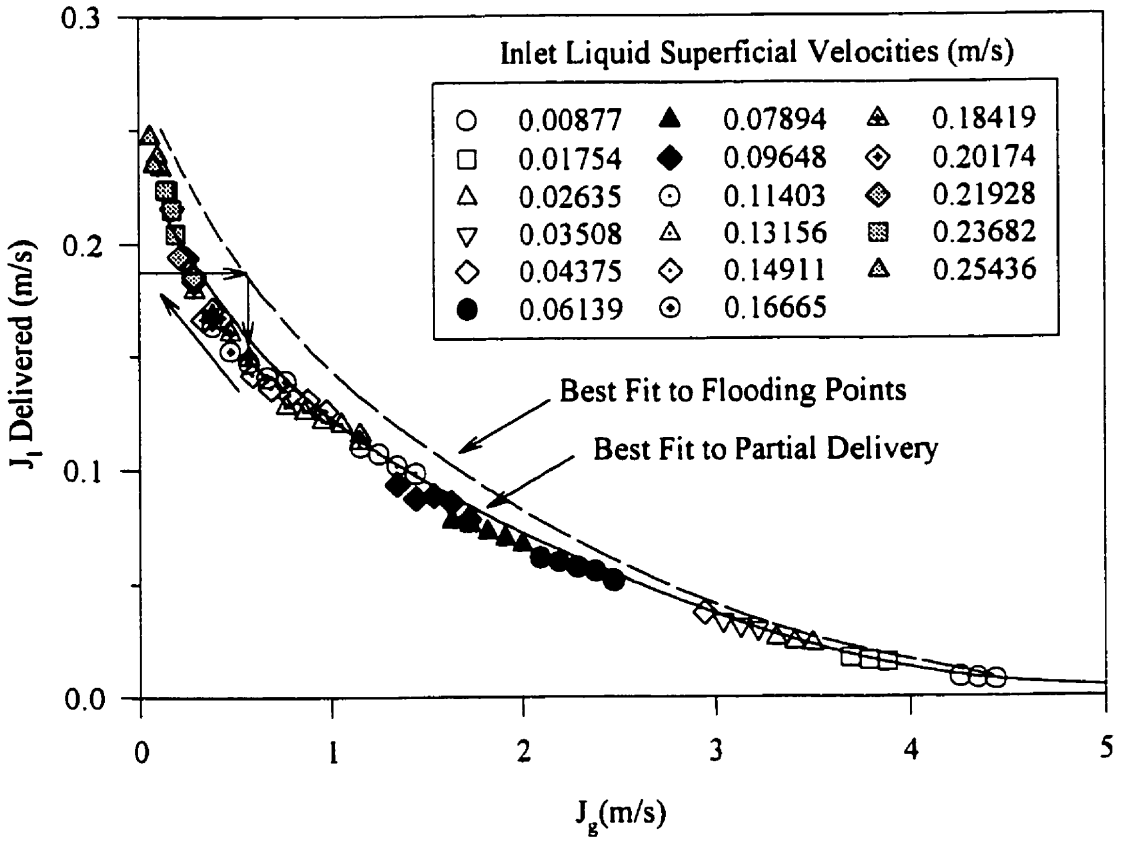

Figure 4.33: Partial delivery results with decreasing gas flow, test section with vertical and horizontal legs (orifice $\beta = 0.90$)

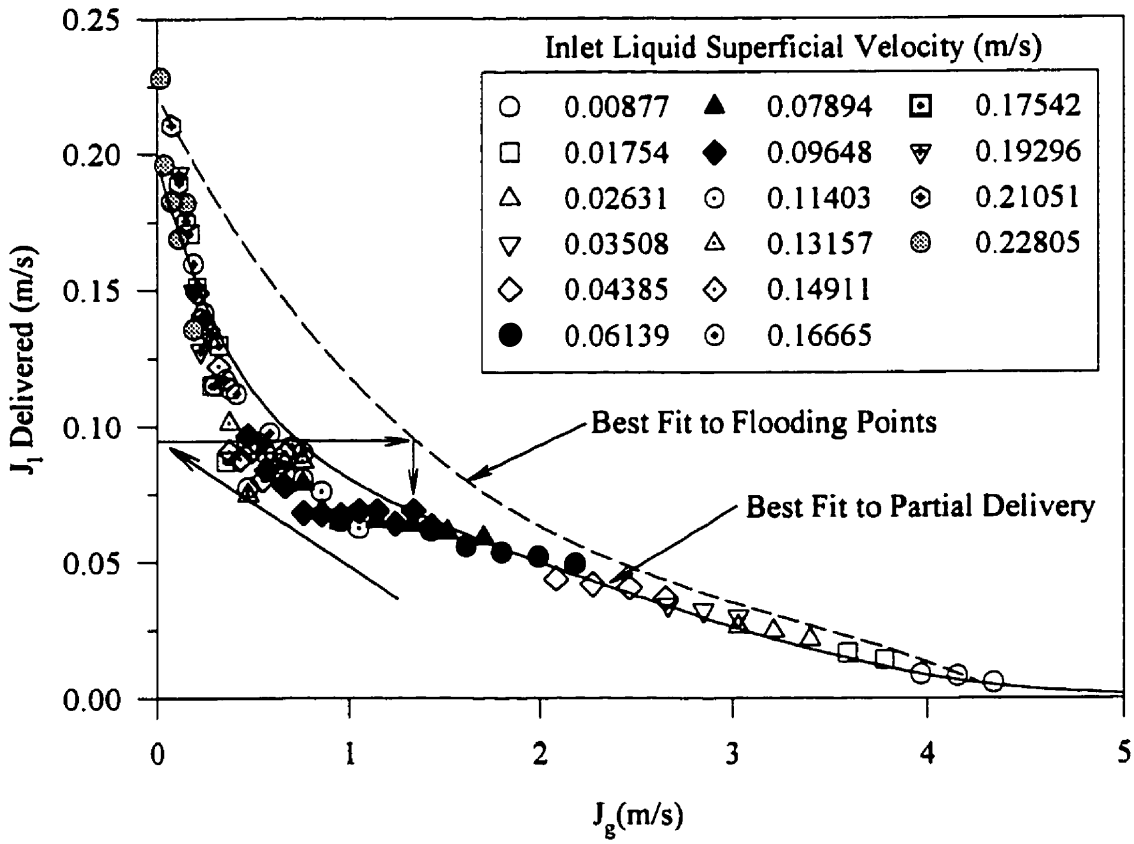

Figure 4.34: Partial delivery results with decreasing gas flow, test section with vertical and horizontal legs (orifice $\beta = 0.83$)

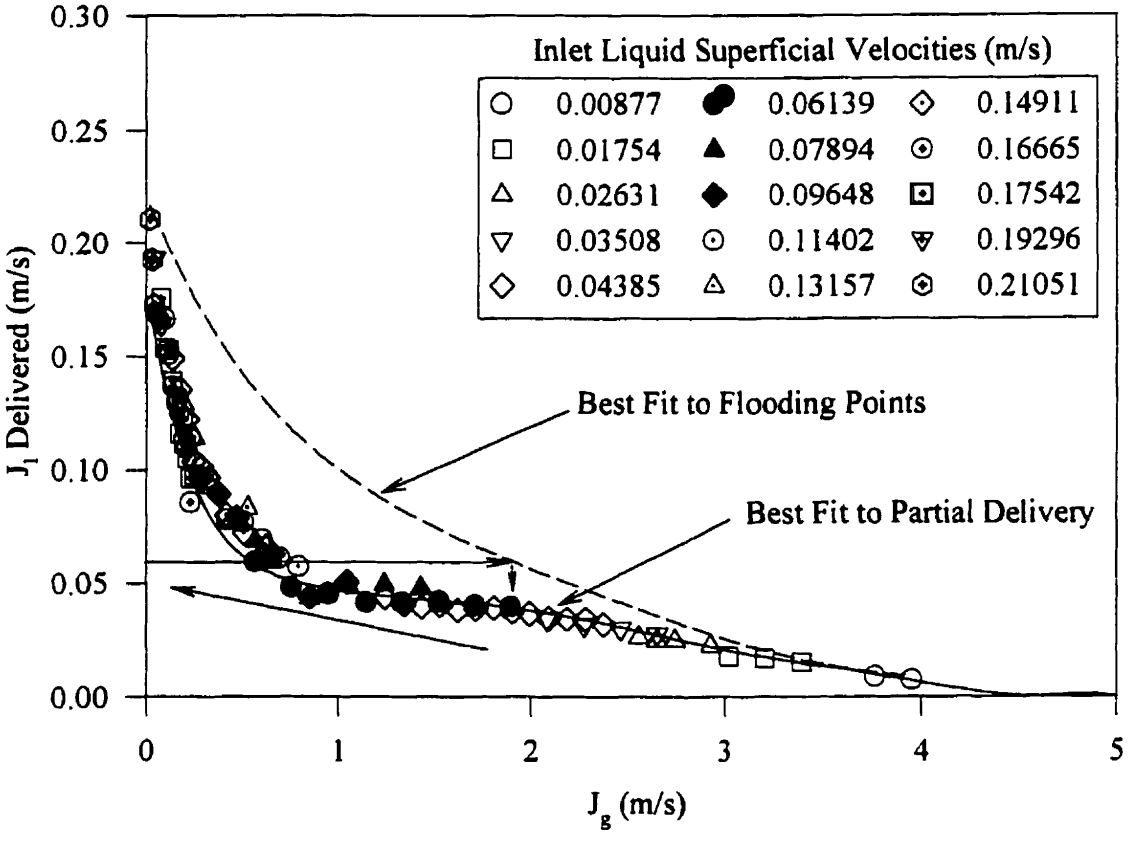

Figure 4.35: Partial delivery results with decreasing gas flow, test section with vertical and horizontal legs (orifice $\beta = 0.77$)

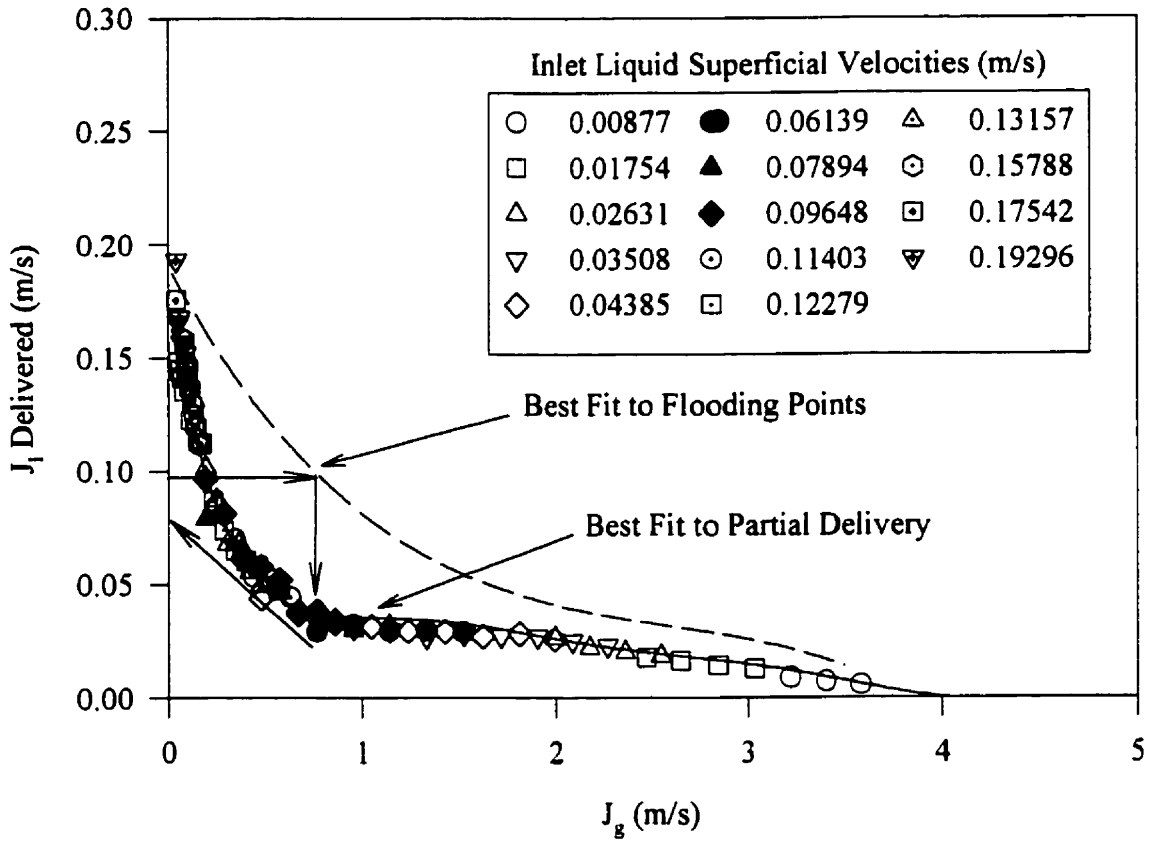

Figure 4.36: Partial delivery results with decreasing gas flow, test section with vertical and horizontal legs (orifice $\beta = 0.72$)

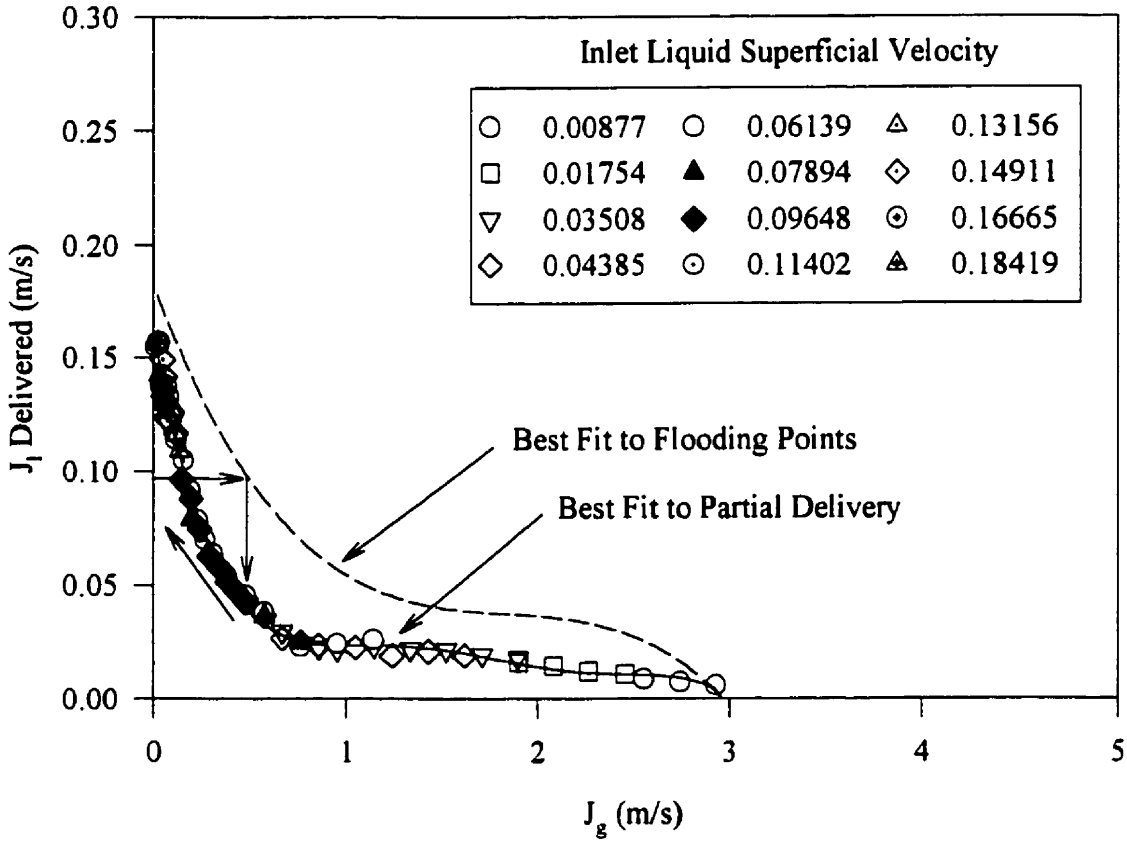

Figure 4.37: Partial delivery results with decreasing gas flow, test section with vertical and horizontal legs (orifice $\beta = 0.66$)

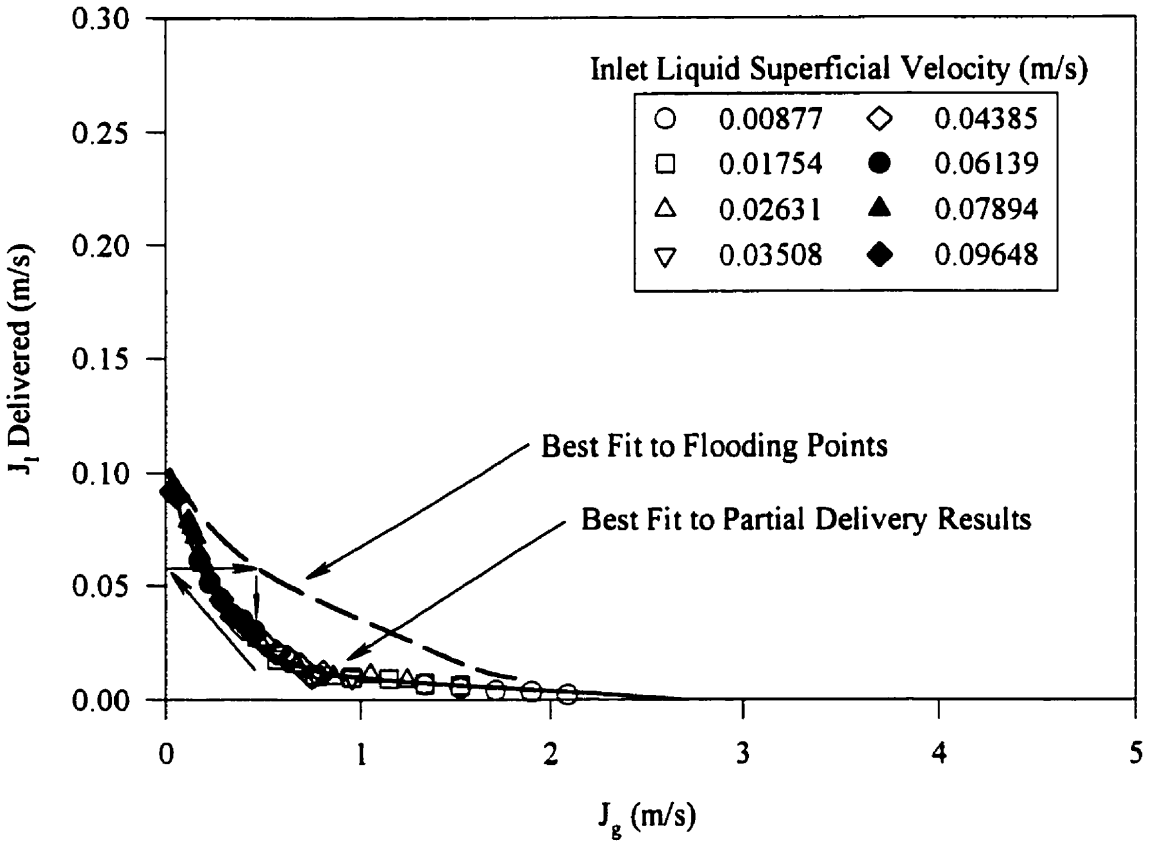

Figure 4.38: Partial delivery results with decreasing gas flow, test section with vertical and horizontal legs (orifice $\beta = 0.55$)

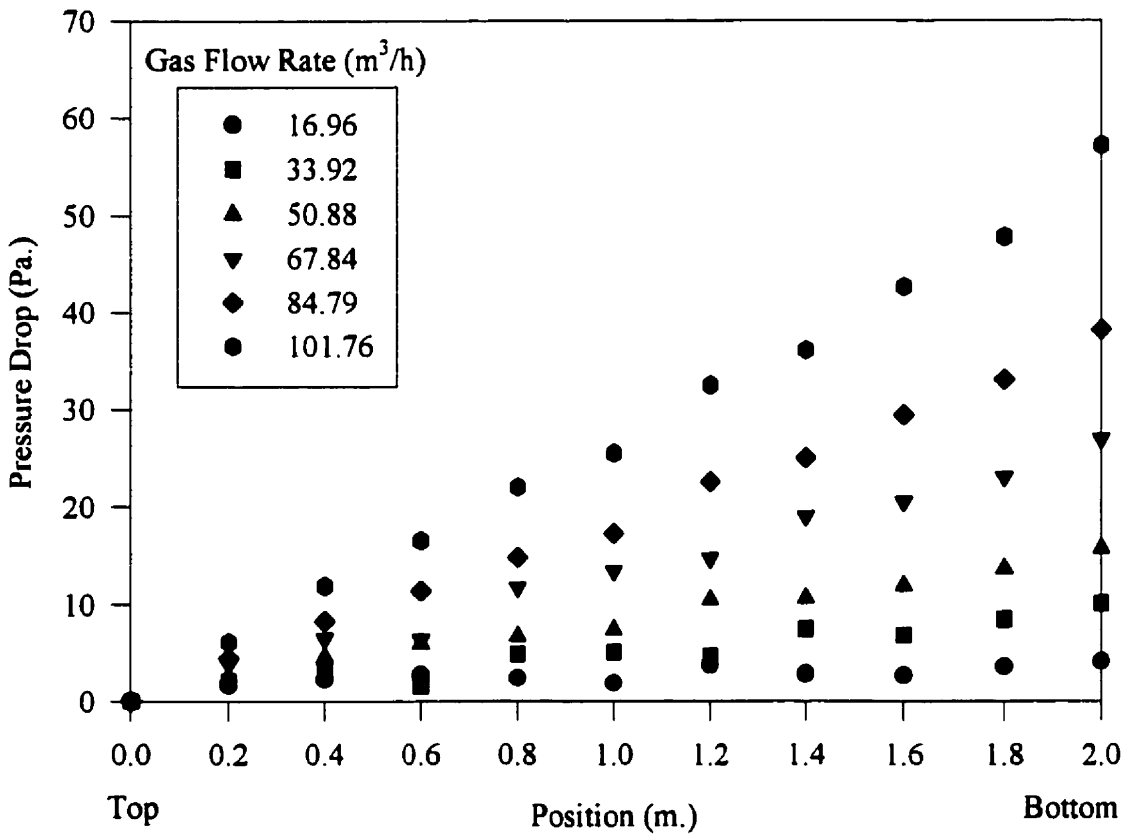

Figure 4.39: Pressure drop $Q_l = 0.1$ (m^3/h), test section with vertical leg only.

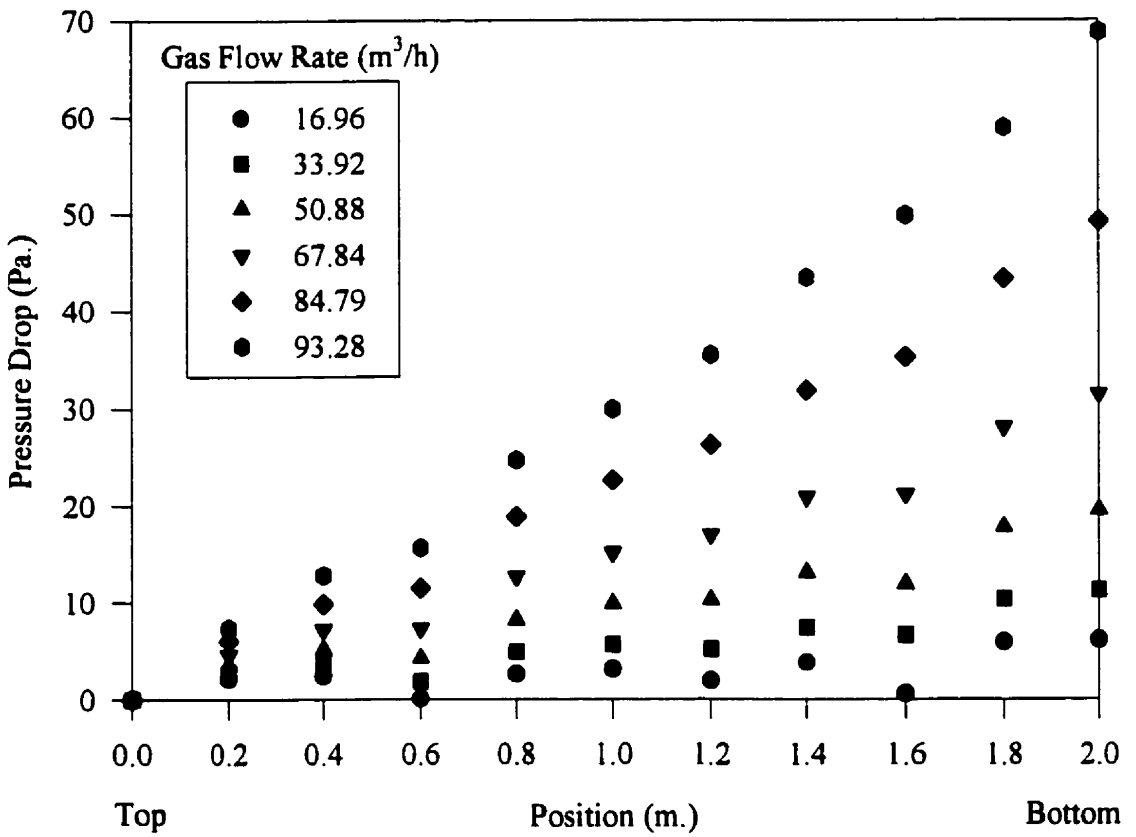

Figure 4.40: Pressure drop $Q_l = 0.25$ (m^3/h), test section with vertical leg only.

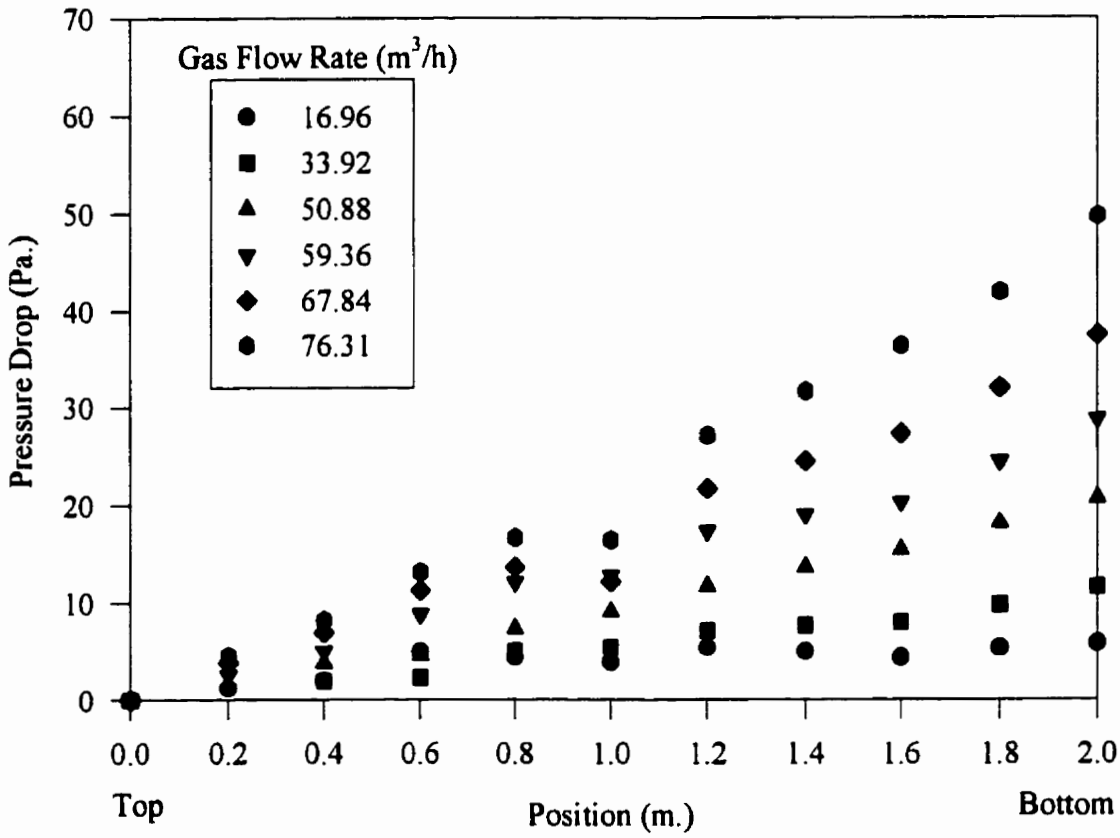

Figure 4.41: Pressure drop $Q_l = 0.5$ (m^3/h), test section with vertical leg only.

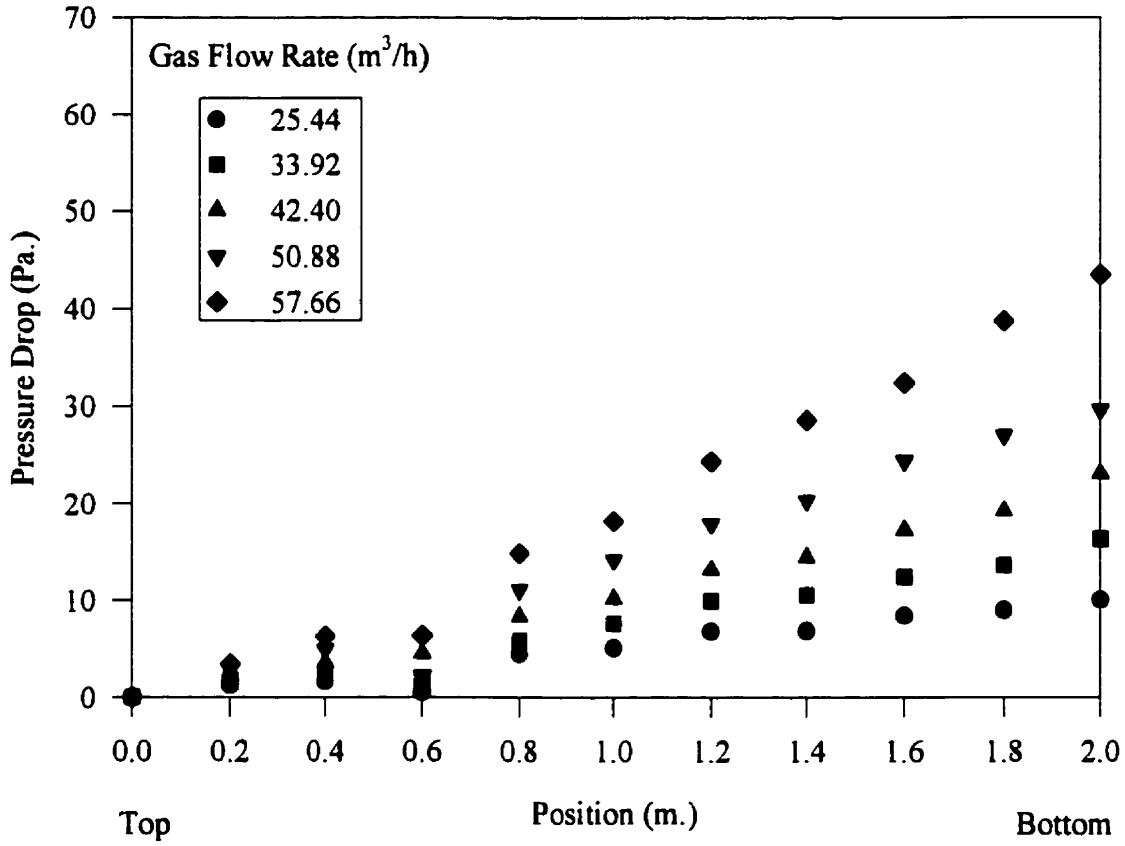

Figure 4.42: Pressure drop $Q_l = 1.0$ (m^3/h), test section with vertical leg only.

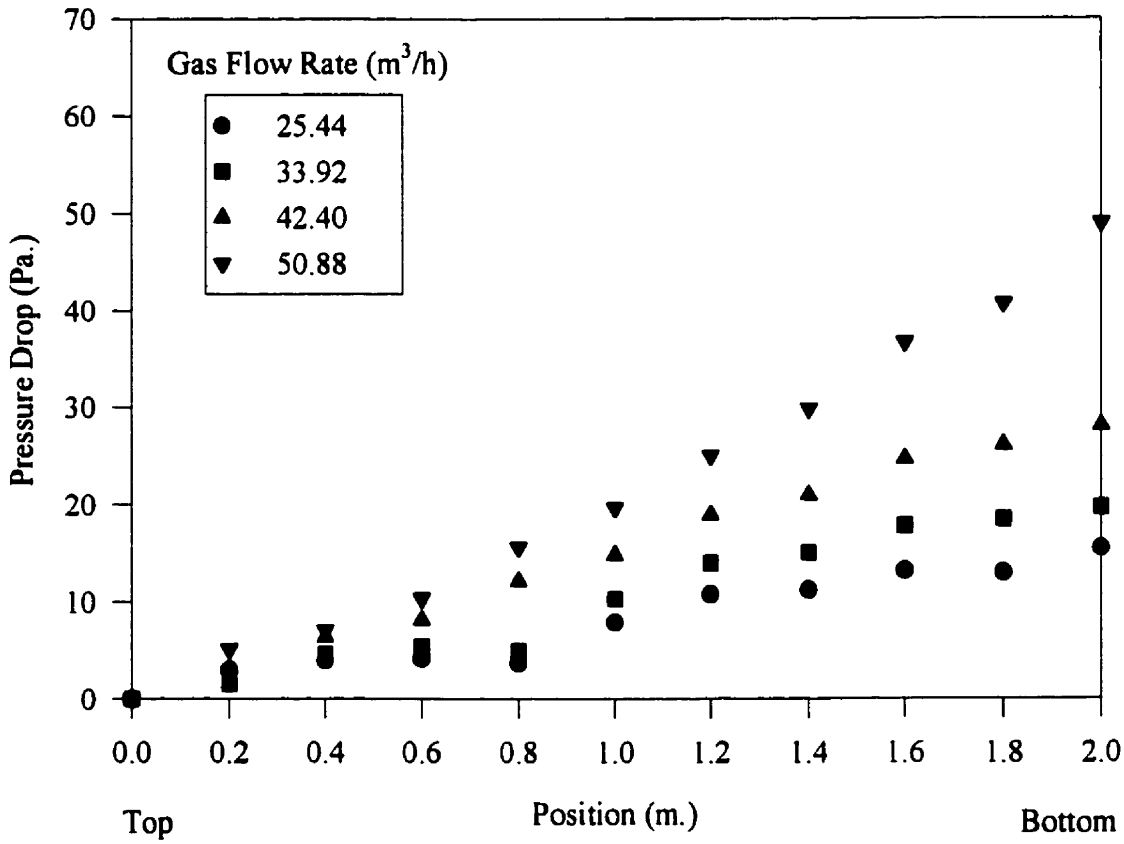

Figure 4.43: Pressure drop $Q_l = 1.5$ (m^3/h), test section with vertical leg only.

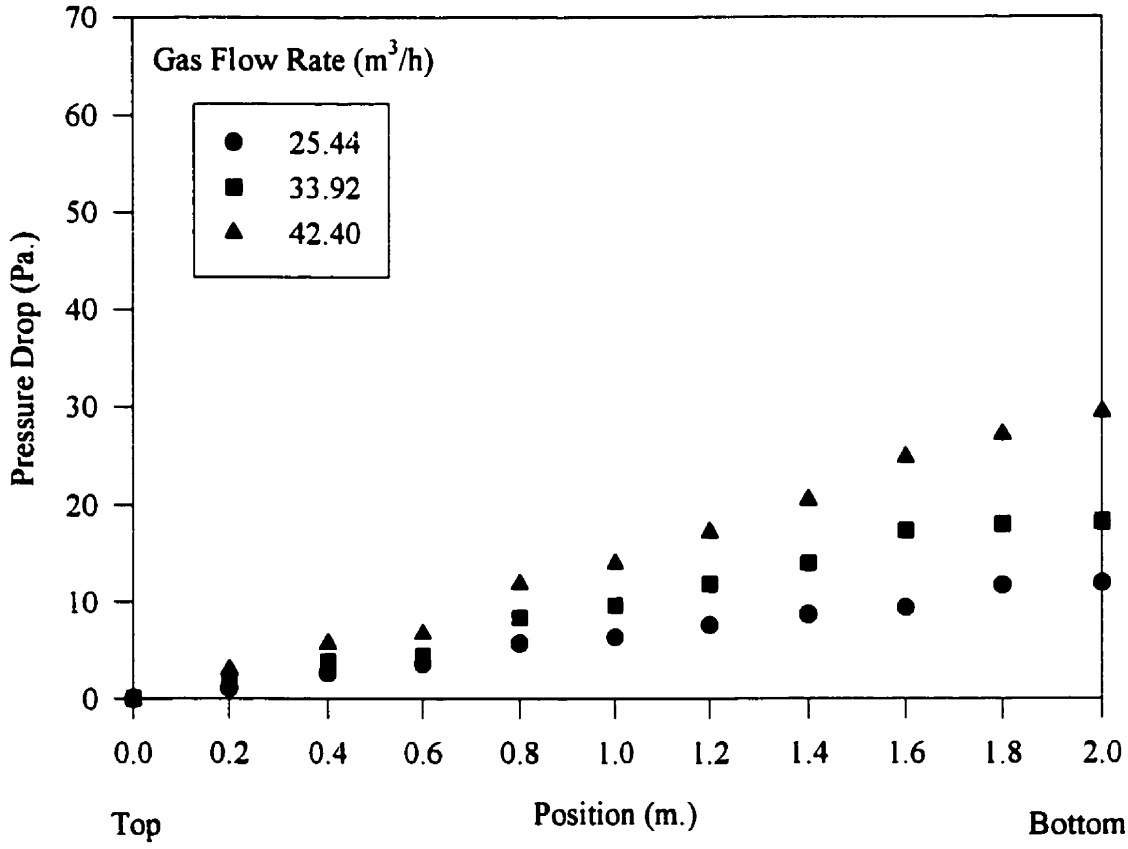

Figure 4.44: Pressure drop $Q_l = 1.75$ (m^3/h), test section with vertical leg only.

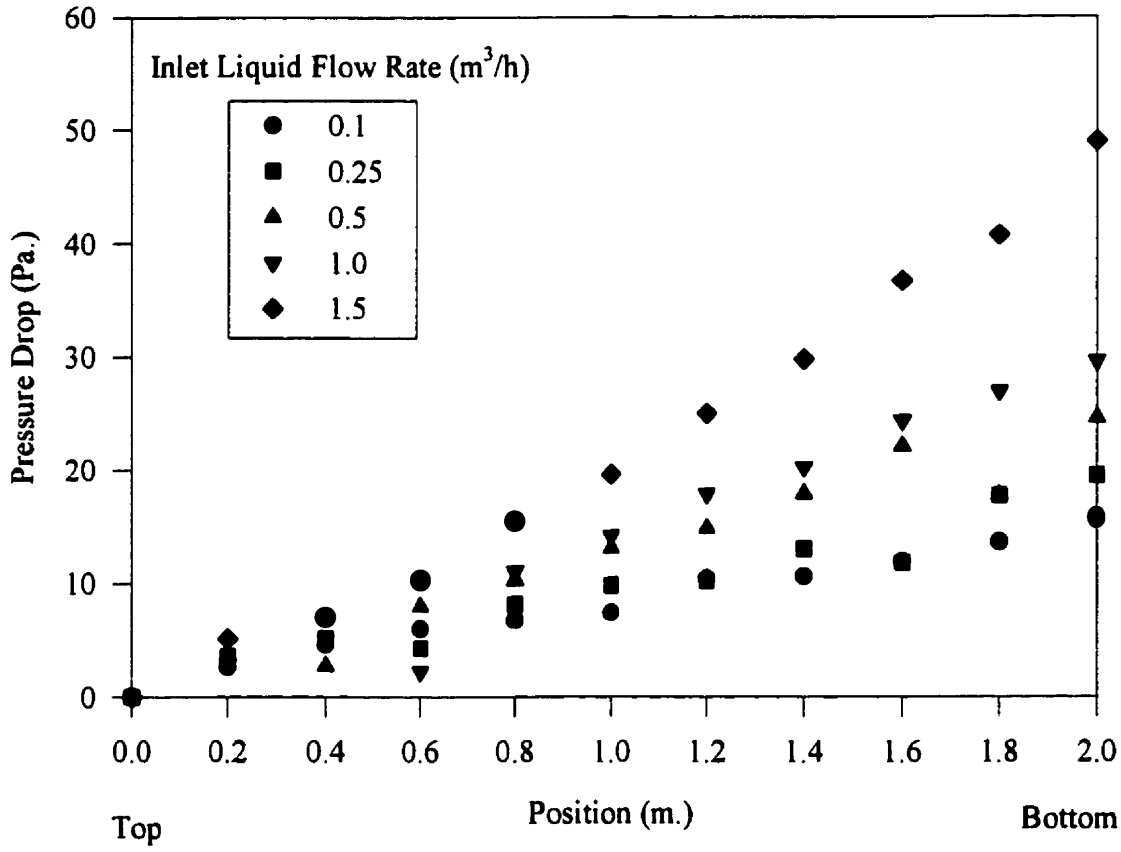

Figure 4.45: Pressure drop $Q_g = 50.88$ (m^3/h) for various liquid flow rates, test section with vertical leg only.

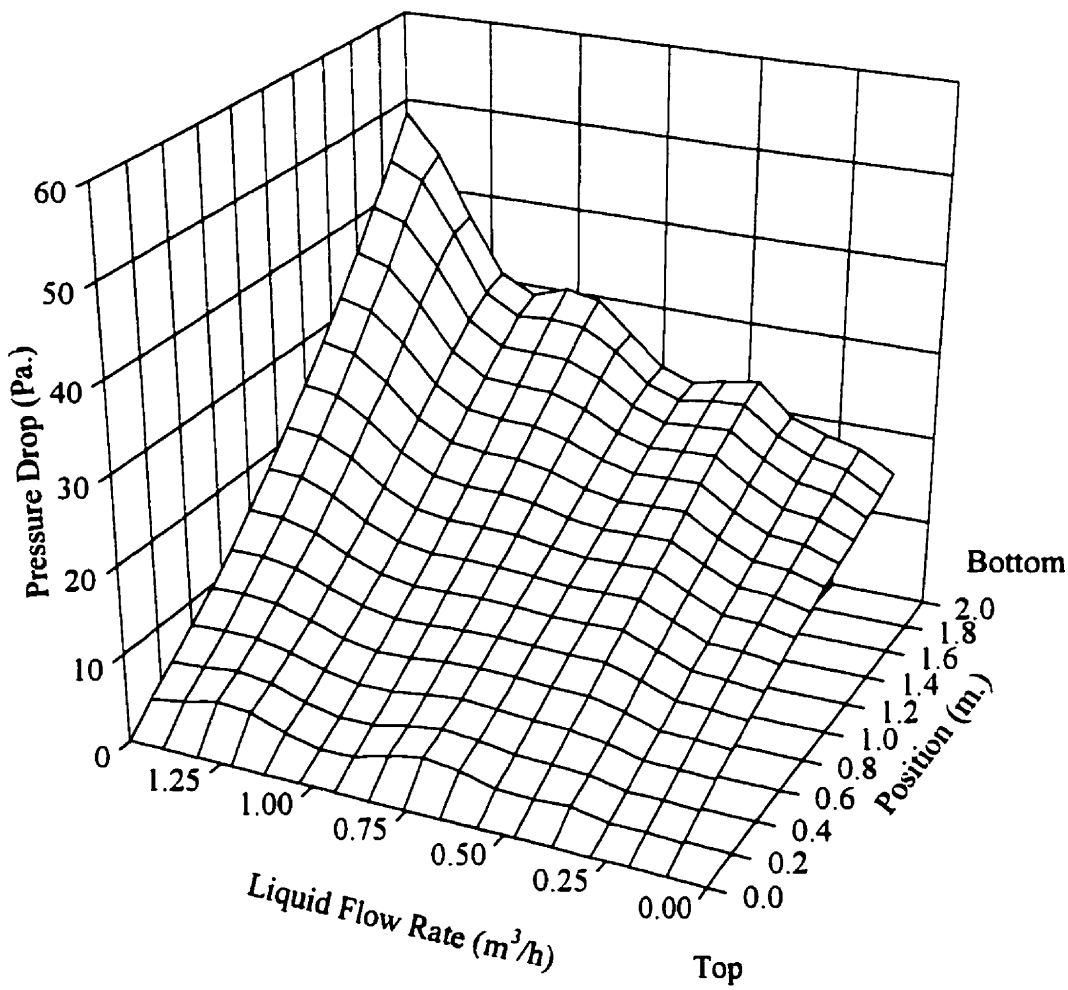

Figure 4.46: Three dimensional view of pressure drop $Q_g = 50.88$ (m^3/h) for various liquid flow rates, test section with vertical leg only.

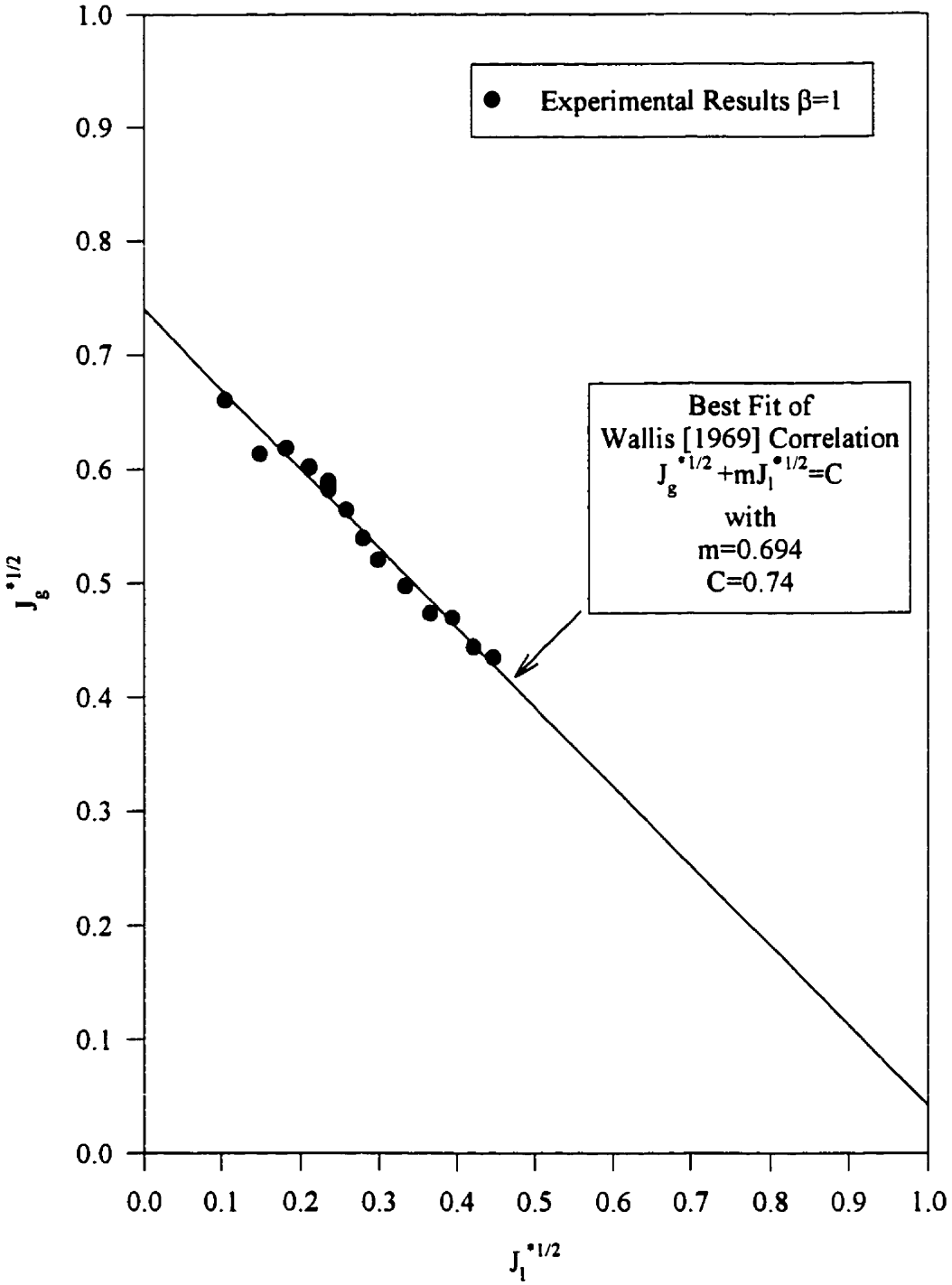

Figure 4.47: Comparison of flooding points obtained in the test section with a vertical leg only and Wallis' correlation (no orifice).

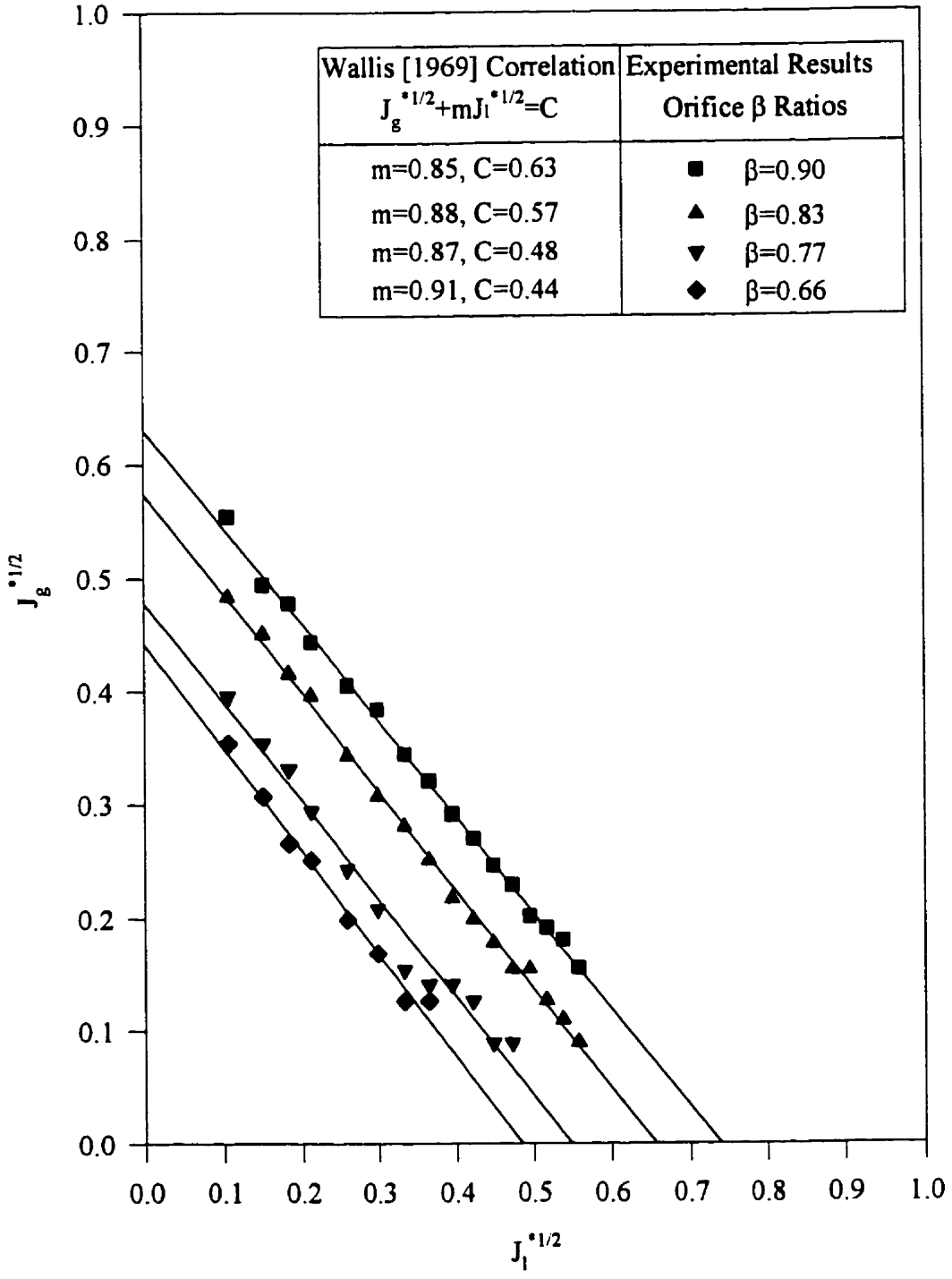

Figure 4.48: Comparison of flooding points obtained in the test section with a vertical leg only and Wallis' correlation (orifices).

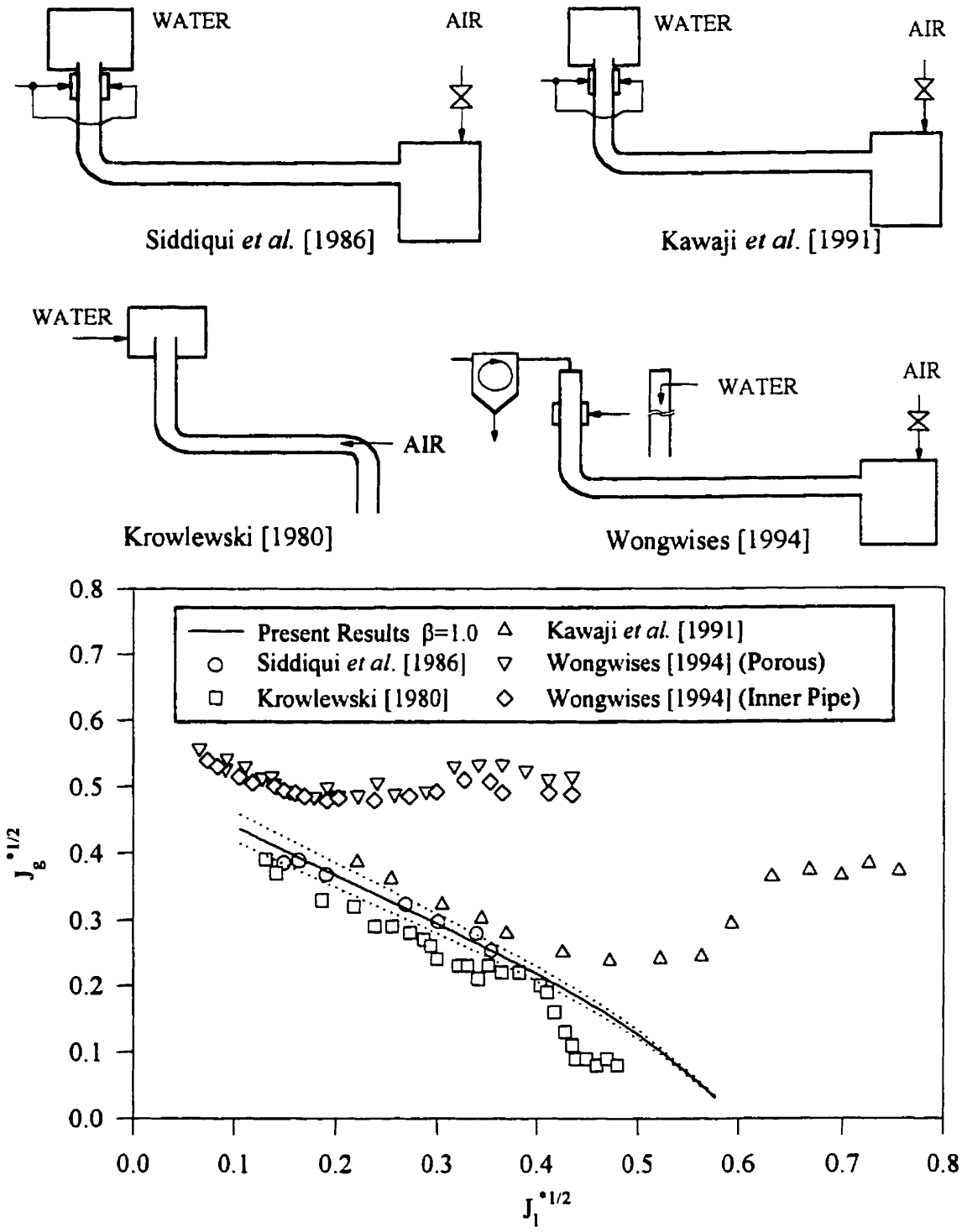

Figure 4.49: Comparison of flooding results with those of other researchers test section with vertical and horizontal leg (no orifice).

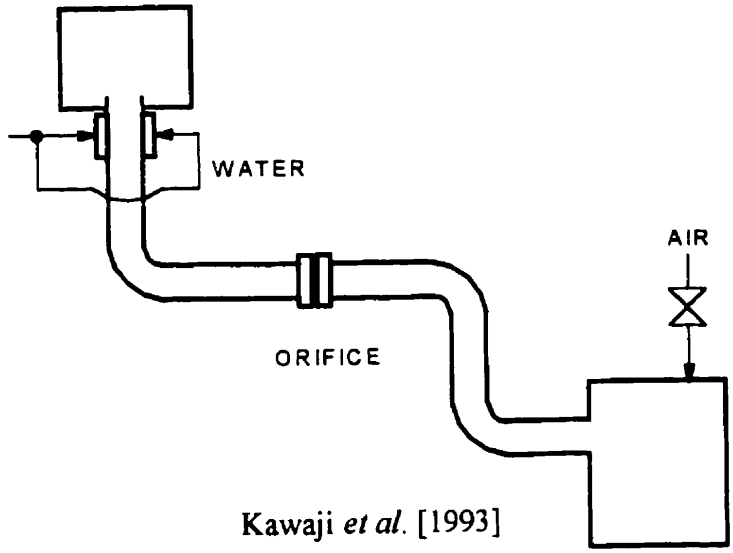

Kawaji *et al.* [1993]

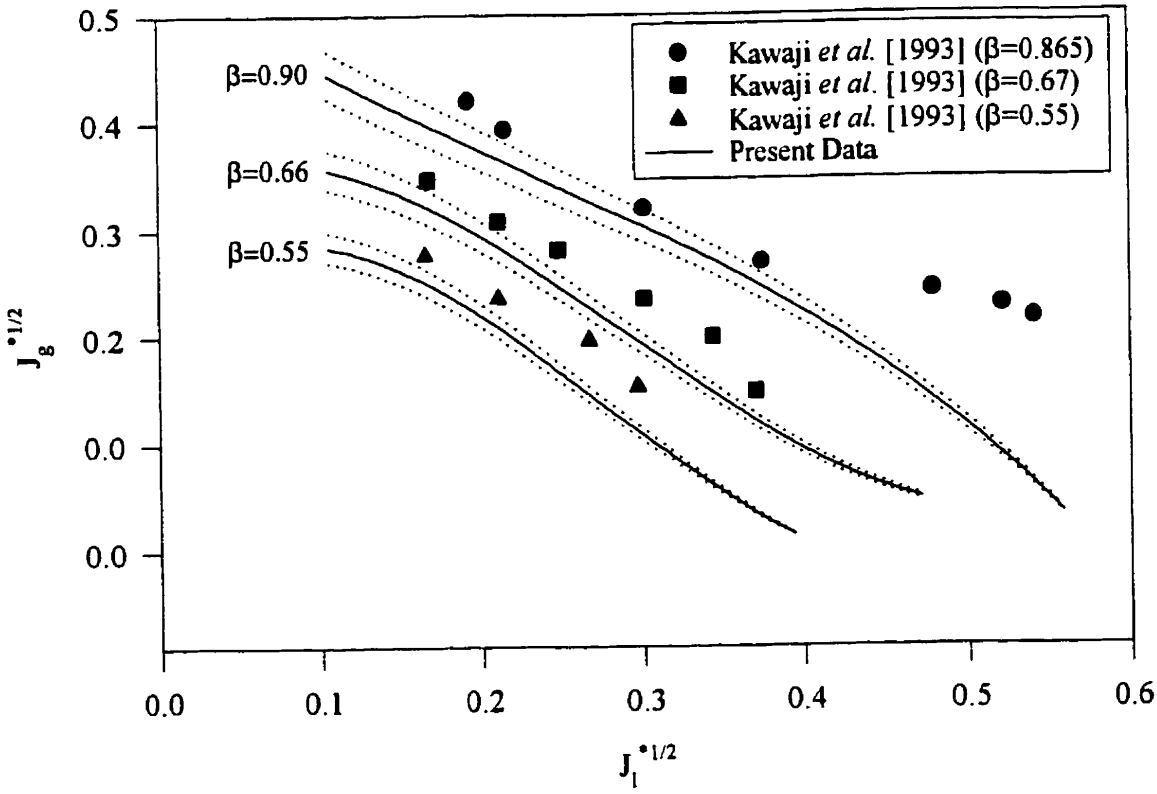

Figure 4.50: Comparison of flooding results with those of other researchers test section with vertical and horizontal leg (orifices).

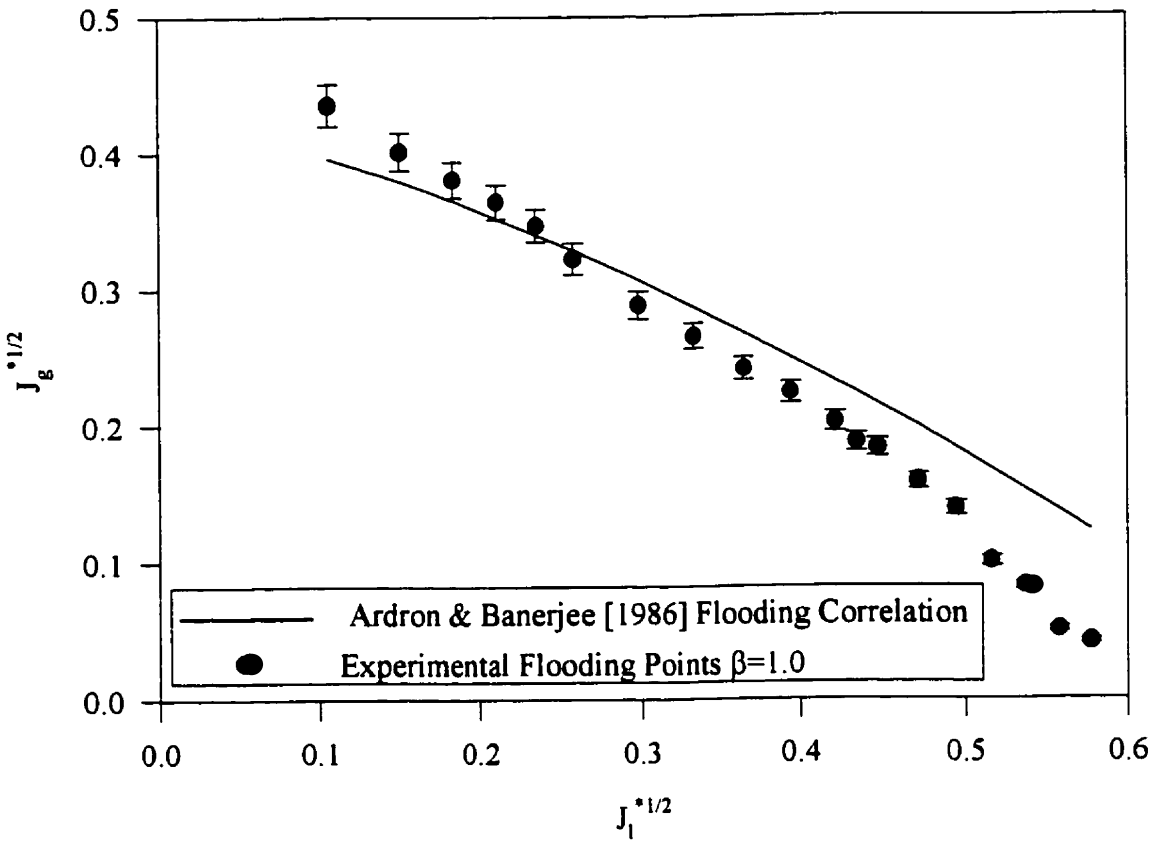

Figure 4.51: Comparison of flooding points obtained in the test section with vertical and horizontal leg and the Ardron and Banerjee flooding correlation (no orifice).

Chapter 5

CCFL MODEL DEVELOPMENT

The focus of the CCF and CCFL modeling efforts have been on the development of phenomenological models capable of predicting the flooding point in a vertical tube without an orifice and in a test section containing both a vertical and a horizontal leg. For the case of the test section containing both vertical and horizontal legs attention was also given to the ability of the model to predict the influence of an orifice placed in the horizontal leg on the flooding point. The models for the vertical and horizontal CCFL will be presented separately. The guiding principle for the model development is [Wilcox 1994]: *"a really good model should introduce the minimum amount of complexity while capturing the essence of the relevant physics."* To this end visual observations of the behaviour of the counter-current flow just prior to and at the onset of flooding were heavily relied upon to guide the model development.

5.1 Model for Vertical CCFL

Visual observations of the nature of the CCF have lead to the adoption of models which describe two different phenomena being retained for testing. Before describing the phenomena being modeled it is important to recall the basic definition of the flooding point which is [Bankoff & Lee 1986]: *"for a given downward liquid flow the maximum upward gas flow rate for which full liquid delivery out the bottom of the tube is maintained, corresponds to the counter-current flooding limit."* Keeping this definition in mind, the model development will focus on two main mechanisms with which flooding may be associated. These mechanisms are:

1. flooding occurs when the gas flow rate is sufficient to entrain a droplet in the gas stream against the force of gravity without being redeposited into the liquid film, and

2. flooding occurs when the gas flow rate is sufficient to cause the velocity of the liquid film at the gas liquid interface to become infinitesimally smaller than zero.

Both of these mechanisms implicitly result in the definition of the flooding point being respected and further coincide with the phenomena observed in the vertical experiments presented in Chapter 4. At low to intermediate liquid flow rates, even at gas flow rates below the flooding point, a number of droplets were observed in the gas core. Thus, it is reasonable to assume that the gas flow rate that is capable of supporting these droplets, without them being redeposited into the liquid film, against the force of gravity corresponds to the flooding point. At high liquid flow rates the transition from full to partial liquid delivery is very sudden, it has been observed that, this transition coincides with a very thick roll wave being seen to travel up the test section in the same direction as the gas flow. In this case the assumption that the flooding point coincides with the gas flow rate required to cause the velocity of the liquid film to pass through zero at the gas liquid interface is also quite logical. At this point the delivered liquid flow rate will be fractionally less than the inlet liquid flow rate, this will result in an increase in the liquid film thickness, and thus an increase in the interfacial shear. This increase in interfacial shear will then result in a partial reversal of the liquid film flow, and in a further increase in the liquid film thickness, and a subsequent further increase in the interfacial shear. This buildup will continue until the force of the gas flow on the liquid film is sufficient to drag the resulting roll wave up the tube against the force of gravity.

There exists in the two–phase flow literature a considerable amount of support for flooding models based on these two mechanisms. Dukler *et al.* [1984] noted that for all the inlet liquid flow rates that they studied; the gas flow rate at which flooding was seen to occur was identically the gas flow rate at which entrainment was first detected. Moalem-Maron & Dukler [1984] noted that a flooding model based on the force balance on a droplet developed solely on theoretical grounds bore a striking resemblance to the experimentally based correlation of Pushkina & Sorokin [1969].

They also noted that such a model provided good agreement with the flooding results presented in Dukler *et al.* [1984]. Despite, the success of this model Moalem-Maron & Dukler [1984] rejected it because of its lack of generality and preferred to base their modeling efforts on a film flow model of the flooding phenomena. Although, it was noted that droplet entrainment was likely to be a cause of flooding under some circumstances. Recently, Jayanti *et al.* [1996] carried out a theoretical investigation of the tube diameter effect on flooding. They observed, that for fixed inlet liquid flow rates, in small diameter tubes the gas velocity required to drive a standing wave upward was much lower than in a large diameter tube. They argued that in large diameter pipes the gas velocity required to entrain and carry droplets upward may be less than that required to transport a wave upward. They therefore claimed, that for large diameter tubes flooding may be associated with droplet transport while in smaller diameter tubes the flooding phenomena may be related to wave (film) transport. The results presented in Chapter 4 were obtained for a fixed tube diameter of 63.5 *mm* for various inlet liquid flow rates. An analogy, albeit imperfect, may however be drawn with the work of Jayanti *et al.* [1996]. At low inlet liquid flow rates the liquid film is much thinner than at high liquid flow rates, while at a given liquid flow rate the liquid film will be much thinner in a large diameter tube than in a small diameter tube. Coincidently, visual observation of the flooding phenomena in the current work, seems to indicate that at low liquid flow rates flooding is related to droplet entrainment while at high liquid flow rates that it is related to film flow reversal.

The two phenomenological models under consideration for the prediction of the flooding point will now be examined in greater detail.

5.2 Droplet Force Balance

The phenomena being modeled in this particular case is represented schematically in Figure 5.1. It involves a balance of the drag and gravitational forces acting on a droplet. The drag force, F_d, will be a function of the drop size and of the drag coefficient while the gravitational force, F_g, for a constant liquid temperature field, will only be a function of the drop size.

For a given drop size, assuming that the drop is spherical, the magnitude of the

gravitational force is given by:

$$F_g = \frac{4}{3}\pi(\frac{d_{max}}{2})^3(\rho_l - \rho_g)g \quad , \tag{5.1}$$

while the magnitude of the drag force is given by:

$$F_d = \frac{1}{2}C_d\pi(\frac{d_{max}}{2})^2\rho_g v_g^2 \quad , \tag{5.2}$$

the gas velocity may be obtained explicitly from the balance of these equations as:

$$v_g = \sqrt{\frac{4d_{max}(\rho_l - \rho_g)g}{3C_d\rho_g}} \quad , \tag{5.3}$$

where the drag coefficient is calculated using Wallis [1969]:

$$C_d = \begin{cases} \frac{24}{Re_d} & \text{for } Re_d < 1 \\ \frac{24}{Re_d}[1 + 0.15Re_d^{0.687}] & \text{for } 1 \leq Re_d < 10^3 \\ 0.45 & \text{for } 10^3 \leq Re_d < 2 \cdot 10^5 \end{cases} \quad , \tag{5.4}$$

with the droplet Reynolds number given by:

$$Re_d = \frac{\rho_g v_g d_{max}}{\mu_g} \quad . \tag{5.5}$$

To close the set of equations given above a method is required to specify d_{max}, which is the largest stable drop size that can exits in a gas stream. Thus, a literature review focusing on droplet size models was carried out.

5.2.1 Drop Size Modelling

A huge amount of information is available in the two–phase flow literature on the subject of drop size modeling. The mechanism of droplet formation in an annular flow which is due to shearing off of the roll wave crests may result in droplets being formed which are larger than the maximum stable drop size. Thus, all of the

models reviewed Ishii & Grolmes [1975], Kataoka *et al.* [1983], Lopes [1984], and Kocamustafaogullari [1993, 1994] are based on an idea first proposed by Hinze [1955] in which a balance of the disruptive and restorative forces acting on the droplet, control the mechanism of droplet disintegration and thus the maximum stable drop size. For a given set of flow conditions a wide range of drop sizes may be observed. It has however been found [Lopes 1984] that while the largest drops account for only a relatively small fraction of the total number of drops that are entrained, they account for a major fraction of the mass and momentum transport. The model development will thus be carried out using the maximum stable drop size.

The mechanism controlling the break-up of a liquid droplet may be regarded as being a balance between the external disruptive stress, τ, and the surface restorative stress, $2\sigma/d$, where σ and d are the surface tension and droplet diameter respectively. Therefore, the condition which controls the maximum stable drop size can be expressed in terms of a critical Weber number which can be defined as:

$$We_c = \frac{\tau d_{max}}{2\sigma} \quad . \tag{5.6}$$

The external disruptive forces may be due to either; the changes in eddy velocities over the length of the droplet, or to the local relative velocity around the droplet. In both cases the external stress can be expressed in terms of the difference in the kinetic energy around the droplet. Lopes [1984] based his model on the first mechanism while Kocamustafaogullari *et al.* [1993, 1994] based their model on the second. Based on these two criteria two different critical Weber numbers may be defined; these are:

$$We_{c_1} = \frac{\rho_g \bar{v}_g'^2 d_{max}}{2\sigma} \quad , \tag{5.7}$$

and

$$We_{c_2} = \frac{\rho_g v_{r_{max}}^2 d_{max}}{2\sigma} \quad . \tag{5.8}$$

In both of these models a means must be found to specify either $\bar{v}_g'^2$ which is the mean square of the spatial velocity fluctuation over the drop length, or $v_{r_{max}}^2$ which is the limiting local relative velocity at which a fluid will flow over a droplet suspended in it.

Both these quantities can be related in some way to the turbulent energy dissipation rate per unit mass, ϵ, thus:

$$\bar{v}_g'^2 \sim (\epsilon d_{max})^{2/3} \quad , \tag{5.9}$$

and

$$v_{r_{max}} \sim [\epsilon d_{max}(\frac{\rho_l}{\rho_g})]^{1/3}(\frac{\rho_l - \rho_g}{\rho_l})^{1/2} \quad . \tag{5.10}$$

Replacing $\bar{v}_g'^2$ and $v_{r_{max}}$ in equations 5.7 and 5.8 by the expressions given by equations 5.9 and 5.10 respectively and assuming that the implied proportionality factors are both on the order of unity, yields:

$$We_{c_1} = \frac{\rho_g \epsilon^{2/3} d_{max}^{5/3}}{\sigma} \quad , \tag{5.11}$$

and

$$We_{c_2} = \rho_g \epsilon^{2/3} d_{max}^{5/3} (\frac{\rho_l}{\rho_g})^{2/3} (\frac{\rho_l - \rho_g}{\rho_l})/\sigma \quad . \tag{5.12}$$

Equations 5.11 and 5.12 can then be solved for the droplet diameter, yielding:

$$d_{max_1} = \left(\frac{\sigma We_{c_1}}{\rho_g}\right)^{3/5} \epsilon^{-2/5} \quad , \tag{5.13}$$

and

$$d_{max_2} = \left(\frac{\sigma We_{c_2}}{\rho_g}\right)^{3/5} \epsilon^{-2/5} (\frac{\rho_l}{\rho_g})^{2/5} (\frac{\rho_l - \rho_g}{\rho_l})^{-3/5} \quad , \tag{5.14}$$

respectively.

Both Lopes [1984] and Kocamustafaogullari *et al.* [1993, 1994] assume that in the case of pipe flow the local energy dissipation rate per unit mass, ϵ, is equal to the average energy dissipation rate per unit mass, $< \epsilon >$, and that the average energy dissipation may be approximated as:

$$< \epsilon >= \left(\frac{< j_g >}{\rho_g}\right)\left(\frac{-dP}{dz}\right) = \left(\frac{< j_g >}{\rho_g}\right)\left(\frac{4\tau_i}{D}\right) \quad , \tag{5.15}$$

where the interfacial shear stress, τ_i, is given by:

$$\tau_i = \frac{1}{2} f_i \rho_g v_r^2 \quad . \tag{5.16}$$

The critical Weber numbers We_{c_1} and We_{c_2} are given by Lopes [1984] and Kocamustafaogullari *et al.* [1993, 1994] as $We_{c_1} = 0.194$ and $We_{c_2} = 12.2$ respectively. It should also be pointed out that a study of the work of Lopes [1984] by Kocamustafaogullari *et al.* [1993, 1994] have lead them to suggest that a better value of the critical Weber number is $We_{c_1} = 0.17$.

The final requirement for the application of either of these drop size models is the specification of the interfacial friction factor. Kocamustafaogullari *et al.* [1993, 1994] used the model of Ishii & Grolmes [1975] in their correlation. In addition to this model a literature review of interfacial friction modeling was also carried out. The available literature on this subject is quite vast. The correlations tested in the present work were taken from a review of interfacial friction modeling presented by Wallis [1987]. The interfacial friction models tested include the following:

Wallis [1987]

$$f_i = 0.005(1 + 300\frac{\delta}{D}) \quad , \tag{5.17}$$

Moeck (Given in Wallis [1987])

$$f_i = 0.005[1 + 545(\frac{2\delta}{D})^{1.42}] \quad , \tag{5.18}$$

Nigmatulin 1 (Given in Wallis [1987])

$$f_i = 0.008[1 + 210(\frac{2\delta}{D})^{1.3}] \quad , \tag{5.19}$$

Nigmatulin 2 [1991]

$$f_i = 0.005 + 0.84(\frac{2\delta}{D})^{1.1} \quad , \tag{5.20}$$

Nigmatulin 3 [1991]

$$f_i = 0.005 + 0.6(\frac{2\delta}{D}) + 5.3 \cdot 10^4(\frac{2\delta}{D})^{5.5} \quad , \tag{5.21}$$

Bharathan [1979]

$$f_i = 0.005 + 406(\frac{\delta}{D})^{2.04} \quad , \tag{5.22}$$

where δ is the film thickness and D is the tube diameter. A comparison of the predicted interfacial friction factors obtained using the above correlations against the experimental results of Dukler *et al.* [1984] is given in Figure 5.2. It can be seen that for relatively low δ/D ratios Bharathan's [1979] correlation yields reasonably good results, however at medium to high values of δ/D the interfacial friction factor is significantly underpredicted. It can also be seen that all of the other correlations significantly underpredict the interfacial friction factor over the entire range of δ/D. All of the above correlations were developed based on data obtained for air–water annular flows and their extension to conditions of steam–water flows may be in question. It has however been pointed out by Hewitt and Hall–Taylor [1970] that the shear stress under diabatic conditions is often approximately equal to that observed in adiabatic flow under the same flow conditions. Nigmatulin [1991] shows a comparison of equation 5.20 against a wide variety of both steam–water and air–water data. This comparison shows that, apart from the data of one researcher, no significant difference exists between the interfacial friction for steam–water and air-water flows. Furthermore, correlations of this type are currently being used in both TRAC [Wallis 1987] and COBRA–TF [Thurgood 1981].

The use of one of the above friction factor correlations in equation 5.16 permits the average energy dissipation rate per unit mass, $< \epsilon >$, to be calculated from equation 5.15. Then the maximum stable drop size, d_{max}, may be obtained using either of the two drop size correlations given by equations 5.13 or 5.14. Finally, the gas velocity required to suspend the droplet in the gas stream can be obtained using equation 5.3.

In order to be able to obtain the interfacial friction factor using any of the aforementioned correlations a means of estimating the liquid film thickness is required.

Assuming that the film can be adequately described by the equation of motion for steady, laminar, one dimensional flow with constant film thickness, in which gravity is the only body force and for which the pressure gradient is assumed to be negligible, the equation of conservation of momentum can be written as:

$$\mu_l \frac{d^2 v(y)}{dy^2} + \rho_l g = 0 \quad . \tag{5.23}$$

The velocity profile in the liquid film can be obtained by integrating equation 5.23. This yields:

$$v(y) = \frac{\rho_l g}{\mu_l}\left(Ay - \frac{y^2}{2}\right) + B \quad . \tag{5.24}$$

Applying the following boundary conditions:

$$v(0) = 0 \quad , \tag{5.25}$$

and

$$\mu_l \frac{\partial v(y)}{\partial y}\bigg|_{y=\delta} = -\tau_i \quad . \tag{5.26}$$

yields the following equation for the velocity profile in the liquid film:

$$v(y) = \frac{\rho_l g}{\mu_l}\left[\left(\delta - \frac{\tau_i}{\rho_l g}\right) y - \frac{y^2}{2}\right] \quad . \tag{5.27}$$

Two special cases will now be considered, these being:

1. zero interfacial shear: $\tau_i = 0$ at $y = \delta$, and
2. zero interfacial velocity: $v(y) = 0$ at $y = \delta$.

For both these cases, the mass flow rate in the liquid film may be obtained using:

$$\dot{m}_l = \rho_l \pi D \delta \int_0^\delta v(y) dy \quad , \tag{5.28}$$

the results for the two cases can then be solved for the film thickness. This yields:

$$\delta = \left[\frac{3\mu_l \dot{m}_l}{g\rho_l^2 \pi D}\right]^{1/3} , \tag{5.29}$$

which is the classic expression for the Nusselt film thickness in the first case, and:

$$\delta = \left[\frac{12\mu_l \dot{m}_l}{g\rho_l^2 \pi D}\right]^{1/3} , \tag{5.30}$$

for the second case. The results of Zabaras [1985] indicate that below the flooding point the measured film thickness agrees very well with that predicted by the Nusselt equation. His results also show that at the flooding point the measured film thickness is quite close to that obtained using equation 5.30. Furthermore, the average film thickness was found to be very nearly constant for two different positions in the test section located at 0.15 and 1.7 m from the point of liquid injection respectively. Thus these two limiting film thicknesses were used in the calculation of the interfacial friction factors given by equations 5.17 to 5.22.

5.2.2 Algorithm for Model Based on Droplet Force Balance

For a given experimental liquid flow rate the above models were used to predict the gas velocity required to suspend a droplet in the gas stream using the following procedure:

1. For a given experimental liquid flow rate calculate the film thickness using either equation 5.29 or equation 5.30,
2. Use this film thickness with one of the given interfacial friction factor correlations to calculate the interfacial friction factor,
3. Use the interfacial friction factor and a guessed gas velocity in equation 5.16 to calculate the interfacial shear stress,
4. Use the interfacial shear stress together with the guessed gas velocity to calculate the average energy dissipation using equation 5.15,

5. Use the average energy dissipation in either equation 5.13 or 5.14 to obtain the maximum stable drop size,

6. Use the drop size and the drag coefficient from equation 5.4 in equation 5.3 to obtain the gas velocity which will support the drop, and

7. If the gas velocity obtained in step 6 is approximately equal to the original guessed velocity, i.e. if ($|v_g^{new} - v_g^{old}| \leq \epsilon$) stop, if not return to step 5.

If the assumption of this mechanism being linked to the flooding phenomena is correct, the resulting gas velocity will correspond to the experimentally observed flooding point.

5.3 Film Flow Modelling

The phenomena being represented in this model is the case of the interfacial shear stress under conditions of vertical annular counter-current flow being sufficient to cause the velocity of the liquid film at the gas liquid interface to be zero.

Assuming the simplest case of steady, laminar, one dimensional flow of a Newtonian fluid the velocity profile in the liquid film is given by equation 5.27 and the mass flow rate in the liquid film is given by equation 5.28.

Solving equation 5.28 as a function of the liquid film thickness yields:

$$\dot{m}_l = \frac{\rho_l^2 g \pi D \delta^2}{\mu_l} \left[\frac{\delta}{3} - \frac{\tau_i}{2\rho_l g} \right] \quad . \tag{5.31}$$

using the definition of the interfacial shear stress, τ_i, which is given by equation 5.16 yields the following expression of the liquid film flow rate:

$$\dot{m}_l = \frac{\rho_l^2 g \pi D \delta^2}{\mu_l} \left[\frac{\delta}{3} - \frac{f_i \rho_g v_r^2}{4\rho_l g} \right] \quad . \tag{5.32}$$

The velocity of the liquid at the gas liquid interface can be obtained from:

$$v(\delta) = \frac{\rho_l g \delta}{\mu_l} \left[\frac{\delta}{2} - \frac{\rho_g f_i v_r^2}{2\rho_l g} \right] \quad . \tag{5.33}$$

For a given liquid flow rate equation 5.32 and 5.33 can be solved for a varying gas flow rates until the condition of zero velocity at $y = \delta$ is reached. The procedure used is:

1. For a given experimental liquid flow rate the film thickness for the condition of $v(\delta) = 0$ is given by equation 5.30,
2. Use this film thickness with one of the given interfacial friction factor correlations to calculate the interfacial friction factor,
3. Use the interfacial friction factor and a guessed gas velocity in equation 5.32 to calculate the velocity of the liquid film at the gas liquid interface,
4. If $v(\delta) \neq 0$ guess another gas flow rate and return to 3; if $|v(\delta)| \leq \epsilon$ stop.

If the above phenomena corresponds to the one that is actually linked to the onset of flooding the gas flow rate required to cause $v(\delta) = 0$ will correspond to the experimental gas flow rate at the flooding point.

5.4 Comparison of Predicted and Experimental Flooding Points – Vertical Flow

A comparison between the experimental flooding points for vertical flow without an orifice carried out using the 63.5 *mm* I.D. test section and the predictions obtained using the correlations of Wallis [1969] (with $m = 1$ & $C = 1$), Alekseev *et al.* [1972], and Bharathan *et al.* [1978] is presented in Figure 5.3. It can be seen that none of these correlations are capable of correctly predicting the experimental results. As shown in Figure 5.4 the parameters m and C in the Wallis [1969] correlation may be adjusted in such a way as to produce a very good agreement with the experimental results. This, however, requires apriori knowledge of the flooding results and thus limits its usefulness as a predictive tool [Tye *et al.* 1995].

The model for the prediction of the flooding point in a vertical test section without an orifice, based on the droplet entrainment mechanism as described above has been compared against the flooding data obtained in our experiments using the 63.5 *mm*

I.D. test section. Comparisons were carried out using two limiting film thicknesses, the Nusselt film thickness and the film thickness corresponding to zero liquid velocity at the gas liquid interface and a number of different correlations for the interfacial friction factor. The results are shown in Figures 5.5 and 5.6 using the Nusselt film thickness and the film thickness corresponding to $V_{il} = 0$ respectively. It can be seen that in general the predicted flooding points do not agree with the experimental results.

As was seen in Figure 5.2 with the exception of Bharathan's correlation which yielded reasonably good results at low values of δ/D all of the correlations tested significantly under predicted the interfacial friction factor. New interfacial friction factors were thus obtained from a best fit of the data of Dukler *et al.* [1984]. A comparison of the experimental and predicted flooding points using the droplet entrainment model for the two limiting film thicknesses using these new interfacial friction factors is shown in Figure 5.7. It can be seen that for the case using the film thickness corresponding to zero interfacial velocity the predicted flooding points are in very good agreement with the experimental results.

Figures 5.8 and 5.9 show a comparison of the predicted and experimental results obtained using the film flow model in which the interfacial friction factors were obtained from Bharathan's [1979] correlation and from the best fit of the data of Dukler *et al.* [1984] respectively. It can be seen that when Bharathan's [1979] correlation is used the agreement between the predicted and experimental results is very poor. For the case when the interfacial friction factor is obtained from the best fit of the data of Dukler *et al.* [1984] it is interesting to note that while the predictions do under estimate the flooding points for higher liquid flow rates the curves of the predictions and the experimental results have very similar shapes.

5.5 Model for Horizontal CCFL

As was the case for the development of the model for the prediction of the counter-current flooding limit in vertical tubes, visual observations of the nature of the CCF and the CCFL in a test section containing both a vertical and a horizontal leg have again been used to guide the model development.

It was observed that as the gas flow rate was increased, entrained droplets began to appear in the gas stream in the vertical leg just above the elbow. At gas flow rates below that corresponding to the flooding point the concentration of entrained droplets was quite small. This concentration increased quite rapidly as the flooding point was reached. It was thus postulated that the onset of flooding was in some way linked to the onset of entrainment.

Thus a mechanistic model based on the following premise has been developed for the prediction of the flooding point in an elbow between a vertical and a horizontal leg:

- flooding occurs as a results of a buildup of the droplets entrained from the crest of the hydraulic jump which occurs inside the elbow.

In order to calculate the height of the hydraulic jump it is necessary to first obtain the depth of the flow upstream of the jump. To do this, it is assumed that the void fraction in the supercritical region in the horizontal leg is equal to that in the vertical leg. This is a reasonable assumption as it has been observed that the hydraulic jump takes place right at the start of the horizontal leg. It is now necessary to find a means of calculating the film thickness and liquid velocity in the vertical leg. Since the flooding point in a test section containing both a vertical and a horizontal run is well below that occuring in vertical flow only, and further, since it has been shown experimentally [Zabaras 1985] that for vertical flow below the flooding point, the measured film thickness under counter-current flow conditions is very close to the Nusselt film thickness it is reasonable to assume, for calculation purposes, that the film thickness is equal to the Nusselt film thickness as given by equation 5.29. The void fraction is then obtained from:

$$\alpha = \left(1 - \frac{2\delta}{D}\right)^2 \quad , \tag{5.34}$$

The film thickness in the horizontal leg, δ_h, corresponding to this void fraction is then calculated by the iterative solution of:

$$\alpha = 1 - \frac{1}{\pi} * \arccos(\frac{D - 2\delta_h}{D}) - \left[\frac{D/2 - \delta_h}{\pi D^2/4} * \sqrt{\delta_h * (D - \delta_h)}\right] \quad , \tag{5.35}$$

The upstream critical depth of the flow and the height of the hydraulic jump can be obtained using Straub's method [French 1985]:

$$\delta_c = \left(\frac{1.01}{D^{0.264}}\right) * \left(\frac{Q_l}{\sqrt{g}}\right)^{0.506} \quad , \tag{5.36}$$

where Q_l is the volumetric flow rate of the liquid phase and δ_c is the critical depth. The height of the hydraulic jump may then be obtained by:

$$\delta_j = \begin{cases} (\delta_c^2/\delta_h) & \text{for } Fr < 1.7 \\ (\delta_c^{1.8}/\delta_h^{0.73}) & \text{for} Fr \geq 1.7 \end{cases} \quad , \tag{5.37}$$

where Fr is the upstream Froude number which is defined as:

$$Fr = \frac{|v_l|}{\sqrt{g\delta_h}} \quad . \tag{5.38}$$

The void fraction at the crest of the hydraulic jump, α_j, is then calculated from:

$$\alpha_j = 1 - \frac{1}{\pi} * \arccos(\frac{D - 2\delta_j}{D}) - \left[\frac{D/2 - \delta_j}{\pi D^2/4} * \sqrt{\delta_j * (D - \delta_j)}\right] \quad , \tag{5.39}$$

and the absolute value of the corresponding liquid velocity is obtained from:

$$|v_l| = \frac{\dot{m}_l}{\rho_l(1 - \alpha_j)\pi D^2/4} \quad , \tag{5.40}$$

where $\dot{m}_l$ is the liquid mass flow rate. **Note: the velocity is defined to be positive in the direction of the gas flow**

The Ishii & Grolmes [1975] criterion for the inception of entrainment is then applied at the crest of the hydraulic jump. This criterion is that the drag force, F_d, acting on the wave crest is greater than the retaining force of the surface tension, F_σ:

$$F_d \geq F_\sigma \quad . \tag{5.41}$$

The drag force on the wave crest is given by:

$$F_d = C_d \lambda a \frac{\rho_g v_r^2}{2} \quad , \tag{5.42}$$

where λ is the wave length, v_r is the relative velocity between the gas and the liquid phases given by $v_r = v_g - v_l$, a is the wave amplitude, and the drag coefficient is given by an analogy to the drag for deformed particles and is taken to be:

$$C_d \approx 1 \quad . \tag{5.43}$$

The retaining force of the surface tension is given by:

$$F_\sigma = C_s \lambda \sigma \quad , \tag{5.44}$$

where C_s is an interfacial shape coefficient, Ishii & Grolmes [1975] specify this coefficient as being:

$$C_s \leq 0.77 \quad . \tag{5.45}$$

The entrainment criterion can thus be obtained by substituting equations 5.42 and 5.44 into equation 5.41:

$$a \frac{\rho_g v_r^2}{2} \geq \frac{C_s \sigma}{C_d} \quad . \tag{5.46}$$

A method must now be found to specify the wave amplitude, a. Ishii & Grolmes [1975] assume that the interfacial shear at the top of the wave crest induces an internal flow which is of the order of magnitude of the film velocity and that the motion of the wave crest with respect to the film can be expressed by a shear flow model. They have thus obtained the following expression for the amplitude of the wave:

$$a = \sqrt{2} C_w \frac{\mu_l}{\rho_l} \sqrt{\frac{\rho_l}{\tau_i}} \frac{1}{\sqrt{f_i}} \quad , \tag{5.47}$$

where C_w is a factor which is used to account for the effect of the surface tension on the internal flow. They argue that, since the hydrodynamics inside the wave crest can be described as a function of the viscous and surface forces, this parameter will

be a function of these forces. Ishii & Grolmes [1975] have obtained the following correlation for the factor C_w:

$$\frac{1}{3C_w} = \begin{cases} 11.78N_\mu^{0.8} & \text{for } N_\mu \leq \frac{1}{15} \\ 1.35 & \text{for } N_\mu > \frac{1}{15} \end{cases} \quad , \tag{5.48}$$

where N_μ is the viscosity number which is defined as:

$$N_\mu = \frac{\mu_l}{\left(\rho_l \sigma \sqrt{\frac{\sigma}{g(\rho_l - \rho_g)}}\right)^{1/2}} \quad . \tag{5.49}$$

They propose that the friction factor, f_i, be calculated using the relationship given by Hughmark [1973]:

$$\sqrt{f_i} = K Re_f^m \quad , \tag{5.50}$$

where Re_f is the film Reynolds number given by:

$$Re_f = \frac{\rho_l \mid v_l \mid \delta_j}{\mu_l} \quad , \tag{5.51}$$

and the constants K and m are given by:

$$\begin{array}{lll} K = 3.73 & m = -0.47 & \text{for } 2 < Re_f < 100 \\ K = 1.962 & m = -1/3 & 100 < Re_f < 1000 \\ K = 0.735 & m = -0.19 & 1000 < Re_f \end{array}$$

and τ_i is given by:

$$\tau_i = f_{gi} \frac{\rho_g v_r^2}{2} \quad , \tag{5.52}$$

where f_{gi} may be specified using any available correlation. For the present study

$$f_{gi} = \frac{0.079}{Re_g^{1/3}} \quad , \tag{5.53}$$

was used. It is important to note that the correlations for the interfacial friction factor which were presented in section 5.1.2 on drop size modelling should not be used for this case as they are applicable only to annular flow. In view of the thickness of the liquid film, δ_j, at the crest of the hydraulic jump, these correlations would yield physically unrealistic values of interfacial friction. In order to apply this model for the prediction of the flooding point in a test section containing vertical and horizontal legs the following procedure is used:

1. For a given experimental liquid flow rate the Nusselt film thickness is calculated using equation 5.29 the corresponding void fraction is then obtained using equation 5.34,

2. The film thickness of the stratified flow before the hydraulic jump, δ_h, is then obtained by an iterative solution of equation 5.35 using the void fraction obtained in the previous step,

3. Equations 5.36 and 5.37 are then used to calculate the critical depth of the flow and the height of the hydraulic jump. The void fraction at the crest of the hydraulic jump is then obtained using equation 5.39 and the corresponding liquid velocity is obtained from equation 5.40.

4. The criterion for the inception of entrainment given by equation 5.46 is then calculated using a guessed gas velocity where the wave amplitude is calculated using equation 5.47 and C_w, $\sqrt{f_i}$, and τ_i are calculated using equations 5.48, 5.50 and 5.52 respectively. The gas velocity is updated until the inequality which defines the point of inception of entrainment is satisfied.

5.5.1 Modification of the Model for Horizontal CCFL to Take into Account the Influence of the Orifice

For the specific case when an orifice is placed in the horizontal leg a provision must be made to take into account its influence on the flooding point. In order to do this it was assumed that the orifice creates a stagnation region in the flow as illustrated in Figure 5.10. This results in the height of the hydraulic jump being offset by the height of this region. The offset height for this case is given by:

$$h_o = (1 - \beta)\frac{D}{2} \quad . \tag{5.54}$$

The results of the application of this correction to take into account the influence of the orifice on the flooding point are shown in Appendix A for all of the orifices used in these experiments. It can be seen that for the four largest orifices tested, i.e. $\beta = 0.90$ to 0.72 Figures A–1 to A-4, the agreement between the predicted and the experimental flooding points is quite good. For the orifices having β ratios of 0.66 and 0.55 Figures A–5 and A–6 however the flooding points are significantly overpredicted. Furthermore it can be seen that the degree of over prediction increases with decreasing orifice β ratios. Thus a correction was made to the calculated offset height which was inversely proportional to the orifice β ratio. The offset height which is added to the height of the hydraulic jump is thus given by:

$$h_o = \frac{(1 - \beta)}{\beta}\frac{D}{2} \quad , \tag{5.55}$$

and the rest of the calculation is carried out in the same manner as for the case without an orifice. A flowchart showing the calculation procedure for the application of this model is given in Figure 5.11.

5.5.2 Comparison of Predicted and Experimental Flooding Points–Horizontal Flow

The results of a comparison between this model and our experimental results for the case without an orifice are shown in Figure 5.12. A comparison of the predicted and experimental flooding points using our data and the Ardron and Banerjee [1986] flooding correlation is also presented. It can be seen that the present model is in better agreement with the experimental results than that of Ardron and Banerjee [1986].

Comparisons of the predictions of the present CCFL model against some of the results of Krowlewski [1980] (system most closely resembling the one used in the current experiments), Wan & Krishnan [1986], Siddiqui *et al.* [1986] and Kawaji *et al.* [1991] are shown in Figures 5.13, 5.15, 5.14 and 5.16 respectively, predictions obtained using the Ardron and Banerjee [1986] flooding correlation are also shown in these figures. It can be seen that for the experiments of Krowlewski [1980], Siddiqui *et al.* [1986]

and Kawaji *et al.* [1991] the predictions of the present model are in very good agreement with the experimental results and in fact better than those obtained using the Ardron and Banerjee [1986] flooding correlation. This correlation does however produce a better agreement with the experiments of Wan & Krishnan [1986] than the CCFL model developed as part of the current research. The comparisons with the experimental results of both Wan & Krishnan [1986] and Kawaji *et al.* [1991] are only carried out over part of the region of the data. The reason for this is that both authors state that at large values of $J_l^{*1/2}$ the flow remains supercritical throughout the horizontal leg. Under these conditions neither the present CCFL model nor the Ardron and Banerjee [1986] flooding correlation are applicable since in both cases flooding is associated with the presence of a hydraulic jump.

The standard deviations of the predictions with respect to the experimental results which are given by:

$$\sigma = \sqrt{\frac{1}{N}\sum (X_{calc} - X_{exp})^2} \quad , \tag{5.56}$$

are presented in Table 5.1 for all the cases that were studied . It can be seen that the standard deviations of the present model are lower than those for the Ardron and Banerjee [1986] flooding correlation for four of the five cases where this correlation was applicable, the only exception being the results of Wan & Krishnan [1986].

The prediction of the flooding point using this model for all of the orifice ratios studied in this project (β=0.90, 0.83, 0.77, 0.72, 0.66 and 0.55) are shown in Figures 5.17–5.22. It should be pointed out that to the best of the authors knowledge there are no models available in the open literature which are capable of predicting the flooding point occuring in an elbow between a vertical and a horizontal leg in which an orifice is placed. It can be seen that in general the agreement between the predicted and experimental flooding points is excellent. For the orifices having β ratios of 0.77, 0.72, and 0.66 for values of $J_l^{1/2}$ greater than 0.35 it can be seen that there is a change in the slope of the experimental results which is not predicted by the current model. The current model predicts the onset of flooding as being due to the inception of entrainment at the crest of a hydraulic jump occuring inside the elbow. For high liquid flow rates, both Wan & Krishnan [1986] and Kawaji [1989] found that the hydraulic jump was shifted towards the exit of the horizontal leg and flooding was

due to slugging at this point. The results of both these researchers exhibit a change in slope at the highest liquid flow rates similar to that observed in the current results. If the phenomena which leads to flooding, at the highest liquid flow rates, is not the one represented by the phenomenological model, it will not be surprising if the model fails to capture the change in slope seen in the experimental results.

A comparison of the predictions of the model against the experimental results of Kawaji [1993] for orifices of (β=0.865, 0.67 and 0.55) are shown in Figures 5.23–5.25. In general, the agreement between the predictions and the experimental results is excellent. At the highest dimensionless liquid superficial velocities for the $\beta = 0.865$ case were Kawaji's data exhibits an unusual trend of the dimensionless superficial gas velocity at flooding being almost constant the predicted and experimental results do however diverge.

Table 5.1: Standard Deviation of Model Predictions vs. Experiments.

Experiments	Model	Standard Deviation σ
Present Work $\beta = 1$	Present Work	0.036
Present Work $\beta = 1$	Ardron & Banerjee [1986]	0.043
Krowlewski [1980]	Present Work	0.042
Krowlewski [1980]	Ardron & Banerjee [1986]	0.096
Wan & Krishnan [1986]	Present Work	0.038
Wan & Krishnan [1986]	Ardron & Banerjee [1986]	0.013
Siddiqui *et al.* [1986]	Present Work	0.019
Siddiqui *et al.* [1986]	Ardron & Banerjee [1986]	0.044
Kawaji *et al.* [1991]	Present Work	0.018
Kawaji *et al.* [1991]	Ardron & Banerjee [1986]	0.026
Present Work $\beta = 0.90$	Present Work	0.050
Present Work $\beta = 0.83$	Present Work	0.048
Present Work $\beta = 0.77$	Present Work	0.046
Present Work $\beta = 0.72$	Present Work	0.032
Present Work $\beta = 0.66$	Present Work	0.033
Present Work $\beta = 0.55$	Present Work	0.021
Kawaji *et al.* [1993] $\beta = 0.865$	Present Work	0.157
Kawaji *et al.* [1993] $\beta = 0.67$	Present Work	0.029
Kawaji *et al.* [1993] $\beta = 0.55$	Present Work	0.023

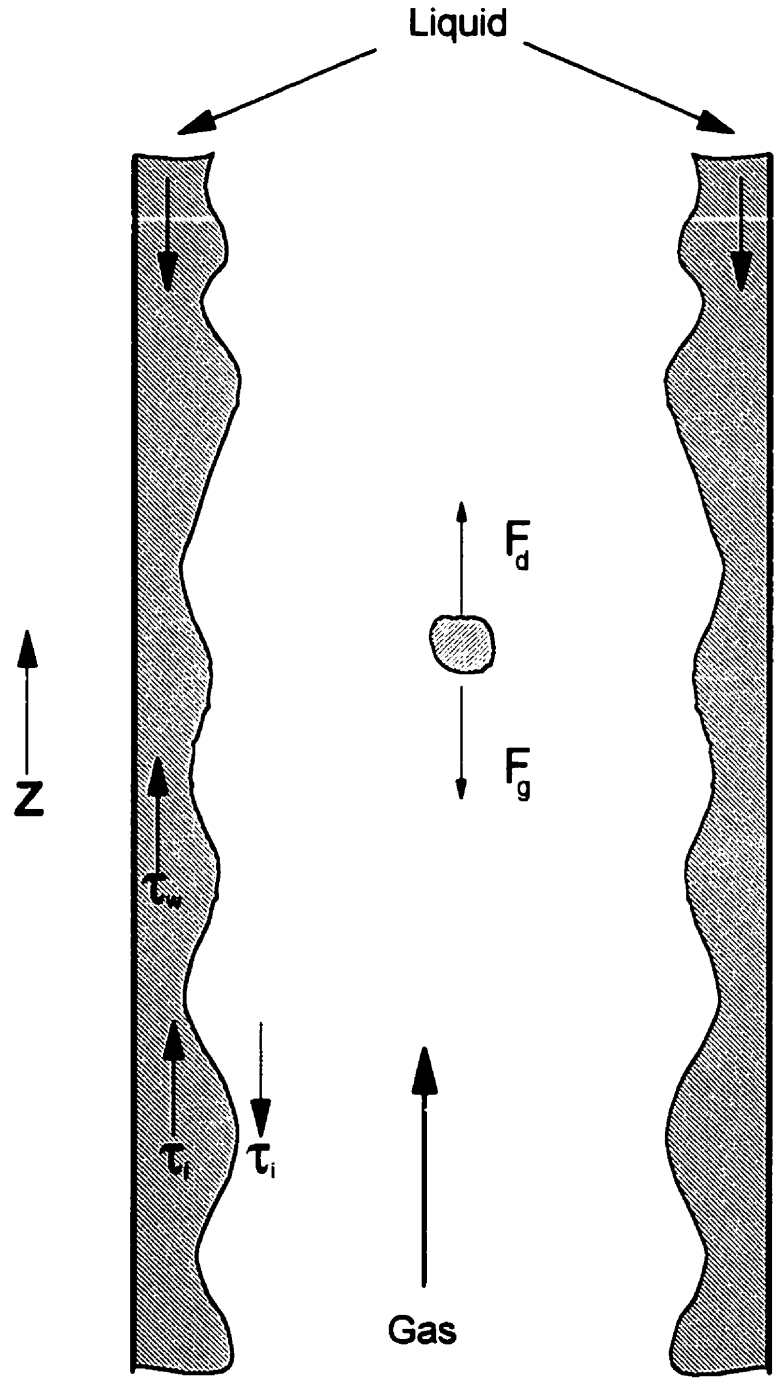

Figure 5.1: Force balance on a drop.

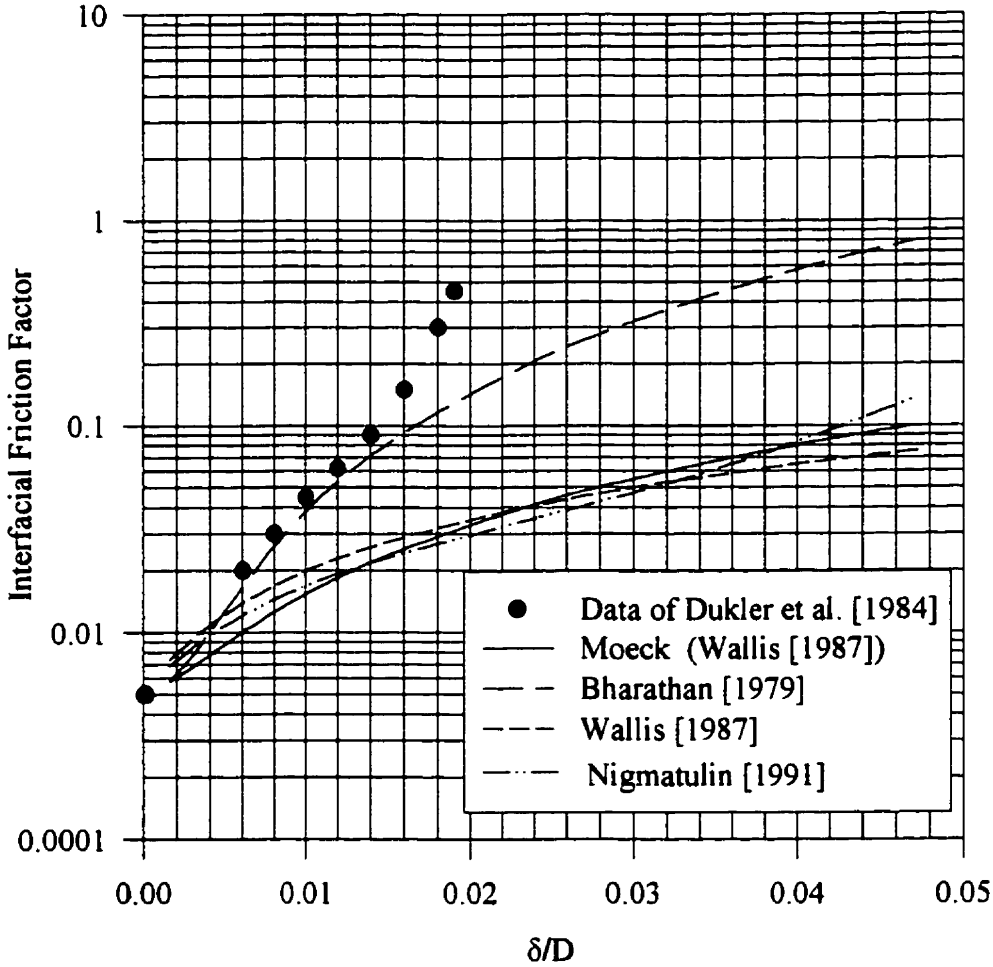

Figure 5.2: Comparison of interfacial friction factor vs. data of Dukler *et al.* [1984]

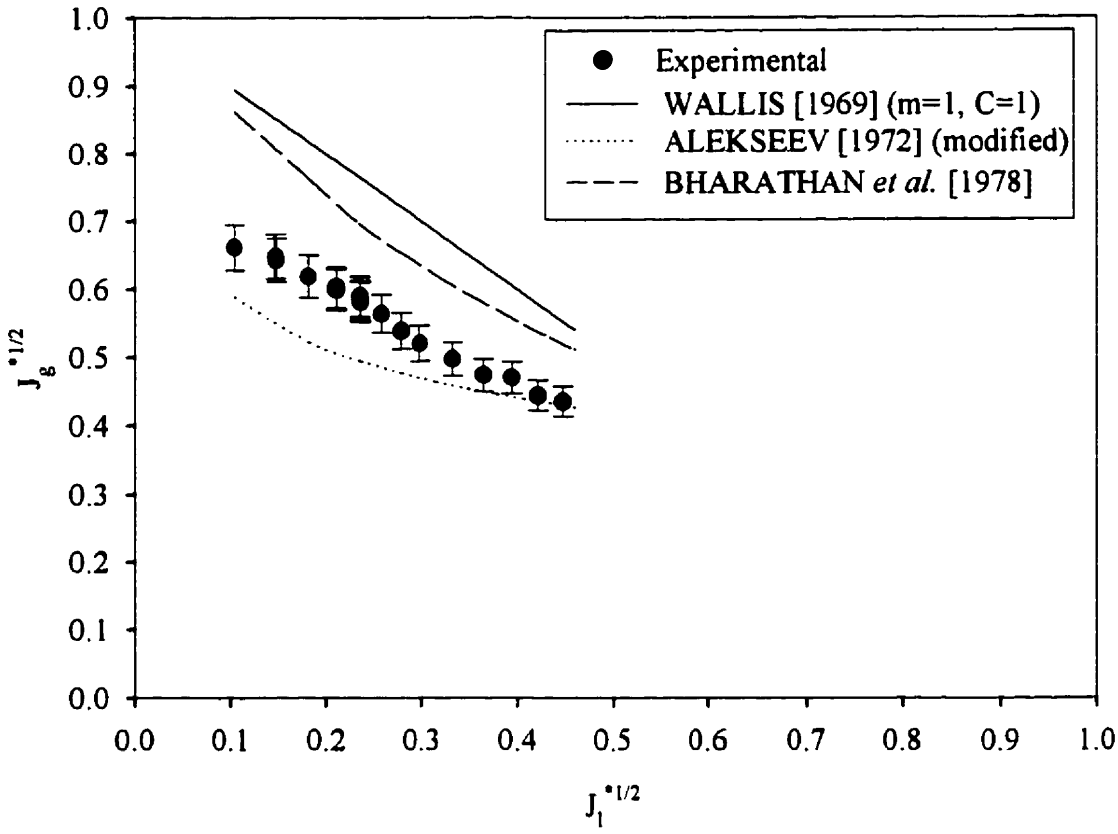

Figure 5.3: Comparison of experimental flooding points and correlations obtained from the literature.

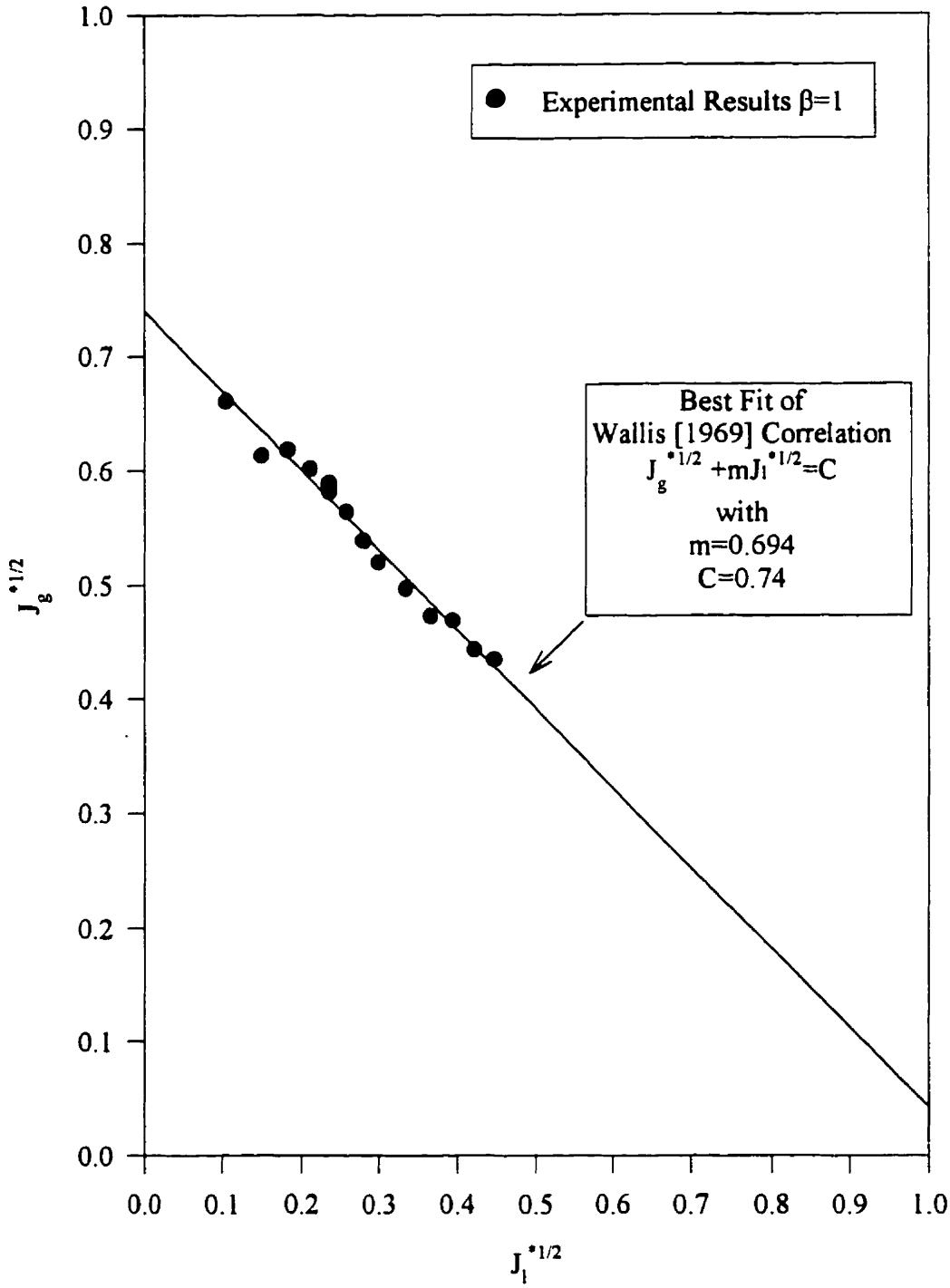

Figure 5.4: Comparison of experimental flooding points and Wallis' correlation.

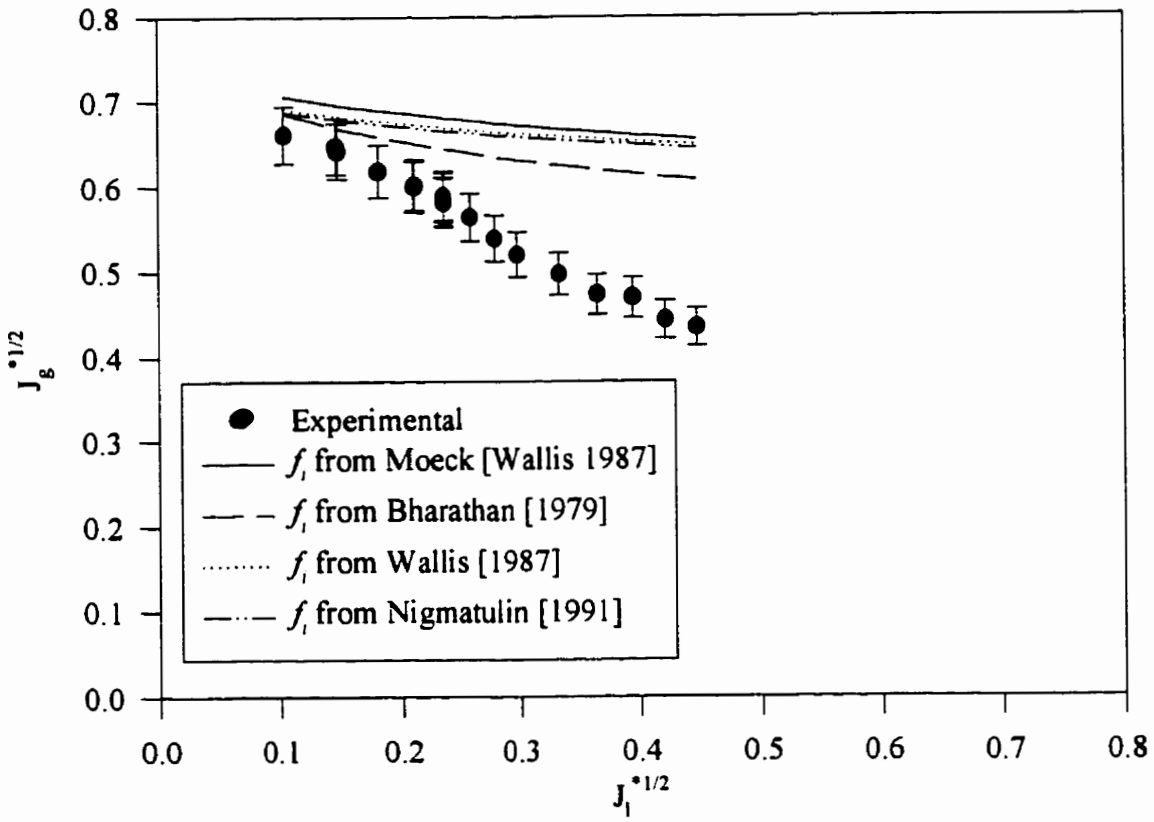

Figure 5.5: Comparison of experimental and predicted flooding points test section with vertical leg only using droplet force balance model with Nusselt film thickness and various interfacial friction correlations.

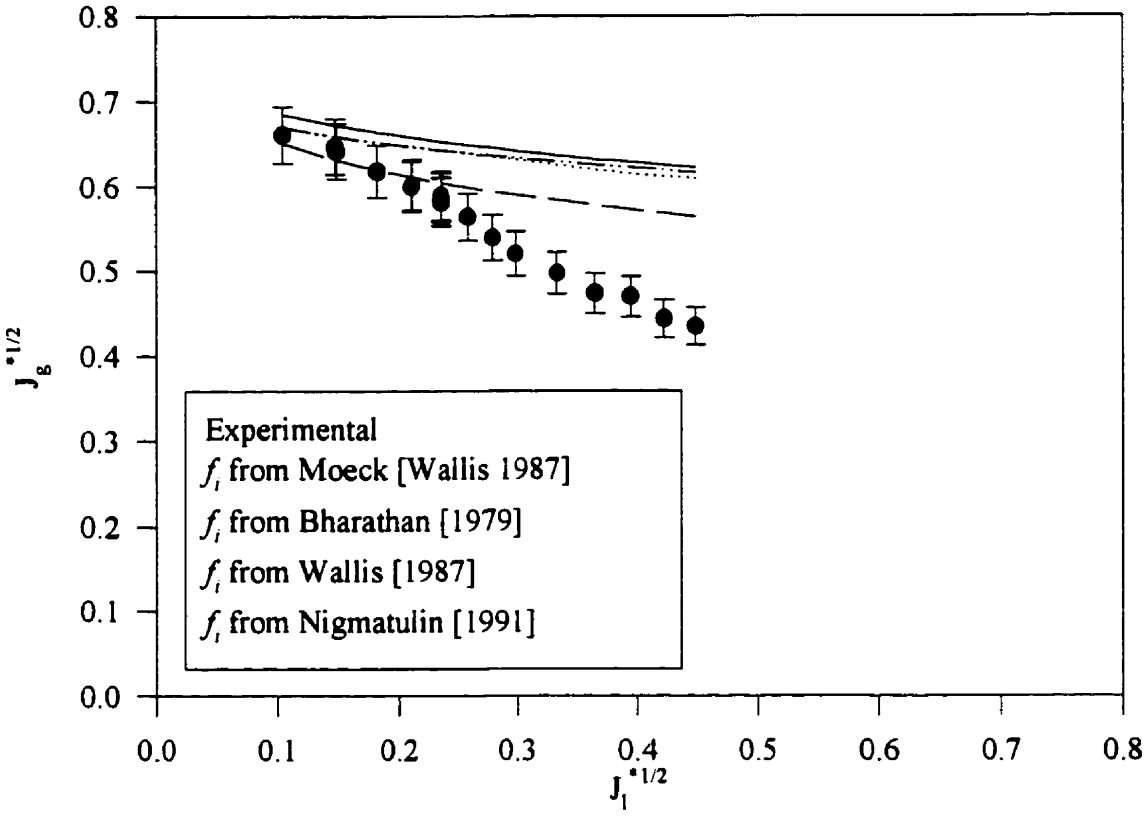

Figure 5.6: Comparison of experimental and predicted flooding points test section with vertical leg only using droplet force balance model with film thickness from $V_{il} = 0$ and various interfacial friction correlations.

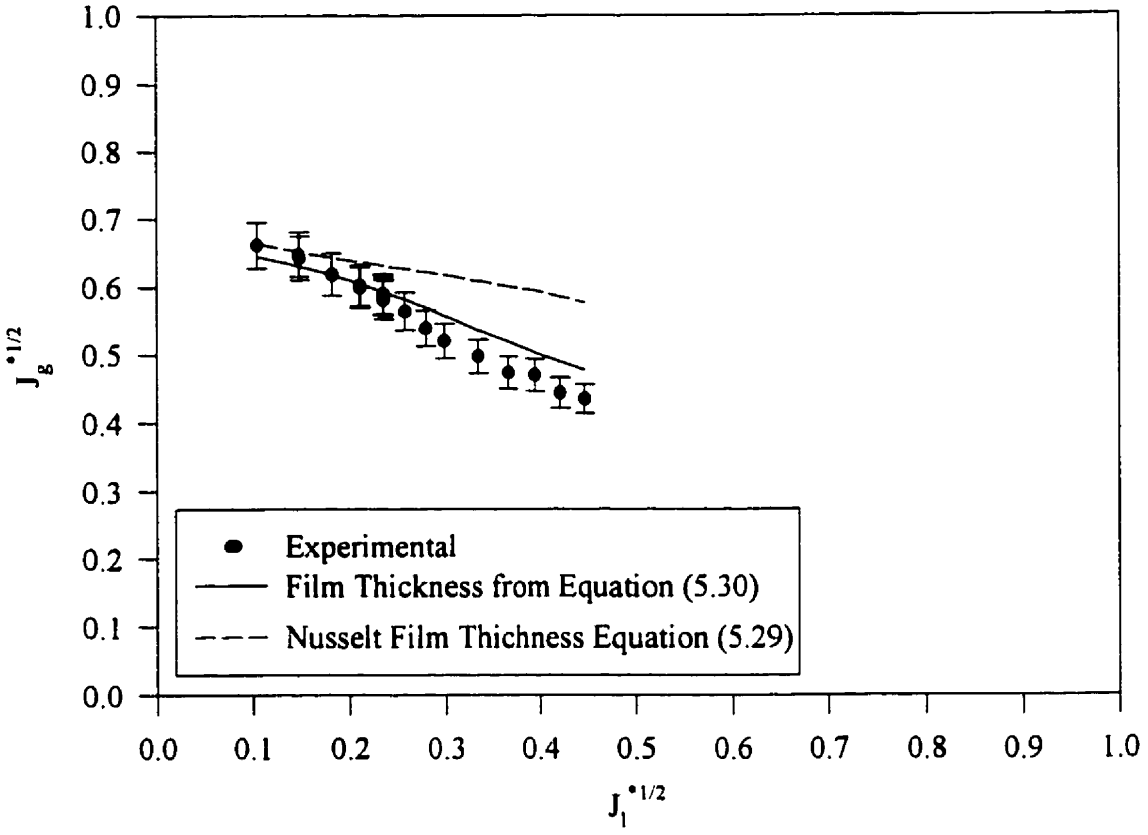

Figure 5.7: Comparison of experimental and predicted flooding points test section with vertical leg only using droplet force balance model with interfacial friction from best fit of Dukler *et al.* [1984] data.

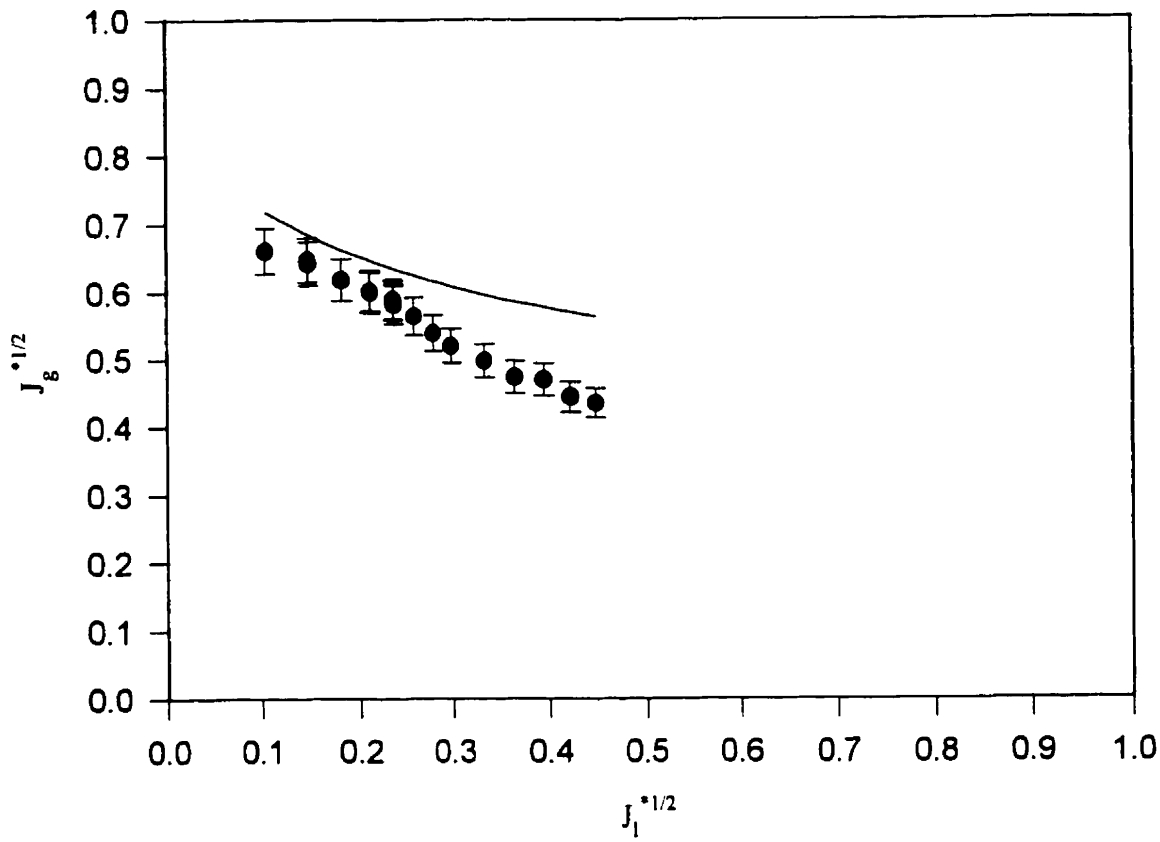

Figure 5.8: Comparison of experimental and predicted flooding points test section with vertical leg only using film reversal model and interfacial friction from the correlation Bharathan [1979].

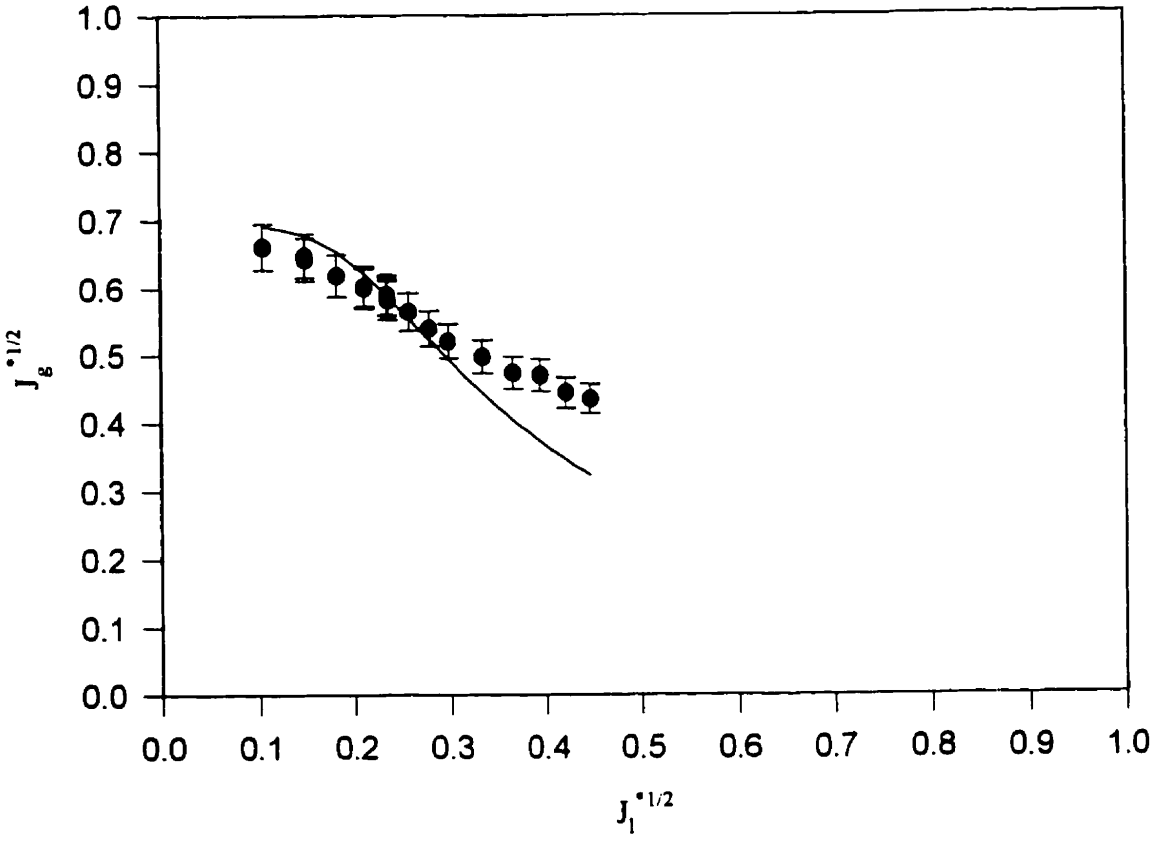

Figure 5.9: Comparison of experimental and predicted flooding points test section with vertical leg only using film reversal model and interfacial friction from best fit of Dukler *et al.* [1984] data.

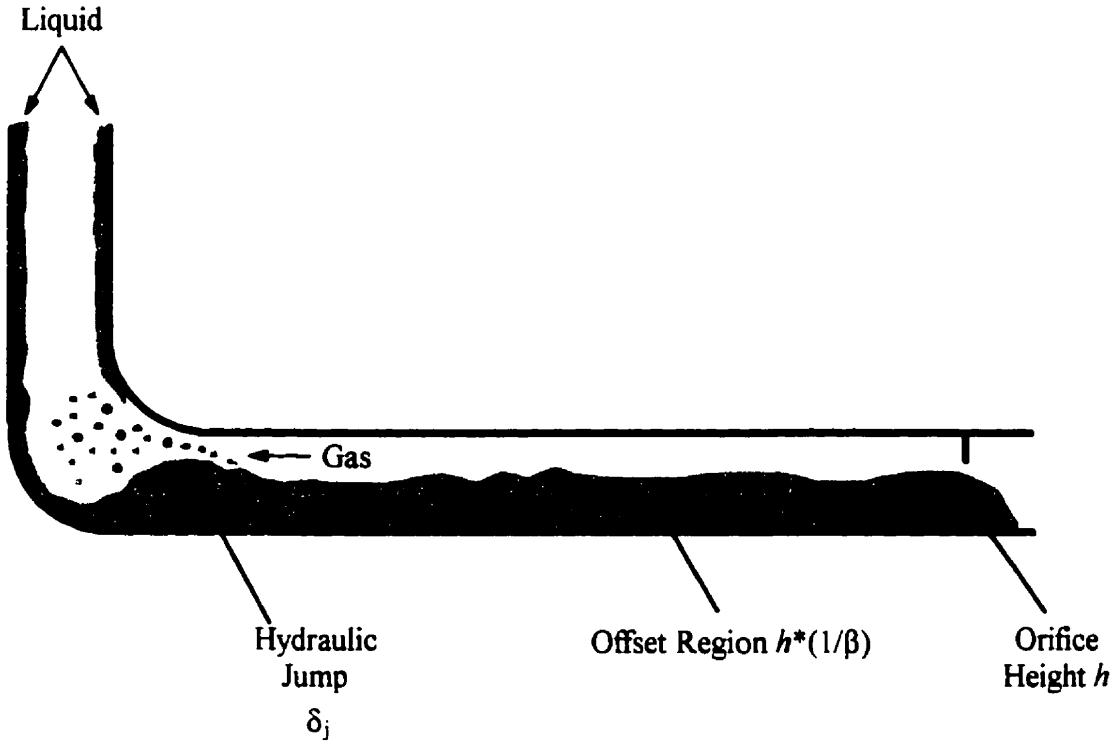

Figure 5.10: Offset region caused by the orifice.

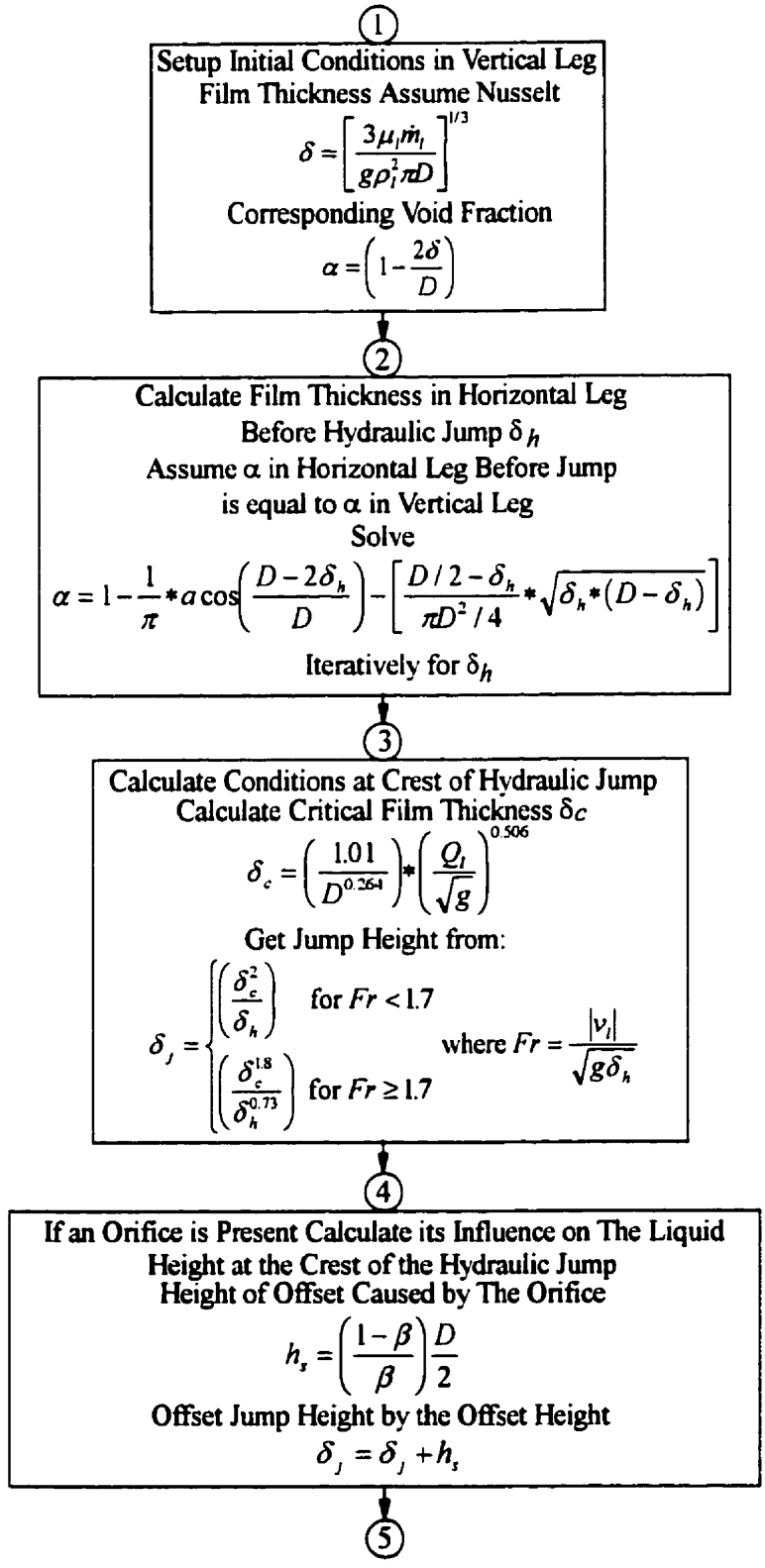

Figure 5.11: Flowchart showing the calculation procedure for the application of the horizontal CCFL model.

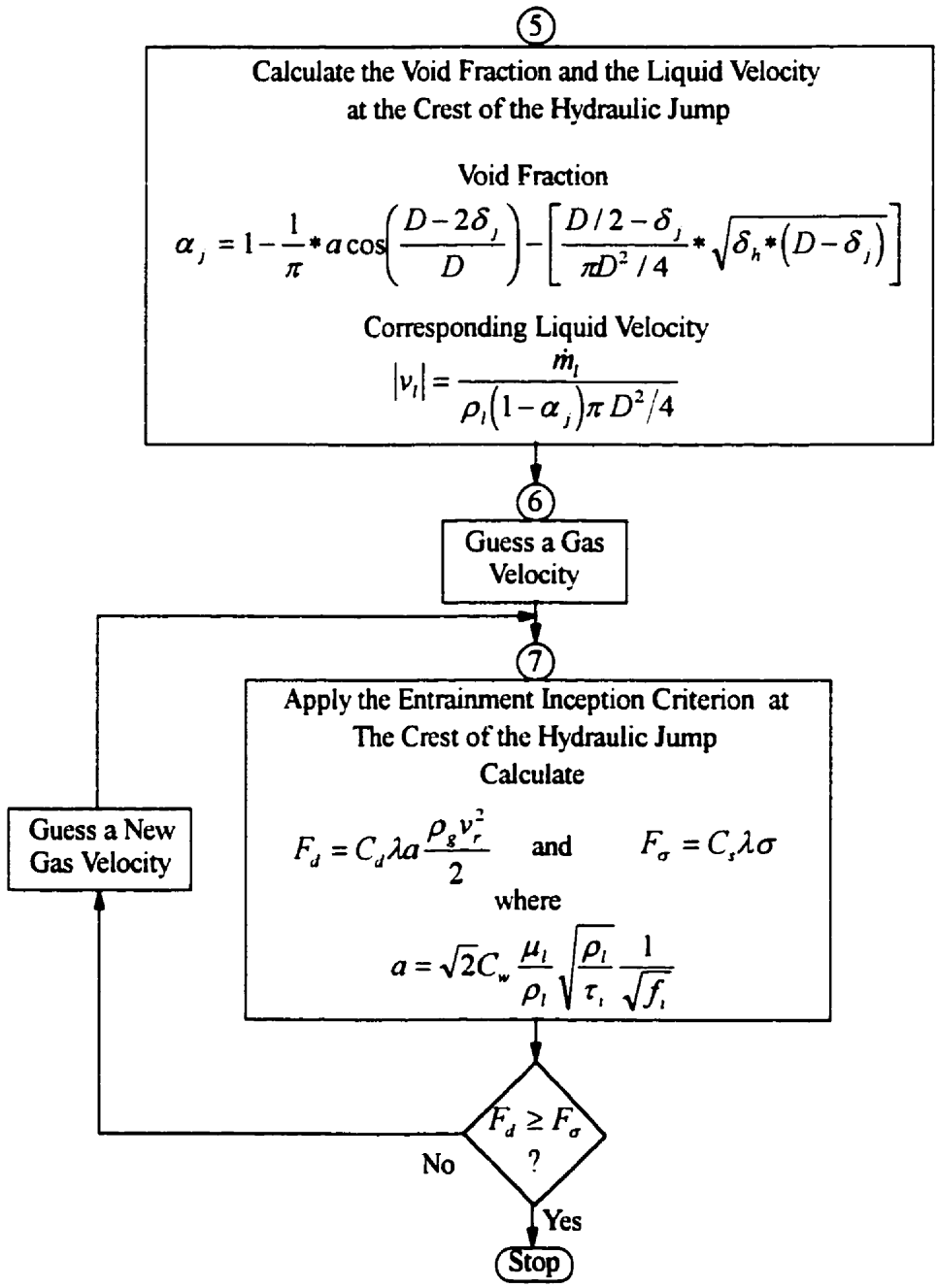

Figure 11 (cont.). Flow Chart of Calculation Procedure for the Application of the Horizontal CCFL Model (Cont.).

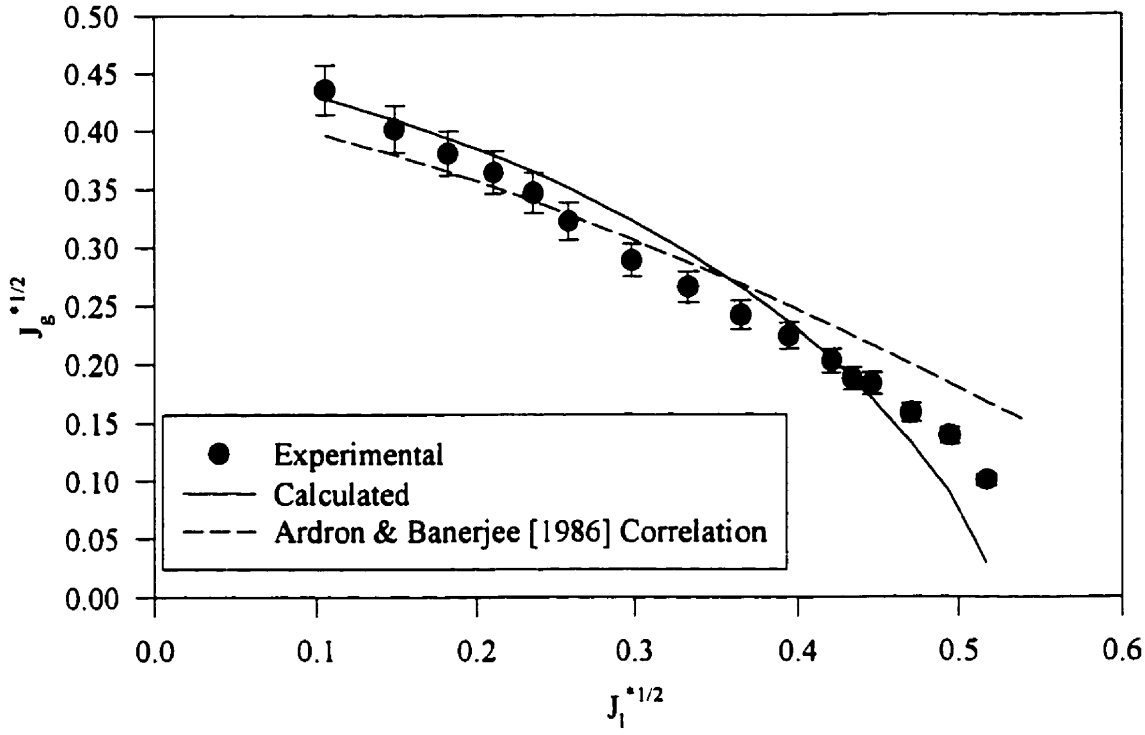

Figure 5.12: Comparison of experimental and predicted flooding points, test section with vertical and horizontal legs no orifice using the horizontal CCFL model.

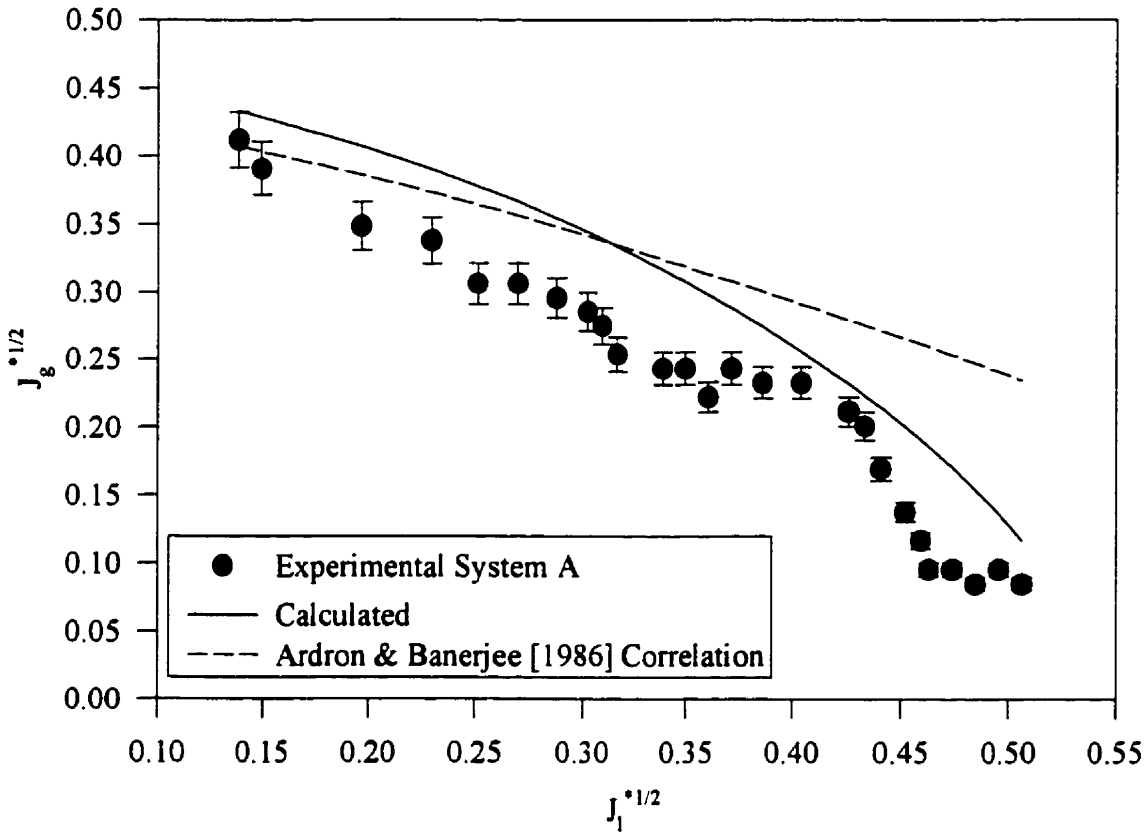

Figure 5.13: Comparison of experimental and predicted flooding points using the horizontal CCFL model and the data of Krowlewski [1980].

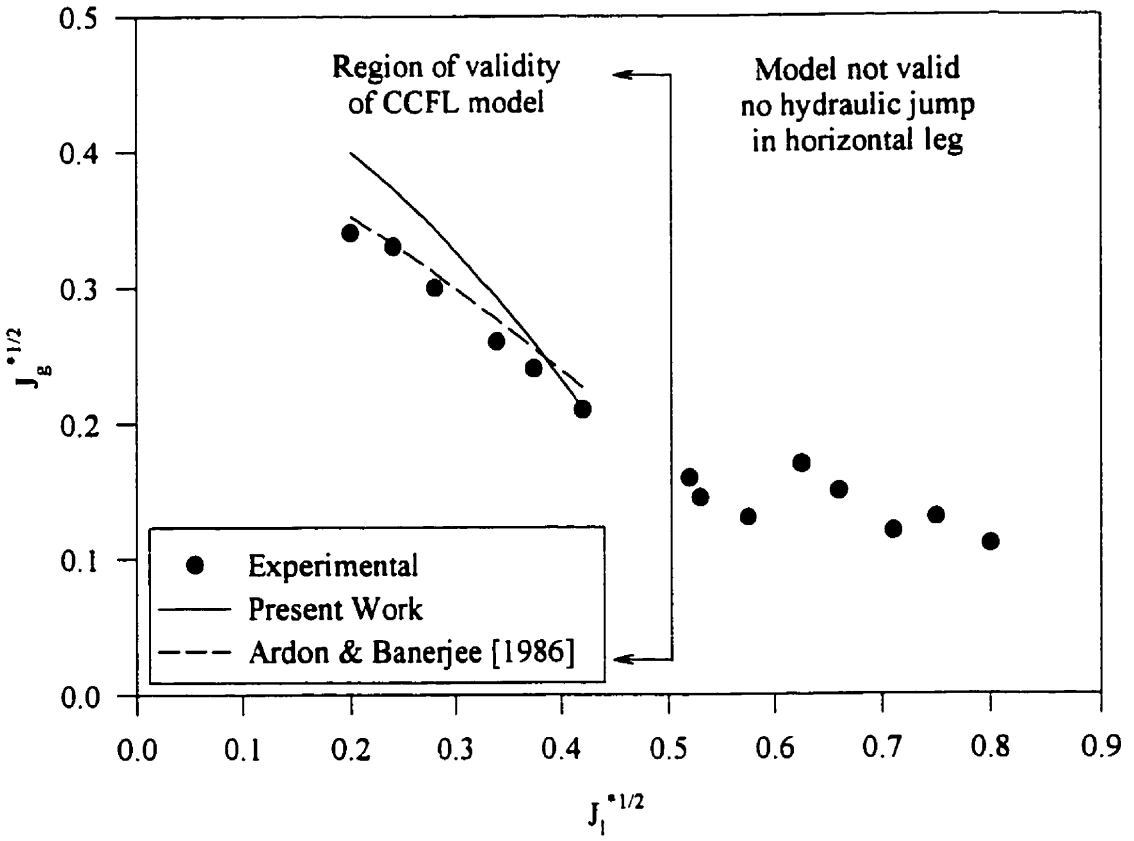

Figure 5.14: Comparison of experimental and predicted flooding points using the horizontal CCFL model and the data of Wan & Krishnan [1986].

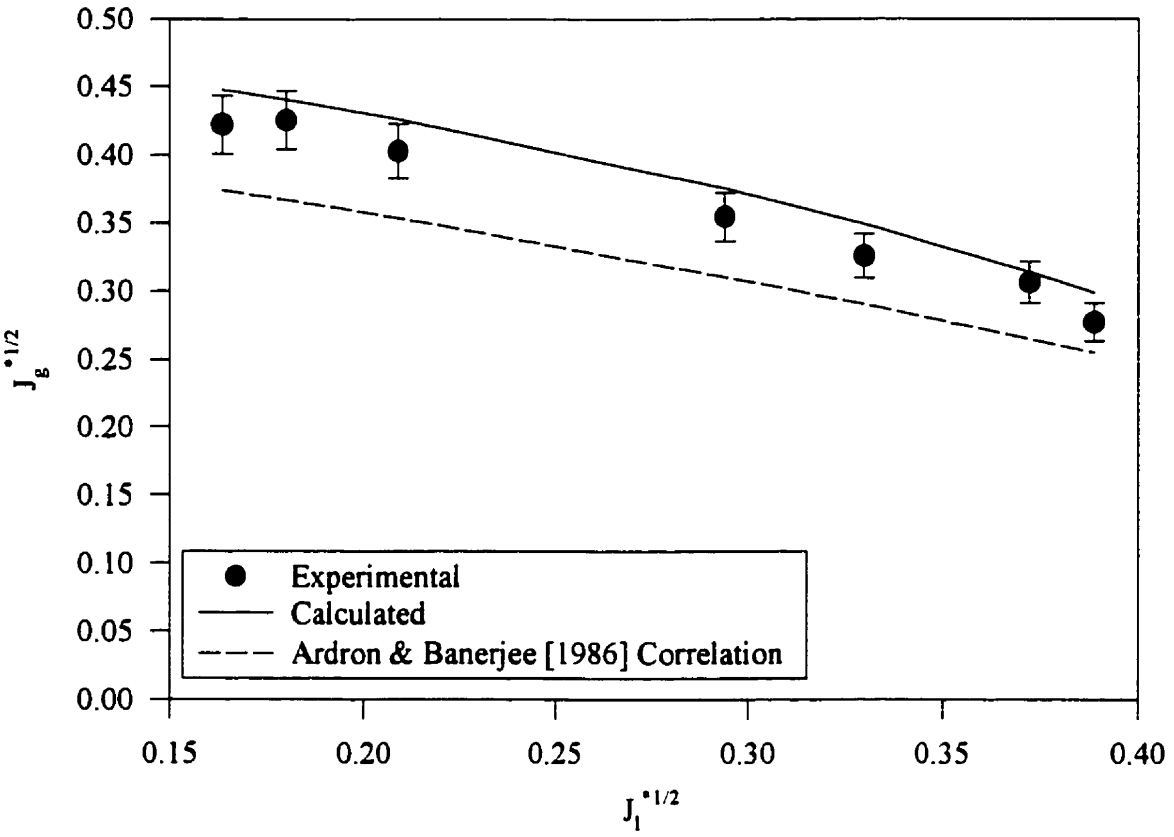

Figure 5.15: Comparison of experimental and predicted flooding points using the horizontal CCFL model and the data of Siddiqui [1986].

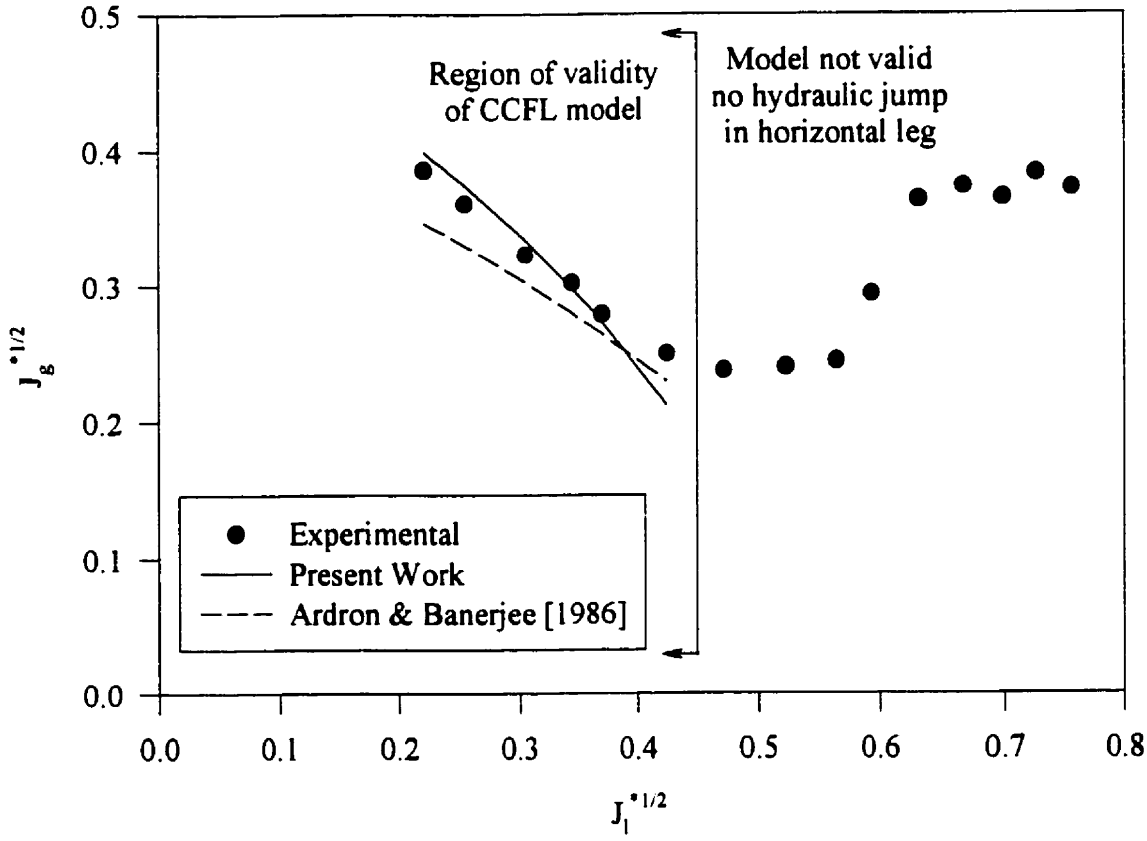

Figure 5.16: Comparison of experimental and predicted flooding points using the horizontal CCFL model and the data of Kawaji [1991].

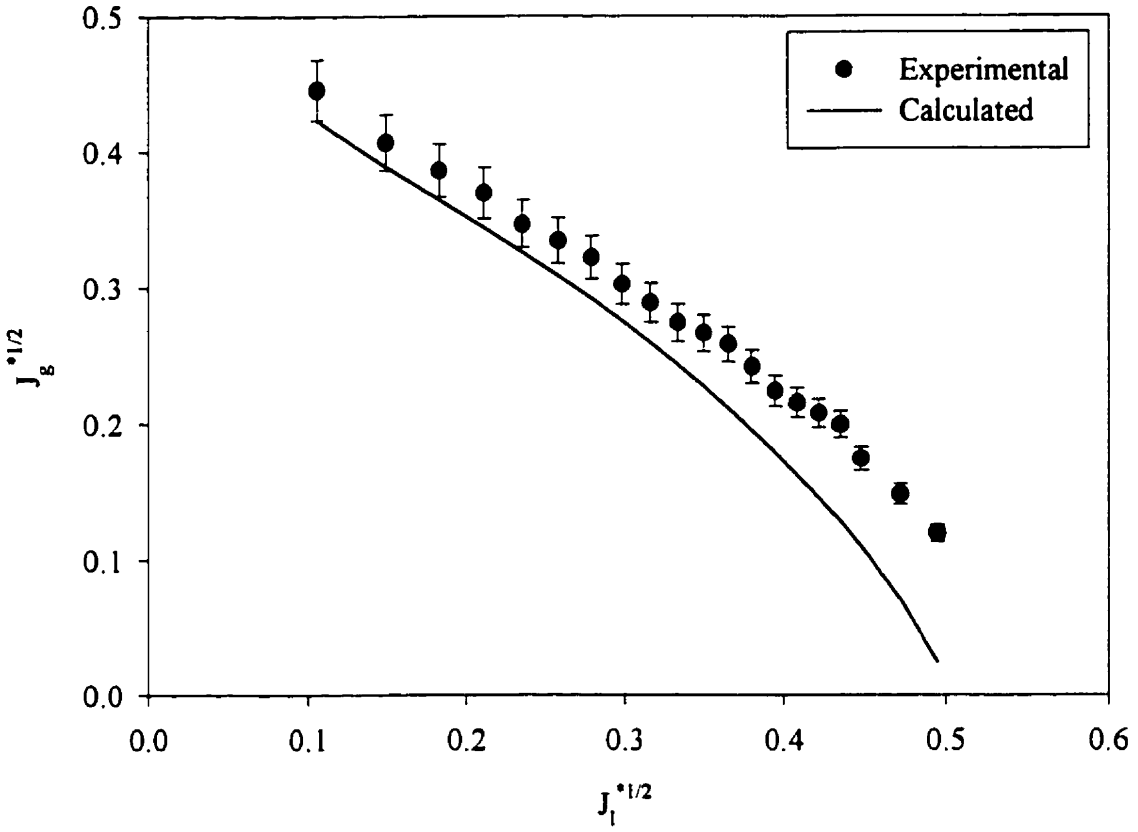

Figure 5.17: Comparison of experimental and predicted flooding points, test section with vertical and horizontal legs orifice $\beta = 0.90$ using the horizontal CCFL model.

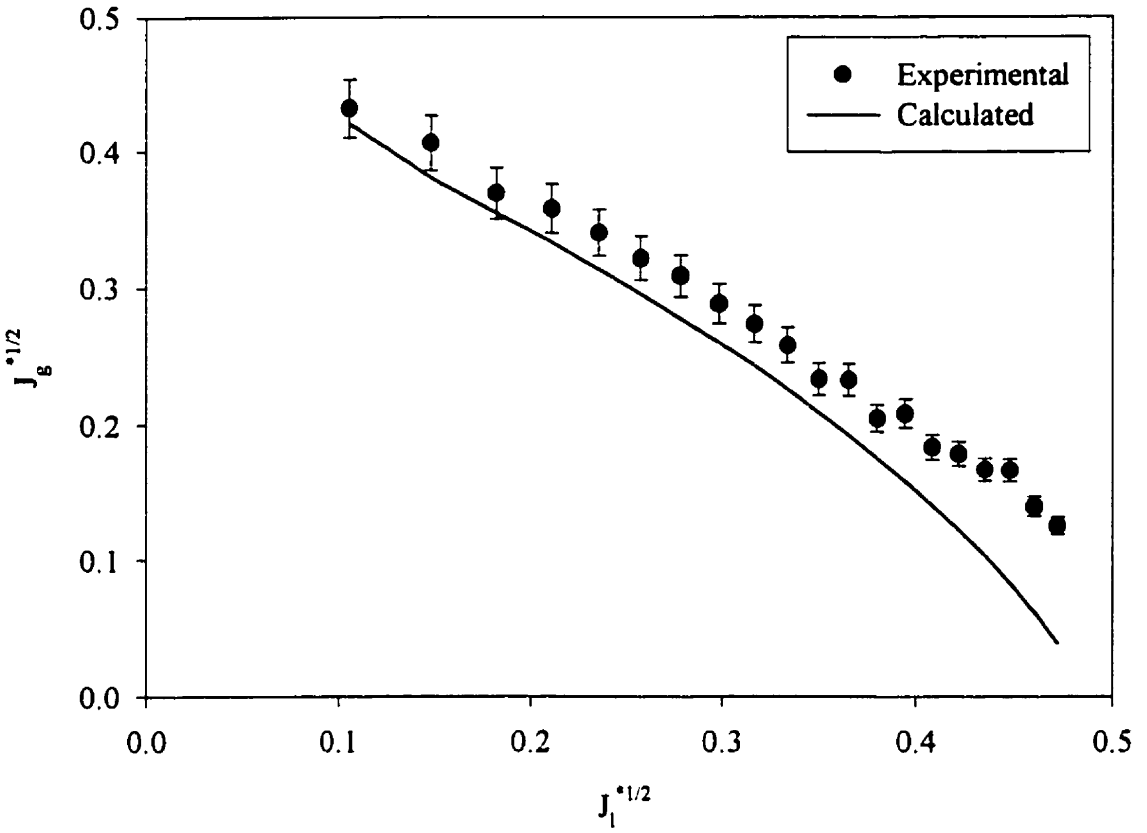

Figure 5.18: Comparison of experimental and predicted flooding points, test section with vertical and horizontal legs orifice $\beta = 0.83$ using the horizontal CCFL model.

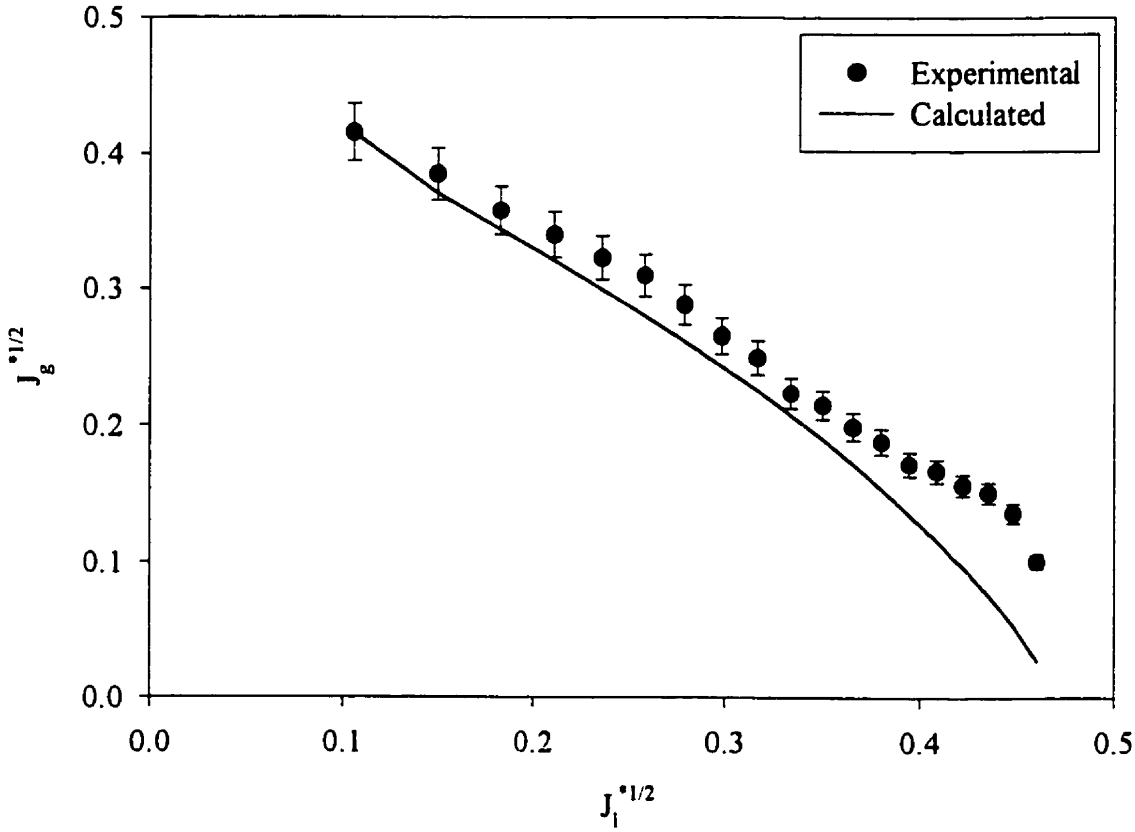

Figure 5.19: Comparison of experimental and predicted flooding points, test section with vertical and horizontal legs orifice $\beta = 0.77$ using the horizontal CCFL model.

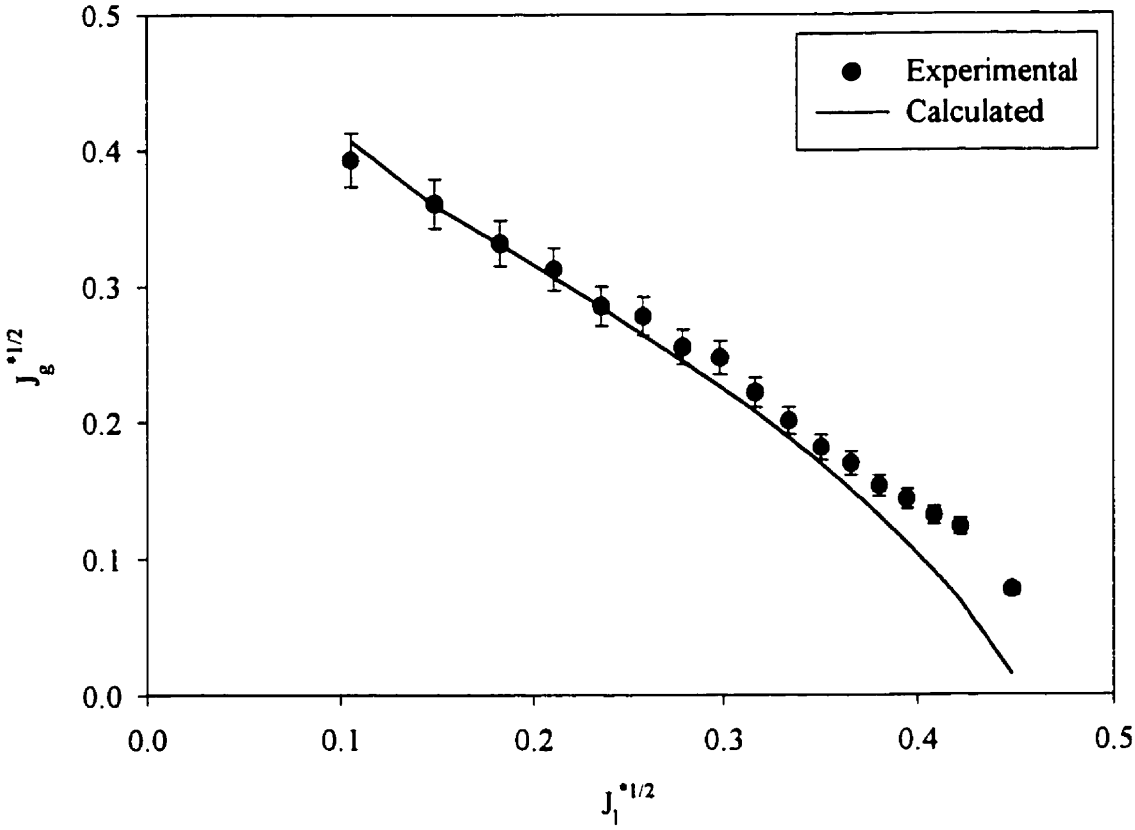

Figure 5.20: Comparison of experimental and predicted flooding points, test section with vertical and horizontal legs orifice $\beta = 0.72$ using the horizontal CCFL model.

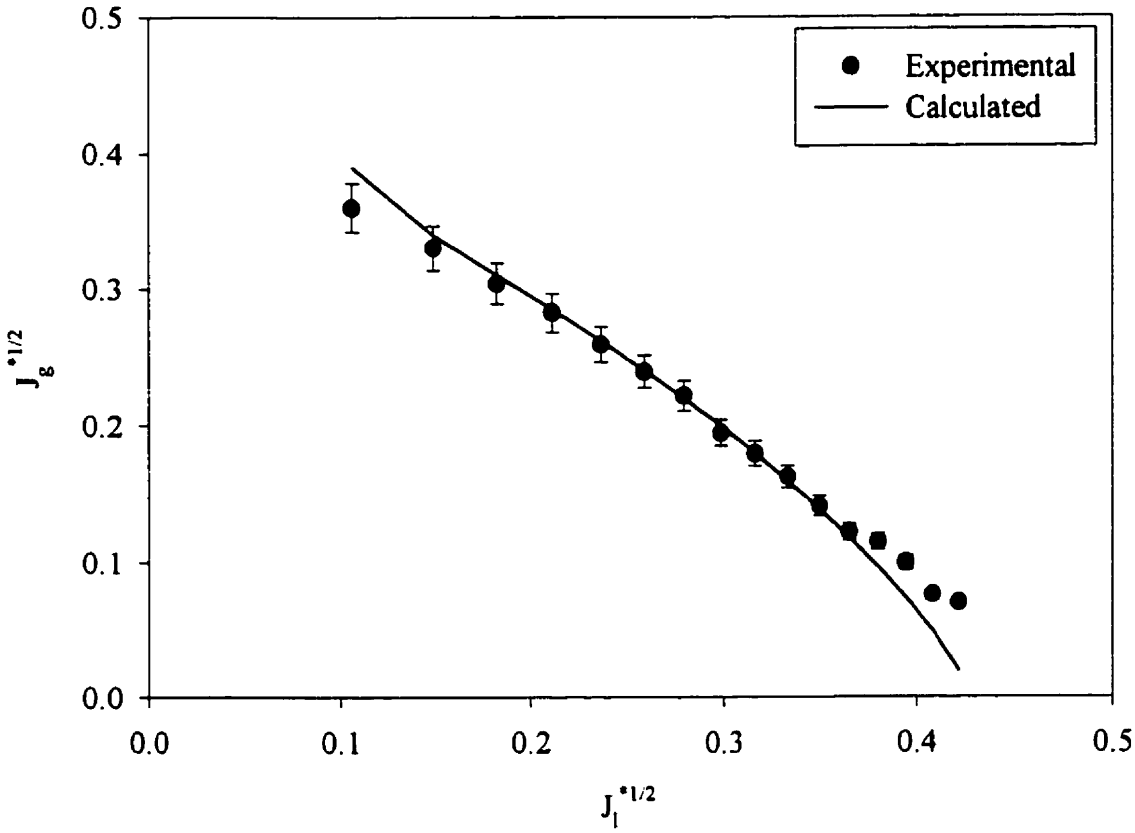

Figure 5.21: Comparison of experimental and predicted flooding points, test section with vertical and horizontal legs orifice $\beta = 0.66$ using the horizontal CCFL model.

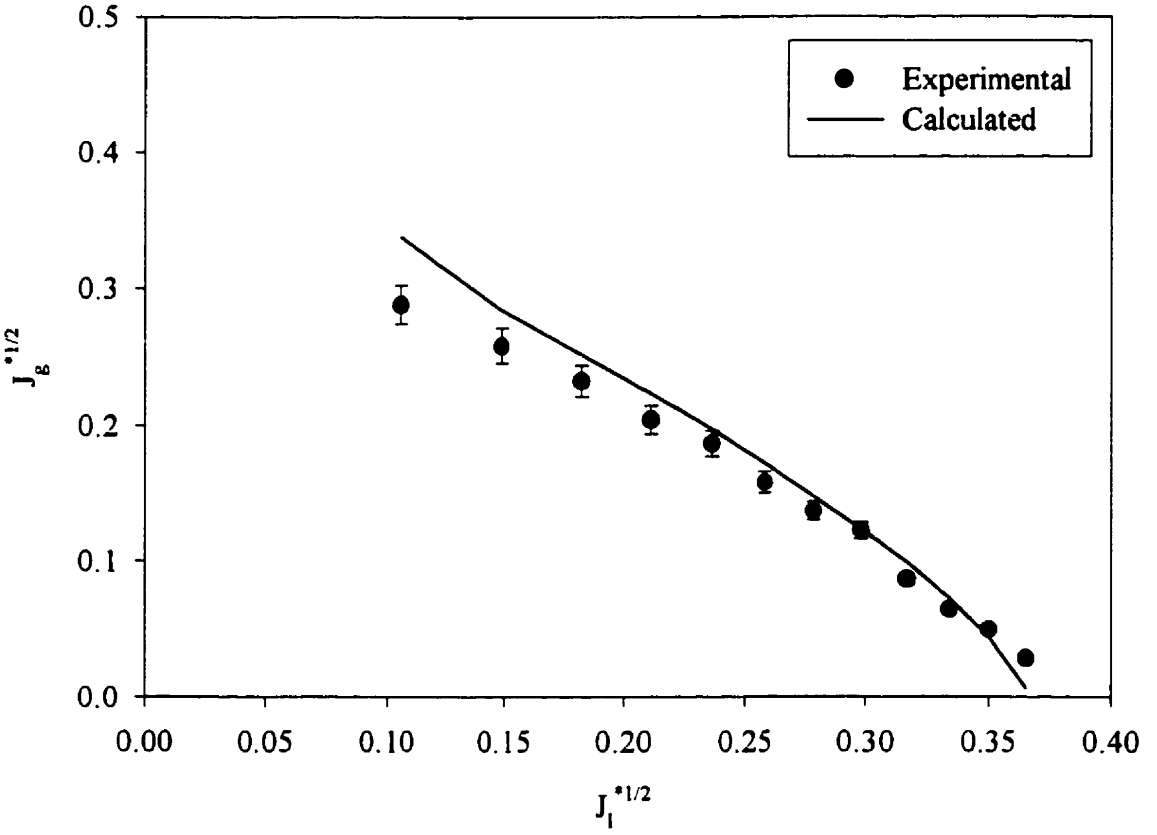

Figure 5.22: Comparison of experimental and predicted flooding points, test section with vertical and horizontal legs orifice $\beta = 0.55$ using the horizontal CCFL model.

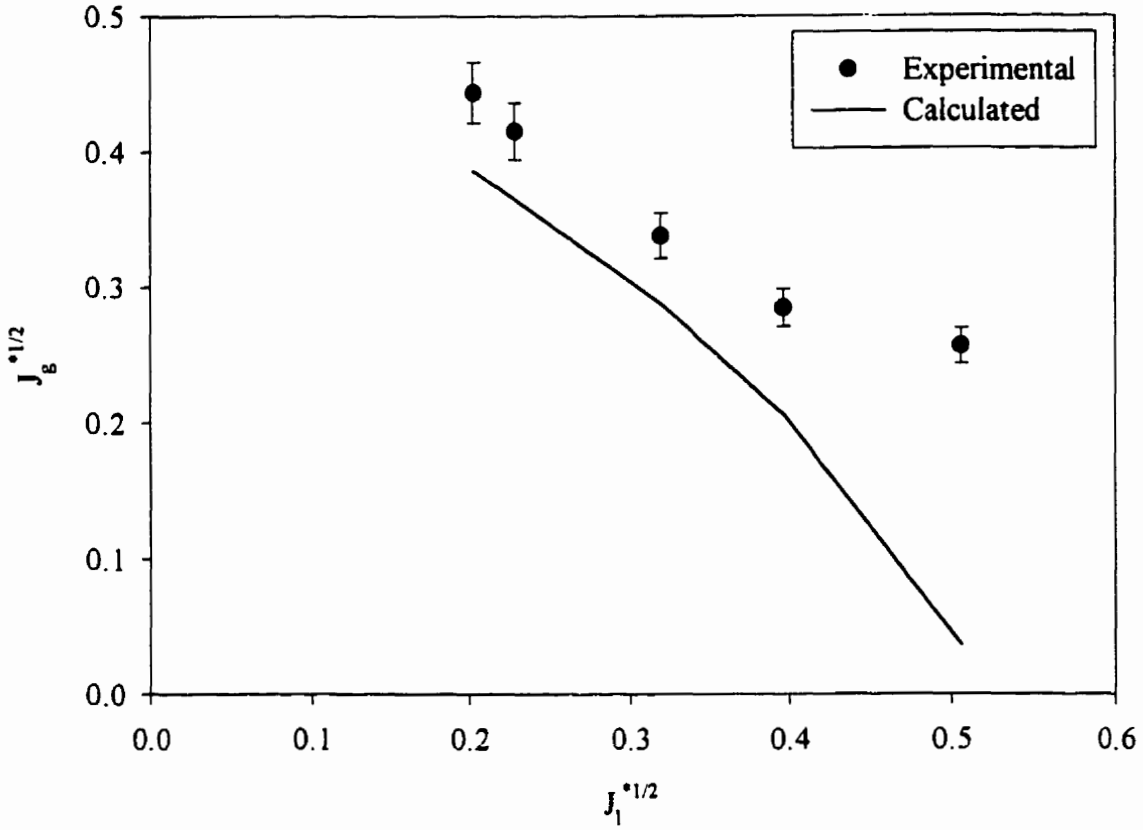

Figure 5.23: Comparison of experimental and predicted flooding points using the horizontal CCFL model and the data of Kawaji *et al.* [1993] orifice $\beta = 0.865$.

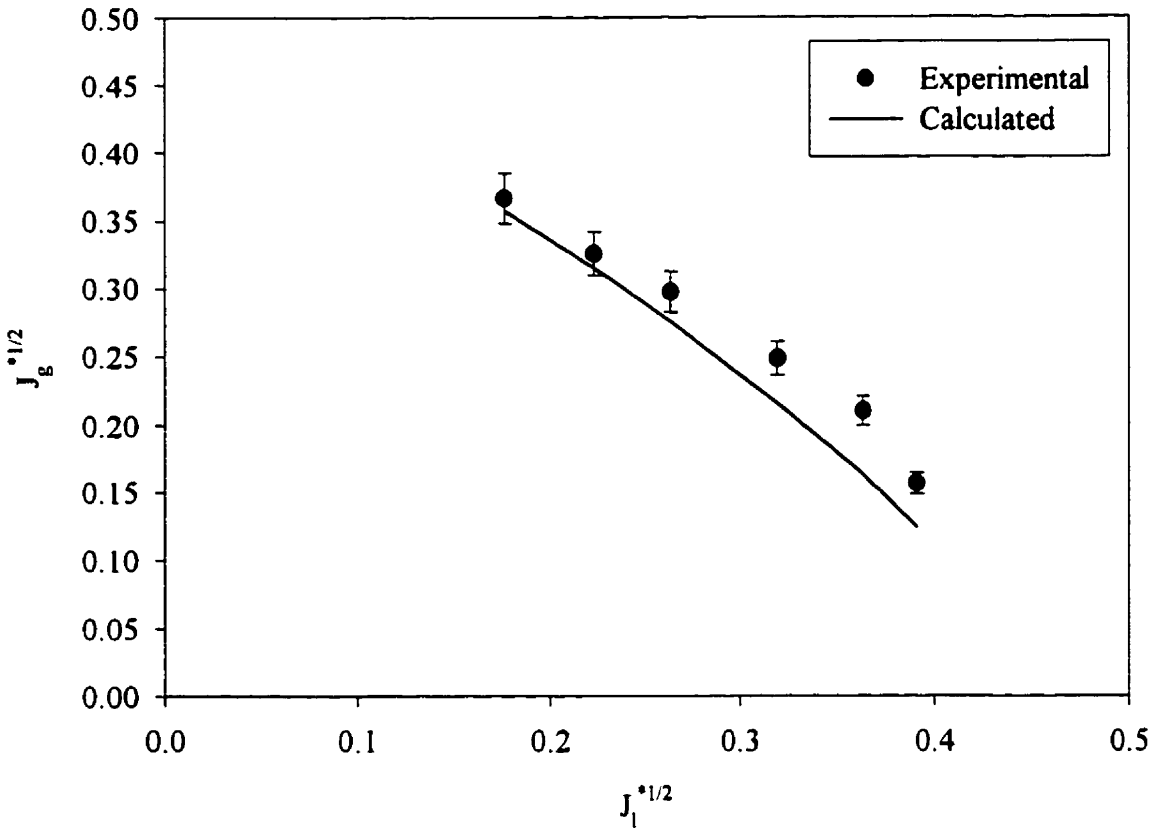

Figure 5.24: Comparison of experimental and predicted flooding points using the horizontal CCFL model and the data of Kawaji *et al.* [1993] orifice $\beta = 0.67$.

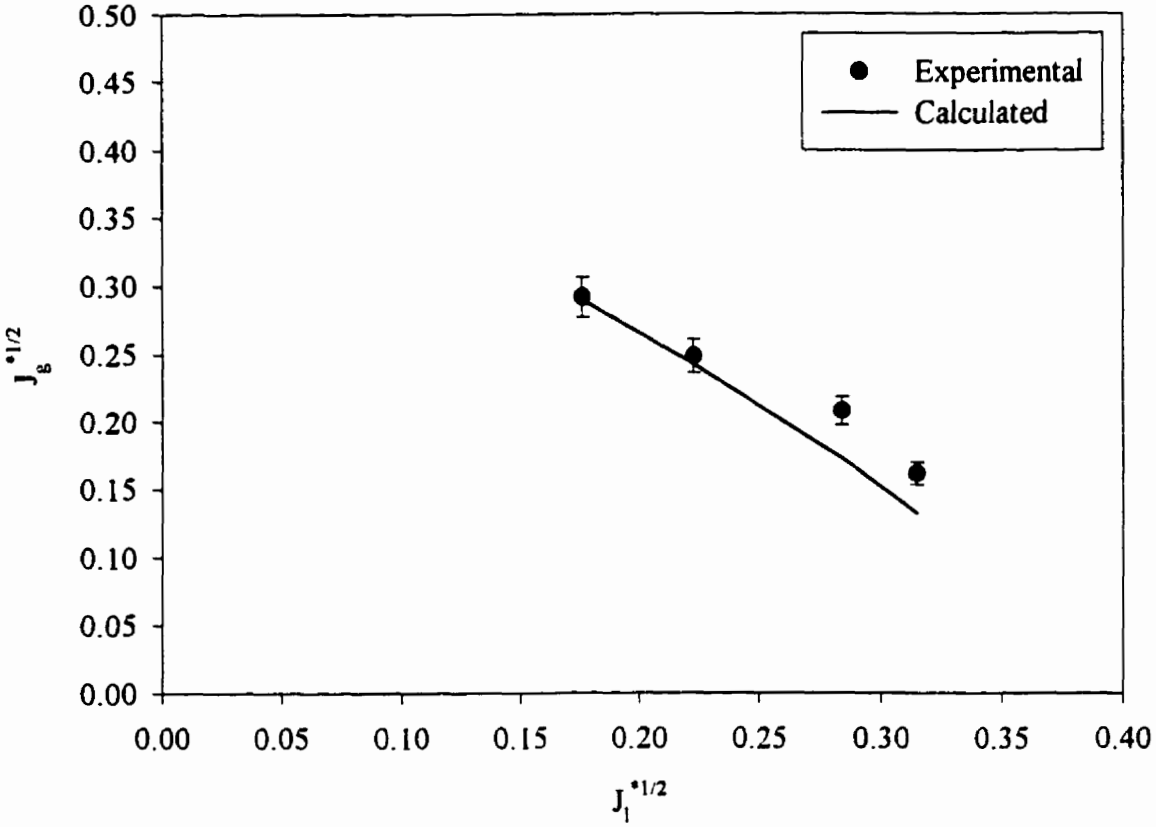

Figure 5.25: Comparison of experimental and predicted flooding points using the horizontal CCFL model and the data of Kawaji *et al.* [1993] orifice $\beta = 0.55$.

Chapter 6

CONCLUSIONS AND RECOMMENDATIONS

In this thesis the results of work carried out to study counter-current flow and flooding phenomena under conditions of both vertical and vertical to horizontal flow have been presented. Two different 63.5 *mm.* I.D. test sections were used for this work. The first containing only a vertical leg and the second having both a vertical and a horizontal leg. In both cases the experiments were carried out both with and without various size orifices placed in the test section. For the test section containing both the vertical and the horizontal legs the orifice was placed in the horizontal leg. Results on the pressure drop under counter-current flow conditions obtained in the test section having only a vertical leg were also presented.

For both the vertical and the horizontal test sections, it was found that for a given liquid flow rate the presence of an orifice greatly reduced the gas flow rate at which flooding occured. Furthermore, this decrease was found to be inversely proportional to the orifice β ratio. Results for the delivered liquid flow rate as a function of the gas flow rate and of the orifice β ratio were obtained using both test sections. These results are unique in that all of the information available in the literature on counter-current flow and flooding for horizontal flow conditions were limited to the determination of the flooding and zero liquid penetration points. Limited information was available in the literature on the partial delivery region for vertical CCF conditions but did not include experiments in which an orifice was present. The important points that come out of the study of the partial delivery region is that while the flooding phenomena does limit the delivered liquid flow rate some coolant will still reach the fuel channels

except under specific conditions which occur only at very large gas flow rates (zero liquid penetration point). It was further observed that for all the cases studied the zero penetration point was only a function of the orifice β ratio and of the gas flow rate and was independent of the inlet liquid flow rate.

The experimental results, for the flooding point only, obtained in the test section containing both the vertical and the horizontal runs were compared to the results of other researchers. In spite of the fact, that none of the test facilities used by the other researchers were identical to the one used in the present study, the results of the other researchers were found to be in good agreement with the present results. The Ardron & Banerjee [1986] correlation was found to do a reasonably good job of predicting our experimental flooding results for the case without an orifice.

Experiments were also carried out to study the hysteresis effect in a test section containing both a vertical and a horizontal leg. These experiments were performed both with and without various sized orifices placed in the horizontal leg. For all the orifices studied, a significant hysteresis effect was observed. It was found that in order to re–establish full liquid delivery after flooding had occured it was necessary to significantly decrease the gas flow rate below that required to initiate flooding. It was also observed that in the post flooding state, the delivered liquid flow rate with decreasing gas flow rate followed the partial delivery curves obtained with increasing gas flow rates.

The experiments for the determination of the pressure drop have shown that for a given liquid flow rate the pressure drop increases with increasing gas flow rate. For a fixed gas flow rate the pressure drop increases with increasing liquid flow rate.

Two phenomenological models for the prediction of the flooding point for vertical counter–current two–phase flows were developed. The first represented flooding as being linked to the mechanism of droplet entrainment while the second related the flooding point to the mechanism of film reversal. A comparison between the predictions of these models and the experimental results obtained during the course of this investigation was presented. It was found that the models were very sensitive to the choice of correlation used for the interfacial friction factor. It has been shown that, with an appropriate choice of the correlation to represent the interfacial friction, the model based on the mechanism of droplet entrainment predicted our experimental results reasonably well. The model based on the mechanism of flow reversal on the

other hand under–predicted the flooding points at high liquid flow rates.

A new model to predict the flooding point in a test section containing vertical and horizontal legs using an extension of a model for entrainment inception applied at the crest of the hydraulic jump was developed. This model is also able to take into account the influence of the various size orifices on the flooding point. This is to the best of the author's knowledge the only model which is capable of predicting the flooding point under vertical to horizontal flow conditions when an orifice is placed in the horizontal leg.

The results of a comparison between this model and our experimental results as well as those of other researchers for cases both with and without an orifice located in the horizontal leg was presented. The predictions were, in general, seen to be in very good agreement with the experimental results.

6.1 Recommendations

The results for the flooding, partial liquid delivery and zero liquid penetration point for conditions of horizontal counter–current two–phase flow presented in this thesis were obtained with the orifice located at one fixed position in the horizontal leg. In order to better represent the various geometrical configurations that are present in the header–feeder system of a CANDU reactor it would be useful to study the influence of the position of the orifice with respect to the elbow between the vertical and horizontal leg on:

1. the flooding point,
2. the partial liquid delivery,
3. the zero liquid penetration point, and
4. the hysteresis effect.

In view of the fact that it has been shown that even after flooding has occured, depending on the gas flow rate, a significant amount of liquid is still delivered to the outlet of the test section, it would be useful to further investigate the phenomena

which occur in and control the partial liquid delivery. These phenomena are mostly linked to the slugging that is seen to occur in this region. In order to be able to accurately model the partial delivery region, the following information would be of great value:

1. slugging frequency,
2. slug velocity,
3. size length, and
4. gas holdup in the slug body.

The aforementioned parameters should be determined as a function of gas and liquid flow rates and orifice size. The final recommendation is that work be done on the development of a model capable of predicting the delivered liquid flow rate results obtained in this work. This would lead to improved predictions of the time required to refill the core of a reactor following certain hypothetical loss of coolant accidents.

BIBLIOGRAPHY

ALEKSEEV, V. P., POBEREZKIN, A. E. & GERASIMOV, P. V. [1972]; "Determination of flooding rates in regular packings." Heat Transfer Soviet Res. 4, pp.159-163.

ARDRON, K. H. & BANERJEE, S. [1986]; "Flooding in an elbow between a vertical and horizontal or near-horizontal pipe. Part II: Theory." Int. J. of Multiphase Flow 12, pp. 543-558.

BANKOFF, S. G. & LEE, S. C. [1986]; "A critical review of the flooding literature." *in*: Multiphase Science and Technology, Vol. 2, Chap.2 (*Edts.*: Hewitt, G. F., Delhaye, J. M. & Zuber, N.). Hemisphere, New York.

BIAGE, M., DELHAYE, J. M. & NAKACH, R. [1989]; "The flooding transition: an experimental appraisal of the chaotic aspect of liquid film flow before the flooding point." AIChE Symposium Series 269, Vol. 85, (Ed. Yilmaz, S. B.), AIChE, pp. 274-279.

BHARATHAN, D., WALLIS, G. B. & RICHTER, H. J. [1978]; "Air-water countercurrent annular flow in vertical tubes." EPRI Report No. NP-786.

BHARATHAN, D., WALLIS, G. B. & RICHTER, H. J. [1979]; "Air-water countercurrent annular flow." EPRI Report, No. NP-1165.

CHANG, H. C. [1986]; "Nonlinear waves on liquid film surfaces. –I. Flooding in a vertical tube." Chem. Eng. Sci. 41, No. 10, pp. 2463-2476.

CELATA, G. P., CUMO, N., FARELLO, G. E. & SETARO, T. [1989]; "The influence of flow obstructions on the flooding phenomena in vertical channels." Int. J. Multiphase Flow 15, pp. 227-239.

CELATA, G. P., CUMO, N., FARELLO, G. E. & SETARO, T. [1991]; "Hysteresis effect in flooding." Int. J. Multiphase Flow 17, No. 2, pp. 283-289.

CETINBUDAKLAR, A. G. & JAMESON, G. J. [1969]; "The mechanism of flooding in vertical countercurrent two-phase flow." Chem. Eng. Sci. 24, pp. 1669-1680.

CHUNG, K. S. [1978]; "Flooding phenomena in countercurrent two-phase flow systems." Ph. D. Thesis, University of California, Berkeley.

CLIFT, R., PRITCHARD, C. L. & NEDDERMAN, R. M. [1966]; "The effect of viscosity on flooding conditions in wetted wall columns." Chem. Eng. Sci. 21, pp. 87-95.

DAVIDSON, M. [1994]; "Étude de l'effet d'une obstruction sur le point d'engorgement en écoulement contre–courant dans un canal vertical." M. Eng. Thesis École Polytechnique.

DEMEKHIN, E. A., TOKAREV, G. Yu. & SHKADOV, V. Ya. [1989]; "Instability and nonlinear waves on a vertical liquid film flowing counter to a turbulent gas flow." Theoretical Foundations of Chemical Engineering 23, No. 1, pp. 54-60.

DUKLER, A. E. & SMITH, L. [1979]; "Two–Phase Interaction in Counter–Current Flow; Studies of the Flooding mechanism." NUREG/CR-0617.

DUKLER, A. E., SMITH, L. & CHOPRA, A., [1984]; "Flooding and upward film flow in tubes. I. Experimental studies." Int. J. Multiphase Flow 10, No. 5, pp. 585-597.

FRENCH, R.H. [1985]; "Open Channel Hydraulics," McGraw–Hill New York.

GOVAN, A. H., [1990]; "Modelling of Vertical Annular and Dispersed Two–Phase Flows." Ph.D. Thesis, Imperial College, University of London, U.K.

GOVAN, A. H., HEWITT, H. J., RICHTER H. J. & SCOTT, A. [1991]; "Flooding and churn flow in vertical pipes." Int. J. Multiphase Flow 17, No. 1, pp. 27-44.

HEWITT, G. F. & WALLIS, G. B. [1963]; "Flooding and associated phenomena in falling film flow in a vertical tube." AERE - R4022, UKAEA, Harwell.

HEWITT, G.F. & HALL-TAYLOR, N.S. [1970]; "Annular Two-Phase Flow," Pregamon Press, Great Britain.

HINZE, J.O. [1955]; "Fundamentals of the Hydrodynamic Mechanism of Splitting in Dispersion Process," A.I.CH.E. Journal Vol. 1, No. 3.

HUGHMARK, G.A. [1973]; "Film Thickness, Entrainment, and Pressure Drop in Upward Annular and Dispersed Flow," AICHE J., Vol. 19.

IMURA, H., KUSUDA, H. & FUNATSU, S. [1977]; "Flooding velocity in a countercurrent two-phase flow." Chem. Eng. Sci. 32, pp. 79-87.

ISHII, M. & GROLMES, M.A. [1975]; "Inception Criteria for Droplet Entrainment in Two-Phase Concurrent Film Flow," AICHE J. Vol. 21.

ISHI, M., CHAWLA, T. C. & ZUBER, N. [1976]; "Constitutive equations for vapor drift velocity in two-phase annular flow." AIChE J. 22, p. 283.

JANYANTI, S., TOKARZ, A., & HEWITT, G.F. [1996]; "Theoretical Investigation of the Diameter Effect on Flooding in Countercurrent Flow," Int. J. Multiphase Flow, Vol. 22, No. 2, pp. 307-324.

KAWAJI, M., THOMSON, L. A. & KRISHNAN, V. S. [1989]; "Analysis of countercurrent flooding data obtained in vertical-to-inclined pipes containing elbows of varying angle." C.N.S. 15th Annular Reactor Simulation Symposium, Missasauga Ont.

KAWAJI, M., THOMSON, L. A. & KRISHNAN, V. S. [1991]; "Countercurrent Flooding in Vertical-to-Inclined Pipes." Exp. Heat Transfer, Vol. 4, pp.95–110.

KAWAJI, M., LOTOCKI, P.A. & KRISHNAN, V.S. [1993]; "Countercurrent Flooding in Pipes Containing Multiple Elbows and an Orifice," JSME, Ser. B, Vol. 36, No. 3. pp.95–110.

KATAOKA, I. *et al.* [1983]; "Generation and Size Distribution of Droplet in Annular Two-Phase Flow," Transactions of the ASME, Fluids Eng. Div., Vol. 105.

KOCAMUSTAFAOGULLARI, G. *et al.* [1993]; "Droplet Size Modeling in Annular Flow,"Proceedings Nureth-6. Grenoble, France, Oct. 5-8.

KOCAMUSTAFAOGULLARI G. *et al.* [1994]; "Maximum and Mean Droplet Sizes in Annular Two-Phase Flow," Int. J. Heat and Mass Transfer, Vol 37, No. 6.

KROWLEWSKI, S.M. [1980]; "Flooding in a Simulated Nuclear Reactor Hot Leg," Bachelor's Thesis, MIT.

LOPES J.C.B. [1984]; "Droplet Sizes, Dynamics and Deposition in Vertical Annular Flow," Ph. D. Thesis, University of Houston, TX.

McQUILLAN, K. W. & WHALLEY, P. B., [1985]; "A comparison between flooding correlations and experimental flooding data for gas-liquid flow in vertical circular tubes." Chem. Eng. Sci. 40, No. 8, pp. 1425-1440.

MOALEM MARON, D., & DUKLER, A. E. [1984]; " Flooding and Upward Film Flow in Vertical Tubes-II, Speculations on Film Flow Mechanisms," Int. J. Multiphase Flow Vol. 10, No. 5.

NIGMATULIN, R.I. [1991]; "Dynamics of Multiphase Media," Hemisphere Publishing Co., N.Y.

NOEL, D.G., SHOUKRI, M., ABDUL-RAZZAK, A. [1994]; "Two-Phase Counter-Current Flow Limitation in Complex Piping Systems." Proc. 15th Annual CNS Conference, Montréal Qc. June 5-8.

NUSSELT, W. [1916]; "Die Obserflacherkondensation des Wasserdamphes," Z. Ver. Dtsch. Ing., 19, pp. 541.

POPOV, N. K. & ROHATGI, U. S. [1986]; "Analysis of counter-current adiabatic flow limitation phenomenon in vertical pipes." Brookhaven National Lab., Upton, N. Y., NUREG/CR-4630.

PUSHKINA, O. L., SOROKIN, Y. L. [1969]; "Breakdown of Liquid Film Motion in Vertical Tubes," Heat Trans. Soviet Res. Vol. 1, No. 5, pp. 56-94.

RICHTER, H. J. [1981]; "Flooding in tubes and annuli." Int. J. of Multiphase 7, pp. 647-658.

SHOUKRI, M., ABDUL-RAZZAK, A. & YAN, C. Q. [1991]; "Hysteresis effects in counter-current gas-liquid flow limitations in a vertical tube," in Proceedings of the International Conference on Multiphase Flows, (Eds. Matsui, G., Serizawa, A. & Tsuji, Y.), Tsukuba, Japan.

SIDDIQUI, H., ARDRON, K. H. & BANERJEE, S. [1986]; "Flooding in an elbow between a vertical and horizontal or near horizontal pipe. Part I: Experiments." Int. J. of Multiphase Flow 12, pp. 531-541.

SUZUKI, S. & UEDA, T. [1977]; "Behaviour of liquid films and flooding in counter-current two-phase flow. - Part I. Flow in circular tubes." Int. J. Multiphase Flow 3, pp. 517-532.

TAITEL, Y. BARNEA, D. & DUKLER, A. E. [1982]; "A film model for prediction of flooding and flow reversal for gas-liquid flow in vertical tubes." Int. J. Multiphase Flow Vol. 8, pp. 1-22.

THURGOOD, M.J. [1981]; "Volume 1: COBRA-TF Equations and Constitutive Relations," Report FATE-81-106, Fluid and Thermal Engineering Section, Battelle PNL, Richland Wash.

TYE, P.F., DAVIDSON, M., MATUSZKIEWICZ, A., [1993]; "Adiabatic Counter-Current Two-Phase Flows in Channels Containing Singularities, Interim Report # 1," Report IGE-153.

TYE, P.F., TEYSSEDOU, A., MATUSZKIEWICZ, A. & TAPUCU, A. [1995]; "Adiabatic Counter-Current Flow in Channels Containing Singularities, Activities for FY-94," Report IGE-181.

TYE, P.F., TEYSSEDOU, A., BDARD, S. [1996]; "Adiabatic Counter-Current Flow in Channels Containing Singularities, Activities for FY-95," Report IGE-213.

TYE, P.F., TEYSSEDOU, A., HERNU, P. [1997]; "Adiabatic Counter-Current Flow in Channels Containing Singularities, Activities for FY-96," Report IGE-225.

WALLIS, G. B. [1961]; "A Theory of One Dimensional Two–Phase and Three–Phase Vertical Flow," Ph.D. Dissertation, Trinity College, Cambridge University, U.K.

WALLIS, G. B. [1969]; "One Dimensional Two–Phase Flow," McGraw–Hill New York.

WALLIS, G. B. & MAKKENCHERY, S. [1974]; "The hanging film phenomenon in vertical annular two-phase flow." J. Fluid Eng. 96, pp. 297-298.

WALLIS, G. B. & KUO, J. T., [1976]; "The behavior of gas–liquid interfaces in vertical tubes." Int. J. Multiphase Flow 2, pp.521-536.

WALLIS, G. B. [1987]; " Interfacial Friction Modeling," Multiphase Science and Technology (G.F. Hewitt, J.M. Delhaye and N. Zuber *Eds.*), Vol. 3. Chapter 3. Hemisphere Publishing Co., N.Y.

WAN, P. T. [1986]; "Counter-Current Steam-Water Flow in an Upright 90^0 Elbow." Proceedings of the 8th International Heat Transfer Conference, (Edts.: Tien, C. L., Carey, V. P. and Ferrell J. K.), San Francisco.

WAN, P. T. and Krishnan, V. S. [1986]; "Air–water flooding in a 90^0 elbow with a slightly inclined lower leg." 7th Annual Conference of the Canadian Nuclear Society, Toronto.

WILCOX, D. C. [1993]; "Turbulence Modeling for CFD." DCW Industries, La Canāda, California, U.S.A.

Wongwises, S. [1994] "Experimental Investigation of Two–Phase Countercurrent Flow Limitation in a Bend Between Horizontal and Inclined Pipes," Exp. Thermal and Fluid Science, Vol. 8, pp. 245–259.

ZABARAS, G. J. [1985]; "Studies of vertical annular gas–liquid flows," Ph. D. Thesis, University of Houston, TX.

ZABARAS, G. J. & DUKLER, A.E. [1988]; "Counter–current gas–liquid annular flow, including the flooding state." American Institute of Chemical Engineers Journal 34, No. 3, pp. 389-396.

ZVIRIN, Y., DUFFEY, R. B. & SUN, K. H. [1979]; "On the derivation of a counter-current flooding theory." Symposium on Fluid Flow and Heat Transfer over Rod or Tube Bundles, ASME, New York, pp.111-119.

Appendix A

ORIFICE OFFSET

This appendix presents the results obtained using equation A.1, which is given below, to calculate the offset height of the hydraulic jump caused by the orifice.

$$h_o = (1 - \beta)\frac{D}{2} \quad . \tag{A.1}$$

It can be seen that for the four largest orifices tested, i.e. $\beta = 0.90$ to 0.72 Figures A-1 to A-4, the agreement between the predicted and the experimental flooding points is quite good. For the orifices having β ratios of 0.66 and 0.55 Figures A-5 and A-6 however the flooding points are significantly overpredicted. Furthermore it can be seen that the degree of over prediction increases with decreasing orifice β ratios.

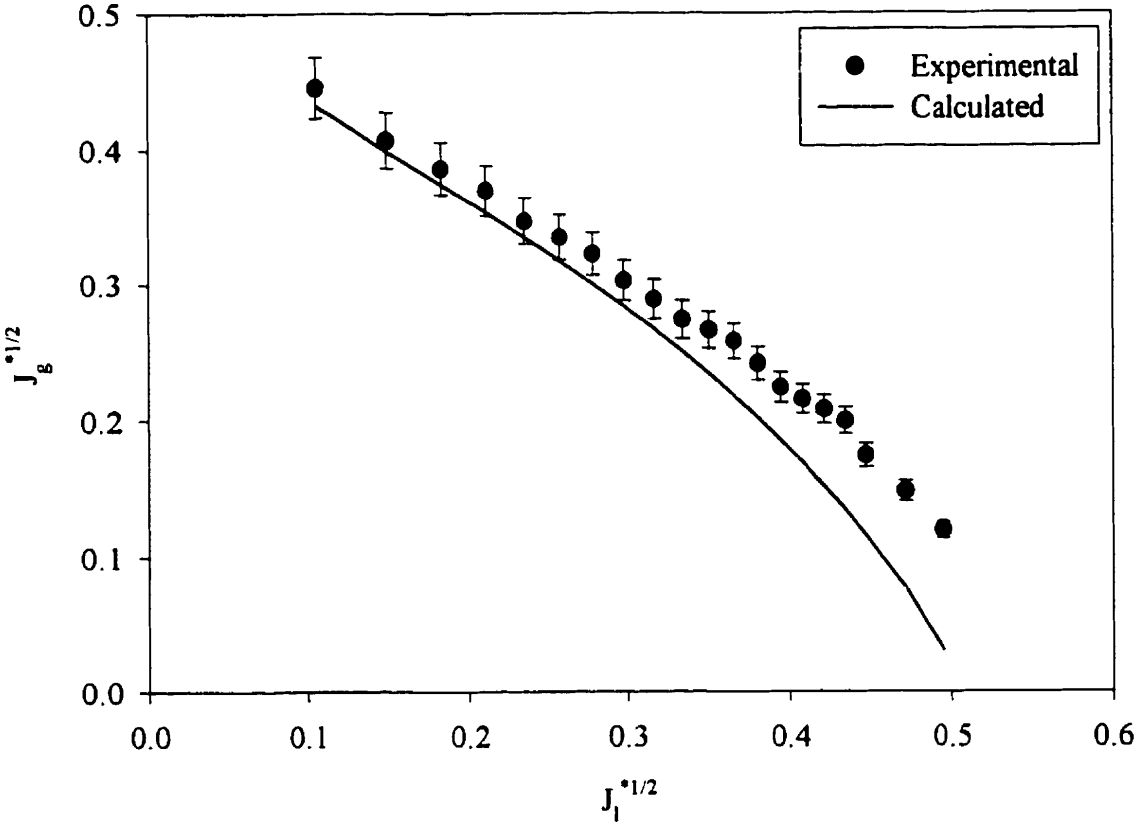

Figure A.1: Test of offset height correction calculated with equation A-1, test section with vertical and horizontal legs orifice $\beta = 0.90$ using the horizontal CCFL model.

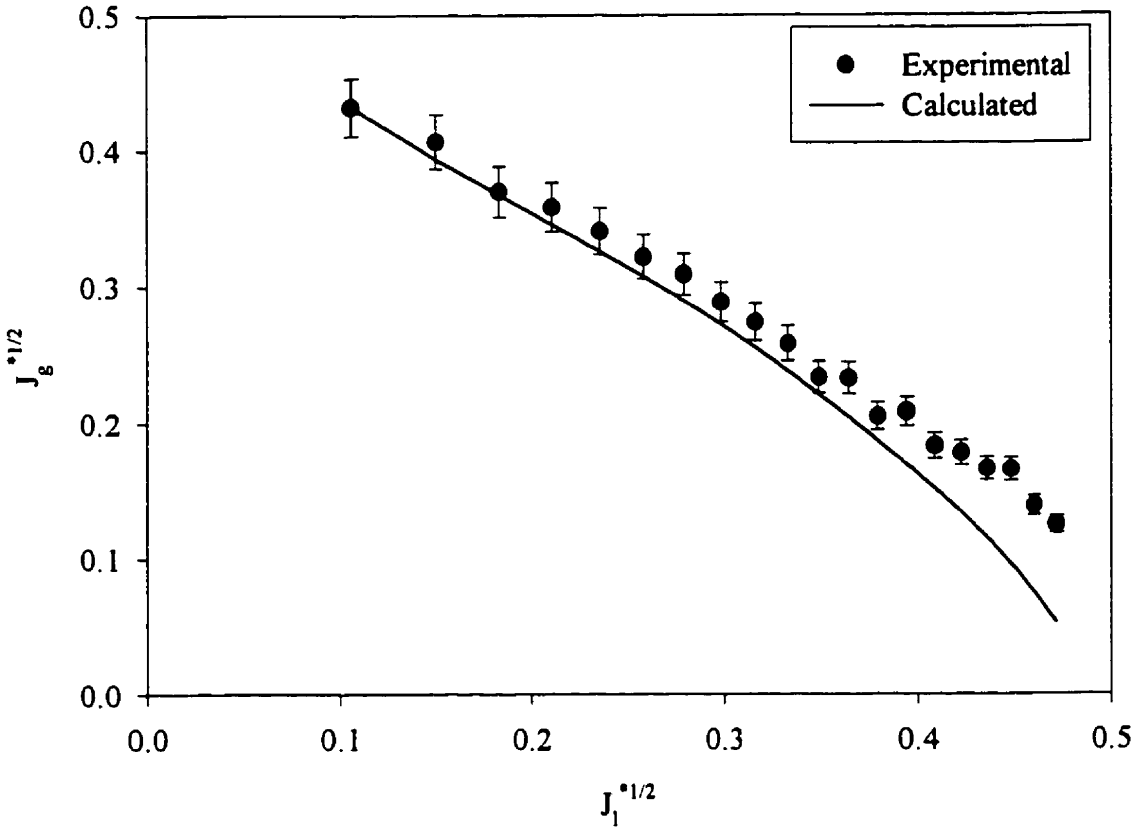

Figure A.2: Test of offset height correction calculated with equation A-1, test section with vertical and horizontal legs orifice $\beta = 0.83$ using the horizontal CCFL model.

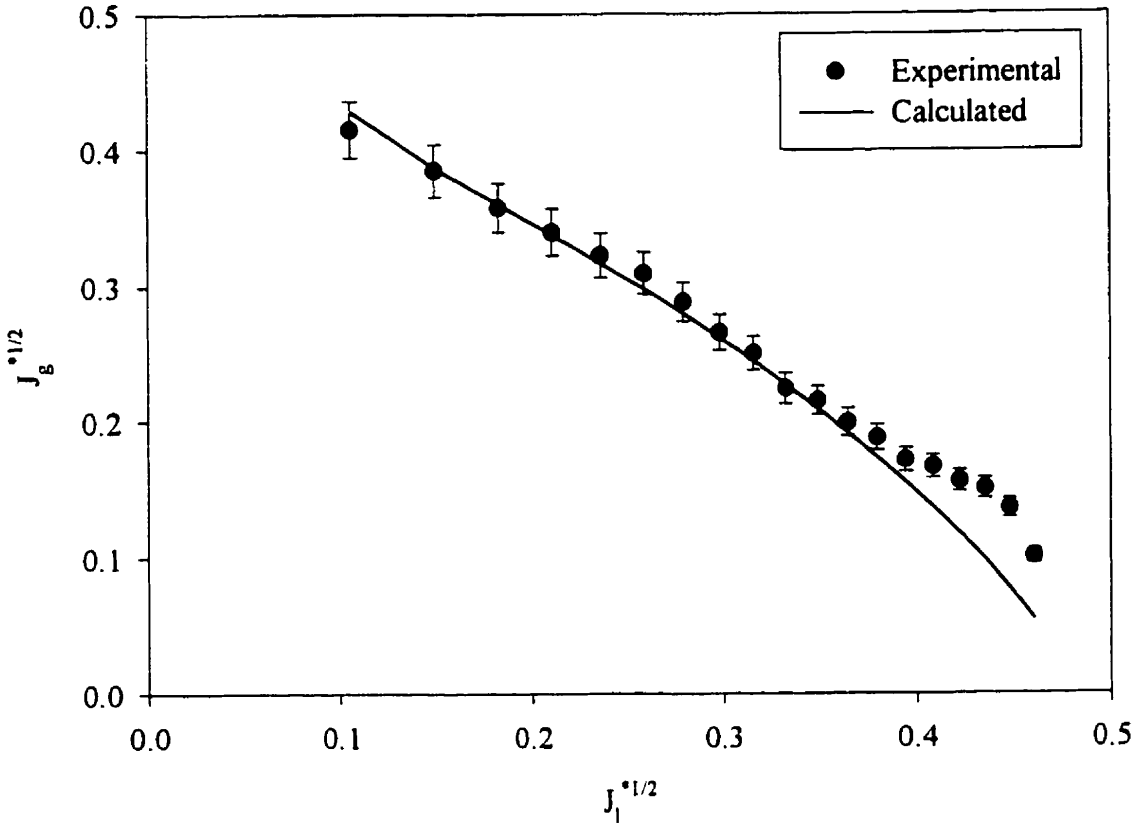

Figure A.3: Test of offset height correction calculated with equation A-1, test section with vertical and horizontal legs orifice $\beta = 0.77$ using the horizontal CCFL model.

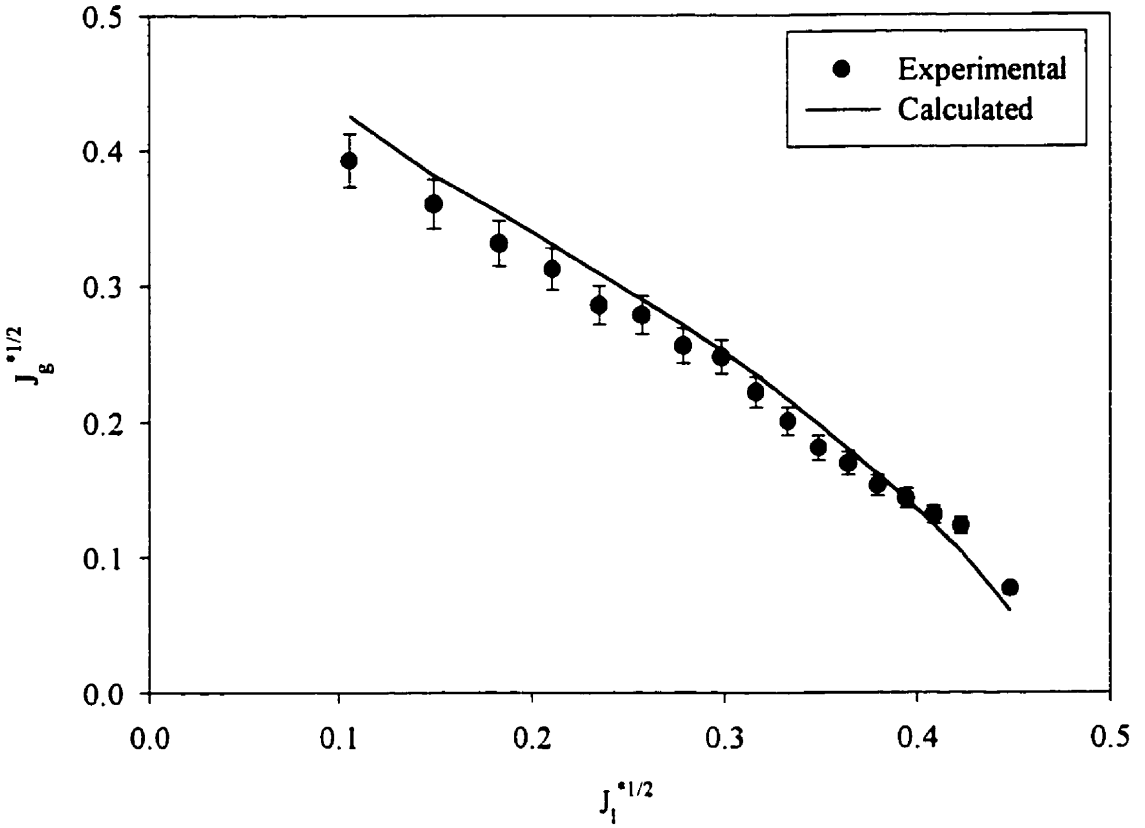

Figure A.4: Test of offset height correction calculated with equation A-1, test section with vertical and horizontal legs orifice $\beta = 0.72$ using the horizontal CCFL model.

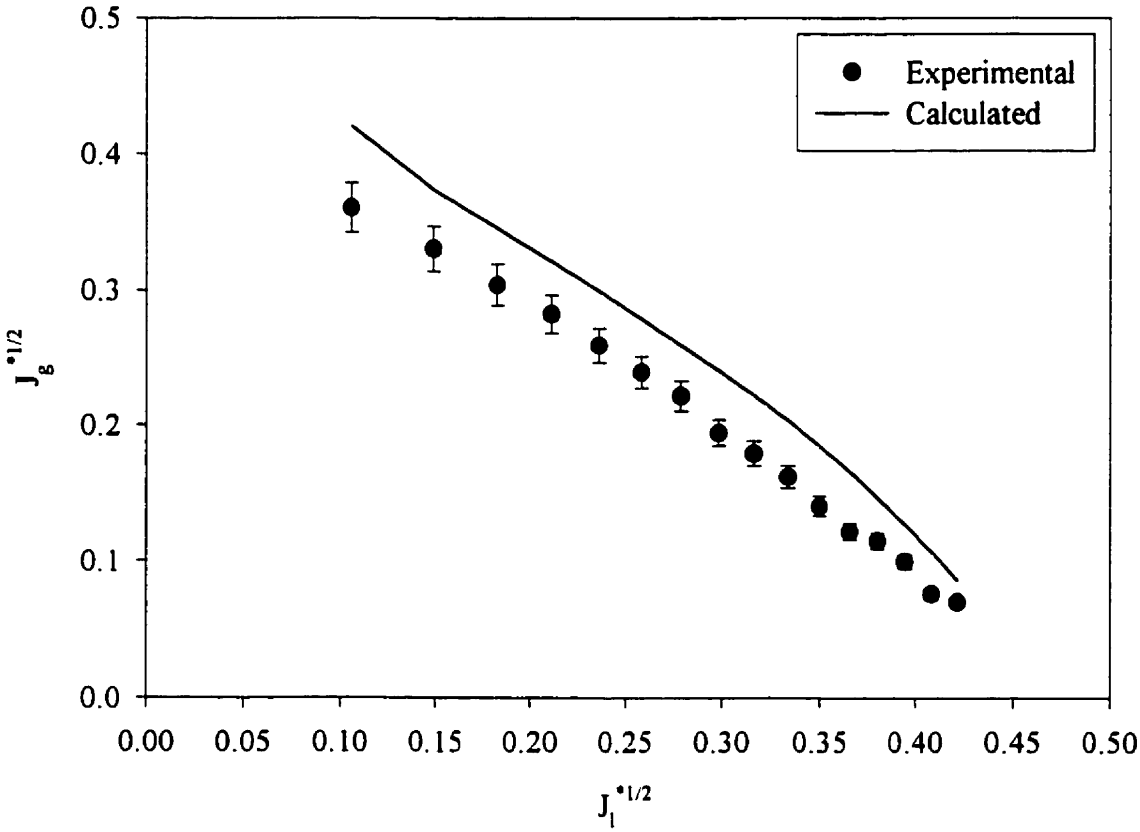

Figure A.5: Test of offset height correction calculated with equation A-1, test section with vertical and horizontal legs orifice $\beta = 0.66$ using the horizontal CCFL model.

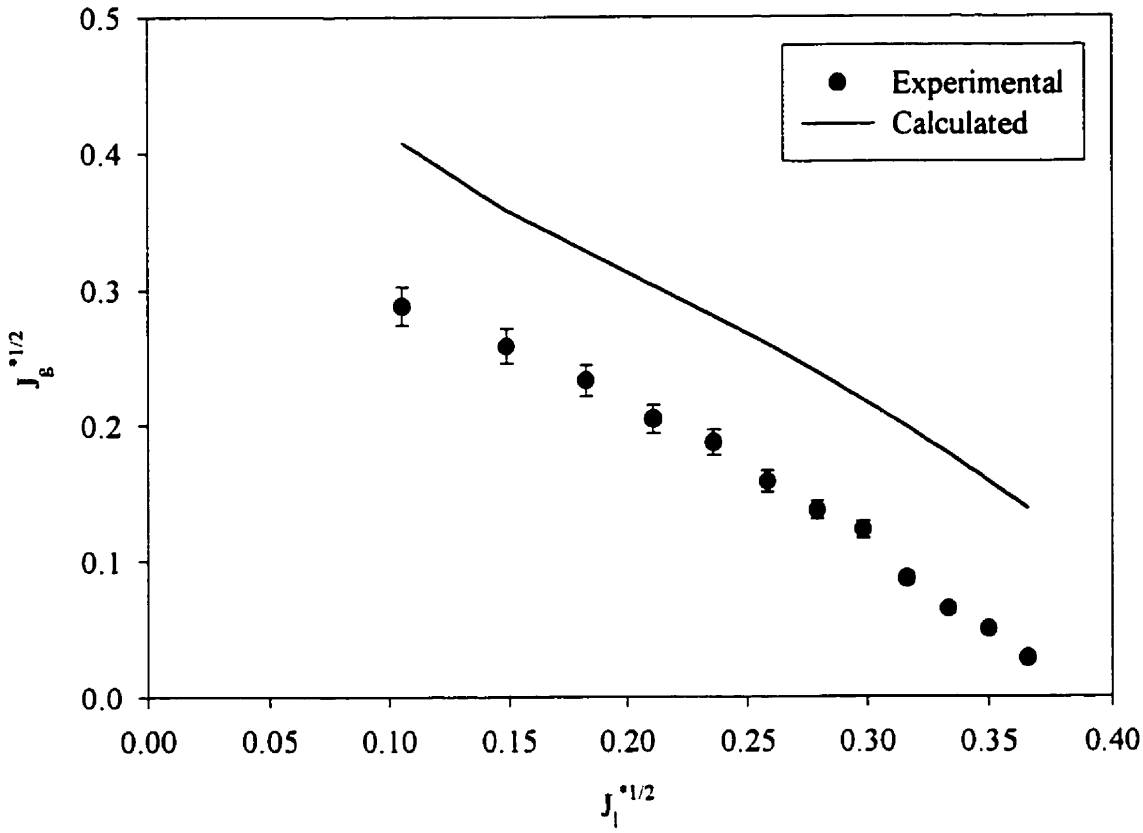

Figure A.6: Test of offset height correction calculated with equation A-1, test section with vertical and horizontal legs orifice $\beta = 0.55$ using the horizontal CCFL model.